HYDRAULIC PERFORMANCE CHARACTERISATION OF VARIABLE RATE IRRIGATION TECHNOLOGY

A Thesis submitted by

Sandile Trevor MSIBI

BSc, MSc (Eng)

For the award of

Doctor of Philosophy

2021

ABSTRACT

Variable-rate irrigation (VRI) technology for centre pivots and lateral moves has been commercially available for over three decades, but its uptake has been limited, with growers citing additional capital and operating costs, the detrimental impact on hydraulic and irrigation performance, as key issues. The hydraulic performance of VRI components are poorly understood in the irrigation engineering community, as evidenced by the common process of simply retro-fitting VRI technology onto existing centre pivots and lateral move machines, without any acknowledgement of the impact these have on the existing hydraulic system. The need to characterise the hydraulic performance of VRI components is essential to allow the accurate hydraulic design of this irrigation equipment for reduced energy consumption, and high irrigation uniformity. As well, the hydraulic performance of VRI components under unsteady hydraulic conditions are even more poorly understood, and this also warranted investigation.

An automated test-rig was developed to capture the hydraulic characteristics of modern VRI components for centre pivots and lateral moves. Highly accurate, calibrated flow and pressure sensors were incorporated into the test-rig. The ability to capture data at high frequency was a unique capability of the test-rig, and was developed specifically to study the unsteady nature of the hydraulic performance of VRI components, and 228 separate tests were completed.

The extensive measured data sets for VRI components, across three different manufacturers, two models, six discharges, and pressures ranging up to 30 m head, provided a unique opportunity to analyse the applicability and fit of standard hydraulic theory for these.

The results highlight that significantly greater head loss occurs through a particularly popular manufacturer's VRI valve compared to others, and warrants special consideration in the selection of these, and if used, specific additional adjustments to machine hydraulics are necessary for optimal hydraulic operation.

The vital importance of the hydraulic characteristic of pressure regulator valves (PRVs) on the overall hydraulic operation of these machines warranted special investigation under steady and unsteady hydraulic conditions. Overall, six separate tests on PRVs were completed.

Due to the incompatibility of published peer-reviewed theories and the hydraulic characteristics measured for these pressure regulators, development of a novel hydraulic model was proposed to more accurately describe the performance, and to be validated against measured results.

Under steady conditions, average outlet pressures for different manufacturer and model combinations vary significantly from the nominal set pressures by up to 0.7 m head.

During unsteady conditions, the complex combination of the mechanical and hydraulic components within PRVs manifest themselves in a hysteresis of outlet pressure when inlet pressures change. A greatly improved explanation of the operation of modern PRVs is reported, for the full range of conditions these valves endure. A novel theoretical model of PRV hydraulic performance was developed based on traditional hydraulic theory and analysis of results from this study, which more accurately describes the performance of these devices.

Overall, an improved understanding of the performance of VRI components has been developed that will allow industry to more accurately design the hydraulic system of VRI equipped centre pivots and lateral moves. This provides the opportunity for improved irrigation performance and lower energy consumption of centre pivot and lateral move systems.

CERTIFICATION OF THESIS

This Thesis is entirely the work of Sandile Trevor MSIBI except where otherwise acknowledged. The work is original and has not previously been submitted for any other award, except where acknowledged.

Principal Supervisor: Associate Professor Joseph Patrick FOLEY

Associate Supervisor: Dr Malcolm Horace GILLIES

Student and supervisors signatures of endorsement are held at the University.

ACKNOWLEDGEMENTS

The fruition of this research is a testament to the invaluable assistance I received from a great number of people during the course of my PhD. I would like to express my sincere gratitude to some of these people, particularly those who were instrumental to the success of my studies.

I would like to acknowledge the expert guidance and excellent support I received from my principal supervisor, Associate Professor Joseph Foley. I am grateful for the time and effort that Joe graciously invested in me to achieve this goal and for always being an inspiration and a mentor. His technical advice, remarks and helpful comments coupled with his great wealth of knowledge and practical experience in irrigation engineering were invaluable to the completion of this work. I am also thankful to my associate supervisor, Dr Malcolm Gillies for his exceptional ideas, technical guidance, and encouragement through all phases of my research.

A big thank you to Dr Richard Landers who provided technical assistance in electronics and LabVIEW software programming, including his help from time to time in the instrumentation of the automatic test-apparatus in Z113 Hydraulics Laboratory at the University of Southern Queensland (USQ). I am also grateful to the staff in the Faculty of Engineering & Surveying and the Centre for Agricultural Engineering (CAE) for providing assistance in research equipment procurement. Great appreciation goes to Komet Irrigation Corporation (Komet Austria GmbH) who offered free units of pressure regulators for this research and paid for their shipment to USQ, Toowoomba Australia.

This PhD would have been impossible without the financial assistance I received from the joint scholarship funding provided by USQ and the Australian Federal Government, and for this I am grateful. I also acknowledge the work opportunities provided by my principal supervisor, to conduct tutorial support activities for

undergraduate students in the faculty, and research work activities in his industry funded projects through CAE.

Words are lacking to express my humble appreciation to the Director of AgriTech Solutions Pty Ltd, Stephen Attard who offered full-time employment at the cessation of my scholarship that coincided with a difficult period when the entire world was affected by COVID-19 and its inevitable imposed restrictions. Steve and his team allowed me to use company resources and work time to complete the write-up of this thesis.

I would also like to express many thanks to all my colleagues for supporting me during this journey, both in the faculty and external, who were present when I needed them. I want to extend my special thanks to Dr Kojo Aikins, a colleague with whom we persevered the PhD journey together and occasionally discussed our research ideas. The moral support and company provided by the Australian citizenry and African communities living in Toowoomba and Australia-wide is greatly acknowledged.

My sincere gratitude also goes to my fearless daughters Asanda and Tami who accepted without any choice to endure the extended period of my absence while I was overseas. To my family, brothers and sisters, especially my late parents who encouraged me throughout my life, I am indebted to you all for the love and support you gave me all these years.

Finally, I thank God for laying the foundation and for using all the people and organisations, institutes and departments mentioned above to help me deliver this thesis.

LIST OF PUBLICATIONS FROM THIS THESIS

Msibi, S.T., Foley, J.P. and Gillies, M.H. (2018), 'Performance of pressure regulation devices for large mobile sprinkler systems', *Irrigation Australia Conference and Exhibition 2018: Addressing the Big Issues*, 13-15 June 2018, Sydney, Australia.

Msibi, S.T., Foley, J.P. and Gillies, M.H. (2018), 'Hydraulic characteristics of automatic VRI sprinkler control valves', *Irrigation Australia Conference and Exhibition 2018: Addressing the Big Issues*, 13-15 June 2018, Sydney, Australia.

Msibi, S.T., Foley, J.P. and Gillies, M.H. (2018), 'Analysis of hydraulic transients in variable-rate irrigation', *Irrigation Australia Conference and Exhibition 2018: Addressing the Big Issues*, 13-15 June 2018, Sydney, Australia.

Msibi, S.T., Foley, J.P. and Gillies, M.H. (2019), 'Hydraulic implications of variable-rate irrigation', *Proceedings of the Australian Society of Sugar Cane Technologists 2019: Broadening Our Horizons*, 30 April-03 May 2019, Toowoomba, Australia.

TABLE OF CONTENTS

LIST OF FIGURES

LIST OF TABLES

LIST OF ABBREVIATIONS

ABS	Australian Bureau of Statistics
ANSI	American National Standards Institute
ASAE	American Society of Agricultural Engineers
CFD	Computational Fluid Dynamics
CP	Centre Pivot irrigation machine
CU	Coefficient of Uniformity
DAQ	Data Acquisition System
EMI	Electro Magnetic Induction
ET	Evapotranspiration
GPS	Global Positioning System
ISO	International Standards Organization
LabVIEW	Laboratory Virtual Instrument Engineering Workbench
LEPA	Low Energy Precision Application
LM	Lateral Move irrigation machine
MPC	Model Predictive Control
NI	National Instruments
PA	Precision Agriculture
PID	Proportional Integral Derivative
PMDI	Precision Mobile Drip Irrigation
PRV	Pressure Regulating Valve
ROI	Return On Investment
USDA-ARS	United States Department of Agriculture – Agriculture Research Service

USDA-NASS	United States Department of Agriculture - National Agricultural Statistics Survey
USA	United States of America
USQ	University of Southern Queensland
VFD	Variable Frequency Drive
VRI	Variable-Rate Irrigation

LIST OF SYMBOLS

g	gravitational acceleration constant
ρ	density of water
p	pressure head in metres of water
μ	kinematic viscosity
V	water velocity
V_e	voltage
γ	hyperbolic mathematical function for switching the slope of regulation curve to produce a turning point
t	time
Q	flow rate or discharge
m	metre head
K	standard minor loss coefficient
K_d	nozzle discharge coefficient
$K_{\_vri}$	minor loss coefficient for VRI valves
$K_{\_prv}$	minor loss coefficient for pressure regulator
C'	coefficient for the slope of regulation curve
D'	constant for adjusting the vertical position of the regulation curve
h_m	standard minor head loss
h_{m_H}	hysteresis minor head loss
h_{m_vri}	minor head loss for VRI valves
h_{m_ST}	static minor head loss for pressure regulators
h_{m_Sv}	variable component of static minor head loss below 1:1 line
h_{m_V}	variable regulation minor head loss

H_{p_F}	falling limb of inlet pressure head
H_{p_R}	rising limb of inlet pressure head
$P_{\_in}$	pressure regulator inlet pressure
$P_{\_set}$	nominal set pressure rating of a pressure regulator
$P_{\_out}$	pressure regulator outlet pressure
TP	maximum turning point of pressure regulator outlet pressure

1. INTRODUCTION

1.1 Introduction

Mobile overhead irrigation (centre pivot and lateral move irrigation machines) has successfully managed to transform agricultural production in the world. This is essentially because of the advantages that these systems have over other irrigation methods. The advantages include low labour and energy requirements, flexibility in terms of operation, ease of automation, as well as high water application uniformity and water application efficiency. The current existing levels of automation in these mechanical systems have enabled them to be integrated with state-of-the-art technologies such as autonomous communication systems and algorithms for data processing from sensing equipment, to achieve high crop water productivity. The Scientific American Magazine (1976) endorsed these machines as the most significant mechanical innovation in agriculture since the replacement of draught horse power by the tractor.

This chapter provides an introduction to the subject of variable-rate irrigation (VRI) technology which is implemented using centre pivot and lateral move (CP&LM) irrigation machines. The discussion begins by highlighting the essential background information on the issues which prompted the advent of VRI. It continues to define and outline how this precision agriculture technology is implemented with CP&LMs to achieve site-specific crop water management while also highlighting the challenges encountered in the process. The discussion culminates to a summary of the research problem and then presents the main aim and objectives for the study. Also included is an outline of the overall structure of the thesis.

1.2 Background

Irrigation is the science and art of artificially applying water to the soil to enhance crop growth. It is practised predominantly in areas with insufficient rainfall to meet crop

water requirements. Irrigation is one of the major consumptive users of water resources globally. Out of the 3800 km^3 of water extracted from the environment annually at a global scale, irrigation consumes about 70 %, with industry and domestic uses accounting for 20 % and 10 % respectively (De Fraiture et al., 2010). More recently, other sectors such as recreation and tourism are beginning to claim substantial amounts of this precious resource. Climate variability and change is also exacerbating the situation by predisposing agricultural production, especially in arid and semi-arid regions, to be the most vulnerable to this phenomenon (Mkhwanazi, 2014, Darko et al., 2017). For instance, the area under irrigation decreased by approximately 537,000 ha between 2002 and 2010 in Australia, due to widespread drought, reduced water allocations, or agricultural establishments selling their water rights to reduce acreage or cease irrigation altogether (Koech, 2012). These challenges make agricultural water management critical, in not only applying water to maintain or improve crop yields, but in targeting applications according to the specific requirements of the soil-crop system.

CP&LM irrigation machines are well-known for their capabilities of uniformly applying controlled, frequent, light amounts of water and chemicals, enabling the efficient management of agricultural resources and therefore protection of the environment. This comes as a result of the design improvements made to these systems since the development of the first CP by Mr Frank Zybach in July 1949 (Luedtke, 2013), which makes them the system of choice for irrigation developments and any future land reclamation projects. They now irrigate about 81.7 % (14.1 million ha) of the total area under sprinkler irrigation in USA (USDA-NASS, 2013). Similar trends have also been observed in regions like Australia, New Zealand, Brazil, as well as in desert areas such as the Sahara and the Middle East. In the Australian cotton industry in particular, the rapid adoption of CP&LMs has been predicted to reach 30 % of total irrigation by 2020 (Raine and Foley, 2002), although they still account for about 15 % of total irrigation nationally (ABS, 2019) due to uncertainty in water regulation.

CP&LMs are self-propelled overhead sprinkler systems with lateral span pipes that are mounted on steel A-frames supported by two-wheeled carriages. The machines are

commonly driven by electric motors and/or oil hydraulic power systems. The major difference is in their operational mode. CPs rotate around a fixed pivot point at the centre of an irrigated field, while LMs travel in a continuous straight path across a rectangular field. This circular movement by CPs means incremental irrigated area increases radially which also increases the rate of water application while applying the same depth along the CP. LMs however apply relatively the same rate of water application over the entire length of the lateral because the area covered by each sprinkler head is the same throughout the irrigated field. Since water cannot be supplied at a fixed point for LMs, it is supplied either from a flexible hose or travelling pumping plant which draws water from a ditch along the side or centre of the field (Figure 1-1). The inability of CPs to economically irrigate rectangular fields, even when implemented with end-guns or an alternative irrigation system for the outfall areas, instigated activity in CP manufacturing to develop LM systems. Younus (2019) conducted extensive end-gun performance evaluations and developed algorithms to improve existing software (TravGUN) tools for simulating end-gun performance.

Figure 1-1: A diesel Gen-set LM irrigating a cotton field at Condamine Plains in southern Queensland, Australia

Apart from the gross alterations in the rigidity of the structure and movement mechanisms, the evolution of CP&LMs into modern systems was necessitated by the challenges and experiences growers had with these systems over the decades.

Increasing energy costs in the 1970's resulted in the development of low pressure sprinkler heads, and Low Energy Precision Application (LEPA) systems, which reduce energy consumption by operating at pressures as low as 41.6 kPa (6 psi). Most sprinklers now operate below 150 kPa (20 psi) and reduce wind drift and evaporation losses as they apply water near the crop canopy, or directly onto the soil surface to increase water application efficiency (Foley, 2008). This low pressure sprinkler technology also enabled these machines to be used for the application of chemicals (chemigation) and fertilisers (fertigation). The downside of LEPA systems is increased surface runoff due to high average application rates (Fraisse, 1994). Mitigation strategies that are implemented include lowering system capacity, adjusting the application patterns using LEPA socks, and cultural practices such as furrow dyking.

The adaptability of CP&LMs to irrigate marginal lands which are otherwise considered not suitable for traditional surface irrigation methods such as sandy soils, heavy clays, and more especially areas with large variations in topography, introduced the need for pressure regulation. Invented in the late 1980s, pressure regulators are used control the performance of CP&LMs sprinkler heads to improve the uniformity and efficiency of water application. It is now a common practice for CP&LM installations to be commissioned with pressure regulators, and existing machines are being modified to include the devices to improve the uniformity and efficiency of water application. Foley and Raine (2001) reported that about 58 % of growers using CP&LMs in the Australian Cotton industry were using pressure regulators in their sprinkler application packages. Mohr (2011) estimated about 90 % of all CP&LMs commissioned in the Australian industry were equipped with pressure regulators, with about 80 % of the machines in Kansas State reported to be pressure regulated (Rogers, 2010).

On CP&LMs, pressure regulators are installed on the sprinkler drop hoses immediately upstream of the nozzle, or on the top of the span pipe, so that every sprinkler head is dedicated to a pressure regulating device. Figure 1-2 illustrates the typical installation of pressure regulators. Over the length of the machine, this equates to a considerable number of devices, and amounts to a significant cost. The objective of this

configuration is to ensure that the regulator output pressure is transferred to the nozzle for optimum sprinkler performance. von Bernuth and Baird (1990) observed that the uniformity of the pressure received by sprinklers depends on the performance characteristics of the regulator, and the hydraulic system design. However, information on the performance characteristics of regulating devices is scarce, with limited studies completed to develop such useful information due to a lack of a suitable testing algorithm. Technologies such as flow control nozzles which uses a flexible orifice to adjust nozzle diameter and roughly maintain constant discharge as pressure fluctuates, have also been developed. Although these special type of nozzles do not require any minimum design pressure, their extensive use in industry was limited (Kranz et al., 1997) by problems of droplet size and distribution patterns when large pressure fluctuations occur.

Figure 1-2: Pressure regulators installed on the upstream of sprinkler heads on a CP&LM

More recently, precision agriculture (PA) or prescription farming as this new trend in managing agricultural inputs is called, requires the ability to apply water and chemicals taking into account the inherent differences in soil productive potential. Research (Zhang et al., 2002, Grisso et al., 2011, Foley et al., 2012, Doerge, 1999, Fraisse et al., 2001, Li et al., 2008) has shown how plant available water capacity, infiltration rates, and hence irrigation requirements can vary due to diverse sources of field variability and how their magnitudes vary in time and space. It is argued however that this

variability can be managed and the economic benefit from inputs maximised by meeting the specific needs of individual plants (Eberhard et al., 2013, Smith et al., 2009). This provides some justification to manage water applications and nutrients based on a predetermined management scheme (Lo et al., 2015).With their existing high levels of automation, CP&LMs have often been chosen as the system of choice for implementing site-specific irrigation using variable-rate irrigation (VRI) technology. Current VRI systems retrofit onto these machines, either new or existing, and enable them to spatially vary irrigation depths by pulsing the flow delivered to sprinkler heads using electrically actuated solenoid valves (Figure 1-3) to meet specific irrigation water requirements of crops in discrete management zones.

Figure 1-3: Configuration of VRI sprinkler solenoid valves in the lateral of CP&LMs (Foley, 2015)

Precision Mobile Drip Irrigation (PMDI) is another recent technique of precision irrigation where drip lines are adapted on CP&LMs to combine the efficiency of drip irrigation with the advantages of these irrigation machines to improve water use efficiency (Figure 1-4). Trials of the systems are reported by Olson (2006), Kisekka et al. (2017), and O'Shaughnessy and Colaizzi (2017).

Figure 1-4: Precision Mobile Drip Irrigation (PMDI) technology with CP&LMs

1.3 Variable-Rate Irrigation

Variable-rate irrigation (VRI) is defined as the practice to spatially vary water application depths across a field to address specific soil, crop, and/or some other requirements. The technology is implemented using CP&LM irrigation machines as introduced previously in Section 1.2 above. It is perceived to have many potential uses that might enhance farm profitability, irrigation water productivity (i.e. yield produced per unit of irrigation water applied), water quality, run-off reduction and reduced pumping for irrigation, resulting in energy savings and reduced deep percolation of water below the root zone (Lo et al., 2015, Lo et al., 2016). However, recent studies targeted at validating and demonstrating the potential benefits of VRI have shown that it is unlikely to realise some of the proposed economic benefits including the reduced consumptive use of water such as evapotranspiration (Lowenberg-DeBoer, 2018).

VRI technology enables CP&LMs to withhold applications for different reasons such as infrastructure, management, soils and topographic variations, for instance avoiding applications in non-cropped areas like roads, rocky outcrops, drainage ditches, and waterways. It is included in the spectrum of precision agriculture (PA) technologies

because advanced site-specific VRI methods can potentially impose treatments in ways that optimise crop response for each unit of water depth applied across different areas of the same field (Evans et al., 2013). Nevertheless, PA uses terminologies such as variable-rate, prescription, site-specific, and spatially variable to connote variable application of seeds, fertilisers, and chemicals. Consequently, Smith and Baillie (2009) defined VRI as prescription irrigation or accurate, precise and possible spatially variable application of water to meet specific requirements of individual plants, following four sequential steps: data acquisition, interpretation, control, and evaluation, as illustrated in Figure 1-5 below.

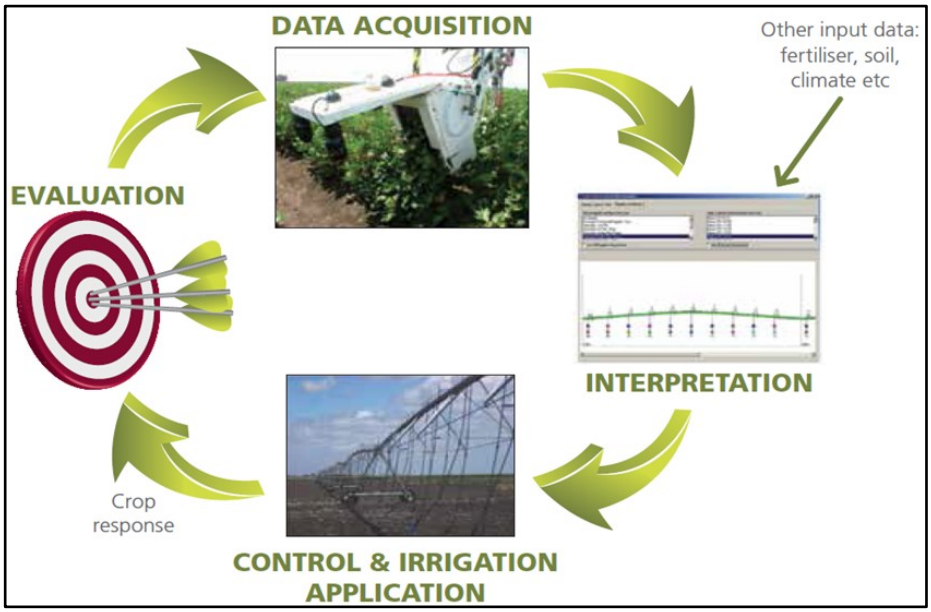

Figure 1-5: Essential elements of a VRI system (Eberhard et al., 2013, Smith and Baillie, 2009)

The development and testing of VRI began shortly after the first patents were filed by the University of Idaho, USA in 1991. However, the VRI system was only commercialised in 2001 following competition for patent rights and other liability issues (McCarthy, 2010), although practical systems became available from 2010 (Evans et al., 2013). Numerous studies have been conducted to demonstrate VRI, in both cold and temperate environments (Figure 1-6), with contemporary research evaluating the potential economic benefits to aid adoption (Lambert et al., 2013, Sui et al., 2015, Zhao et al., 2015). Water savings of up to 27 %, and a 15 % energy saving have been reported for specific crops in some regions. However, these studies have concluded that the savings are too low compared to the capital cost of investing in

VRI. Consequently, growers are consistently losing interest in using this technology, as discussed in Section 1.3.4.

(a) Vertical mounting - no freeze prevention (b) Horizontal mounting – freeze prevention

Figure 1-6: VRI valve configurations for CP&LMs in cold and warm temperatures

1.3.1 *Configuration of VRI Systems*

VRI systems easily retrofit onto existing CP&LMs due to the current existing level of automation in these mechanized self-propelled sprinkler systems. VRI packages are also available for new CP&LM installations. There are four types of VRI systems that have been developed in industry to date, and their configurations vary. *Speed* controlled VRI systems require no additional hardware components because all pivots have an angle encoder at the very top of the CP point that can measure the angle of the pivot arm to a pre-set radial position and a control panel capable of configuring variable speeds as the machine traverses the field. This type of VRI is considered to be an attractive low cost entry into precision irrigation. *Zone* controlled VRI systems comprise a CP&LM harnessed with an array of VRI sprinkler solenoid valves and control boxes for information relay from a VRI control panel, software for decision support to generate prescriptions, and a method for position determination (GPS) to understand sprinkler heads based on field location (Figure 1-7).

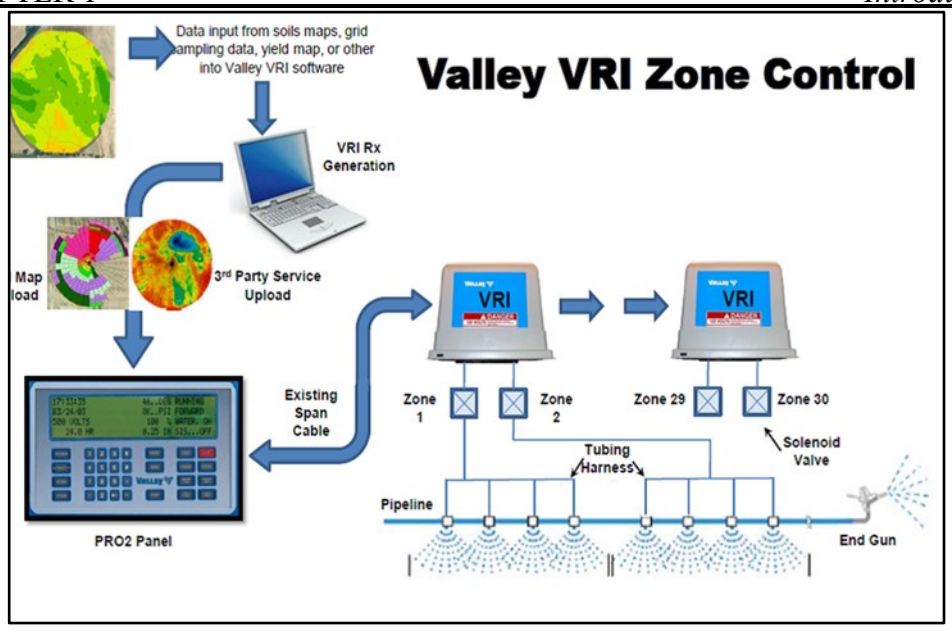

Figure 1-7 : Features of a zone-controlled VRI system from Valley Irrigation (LaRue, 2011)

Advanced zone controlled VRI uses state of the art sensing systems (crop water stress) for real-time adaptive irrigation control with the rest of the components identical to *zone* control systems (Evans et al., 2013). The on-and-off pulsing of sprinkler banks for *zone* controlled and *advanced zone* controlled VRI is controlled by one solenoid valve located in the VRI tower box, with the rest of array of valves controlled hydraulically through a plastic tube connected to the solenoid valve. VRI *individual sprinkler* (VRI-iS) controlled systems are also identical to *zone* and *advanced zone* controlled systems except that they offer capabilities to control individual sprinklers for improved management.

1.3.2 *Methods of Delivering Variable Water Applications*

Several techniques have been implemented with CP&LMs to achieve spatially varied irrigation. The early versions of VRI were predominantly *speed* controlled systems which varied the applied water depths sector-wise by independently varying the speed of the master drive tower in CPs. This technology is also applicable for LMs in their continuous straight movement across the field. *Zone* controlled systems however, introduced new methods of ensuring the target water depths are delivered to each irrigation management zone to improve water use efficiency. This approach requires

some specialised level of control to the depth of water applied by each sprinkler head, thus leading to the development of the following application techniques.

1.3.2.1 Manifold sprinklers

A combination of individual sprinkler heads at a single location or a manifold combination of different sized sprinkler nozzles are used to create a stepwise range of application rates. This approach has been used by the University of Idaho (McCann and Stark, 1993, McCann et al., 1997, King and Wall, 1998) and the USDA-ARS group in Florence, South Carolina (Camp and Sadler, 1994, Camp et al., 1998, Wall et al., 1996, Omary et al., 1997, Sadler et al., 2000, Sadler et al., 2002). Duke et al. (1997) and White (2007) also modified a LM to provide variable water and nutrient application using discrete sprinkler nozzles mounted on manifold pipes.

1.3.2.2 Variable flow rate sprinklers

In another way to vary sprinkler discharge, a retractable concentric pin is used to vary the flow of a sprinkler by varying the open nozzle cross-sectional area with a linear actuator that can insert and remove the pin inside the nozzle bore (King and Kincaid, 1996, King et al., 1997, King et al., 1998, King and Kincaid, 2004, King et al., 2005, Armindo et al., 2011, Armindo and Botrel, 2012). Nonetheless, despite the efforts toward the development of this type of variable flow sprinkler head for site-specific irrigation, they have received very limited adoption in industry as they are not commercially manufactured (Evans et al., 2013).

1.3.2.3 Pulsing solenoid valves

The most common method to generate variable sprinkler discharges for VRI on CP&LMs is where individual, or groups of sprinkler heads, are pulsed on-an-off by energising solenoid valves to create time-proportional flow control. This pulsing technique is now a standard method for commercial VRI systems, and has been implemented widely after research activity, e.g. the collaboration between Farmscan Ag and the University of Georgia (Perry et al., 2002, Perry and Pocknee, 2003), the United States Department of Agriculture and Agricultural Research Service (USDA-

ARS) in Fort Collins, Colorado (Fraisse et al., 1995), Clemson University (Han et al., 2009), and WMC Technology Limited in New Zealand (Bradbury and Ricketts, 2014).

A range of commonly used solenoid actuated VRI valves are available in different materials, i.e. brass, cast iron, and engineering grade reinforced polymers. These generally have a globe or Saunders-type of body design as shown in Figure 1-8.

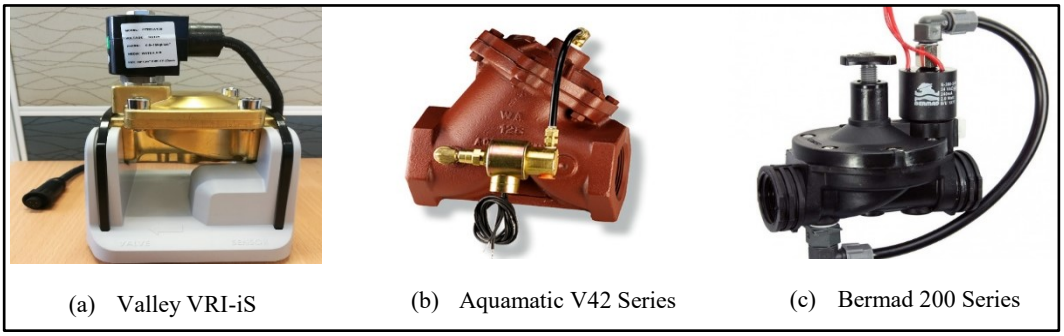

(a) Valley VRI-iS (b) Aquamatic V42 Series (c) Bermad 200 Series

Figure 1-8: Some of the most common electric solenoid actuated valves used in industry for VRI on CP&LMs

1.3.3 *Implementation of VRI Strategies*

Knowledge of information about crop stress is important for optimal irrigation management. The types of crop stress can be classified as abiotic, which may include differences in soil, slope, rock outcrop, drainage ditches, and waterways, and biotic which includes insect pressure, or plant diseases (Casanova et al., 2014). VRI utilises data from these factors to develop algorithms that can generate controlled irrigation applications via prescription maps. A prescription map is an electronic data file that is loaded on the VRI control panel of CP&LMs, and contains a set of instructions composed of specific input rates of irrigation depths to be applied in discrete management zones. This special map is considered to be the heart of VRI because it controls the operation of VRI CP&LMs. The VRI control strategies that are implemented in industry are:

1.3.3.1 Historical Bases for VRI Map Generation

Historical map-based VRI control strategies may use remote sensing, yield monitoring, and manually collected soil mapping or Electromagnetic Induction (EMI)

techniques to collect variability data for irrigation adjustments. This information is processed and prescription maps created and loaded on CP&LM to control the depths applied by individual sprinklers, utilising GPS guidance to locate different water management zones. This technique has been implemented by Grisso et al. (2009), Grisso et al. (2011), Foley et al. (2012), and O'Shaughnessy et al. (2015). The downside of historical map-based strategies is the ignorance of intra-seasonal and inter-seasonal variability, since prescription maps are not usually changed between, and through consecutive growing seasons

1.3.3.2 Sensor-Based VRI Strategies

Sensor-based VRI control strategies achieve adaptive control of site-specific irrigation through input from sensors to control variable water applications. The sensors can directly or indirectly measure soil moisture deficit, plant stress, or other parameters that can be used to determine crop water requirements. These strategies are capable of continuously measuring crop water stress to generate dynamic prescription maps for adaptive irrigation scheduling. For instance, Casanova et al. (2014) developed a wireless computer vision system to detect crop biotic stress, while infrared thermometry (O'Shaughnessy et al., 2011) and canopy reflectance (Stone et al., 2016) sensors were used to determine crop water requirements in real-time in CPs irrigated crops. Capital costs were a major challenge, and now these sensors are being miniaturized and made commercially available at relatively low costs (O'Shaughnessy et al., 2015).

1.3.3.3 Model-Predictive Control Strategies

Model Predictive Control (MPC) VRI strategies are advanced process control strategies that use crop production models to aid the irrigation decision making process. Some use the available weather-soil-and-plant information to calibrate bio-physical crop models (McCarthy et al., 2014) in order to determine the optimal irrigation depth and timing that will achieve the desired performance objective. Barker et al. (2019) implemented a remote sensing-based evapotranspiration (ET) model with Landsat imagery to calibrate VRI equipped CP for full irrigation (VRI-Full and Uniform-Full irrigation), and deficit irrigation (VRI-Deficit and Uniform-Deficit

irrigation) for maize and soybean. McCarthy et al. (2014) reported the superiority of MPC (higher yields and water use efficiency) over sensor-based strategies, but highlighted the necessity for more accurate field measurements to accurately calibrate the crop models.

1.3.4 *Adoption of VRI Technology*

An international review of VRI utilisation and its global footprint indicates that adoption has been very poor despite its cited potential to impact crop productivity, water use, energy efficiency, and environmental conservation. The advantages and disadvantages of VRI are summarised in O'Shaughnessy et al. (2019). Evans et al. (2013) estimated about 95% of all VRI systems in the world to be in the USA with Australia, New Zealand, and South Africa accounting for most of the remaining installations. However, these statistics only account for less than about 200 machines, as Evans et al. (2013) estimates only 25% of these to be currently using the technology for improved crop water management. Evans et al. (2013) also estimated that there were less than 500 *speed* controlled VRI systems currently in fields around the world, but it is not known how many are being used by growers for site-specific irrigation management. A manufacturer's representative also acknowledged the under-utilisation, where growers with the systems are no longer continuing to use them, e.g. only four out of 100 who purchased Farmscan VRI systems in Georgia are still using the technology (McCarthy et al., 2011). However, the number of *speed* controlled VRI systems installed today is large because of that capability that comes built in to modern CPs (Section 1.3.1).

The limited uptake of VRI generally is attributed to significant additional capital cost, uncertainty of economic returns and subsequent profit, and high levels of technical sophistication to use, amongst other factors. In an extensive analysis of VRI applications for potato production in Alberta Canada, Pieterse (2014) emphasised the need for more research to establish site-specific or local economics of the potential benefits, since farmers were already frustrated with VRI technology. Incentives and legislation are now being used as adoption drivers in countries like New Zealand based

on requirements to limit animal waste effluents to waterways and animal watering points.

1.3.5 *Water Application Uniformity of VRI CP&LM Machines*

ANSI/ASAE S436.1 and ISO 11545:2009 describe the standard procedures for evaluating the uniformity of water application for CP&LMs. These methods are applicable for conventional machines that are intended to apply uniform depths along their entire radius. In VRI-based machines, water depths are applied variably across the field to match specific irrigation requirements in different zones. Generally, the number of these zones depend on the extent of variability in the irrigated field. The lack of a suitable algorithm for assessing the uniformity of machines operating with VRI enables researchers (Chavez et al., 2010, Hezarjaribi and SourellL, 2008, Yari et al., 2017) to apply ANSI/ASAE S436.1 and ISO 11545:2009 on groups of nozzles pulsing at constant rates. Consequently, experiments were characterised by a combination of time consuming and resource intensive catch can tests arranged in transects, arc-wise, and in grid patterns (Figure 1-9), a phenomenon called zone uniformity where poor uniformities (CU) greater than 80 % and less than 90 % were reported.

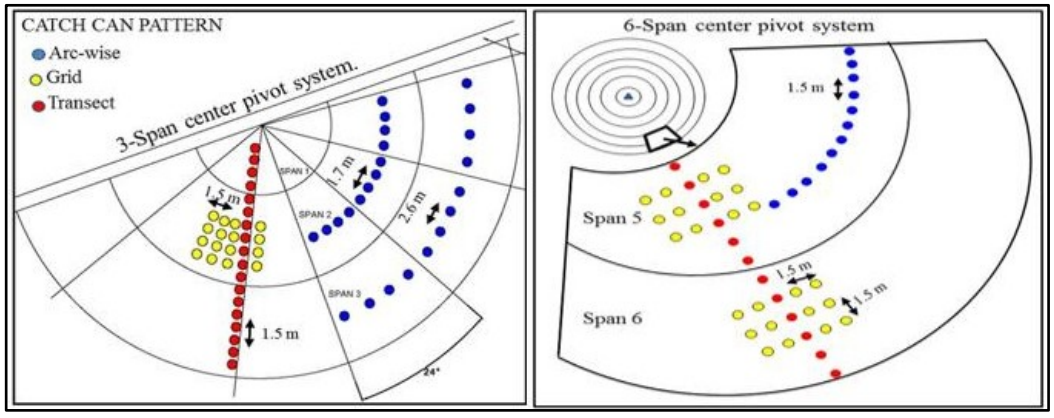

Figure 1-9: Catch can layout during a VRI CP evaluation (O'Shaughnessy et al., 2013)

Problems associated with the performance evaluation of VRI machines are related to overlapping sprinkler patterns between adjacent sprinkler controlled management zones. Sui and Fisher (2015) observed that the overlap is usually aggravated with larger numbers of management zones. Overlaps of up to 6 m on either sides of

management zones have been reported (O'Shaughnessy and Evett, 2015). However, the long term effect of this non-uniformity on crop performance has not been studied. Sensitivity analyses demonstrate that CU values for VRI machines are relatively similar to those of conventional machines when overlap measurements are excluded from the analysis. However, the practice of data exclusion is only limited to a maximum 3% of total catchments, as provided for in the ASAE/ANSI Standard 436.1. Other methods such as yield comparisons between VRI and non-VRI CP&LMs are being used to assess the performance of VRI (King et al., 2006, Hedley et al., 2011).

1.4 Summary and Research Gap

While there has been tremendous impetus to retrofit and calibrate pressure regulated CP&LMs for site-specific irrigation using VRI technology, the interactions between the hydraulic performance characteristics of VRI equipment and the hydraulic system of these machines has been ignored. The design of VRI CP&LMs is principally governed by field variability assessments of soil, topographic, and crop characteristics, with no attempts made to integrate the hydraulics of the technology. This becomes critical when considering the unsteady conditions introduced by on-and-off pulsing of solenoid valves, the additional head loss from the array of valves, as well as variable system pressure during VRI operation in different management units, which are all too often compounded by the precursory lack of ideal comprehension of pressure regulator performance. Foley and Smith (2011) also reported that most irrigation related problems are attributed to a lack of understanding of hydraulics and poor system design. If such technical information is established and the necessary remedies are well integrated, the performance and uptake of VRI systems can improve significantly. Despite the fact that these technical remedies will not address the capital costs of VRI and the complexity of generating irrigation prescriptions, the following main research questions need to be addressed for the successful implementation of VRI technology in industry to improve irrigation performance and water use efficiency:

(a) What is the impact of retrofitting VRI valves on the total pressure head of CP&LM irrigation machines?

(b) Does pulsing and cycling of VRI valves to control sprinkler discharge generate pressure wave transients in CP&LM irrigation machines?

(c) What are the actual performance characteristics of pressure regulating valves used in CP&LM irrigation machines?

(d) What is the impact of VRI transients on the pressure regulation of CP&LM irrigation machines?

1.5 Research Aim and Hypothesis

The broad aim of this research is to develop advanced automatic hydraulic measurement techniques and utilise these to characterise and model the effects of retrofitting pulsing solenoid VRI valves on the hydraulic performance of CP&LM irrigation machines.

The general overarching hypothesis is that the on-and-off pulsing of VRI valves generates unsteady conditions and pressure wave transients which impact on the hydraulic performance of CP&LM irrigation machines, more especially pressure regulation of sprinkler heads.

This research makes proposition and will provide evidence to the following hypotheses:

(i) *The hydraulic characterisation of variable-rate irrigation components can be accurately measured for steady and unsteady hydraulic conditions.*

(ii) *Characterising the varied performance of VRI components provides the ability to more accurately design hydraulics of CP&LM systems for improved irrigation performance and greater industry uptake of VRI.*

1.6 Objectives of the Study

The main objectives of this research work were to:

1. Design and construct an automated experimental measurement apparatus for characterising the hydraulic performance of VRI valves and CP&LM pressure regulators,
2. Develop an appropriate testing methodology for (1) to characterise the hydraulic performance of VRI valves and CP&LM pressure regulators,
3. Evaluate the minor head loss of solenoid actuated VRI valves, and develop empirical techniques for modelling their impacts on the hydraulics of CP&LM irrigation machines retrofitted with VRI,
4. Investigate the nature and relative magnitudes of hydraulic transients generated by VRI pulsing, and the significance on machine hydraulics and ultimate irrigation performance.
5. Evaluate the hydraulic performance characteristics of CP&LM pressure regulators,
6. Evaluate the impacts of VRI transients on the hydraulic performance of CP&LM pressure regulators, and
7. Develop a new mathematical model for predicting the hydraulic performance of pressure regulators in unsteady conditions experienced by modern CP&LMs.

1.7 Structure of the Thesis

This chapter (**Chapter 1**) has provided a brief background to the subject area of VRI CP&LM irrigation and has introduced the main objectives for the remaining eight chapters of this thesis. The relationship between chapters is shown in Figure 1-10.

Chapter 2 serves as a comprehensive review of the theory of hydraulics of VRI machines. In doing so, the review attempts to integrate the theory of hydraulic transients with the fundamental hydraulic principles of CP&LMs to develop a

theoretical understanding of the hydraulic performance characteristics of VRI CP&LMs since such technical information is non-existent. The idea is to highlight the potential issues that may be introduced by retrofitting and pulsing VRI on these irrigation machines. Chapter 2 also reviews the performance characterisation of CP&LM pressure regulators to highlight the limitations of measurement criteria, which often lead to poor comprehension of pressure regulator performance and subsequently incorrect application. The mathematical models used to describe pressure regulator performance, as well as their limitations are also reviewed. Lastly, the theoretical impacts of VRI pulsing on pressure regulator performance are developed to aid the development of a suitable test procedure.

Chapter 3 discusses the development of a novel automatic multi-function measurement system for use in Z113 Hydraulics Laboratory to develop the required technical information about solenoid VRI valves and CP&LM pressure regulators. The chapter discusses the special equipment selection and their respective specifications, as well as how these critical components are assembled into a testing kit. It also includes the development of multiple algorithms for implementing the test-apparatus to establish the hydraulic measurements sought in this research. The coding of the algorithms using LabVIEW software graphical programming language into an automatic data acquisition (DAQ) software interface, and its integration with sensing gear to control the test apparatus are discussed. In addition to the layout of the test-apparatus, the resulting testing phases and their measurement capabilities are outlined.

Chapter 4 is a discussion of the development of a novel testing methodology that is employed with the novel automatic multi-function hydraulic test-apparatus to develop the experimental data needed to interpret VRI and its implications in CP&LM irrigation. Chapter 4 also covers a discussion on the extensive calibrations undertaken on the test-apparatus before implementing the new test methodology. The statistical measures employed to solicit the appropriate sample sizes, numbers of tests, and test repetitions are also presented in this chapter, as well as the analytical techniques employed to interpret the measured datasets.

Chapter 5 presents the results and analysis of the numerous hydraulic experiments that were conducted in the Hydraulics Laboratory to achieve the objectives of the research. They include minor head losses and minor loss coefficients for the tested VRI valves, peak hydraulic heads from VRI pulsing and hydraulic transient analysis. The chapter also presents a series of results and analysis on the hydraulic performance parameters of CP&LM pressure regulators.

Chapter 6 is a critical review, analysis, and evaluation of common existing pressure regulator mathematical models that are used to predict pressure regulator performance. This process attempts to identify the strengths and limitations of these pressure regulator models in order to justify the need of, and proposition an improved model for use in pressure regulation modelling, especially within the practical and operating conditions of CP&LM irrigation machines retrofitted with VRI.

Chapter 7 describes the development of the new pressure regulator mathematical model for use with CP&LM irrigation machines equipped with pressure regulators. The processes conducted in deriving the mathematical concepts and sub-models that can implemented in hydraulic model to correctly predict pressure regulator outlet pressures are discussed. The chapter also demonstrates the model utilisation in predict the regulator outlet pressures, as well the non-statistical validation process using measured data.

Chapter 8 presents a succinct discussion of the implications of all the results of the hydraulic measurements conducted on pulsing solenoid VRI valves and CP&LM pressure regulators. It discusses the impacts of VRI technology on the hydraulic performance of CP&LM irrigation machines including pressure regulation of CP&LMs. The importance of the new mathematical model with respect to precise modelling of regulator outlet pressures and how this improves the hydraulic design of pressure regulated CP&LMs is also covered.

Chapter 9 presents the conclusions drawn from the extensive work conducted in this research and suggests recommendations for future study.

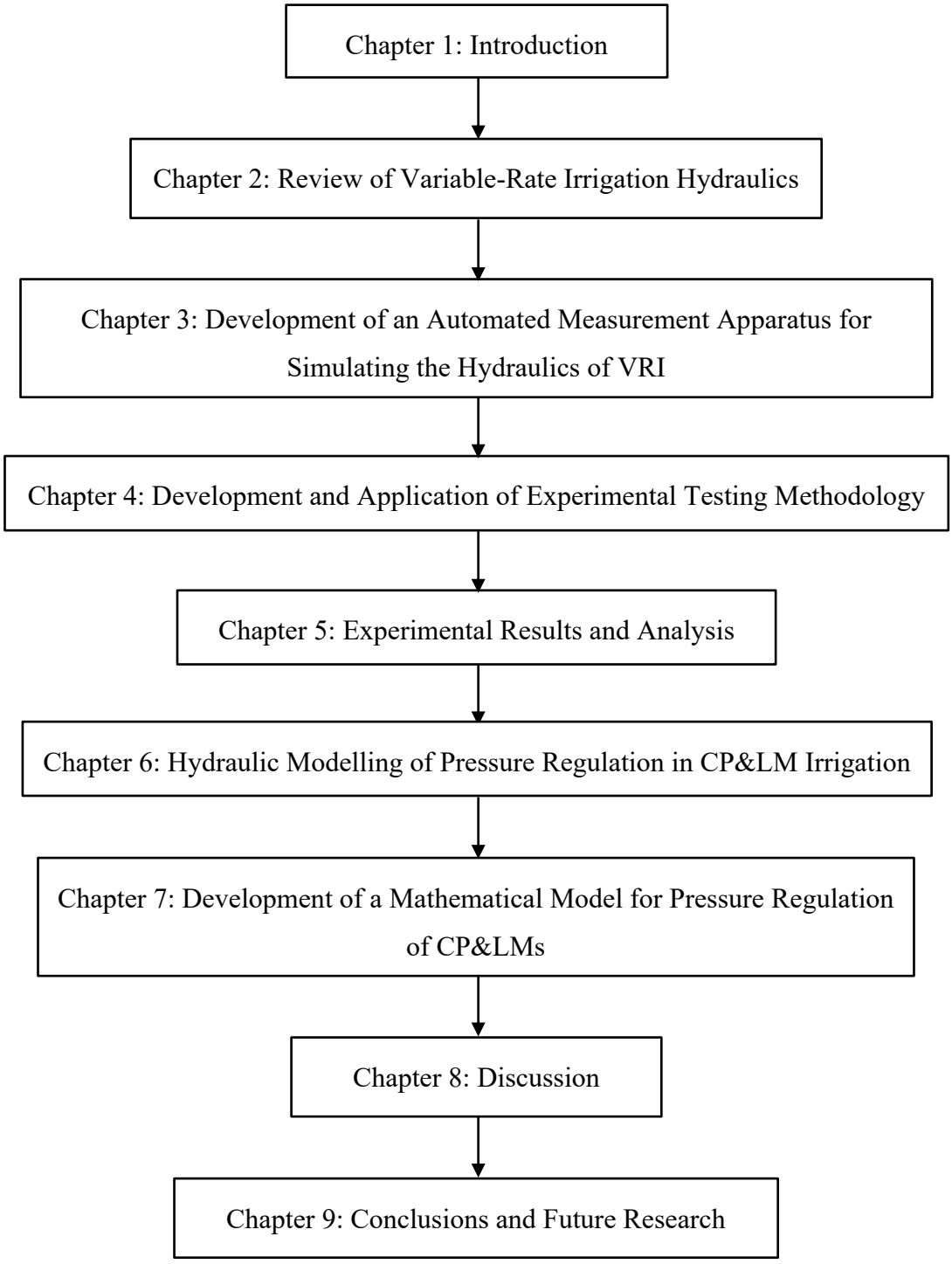

Figure 1.10 : Structure of the Thesis

2. REVIEW OF VARIABLE-RATE IRRIGATION HYDRAULICS

2.1 Introduction

Before proceeding with any characterisation and modelling, it would be customary to recognise the body of research on the theory and field behaviour of the hydraulics VRI technology. However, due to a lack of technical information in this subject, this chapter uses the physical structure and operational mode (pulsing sequencing) of VRI equipment (Section 1.3.1 and Section 1.3.2.3) in conjunction with the theory of hydraulic transients and unsteady flow, to infer these to the fundamental hydraulic principles of CP&LMs. The idea is to provide a basic theoretical perspective on the interactions and potential impacts of retrofitting VRI on these machines, to justify the types of hydraulic experiments and testing needed to develop a robust hydraulic theory and modelling techniques that will enable the interpretation of VRI impacts on CP&LM hydraulics. To provide a full comprehension of transients and unsteady flow, it is necessary to first review the basic principles of fluid motion especially pressure and discharge.

2.2 Fundamentals of Fluid Dynamics

Any attempt to move fluids such as water requires energy per unit weight to increase the velocity, lift it to higher elevations, and to overcome friction resistance and minor losses in hydraulic systems. The energy required to overcome these forces can be supplied from different sources, with the most common being centrifugal pumps in pressurised irrigation applications. The branch of engineering which deals with this type of fluids is called *hydraulics* and is the focus of this dissertation.

2.2.1 *Pressure*

Pressure is defined as a continuous force applied perpendicular to a surface area over which that force is distributed. In fluids, this results from the motion and the transfer of momentum from molecules to the object from which pressure is said to act. This amount of pressure is mathematically expressed by Equation 2.1, with the SI units Pascal, as:

$$P = \frac{F}{A} \tag{2.1}$$

where: P = pressure (Pa), F = magnitude of the normal force (N), and A = area of the contact surface (m^2).

Pressure is commonly interpreted as gauge pressure and absolute pressure. Gauge pressure is an arbitrary pressure measurement relative to local atmospheric pressure. Gauge pressure may be positive or negative (Hamill, 2011). Pressure can be represented in two ways; (1) as a force per unit area (Pa), (2) as an equivalent height (head) of a column of fluid (metres head). Pressure is not constant everywhere in a body of water, but it varies with elevation or depth of water (Equation 2.2). Head is mathematically defined as energy per unit weight of the liquid being pumped (Equation 2.3) and has units of metres head.

$$P = \rho g h \tag{2.2}$$

$$h = \frac{P}{\rho g} \tag{2.3}$$

where: g = gravitational acceleration (m/s^2), h = fluid column height or metres head of liquid which is water in this case (m H_2O), and ρ = density of the liquid in kilograms per cubic metre (kg/m^3).

The head components of interest in hydraulics are elevation head, pressure head, and kinetic or velocity head, and when summed mathematically, can be expressed by the Bernoulli equation (Chadwick and Morfett, 2002):

$$\frac{p_1}{\rho g} + \frac{V^2}{2g} + z_1 \qquad 2.4$$

where: p = water pressure head (m), ρ = fluid density (kg/m^3), g = gravitational acceleration (m/s^2), V = section mean velocity (m/s), Z = elevation or head per unit weight of water (m head H_2O).

These three separate components are vital in the design of irrigation systems because they determine the magnitude of the total head required to operate the system. In lower pressure systems like modern CP&LMs, only the energy gradient correctly accounts for all components, including the velocity head, when determining the total head required in the system (Foley, 2019). The principles of conservation of energy states that energy is always conserved; it can change from one form to another, but it cannot be destroyed. In pressurized irrigation systems, if the sum of the elevation head, pressure head, and velocity head are not constant between any two points as the water flows between them, then there must be head that is either being added by a pump or consumed by friction or some other minor losses, as shown in Equation 2.5 (Waller and Yitayew, 2015).

$$\frac{p_1}{\rho g} + \frac{V_1^2}{2g} + z_1 + h_p = \frac{p_2}{\rho g} + \frac{V_2^2}{2g} + z_2 + h_f + h_m \qquad 2.5$$

where: h_p = supply or pumping head (m head), h_f= friction head loss (m head), and. h_m = minor head loss (m head).

2.2.2 *Discharge*

The amount of fluid passing through a section of pipe per unit time is referred to as discharge or flow rate. The discharge can be calculated from the two components, the velocity of flow, and the cross-sectional area of the flowing fluid. The continuity

equation (Equation 2.6 and 2.7), based on the conservation of mass, states that discharge into any hydraulic system should be equal to the discharge exiting the system.

$$Q = AV \tag{2.6}$$

$$A_1V_1 = A_2V_2 \tag{2.7}$$

where: Q = flow rate (m^3/s), A = cross sectional area of flow pipe (m^2), and V = flow velocity (m/s).

This equation can be used with the Bernoulli equation (Equation 2.4) to calculate velocity. Flows measured at a specific section in a hydraulic system that are linked to a time scale are named as steady flows and unsteady flows, while the distance scale classifies flows into either uniform or non-uniform steady or unsteady flows. The flow classification that is linked to a time scale shall be the focus of this dissertation.

2.2.3 *Steady Flow and Unsteady Flow*

A steady flow is a flow condition that occurs when the discharge and velocity do not vary with time at a specific point of cross-section in a hydraulic system. However, perfectly steady flow conditions seldom occur due to oscillations from pumps and water supply systems. Hence the permissible variations for flow conditions to be considered steady are limited to below 1 or 2 % (Larock et al., 1999).

Unsteady flow conditions occur in a flow of constant cross-section when the discharge and velocity vary with time. The variations in flow in this case would normally exceed 1 or 2 % (Larock et al., 1999). The types of unsteady flow conditions that occur in CP&LMs have traditionally been a result of fluctuations in ground water tables, and/or changes in field elevation as the systems traverse irrigated fields. More recently, the on-and-off pulsing of VRI valves, which is the main subject of this dissertation, can

now also introduce unsteady conditions in these mechanized self-propelled sprinkler systems.

2.3 Hydraulic Transients

A hydraulic transient is a form of temporary pressure wave, surge or shock wave that occur as result of a disturbance in flow in a hydraulic system. The disturbance is usually caused by events such closure or opening of valves due to different discharge requirements, starting or stopping of pumps, or the presence of entrapped air (Tadić Ananić and Gjetvaj, 2017). These includes phenomena like water hammer, which causes abrupt changes in fluid velocity and generates unsteady conditions and the propagation of pressure wave transients in the system (Tullis, 1989, Covas et al., 2012). The transient pressure waves travel at the speed of sound through the system, and can occur in pipelines transporting water over considerable distances. Boulos et al. (2005) observed that the magnitude of the transients depend on the elasticity of the pumped fluid and the rigidity of the pipe material. At normal temperatures, water pipelines can be subjected to pressure waves traveling in excess of 1,200 m/s (Adamkowski and Lewandowski, 2012) because of the slightly compressible nature of water.

The effects of the water hammer events can be effectively multiplied many times by the geometry of a piping system if the pressure wave is allowed to reflect, or bounce back and forth within the hydraulic system, as shown in Figure 2-1 below.

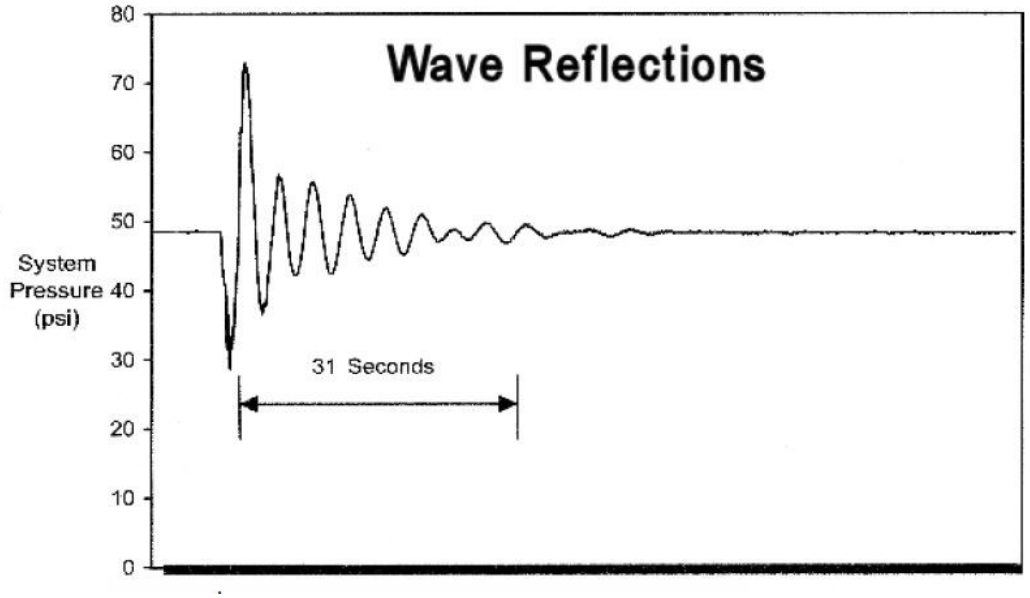

Figure 2-1: Water hammer profile from a single valve closure in a hydraulic system (Workman, 2011)

Entrapped air can also cause problems of water hammer in pressurized systems (Chaudhry, 1979). Since air, is highly compressible, its compression and propagation along the pipeline may cause changes in flow velocity which ultimately result in considerable pressure variations in the system. Covas et al. (2012) reported that a small amount of air as 0.01% in volume can justify differences in wave speeds.

Pressure transients are known to have undesirable effects such as pipe integrity fatigue, and on occasion catastrophic effects such as the subsequent rupture when no transient control mechanisms are in place. This occurs because they are capable of generating pressure head waves that can exceed the design limitations and maximum pressure ratings of the pipe and system equipment. This follows from Newton's Second Law of Motion that the resultant force generated by a moving object when it suddenly stops is equal to the rate of change of momentum (Tullis, 1989). In other occasions, the transients can result in sub-atmospheric pressures, which can lead to the occurrence of cavitation. Hence, hydraulic calculations of unsteady flow have to be made in the scope of design work to determine potential extremes of pressure head in the system, so as to provide adequate control of hydraulic transients.

Industry standards for pressure ratings of pipes are based on static pressure, without regard for surge conditions which often take place. ASAE S376.1 also recommends a valve filling velocity of not more than 0.1 m/s to prevent the catastrophic effects of pressure surge. The US Natural Resources Conservation Service, Conservation Practice Standard 430recommends working pressure not exceeding a maximum of 72 % of the pipe pressure rating. The standard also recommends that pipeline flow velocities be limited to 1.5 m/s. The effects of an abrupt change in velocity on the pressure head is determined by the Joukowsky equation:

$$\Delta H = \frac{c}{g}\Delta V \qquad 2.8$$

where: ΔH = pressure rise in the fluid (m head), c = wave celerity or speed at which the pressure wave travels throughout the pipe (m/s), g = gravitational acceleration (m/s^2), and ΔV = change in fluid velocity (m/s).

The pressure wave speed or wave celerity for different pipe materials can be determined by:

$$c = \sqrt{\frac{1}{\rho\left[\frac{1}{K} + \frac{D}{Ee}\right]}} \qquad 2.9$$

where: ρ = fluid density (kg/m^3), D = pipe diameter (m), K = bulk modulus of elasticity of the fluid (10^6 N/m^2), E = Young's modulus of elasticity of the pipe material (10^6 N/m^2), and e = wall thickness of the pipe (m).

While the subject of hydraulic transients is well developed, with complex classical transient solvers and modelling tools now available, Workman (2011) argues that the profile of a pressure wave form is the least investigated and understood variable in cyclic behaviour of piped systems. The shape of the wave form describes how rapidly the pressure rises and falls, and how long it stays at peak and lower levels. Figure 2-2 illustrate some common pressure wave form characteristics that occur in transients. However, the most commonly used type of wave form in hydraulic transient research is the sine wave, which describes continuous smooth periodic oscillations.

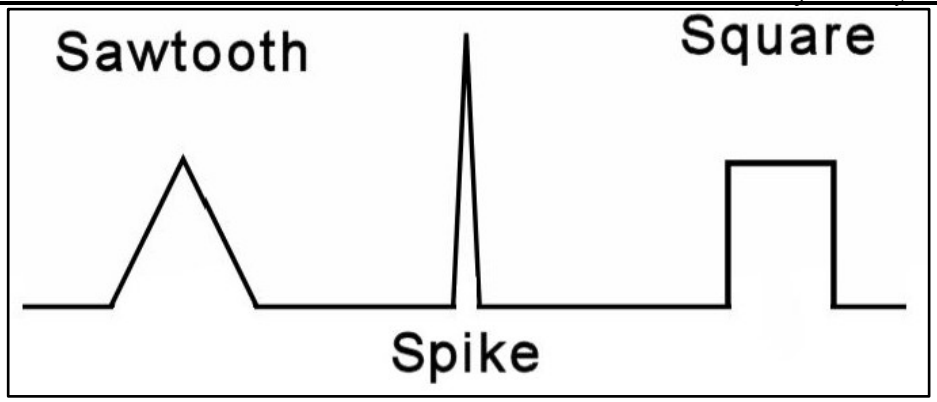

Figure 2-2: Types of pressure wave forms or surge profiles generated from hydraulic transients

Within the scope of the present study, VRI systems pulse solenoid actuated valves on-and-off to create time-proportional flow control through sprinkler heads on CP&LMs. While information regarding this operational mode for VRI machines is lacking, research has shown that electric control valves are a good cause of water hammer because of the combination of high flow velocities and the instantaneous on-and-off action of the valves. Workman (2011) reported that 85 % of the flow rate will be controlled in the last 15 % of the closure duration in most valves, with the majority of the flow change expected in the early portion of the opening duration. When pulsing and cycling occurs over extended periods, the tolerance limit for pressure surges of a system decreases.

2.3.1 *Conclusion*

Pressure head is an important measure of the performance of hydraulic systems in pressurised CP&LM irrigation machines. However, common practices such as the on-and-off pulsing of control valves, as is the case for VRI introduce unsteady conditions which may affect the pressure state as well as the discharge of a system. Depending on the hydraulic conditions, this likely results in the propagation of pressure wave transients which can lead to undesirable and/or instabilities in system operation and performance such as water hammer, and catastrophes like pipeline failure.

2.4 Hydraulics of VRI CP&LM Machines

Studies (Fraisse et al., 1993, Fraisse, 1994, Camp and Sadler, 1994, Omary et al., 1997, Han et al., 2009, Rackers, 2011, McCarthy et al., 2015, McCarthy and Foley, 2017) have shown how VRI technology retrofits into CP&LMs and how this novel irrigation management practice is implemented to achieve site-specific crop water management. Contemporary research is focusing on validating and demonstrating the proposed benefits of using the technology (Yari et al., 2017, Lo, 2015, Lambert et al., 2013, Al-Kufaishi et al., 2006). Nonetheless, there has been no previous attempt to establish an understanding of the hydraulic characteristics of VRI and its interactions with the complete hydraulic system (Zhao et al., 2016). Evans et al. (2013) observed that VRI research and development has been concentrated on improving decision support systems to advance irrigation scheduling and prescription map development. Therefore, to develop a hydraulic understanding of the interactions between VRI equipment and CP&LMs, a review of the fundamental hydraulic principles of CP&LMs becomes paramount, especially when integrated with the VRI transient theory developed in the previous sections.

2.4.1 *Pipe Friction Losses*

Friction head losses are a result of shear between the fluid and pipe walls, and internal shear between fluid particles. These head losses are proportional to the length of pipe in which the water is flowing. The Darcy-Weisbach equation (Equation 2.10) is used to determine the friction head loss in pipelines, and is given as:

$$h_f = f\frac{L}{D}\frac{V^2}{2g} \qquad 2.10$$

where: h_f = friction head loss (m), f = Darcy-Weisbach friction coefficient, L= length of pipeline (m), D = internal pipe diameter (m), V = mean water velocity in the pipeline (m/s), and g = gravitational acceleration (m/s^2). The friction coefficient f is determined by the Colebrook-White equation for turbulent flows:

$$\frac{1}{\sqrt{f}} = 1.14 - 2\log\left(\frac{e}{D} + \frac{9.35}{R_e\sqrt{f}}\right) \qquad 2.11$$

where: e = roughness height of pipe (m), Re = Reynolds Number ($V\,D$ / μ), and μ = kinematic viscosity (m^2/s).

However, since the Colebrook-White equation is non-factorable in f, it is awkward to use, except for using its graphical representation in the Moody diagram. Hence, a simplified equation for use in regard to pipe friction is that developed by Hazen-Williams (Equation 2.12).

$$h_f = 1.212\text{x}10^{12} L \frac{\left(\frac{Q}{C}\right)^{1.852}}{d^{4.871}} \qquad 2.12$$

where: C = friction coefficient, which is a function of pipe material characteristics, and Q = pipe discharge (m^3/s).

The Hazen-Williams equation also has limitations as it was developed empirically. Therefore, care must be taken when it is used. It works well for moderately smooth pipes but is not entirely accurate for rough pipe materials, diameters less than 50 mm, or laminar flow conditions (Fraisse et al., 1995), and velocities greater 3 m/s. It is also stated that this equation is not entirely suitable for friction coefficient values C which are less than 100. James (1982) reported that a C=135 provided good agreement with field data for CP&LM pipes of galvanized steel construction.

Since the flow, and hence velocity changes at every sprinkler head along the lateral, computing friction losses is laborious by simple hydraulics. This process has been simplified by Christiansen (1942) who developed an adjustment factor, F to correct friction losses calculated for pipelines transporting the total flow through the entire length. This procedure works adequately for laterals with multiple outlets having equal spacing between sprinklers and having equal discharges, which is usually the case for

LM machines. Equation 2.13 is used to calculate the *F* factor assuming the first outlet is located from one sprinkler spacing from the lateral inlet.

$$F_c = \frac{1}{m+1} + \frac{1}{2N} + \frac{\sqrt{m-1}}{6N^2} \qquad 2.13$$

where: m = velocity exponent of the friction equation, and N = number of outlets on the lateral. This equation was modified by Jensen and Fratini (1957) to account for a sprinkler situated at half the sprinkler spacing from the lateral inlet into the following:

$$F_n = \frac{1}{2N-1} + \frac{2}{(2N-2)N^m}\left[(N-1)^m + (N-2)^m + ...+1^m\right] \qquad 2.14$$

For the case when the first sprinkler outlet is right at the entrance to the sub-main or mainline, the following equation is used:

$$F_x = \frac{NF_c - 1}{N-1} \qquad 2.15$$

CPs have a special type of lateral with a uniform increasing discharge per unit length. As result, the *F* factor for these machines is different from the one obtained for LMs. The *F* value for standard CPs has been established and is denoted as $F_p = 0.555$, while that of LMs is $F = 0.36$ (Keller and Bliesner, 1990). The reason that F_p is larger than F_c is because there is much less reduction in flow near the inlet end of a CP, resulting to the innermost circular areas being too small compared to the average circular area irrigated per outlet. This implies that LMs are more efficient in terms of energy conservation when compared to CPs. To simplify the use of Equations 2.13, 2.14, and 2.15, *F* values for a given number of outlets are usually tabulated in most sprinkler designs. Apart from being unsuitable for variable sprinkler discharge, the downside of this approach is that it has limitations where variable sprinkler spacing is designed. In addition, the position of the first sprinkler on both machines is also at a considerable distance. In addition to the limitations of these simplistic approaches, they are not applicable to VRI machines because the distribution of flow in the lateral span pipe is not constant.

Chu and Moe (1972) used a differential approach to derive an expression for the head loss distribution assuming an infinite number of tiny sprinklers evenly spaced along the lateral. The Scobey formula was used to calculate the friction head loss and it was found to be 54 % of the head loss for laterals operating as a supply line with the discharge at the pivot point. Correction factors and analytical equations for machines operating with end guns (Anwar, 2000), and multi-diameter laterals with and without end guns (Valiantzas and Dercas, 2005) are also reported.

2.4.2 *Minor Losses*

Local or minor head losses occur as a result of the formation of eddies which causes a pressure drop when water flows through valves, bends, and fittings. Generally, the losses are estimated to be proportional to the velocity head in the pipe and the minor loss coefficient *K* (Keller and Bliesner, 1990). The head loss in the branching pipes or sprinkler drop tubes affects the sprinkler nozzle pressure head when supply pressure is limiting (Kincaid and Heermann, 1970). In general guidelines, minor losses are approximated to be at 10 % of the total system head loss of an irrigation system, as reported in the FAO irrigation design guidelines although Phocaides (2007) estimates these to be 15 %. Within the scope of the present study, VRI valves are plumbed onto the sockets connecting sprinkler drop tubes to form an array in the lateral spans of CP&LMs. Thus, the total minor head losses for VRI machines should include a minor loss component through these sprinkler control valves.

Minor losses across valves vary due to flow rate, and the type, size and geometry of the valve (Phocaides, 2007). Numerous relationships between flow and head loss have been developed using experimentally measured losses and flow characteristics. This led to the development of a universally accepted relationship between pressure drop, velocity head, and minor loss coefficient:

$$h_m = K\frac{V^2}{2g} \qquad 2.16$$

where: h_m = minor head loss (m), K = minor loss coefficient, V = mean flow velocity through the valve (m/s), and g = gravitational acceleration (m/s^2).

When the valve loss coefficient, K, is not specified or it is unknown, as is the case for VRI valve, the head loss can be measured directly through empirical measures and the minor loss coefficient calculated using the following equation:

$$K = \frac{h_m}{V^2 / 2g} \tag{2.17}$$

The minor head loss is sometimes also conveniently expressed in terms of pipe length that will produce an equivalent head loss through friction alone. The equivalent length of pipe is inversely proportional to the Darcy friction factor, and proportional to the loss coefficient and pipe diameter:

$$l_{eq} = \frac{KD}{f} \tag{2.18}$$

where: l_{eq} is the equivalent length of pipe, K is the minor loss coefficient, D is the internal diameter of pipe, and f is the Darcy friction factor.

Valves of the same general type, but from different manufacturers, and different sizes, are not geometrically similar. Thus, the minor loss for a particular type and size of valve can differ considerably among different brands and types. Fraisse (1994) demonstrated that irrigation control valves of different models and manufacturers would have different hydraulic characteristics.

2.4.3 *Elevation Changes*

Unlike solid-set sprinklers with permanently stationary laterals, CP&LMs have the potential to experience variations in field elevation, and hence pressure changes, as they traverse the field. This causes deviations from the desired individual sprinkler discharge. The effect of this change is more significant on low pressure systems than high pressure systems, since it depends on the magnitude of the pressure head on level

terrain, when compared to the quantum of elevation change (Fraisse et al., 1995). This is principally because the sprinkler package is normally designed for no elevation change between the supply point and the end tower, such that the flow of water out of each sprinkler will be less than that designed when the lateral elevation is higher, or greater than designed when the lateral elevation is lower than the pivot point or cart, all other things being equal. As a result, when unregulated CP&LMs are irrigating downhill, more water is applied near the end tower and less water will be applied in this position when the machines are pointing uphill (Figure 2-3 and Figure 2-4).

Figure 2-3: A CP&LM operating across varying field elevations (Santiesteban, 2011)

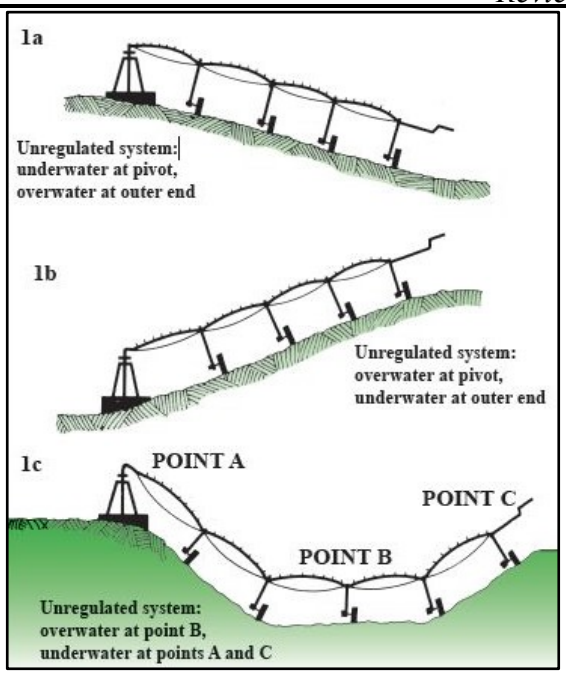

Figure 2-4: Water application characteristics of unregulated CPs operating in variable terrains (Kranz et al., 1997)

The variation in nozzle discharge as a result of elevation change is a function of nozzle discharge coefficients, pipe friction loss, pump-discharge head characteristics (Allen et al., 2000), and on-and-off cycling of end-guns for CPs (Kranz et al., 1997). Table 2-1 illustrates the magnitude of elevation changes that will result in a 10 % change in sprinkler flow rate for a range of sprinkler operating pressures. It is evident that when the operating pressure is greater, a greater difference in elevation is required to cause the 10 % variation in discharge.

Table 2-1: Operating pressures and corresponding elevation changes which cause a 10 % variation in sprinkler discharge adapted from Kranz et al. (1997)

Operating Pressure (kPa)	103.4	172.3	241.3	310.3	379.2	448.2	517.1	586
Elevation Difference (m)	2.1	3.3	4.5	6.0	7.2	8.7	9.9	11.1

2.4.4 *Sprinkler Hydraulics*

While accounting for about 10 % of the capital cost of a CP or LM, the sprinkler package is the most important component in these machines because it is the main device that is used to apply or distribute irrigation water depths to the crop and soil. Sprinklers consist of a nozzle and a deflector plate, some of which rotate, while others are stationary. To date, there has been a range of new sprinkler packages that have been introduced by industry to improve the uniformity and efficiency of water application for these machines. This type of sprinkler package is applicable to machines found in arid regions where drop tubes are used. In humid regions, impact sprinklers are still common. The relationship between discharge and pressure for a sprinkler is mathematically expressed by Equation 2.19 or Equation 2.20. Beccard and Heermann (1981) used the orifice discharge equation based on Torricelli's theorem to determine the flow rate for an individual sprinkler.

$$q = K_d \sqrt{P} \qquad 2.19$$

where: q = sprinkler discharge (L/s), K_d = nozzle discharge coefficient, and P = pressure at base of sprinkler, Or:

$$q = C_d a_0 \sqrt{2gh_i} \qquad 2.20$$

where: q = sprinkler nozzle discharge (m^3/s), C_d = orifice discharge coefficient, a_0 = cross sectional area of orifice (m^2), g = gravitational acceleration (m/s^2), and h_i = pressure head at the base of sprinkler (m).

The individual sprinkler nozzle discharge considering the sprinkler spacing along the CP lateral is given by:

$$q_r = rS_s \frac{2Q_s}{R^2} \qquad 2.21$$

where: q_r = sprinkler nozzle discharge (m^3/h), rS_r = sprinkler spacing at a distance r from the pivot point (m), Q = system discharge (m^3/h), R = maximum effective radius of Lateral (m).

The selection of an appropriate sprinkler package for CP&LMs requires proper knowledge of the pressure head distribution along the lateral. For CPs, this is complicated by the increasing discharges as you move toward the end of the lateral, while the pipe diameter remains constant. Hence, the pressure at any point along the lateral is given by:

$$P_j = P_o - \frac{P_{lp} \text{x} L \text{x} f_p(R)}{100} - IE_g \qquad 2.22$$

where: P_o = pressure at the inlet to the pivot (m head), P_{lp} = pressure loss in the pivot lateral pipe (m head/ 100 m), L = radial length (m) to j, E_g = elevation gain at j (m), I = conversion factor of 0.1017 between with metre head and kPa, and $f_p(R)$ = dimensionless pressure distribution factor at distance R. R is about 0.555 for most CPs without an end gun and 0.56 with an end gun (Section 2.4.1). A value of 0.36 is used for R on LM systems due to the more equal distribution of flow from the outlets along the lateral. This can relationship also be calculated by the Hazen-Williams equation using a C factor of 140 or 145 for galvanized or epoxy lined steel pipes.

Overall, the total pressure head at the centre of a CP or LM, h_l, is summarised as:

$$h_l = h_f + h_{\Delta e} + h_s + h_r + h_m \qquad 2.23$$

where: h_f = friction head loss on lateral pipe (m), Δh_e = elevation difference to end sprinkler in the field (m), h_s = sprinkler operating pressure (end pressure) (m), h_r = minor loss through pressure regulator (m), h_m = minor loss through valves and fittings (m).

2.4.5 *Pressure Regulation*

Section 2.4.3 has discussed how elevation affects pressure head in CP&LMs, and how this impacts the pressure head of a sprinkler. VRI pulsing is also hypothesised by this research to cause unsteady flow conditions and pressure surges which may have adverse effects on the hydraulic performance of these machines. Additionally, a large proportion of CP&LMs, especially in the USA, are reportedly supplied from underground wells (Luedtke, 2013), and fluctuations or drawdown in water tables

during pumping may present undesirable effects on system pressure head. Pressure regulators are used to limit the variation in inlet pressure to a prescribed outlet pressure, regardless of changes in system pressure to ensure that the ideal pressure for optimum sprinkler performance is maintained. The recommendation for using these devices is when pressure variation exceeds 20 % of the sprinkler design pressure, which is likely to cause discharge variations greater than 10 % (Rogers, 2010).

2.4.5.1 Physical Description and Fundamentals of Pressure Regulation

A pressure regulator is an inline, spring-loaded valve designed to regulate system pressure downstream of its placement (Figure 2-5). Pressure regulators are different from ordinary valves because they do not require constant adjustment of the water flow to achieve a constant downstream pressure. Instead, they automatically modulate their area of opening as upstream pressure varies so that pressure loss through the valve will change proportionally to maintain the downstream pressure at a relatively constant base. Since pressure regulators function by dissipating energy, they always require upstream pressures greater than the desired downstream pressure. This minimum pressure is approximated to be about 1.5 times of the nominal pressure setting of the regulator (Kranz et al., 1997, Santiesteban, 2011), or 34.5 kPa above the regulator set pressure. This implies that there is an additional energy cost of 3.5 m to operate pressure regulated CP&LM machines efficiently, which is believed to be paid off by the increased crop yields as a result of improved water application efficiency.

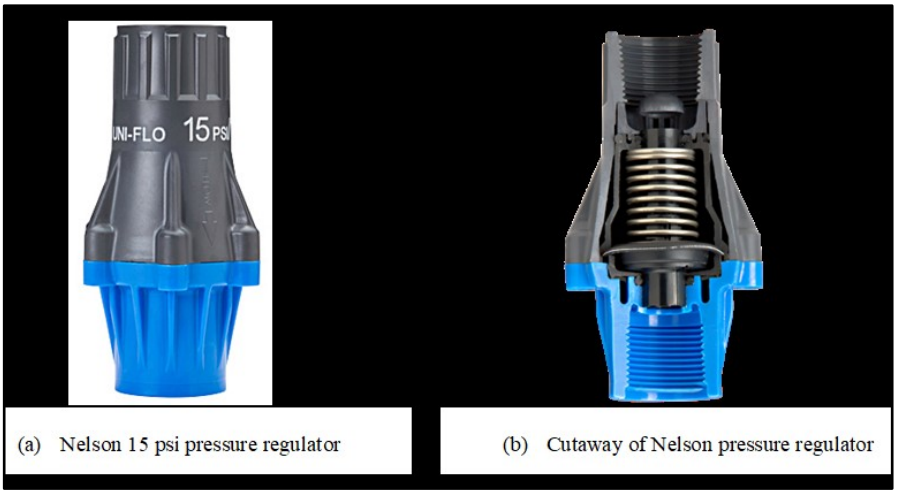

Figure 2-5: A 15 psi Nelson pressure regulator showing internal components

All pressure regulators consist of similar components which function collectively to maintain a non-adjustable prescribed constant outlet pressure. Depending on the brand and manufacturer, nine or ten individual components constitute a pressure regulating valve. They include an inlet strut seat which is sometimes referred to as a flow redistribution plug inside the inlet, a flow tube which is encased by a rubber diaphragm towards the outlet, compression spring, three O-rings, internal casing, upper external casing, lower external casing, and six Philip screws. Other pressure regulator brands do not require screws. The main difference between pressure regulator models of the same brand is the properties of the spring utilised. These properties determine the regulator set pressure. The number of coils and thickness of the spring wire increase with an increase in pressure rating.

2.4.5.2 Manufacturers of CP&LM Pressure Regulators

Nelson

Nelson Irrigation Corporation in USA manufactures Nelson type of pressure regulators which and comes in two different models; *UNIVERSAL-FLO* regulator, and the *HI-FLO* regulator. Both models are manufactured with a range of different pressure settings from 41.4 to 345 kPa (6 to 50 psi). There are three different types of connections available with the Nelson pressure regulator models, with choice depending on the intended application. The pressure regulator models are the same in design, except for flow rates for the different pressure settings. The different flow rates are a result of the differences in the cross-sectional area of the flow tube. Mohr (2011) reported the 70 kPa regulator with a flow setting of 0.0305 – 0.7555 L/s to be the most common device used in CP&LMs in Australia.

Senninger

Senninger Irrigation Inc manufactures four pressure regulator models, *PRL*, *PSR & PSR-2*, *PMR-MF*, and *PRU*. The *PRL* model handles flow ranges from 0.03 – 0.51 L/s at 41.4 to 275.8 kPa (6 to 40 psi), *PSR & PSR2* model from 0.03 – 0.95 L/s at 41.4 to 345 kPa (6 to 50 psi), *PMR-MF* model from 0.13 – 1.3 L/s at 41.4 to 414 kPa (6 to 60 psi), and *PRU* model from 1.3 - 6.3 L/s at 68.9 to 414 kPa (10 to 60 psi). Connections

for Senninger regulators are the National Pipe Thread (NPT), British Standard Pipe Thread (BSP or BSPT), and Hose Thread (HT).

Rain Bird

Rain Bird manufactures only two types of pressure regulators used in CP&LMs. They are the L - Series and M - Series types. Pressures ratings are available from 41.4 to 345 kPa (6 to 50 psi).

Valmont

Valmont retail the *Valley All-Range Pressure Regulator*. This type of pressure regulator is designed specifically for the Valley Low Energy Nozzle (LEN) fixed spray. It is available with increments of pressure settings from 41.4 to 207 kPa (6 to 30 psi). However, since Valley specializes in the manufacture of CP&LMs, pressure regulators and sprinkler packages for their machines are manufactured by Senninger Irrigation.

Komet

The *All-Flow Komet Precision Regulator* (KPR) is a new product in the market and is currently available in 41.4 to 138 kPa (6, 10, 15, and 20 psi) models. Komet Irrigation specifies that their product has very low hysteresis due to its unique design. The KPR is designed to cover the whole range of sprinkler nozzles (1.6 to 10.3 mm or 8 to 52/128") used in CP&LMs.

2.4.5.3 Characterisation of Pressure Regulator Performance

von Bernuth and Baird (1990) pioneered research on the performance characterisation of CP&LM pressure regulators. This extensive work including von Bernuth and Baird (1987) is hypothesised by this research, to have laid the foundations of the development of ISO 10522:1993, which is the universal standard that outlines the general procedure, requirements and criteria for characterising and testing the performance of pressure regulating valves used in sprinkler irrigation. However, only

few studies (Kranz et al., 1997, Rogers, 2010, Mohr, 2011, Araujo et al., 2017, Junior et al., 2018, Burt, 2013) have been completed to understand the performance characteristics of pressure regulators, with a focus of predicting their performance when operated with CP&LMs.

A general consensus on the pressure regulator performance characteristics is illustrated in Figure 2-6. The minimum value of inlet pressure corresponding to the outlet pressure within the tolerance range is called the initial regulation pressure. This tolerance or average deviation in outlet pressure due to varying inlet pressures is about 7 kPa or 10 % for a 70 kPa (10 psi) regulator. A lower initial regulating pressure corresponds to a wider regulating range, while a higher initial regulating pressure will correspond to a narrow regulation range (Zhang and Li, 2017).

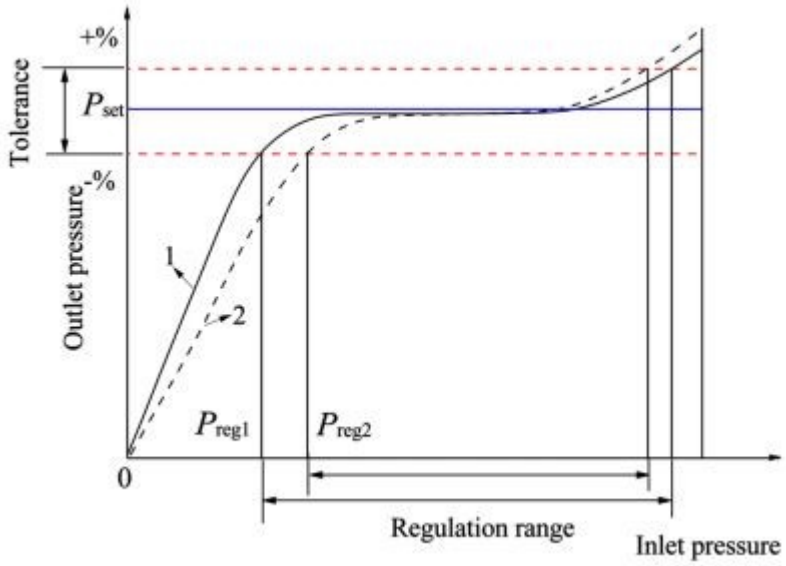

Figure 2-6: Schematic of pressure regulation curve (Zhang and Li, 2017)

The slope of the performance lines on the unregulated segment of the regulation curve characterised as initial regulation pressure is taken as an evaluating parameter, and a value closer to one indicates better performance. The criteria for determining the slopes for each line segment using coordinates of the initial and end segments is expressed by von Bernuth and Baird (1990). Zhang and Li (2017) defined the slope of the performance line of the unregulated segment as:

$$\eta = \frac{(1-\delta)P_{set}}{P_{reg}} \qquad 2.24$$

where: δ is the tolerance range (the values of δ for different gradation are 0.1 and 0.2, respectively), P_{set} is the pre-set pressure (MPa), P_{reg} is the initial regulation pressure (MPa).

A review of the literature shows that there is a substantial conflict of opinions regarding the true nature of the regulating characteristics of pressure regulators. This is also demonstrated in the lack of suitable mathematical models that accurately describe pressure regulator performance for modern low pressure CP&LM irrigation machines (Section 2.4.5.4). For instance, von Bernuth and Baird (1990) describe hysteresis of outlet pressure (Figure 2-7) using four straight line segments, where two segments follow the rising pressure limb of the hysteresis curve, while the other two follow the falling pressure limb of the hysteresis curve. Keller and Bliesner (1990) incorrectly describe the outlet pressure tracking along the lower leg of the hysteresis curve when inlet pressure is increasing, and that it follows the upper leg when inlet pressure is decreasing. As well, other authors (Burt, 2013, Kincaid et al., 1987) also suggest design pressures in the order of 3.5 m to 5 m head is required for pressure regulators to function correctly. In their comparisons of experimental versus numerically simulated results, Zhang and Li (2017) demonstrated a lack of good understanding of the hydraulic parameters placed on pressure regulation mechanisms to clearly define pressure regulator performance. They plotted inlet pressure ratios on the y-axis while the x-axis was plotted with the dependent variable of outlet pressure ratio.

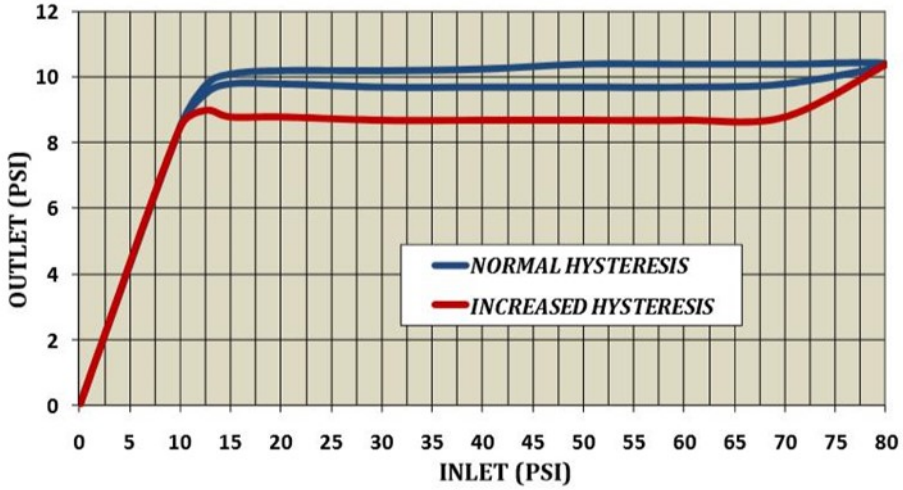

Figure 2-7: Hysteresis curve showing the rising and falling limbs with increasing and decreasing supply pressures (Santiesteban, 2011)

In some CP&LM installations, pressure regulators of the same pressure settings are installed on the upstream end of dropper on the lateral pipe outlets together with additional secondary regulators installed adjacent to the nozzle (Santiesteban, 2011). Zerihun et al. (2019) simulated the hydraulic performance of a LM equipped with pressure regulators to predict the pressure head along the lateral at the inlet of pressure regulators. However, the simulation model did not accurately represent the true energy gradient for the LM, because it was assumed that pressure regulators have the nominal set pressure as the actual outlet pressure.

Consequently, these separate misunderstandings highlight a comprehensive lack of understanding of the hydraulic performance characteristics of pressure regulators under normal operation, and would erroneously represent the CP&LM hydraulic performance when unsteady conditions occur in CP&LMs in the field. In addition, pressure regulation performance research is needed because of their extensive utilisation in recent modern CP&LM irrigation developments.

Previous studies have shown that the hydraulic characterisation of the complex individual interconnected processes involved in the regulating mechanism is ignored. The focus is on measuring the differential pressure head across the devices, to determine only the final output pressure being received by the nozzle, the effects of

wear and tear on regulated pressure for regulating valves that have been operational for extended hours (Lima et al., 2003), as well as the effects of regulated applications depths on crop yield (Araujo et al., 2017). The only work that explores the characterisation of pressure regulator performance to a great extent, are reported by von Bernuth and Baird (1990), Mohr (2011), Zhang and Li (2017), and Junior et al. (2018).The authors recognised the lack of a classical procedure that can be employed for the effective characterisation of the complex nature of pressure regulation process, which could be reason for the limited information on this phenomenon.

For VRI machines, the impacts of unsteady flow from pressure transients on pressure regulator performance is not expressed in the existing literature. The pressure changes that have been studied so far are a result of elevation changes, which gradually occur as CP&LMs move across sloping fields. Therefore, the effects of fast pressure wave transients and the resulting unsteady conditions on regulator performance requires a broader understanding to effectively manage VRI machines for optimal irrigation performance. However, it is worth noting the discussions above that, there is still a great amount of work needed to fully understand pressure regulator performance, before any VRI impacts can investigated.

2.4.5.4 Limitations of ISO Testing Standards

International Standards Organisation (ISO) provide general guidelines for characterising and testing irrigation accessories such as irrigation valves and pressure regulators. The ISO Standard 9644:2008 provides the criteria for characterising the hydraulic performance of irrigation valves, while the guidelines for characterising the hydraulic performance of pressure regulators are contained in ISO Standard 10522:1993. However, Mohr (2011) and Junior et al. (2018), using the generic ideas from these ISO standards, demonstrated that it is possible to integrate advanced and specialised equipment to develop smart testing apparatuses that can help determine the hydraulic characteristics of complex irrigation accessories. The studies concluded that there is a need for a more sophisticated and enhanced automatic measurement system to be used to accurately characterise complex devices such as pressure regulators. In addition, and in conjunction with the introduction of pulsing solenoid valves in

CP&LM irrigation, the review found that ISO Standard 9644:2008 does not provide a procedure for characterising the performance of automatic control valves such as pulsing solenoid VRI valves. The ISO Standard 10522:1993 for testing pressure regulators is also found to be very basic and cannot provide comprehensive procedures for complex and autonomous testing needed for pressure regulators. Junior et al. (2018) recommended a review of this standard to include additional procedures for understanding pressure regulator performance very explicitly.

2.4.6 *Conclusion*

The hydraulic performance of pressure regulated CP&LMs before they are retrofitted with VRI are not adequately understood. Pressure regulation understanding has eluded the irrigation community, with machines now equipped with pressure regulators as a commissioning standard. The lack of precise and robust pressure regulator mathematical models has also reduced understanding of the significance of these important devices in pressurised irrigation system performance. This has a compounding effect on the hydraulics now that these machines are retrofitted with pulsing solenoid VRI valves without clear performance characteristics, and when no hydraulic re-design is undertaken during the retrofitting process. It is not known if pressure regulators can withstand the unsteady conditions experienced by VRI CP&LMs to maintain pre-set pressure required by nozzles. As a result, the performance of VRI equipped CP&LMs may be outside the acceptable irrigation engineering design norms, until improved hydraulic understanding is well integrated in these systems.

2.5 Overall Conclusion and Justification for the Study

The literature reviewed in the foregoing sections of this chapter demonstrates that hydraulic systems that are identical in operation (pulsing cycles) as VRI are capable of introducing unsteady flow conditions and pressure surges that can have serious impacts on the hydraulic performance of a system. However, the review has identified that the hydraulic performance of VRI machines have been ignored, mainly because the hydraulic characteristics of VRI equipment is unknown, and no attempt has been

made to establish their performance characteristics. The review has also identified that pressure regulation of CP&LMs is not well understood, with limited research completed to develop such critical information, more importantly now that these machines can be operated predominantly under unsteady-state conditions. The main reason is the lack of a suitable testing algorithm as ISO testing standards are also limited in procedures for characterisation and mathematical modelling of the inherently complex pressure regulation process. Therefore, all these technical problems concerning the hydraulics of pressure regulated VRI CP&LMs can be rectified by addressing the research objectives outlined in Section 1.6 of this thesis.

3. DEVELOPMENT OF AN AUTOMATED MEASUREMENT APPARATUS FOR SIMULATING THE HYDRAULICS OF VRI

3.1 Introduction

Chapter 2 has highlighted that the hydraulic performance of VRI CP&LMs including pressure regulation of these machines before they are retrofitted with VRI technology is not well understood. From the discussion, it is apparent that the underlying reasons are twofold; (i) the hydraulic performance characteristics of VRI equipment are non-existent, and (ii) the comprehensive understanding of the hydraulic performance characteristics of pressure regulating valves used in CP&LMs is lacking. However, Section 2.5.5.4 demonstrates clearly that the major limitation surrounding the performance characterisation of solenoid VRI valves and pressure regulators is due to the lack of suitable testing procedures, as ISO Standards 9644:2008 and 10522:1993 are very limited. Junior et al. (2018) suggested a review of these standards to be concurrent with technological advances in the irrigation industry.

Previous studies have shown however, that it is possible to strategically arrange or integrate a range of sophisticated components with hydraulic equipment to establish measurement data. Some of these components include electronics equipment and high precision sensing equipment. This criterion provides the basis for exploring design options and conceptualisation of a novel automatic measurement system encompassing an appropriate testing methodology for the hydraulic performance characterisation of VRI valves and pressure regulators. The novel system being proposed here is envisaged to have adequate capability to simulate and measure the hydraulic performance characteristics of pressure regulators and VRI valves when operating in the field. When such a test methodology has been successfully commissioned and validated, it will serve as a basis for the review and amendment of ISO standards relevant to modern irrigation technological advancements. von Bernuth and Baird (1990) proposed that automatic test procedures are a requisite for the

comprehensive characterisation of such irrigation equipment components. Trials of such a system are reported by Junior et al. (2018), where a proportional integral derivative (PID) controller was used to calculate pre-set pressure error and apply an output signal to a variable frequency drive (VFD).

To achieve the objectives of this research, a novel automatic multi-function experimental hydraulic measurement apparatus was developed. The automatic multi-function test apparatus is a state machine which integrates a data acquisition (DAQ) system controlled by a National Instruments (NI) LabVIEW software. The design process, equipment specifications, construction, calibrations and operation of the apparatus, including hardware and software components, are described in this chapter. The system development was based on modifications and improvements of a prototype system developed by Mohr (2011), and some of the basic equipment and set-up conditions were identical. Mohr (2011) commissioned a test apparatus which characterised pressure regulator performance on the basis of manual control and incremental adjustment of test parameters, pressure head and discharge. Automation was provided only for data logging. This semi-automated apparatus was an improvement to a design proposed by von Bernuth and Baird (1990) as illustrated in Figure 3-1.

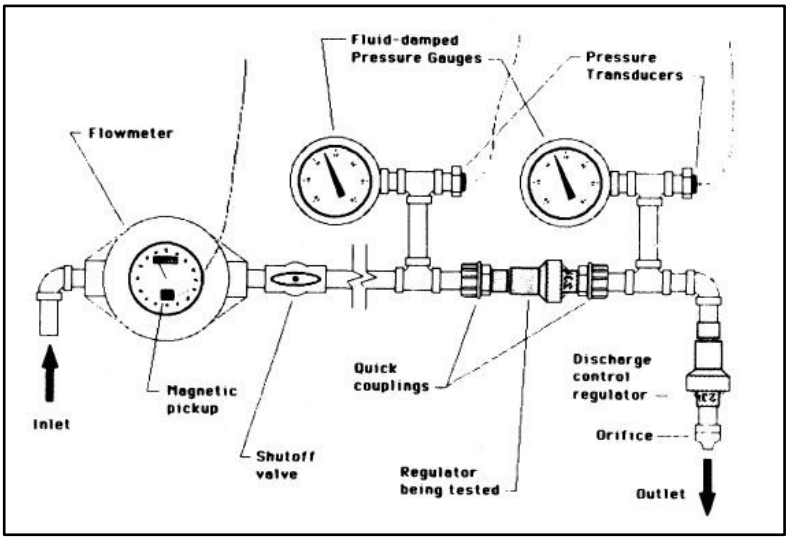

Figure 3-1: Schematic drawing of pressure regulator test stand developed by von Bernuth and Baird (1990)

3.2 Description of System Development and Operation

The primary objective (objective 1) of this research is the design and development of an automatic multi-function hydraulic measurement system that could permit comprehensive characterisation of VRI valves and CP&LM pressure regulators, in order to address the objectives (2 to 7 all inclusive) of this research as outlined in Section 1.6. The overall goal is to develop hydraulic modelling techniques that can simplify the hydraulic assessment processes required when designing or retrofitting and managing VRI machines. The design specifications adapted ISO standards, 9644:2008 and 10522:1993, to incorporate a series of modifications and improvements that enable a system with suitable capability to execute the measuring tasks. The system was designed to measure the amount of pressure head loss through VRI valves (Stage 1), the nature and relative magnitudes of pressure wave transients from VRI valve pulsing (Stage 2), a suite (four different types) of complementary testing processes which describe the functional characteristics of pressure regulators (Stage 3), and the hydraulic response of pressure regulators to the effects of VRI transients (Stage 4). In order to achieve the four different testing phases, the automatic hydraulic measurement apparatus had to meet the following design criteria:

- Capability to control the operation of the different electric VRI solenoid valves being tested.
- Automatic operation of test-rig control valves, predominantly for hysteresis testing.
- Automatic data acquisition (DAQ) of pressure head, discharge, and temperature measurements.

The Engineering Hydraulics Laboratory (Z113) which is located at the Faculty of Engineering and Surveying at the University of Southern Queensland (USQ) was used to set-up the test apparatus. This lab was selected because it houses a range of infrastructure that is used for conducting hydraulic testing and modelling, where some of the equipment were critical and vital to the development of the apparatus. Hence, the automatic hydraulic measurement apparatus consisted of six (6) main components which included:

- Constant head water supply
- Test-rig piping and fittings
- Desktop PC running LabVIEW software
- Relay board connecting solenoid valves to a DC lab power supply
- Automatic DAQ modules receiving signals from flow meter, pressure sensitive transducers, and a resistance temperature sensor, and
- Electronically actuated test-rig control valves and a precision downstream orifice.

To ensure that the measuring apparatus represented physical operating conditions of VRI machines, the design pressures and nozzle flow rate ranges were carefully selected using the design specifications of a local 50 ha VRI CP which is used for research activities by the Centre for Agricultural Engineering (CAE) at USQ. The pressure and nozzle flow rates selected could also represent typical LM operational conditions. The maximum design flow rate was 0.75 L/s, which occurs on sprinklers near the end of very large CP machines while 0.05 L/s was selected as the minimum flow rate as this would occur in the innermost sprinklers of a CP. Additional intermediate flow rates were selected at approximately equal intervals to represent flow rates at specific points along the machine radius. These flow rates were successively measured in an increasing and decreasing manner during testing. A downstream precision orifice nozzle (orifice diameter = 9.72mm) was installed to control flow rate through the apparatus in conjunction with a pair of electronically actuated valves. Water is supplied from a constant header tank providing 16.181 m (Mohr, 2011) of stable head through a 200 mm high density polyethylene pipe. The piping in the test apparatus was made of a 19.05 mm nominal bore (wall thickness = 2.64 mm) galvanized steel pipe with appropriate water-tight fittings to enable quick installation and removal of each test specimen. Each of the system components is described in further detail in the following sub-sections.

3.2.1 *Constant Head Water Supply*

As mentioned previously in Section 3.2, the VRI component and pressure regulator testing apparatus was set-up in the Engineering Hydraulics Laboratory at USQ. A constant head water supply system is available in this lab and provides a convenient stable supply pressure head into the laboratory. The system is made up of a 30,000 L underground storage tank which is situated underneath the laboratory, with four different sized Grundfos centrifugal pumps lifting water into two header tanks (Figure 3-2). The total flow rate for these pumps to these header tanks is about 80 L/s. The header tank system is comprised of low and high header tanks supported by the side of the Engineering building. The tanks each consist of an inner shorter tank with a long weir edge, and an outer overflow capture tank. The inner shorter tank receives water from the pump-sets, and supplies water through a 200 mm PE100 PN10 polyethylene pipe to three equally spaced manually operated butterfly valves in the laboratory. The outer overflow capture tank receives excess water flowing over the long weir edge, returning it to the underground storage by gravity.

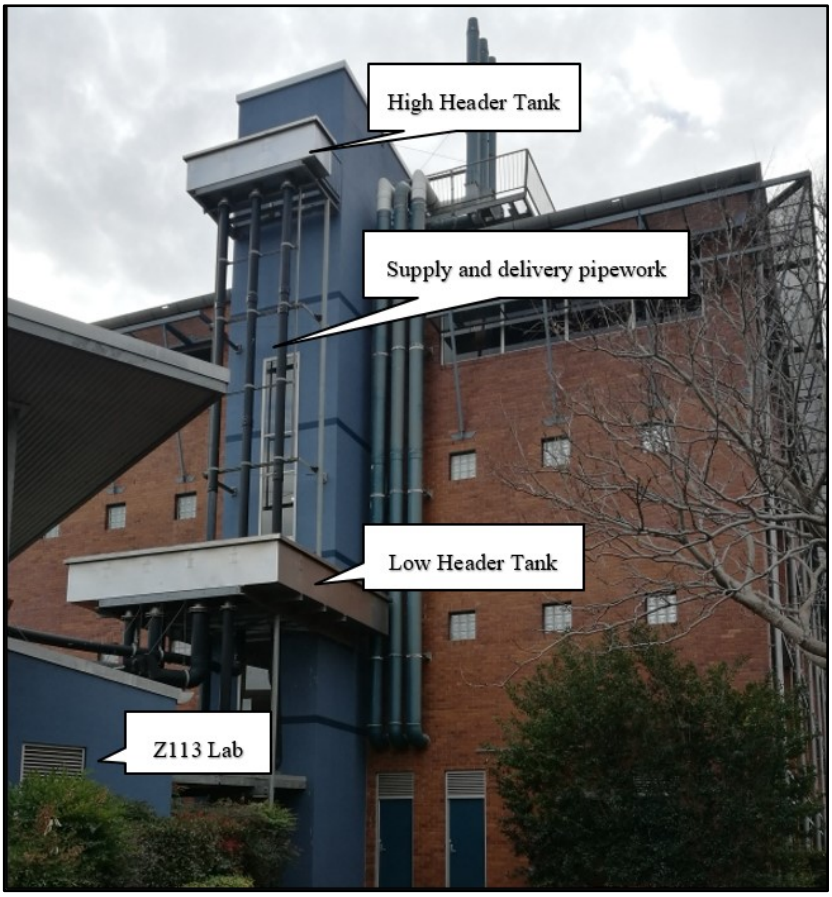

Figure 3-2: Header tank system set-up at the Engineering Block leading to the Z113 Hydraulics Laboratory in the lower left of the image

To maintain a constant head supply during testing, continuous pumping occurs so that the inner shorter tank continuously overflows to the outer capture tank back to the underground storage. In this type of experiments, two of the smallest pumps, Grundfos NP65 50 125/128 model 96443 with a combined water duty of 20 L/s were used. The pumps are each driven by a 2-pole 3.0 kW electric motor. The system provides a stable constant supply head of approximately 15 m to a test bench erected about 1 m above the floor. A galvanized steel plate machined to suit the downstream flange of the supply line butterfly valve was used to connect the test apparatus to the constant head supply through a 50 mm outlet. An equivalent size flexible corrugated piping was used to connect the test-rig directly to the header tank, or through a booster pump, depending on testing requirements. Discharge from the test apparatus was drained onto the sloped floor where it returned in concealed gutters back to the underground storage.

3.2.2 *Test-Rig Piping and Fittings*

The plumbing and connection of the hydraulic testing apparatus was based on a 19.05 mm nominal bore galvanized steel pipe, Schedule 40, with a wall thickness of 2.64 mm and modulus of elasticity equal to 2.25 x 10^{11} N/m^2. The rationale for selecting this pipe size and material are twofold; (i) the standard size of the solenoid valves and pressure regulators to be tested was 19.05 mm (3/4 inch), and fittings for this size were readily available, and (ii) the requirement to test and investigate the nature and relative magnitudes of hydraulic transients generated by VRI pulsing (Stage 2), without any potential for dissipation or dampening of the pressure waves propagated due to axial deformation of the pipe rig. Ramos et al. (2009) reported that PVC pipes exhibit lower hydraulic heads during peaks of hydraulic transients when compared to metal and concrete pipes due to their viscoelastic properties, while slightly lower hydraulic heads were observed by Covas et al. (2012) as a result of vibrations and axial deformation of a coiled copper pipe rig not rigidly anchored on supports. Wan and Mao (2016) demonstrated that a steel mesh reinforcement on polyethylene pipes can significantly increase the shock wave speed, thus causing severe peak pressure and hydraulic surges.

The set-up of the hydraulic apparatus, together with sensing devices, and the LabVIEW automatic DAQ system is illustrated in Figure 3-3. The test-rig was a simple configuration of the type; reservoir, pipe, and valve system. The upstream end of the test-rig was equipped with a set of valves to enable changing the configuration to include a booster pump between the reservoir and the apparatus. It was also designed to be flexible for other configurations that allowed more than one type of valve, e.g. the set-up which included both the solenoid valve and pressure regulator (Stage 4). A custom-built table (1.5 m x 0.6 m x 0.7 m) with slotted bottom ends (0.2 m x 0.15 m) was mounted over a 3.0 m x 0.8 m x 1.0 m bench which served as a platform for the test-rig piping. The internal vertical wall of this special table was used to mount the DAQ modules, the relay board, and the flow meter transmitter, including restraints for the electrical wiring, so as to isolate these and avoid wetting by the main rig piping and test specimens. The desktop computer, power board, and DC power supply were positioned on top of the custom table which, separated and confined the wet and dry

components of the test-rig. The 19.05 mm test-rig piping was connected to the 50 mm galvanized steel outlet through appropriate reducers and fittings.

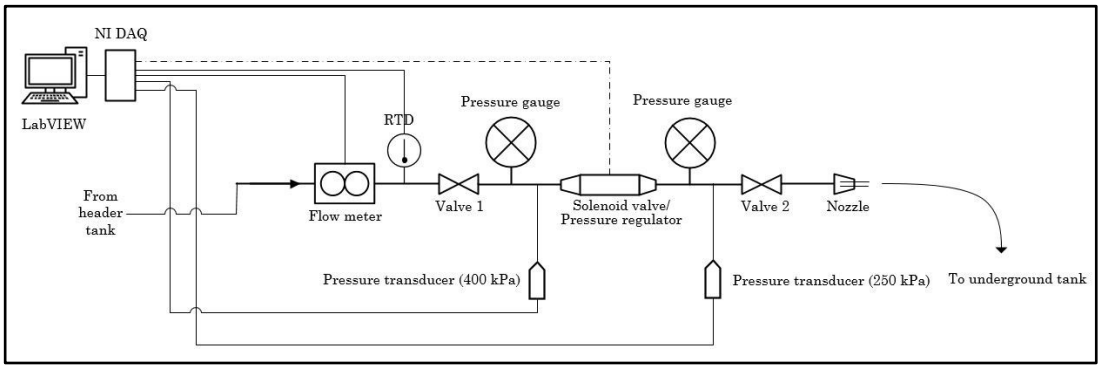

Figure 3-3: Instrumentation flow chart of the developed automatic multi-function measurement apparatus

The booster pump used for the high pressure set of experiments in this testing is a Southern Cross *Mark* HX-C medium head end-suction centrifugal pump that is coupled to a high efficiency (IEC 34) 2-pole 3.0 kW Brook Hansen electric motor. The pump and motor are coupled using a V- belt (dual) and pulley system as shown in Figure 3-4. The switchgear (NHP Sprecher + Schuh CAT3 with IP 66) for the 3-phase electric motor is a DOL (Direct-On-Line) and is mounted on a steel frame supporting both the pump and motor, with sufficient 4-core cabling (~20 m) to a 3-phase power supply. DOL starters are desirable for electric motors not exceeding 7.5 kW because their high inrush current at start up does not cause excessive voltage drop in the supply circuit. A soft starter or Star Delta switchgear is otherwise used for bigger motors where the inrush current (about 300 % of full load current) can cause significant voltage drop. The revolving coupling mechanism in this pump set is machine guarded with a fabricated sheet metal frame to prevent hazards during pumping.

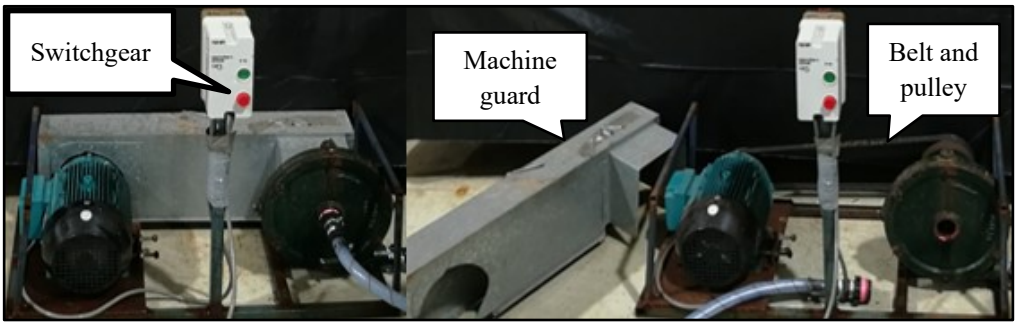

Figure 3-4: Setup of the booster pump used in the experiments showing a belt and pulley drive coupling mechanism with a machine guard arrangement

3.2.3 *The LabVIEW Data Acquisition Software*

Integration of an automatic DAQ system in the hydraulic apparatus to enable automatic measurement and control of the experimental testing, required a National Instruments (NI) LabVIEW computer software. The LabVIEW software programming language is designed specifically for scientific and laboratory experiments, and it acts as an interface between compatible PCs and laboratory sensors and instruments. The code was written using LabVIEW 2017 to produce a stand-alone executable program capable of operating on any PC running Microsoft Windows or Linux systems. The software code was compiled to operate under Windows XP or later versions, and the PC used for this experimental testing was running Microsoft Windows 10. The LabVIEW graphical user interface was designed with the "NI Automation and Measurement Explorer" for software setting changes and online help, so as to be simple and intuitive. The LabVIEW state machine construction allowed several steps to be linked in series so that each individual step can be executed easily with loop systems. The schematics of the LabVIEW code for each test method are shown in Appendix C. Execution of cases in the structure was determined by the output from the previous case or first execution by the control selector input.

The design of the LabVIEW computer program was based on parameters deemed to be essential for the comprehensive characterisation of the hydraulic performance of VRI valves and pressure regulators. These measured parameters included flow rate, upstream pressure, downstream pressure or differential pressure across test specimens, and water temperature. Each of these parameters were measured with advanced high precision sensing equipment transmitting signals to the LabVIEW software, and were recorded and stored in *.lmv* data files. In order to address each of the ensuing specific objectives of this study, the lab work was split into four different testing phases; Stage 1 designed for the characterisation of minor loss from solenoid actuated VRI valves, Stage 2 for the characterisation of hydraulic transients from VRI valves pulsing, Stage 3 for the characterisation of pressure regulator performance including hysteresis, and Stage 4 for the characterisation of transient-impacted pressure regulator performance.

Figure 3-5 shows the main window of the LabVIEW computer program which was compiled and packaged from four individual sets of codes of the four stages of testing. Once input parameters are set, clicking a particular testing stage prompt the interfaces in Section 3.2.3.1 to 3.2.3.4. The four discrete experimental testing phases have unique controls for monitoring and fine tuning of test parameters, and test durations, as well as different data saving options. The sections below describe the operational functions and capabilities of each of the testing phases.

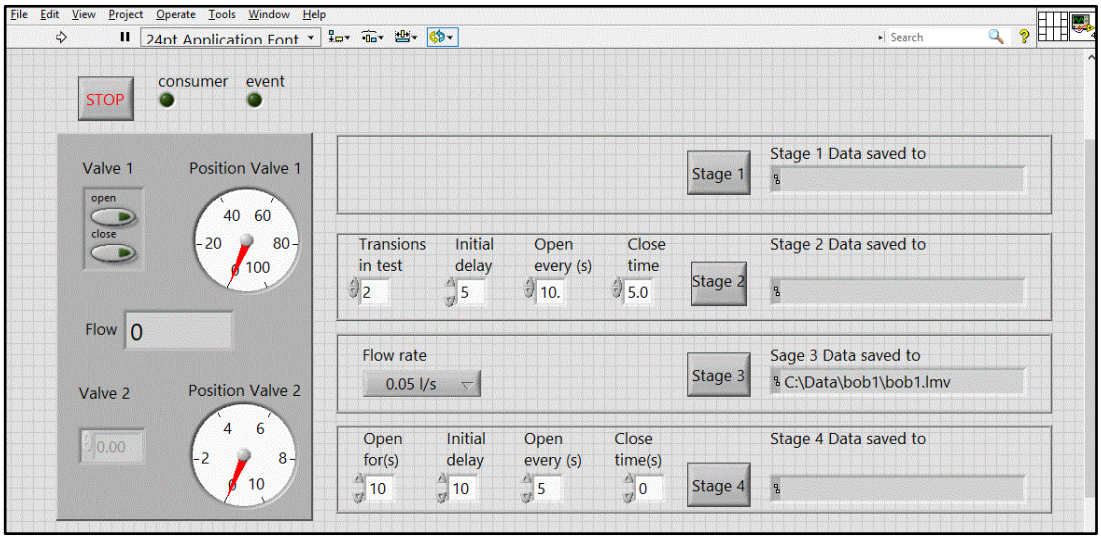

Figure 3-5: LabVIEW software main window showing the four different testing stages

3.2.3.1 Stage 1: Minor Head Loss Measurement

The LabVIEW computer program in Stage 1 (Figure 3-6) enables the selection of a test flow rate that can automatically trigger the opening and control of the automatic valves to maintain this particular flow rate. The downstream throttling valve could be further controlled by manually inputting a specific voltage to arrive at a specific flow and input pressure, while continuously measuring water temperature. The program also enables the user to alter test durations and select suitable file locations for data saving on the PC. The DAQ system in Stage 1 was designed to sample data at a frequency of 1 kHz and then record averages 10 times per second. Since this methodology only required the relay board to energise the solenoids to keep the valves open, this procedure was also capable of being used to characterise the minor loss and to gather other pressure regulator performance characteristics.

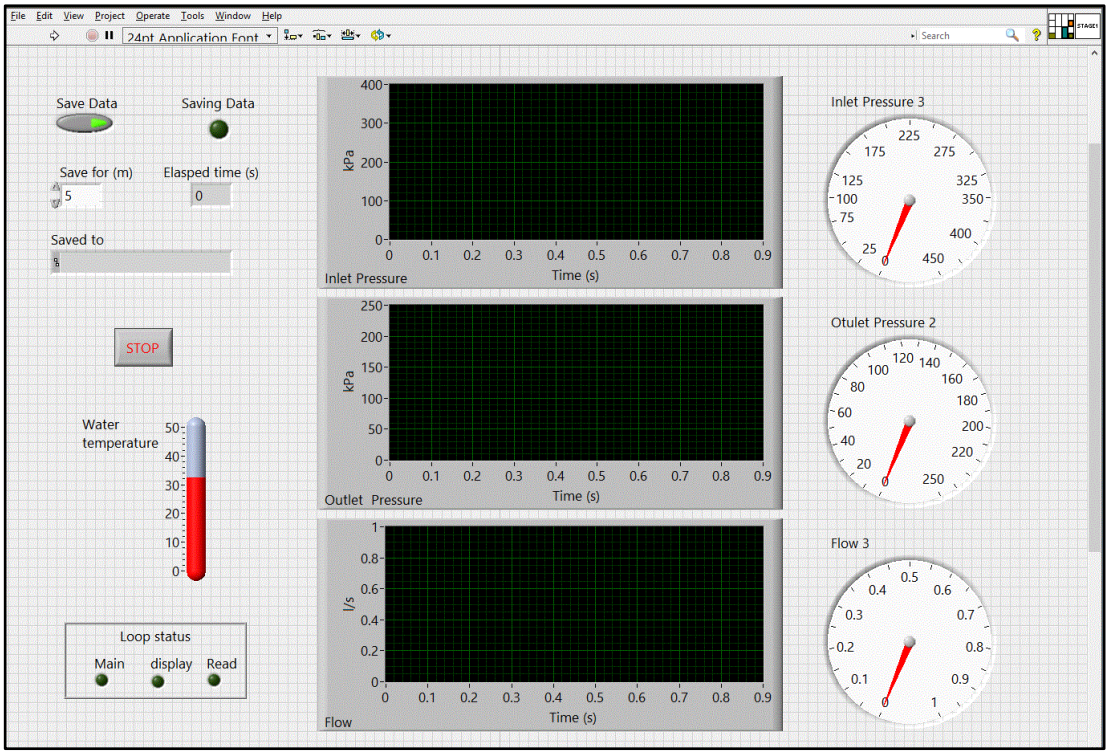

Figure 3-6: Stage 1 window for measuring minor head loss in VRI valves

3.2.3.2 Stage 2: Measurement of Hydraulic Transients

The algorithm that was written for measuring pressure and discharge under the influence of on-and-off pulsing of VRI valves is shown in Figure 3-7. The LabVIEW algorithm for the Stage 2 method was written with a sine wave type of wave form to characterise the nature of pressure waves transients generated from VRI pulsing. The inputs to the program were: (1) an open position duration, (2) time delay, (3) close position duration, all in seconds, and (4) the number of transitions desired for each set of experiment over a duty cycle of 60 seconds. This type of duty cycle was selected to allow ample time for the stabilization of pressure and discharge in the test-rig before a transient was generated. LabVIEW was used to control the operating position of the solenoid valves. The theoretical effects of the fast opening and the fast closing of valves are discussed in detail in Section 2.3. Therefore, a measurement system that could accurately capture the speed and magnitude of pressure wave transients needs to capture pressure readings at least double the frequency of the transients. The DAQ system was set at a frequency of 10 kHz and was configured to write all 10 000 records of raw data for each second to the data file.

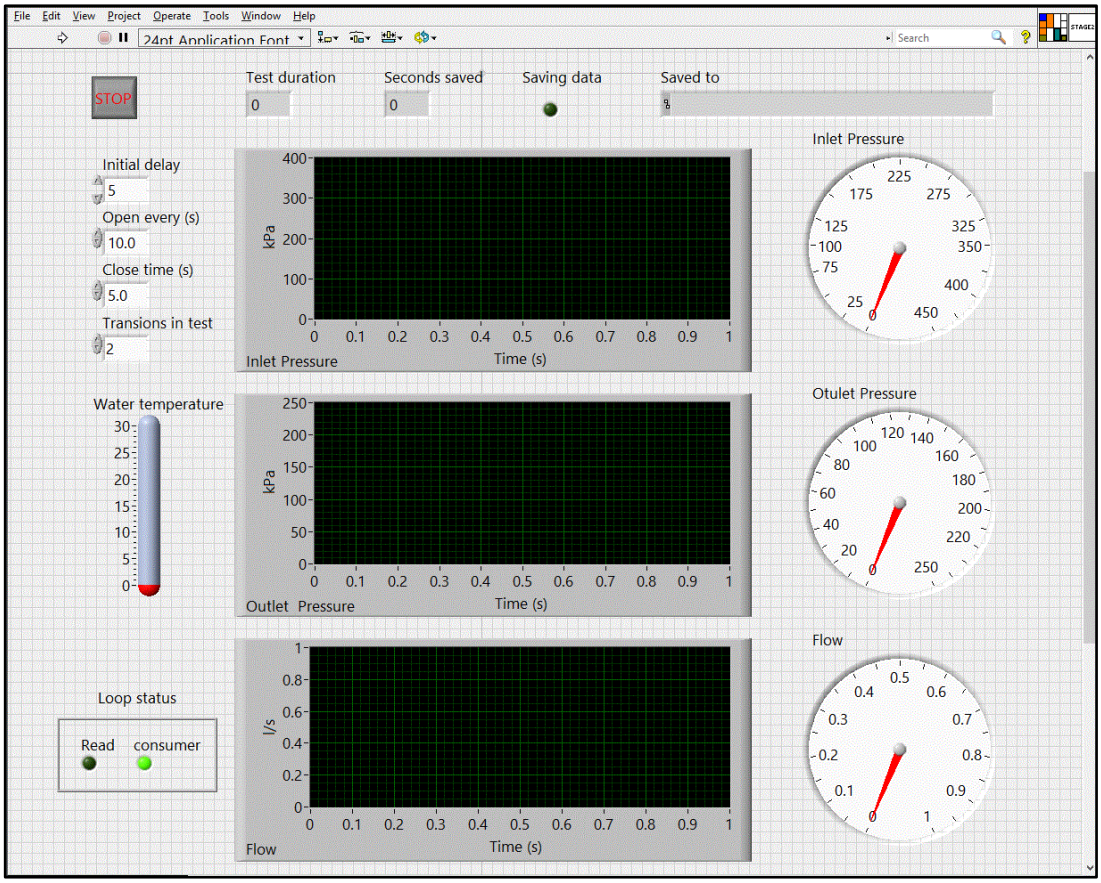

Figure 3-7: Stage 2 window for measuring the propagation of pressure wave transients from VRI valve pulsing

3.2.3.3 Stage 3: Pressure Regulator Hysteresis Characterisation

A more sophisticated process is needed to understand pressure regulator outlet pressure hysteresis. Manufacturers do not provide enough technical detail to fully understand their regulator hysteresis, but instead they only mention that their products have a very low hysteresis to suggest that they perform according to their design specifications. However, the various physical operating conditions of CP&LMs on hilly terrains, with fluctuating groundwater tables, and during the on-and-off pulsing of VRI valves will test the capability of the devices to withstand these conditions and maintain a constant outlet pressure, as has been reported anecdotally.

Figure 3-8 shows a LabVIEW software interface that was developed for characterising pressure regulator hysteresis. It utilises voltage signals to automatically actuate the stepper-motor driven Belimo control valves as described in Section 3.2.6, so that the

upstream valve opens one step while the DAQ system completes a check to determine if the flow if is within a set tolerance band, before the downstream valve can automatically adjust to stabilise flow in cases when it is outside the tolerance band. The logic developed and used is that the downstream test-rig control valve should open first to a 100 % (fully- open) position while inlet pressure is below any set point when an experiment is started. Once this is achieved, the upstream control valve then opens to about 20 % to allow the first flow passage in the test apparatus. Depending on the tested discharge, the LabVIEW DAQ system controls the incremental step movement of the control valve upstream so that it opens every single step with a feedback loop to check flow rate. If the flow rate is below the set band, the valve will make consecutive incremental step movements until it reaches or is slightly above the set point, and then allow the downstream valve to start closing to maintain this discharge. Pressure in the test apparatus is controlled by the movement of these control valves (Table 3-1), and is subject to the supply pressure from the header tank and Southern Cross pump. This process repeats to typically maintain a set flow variation within 0.001 %, upon which the system will continue saving data and allowing the upstream valve to make further incremental steps, and save data until the full range of input test parameters is complete. The flow check process is designed to be visible on the LabVIEW interface. A look-up option for historic flow rates, and a pressure limit for confining the inlet pressure to a fixed threshold when the upstream valve is continuously opening are also incorporated and provided in this interface screen. The pressure regulator hysteresis testing process samples the supply pressure, flow rate, control voltage for the two automatic valves, water temperature, and the final regulator outlet pressure at 1 kHz frequency.

This automatic hysteresis measurement procedure allows the collection of data points across the full range of the hysteresis curve to simulate unsteady conditions experienced by regulators when controlling nozzle flow rates of CP&LMs in irrigated fields. Mohr (2011) and Junior et al. (2018) used a system with 50 kPa incremental adjustments in supply pressure using manual control valves, as generally suggested ISO Standard 10522:1993, with automation only used for data acquisition.

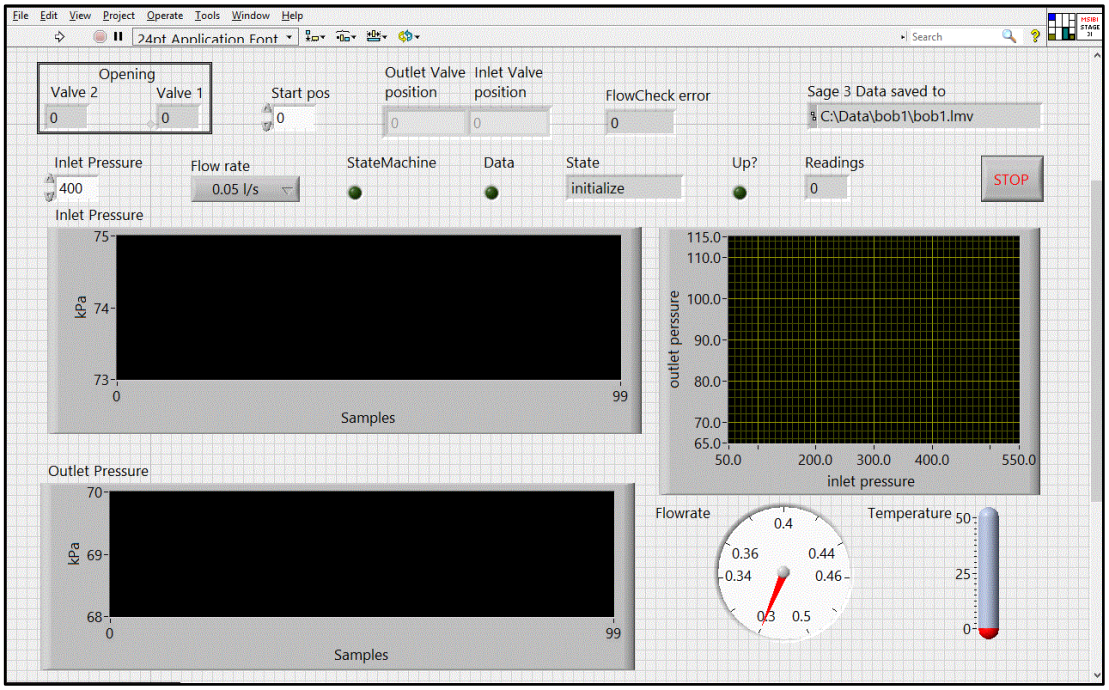

Figure 3-8: Stage 3 window for pressure regulator hysteresis characterisation

3.2.3.4 Stage 4: Response of Pressure Regulators to VRI Transients

Pressure regulators are reported by manufacturers to be capable of maintaining a constant outlet pressure when the supply pressure varies, for all conditions, when it is at least 3.5 m greater than the set pressure. Some manufactures even suggest that the devices can maintain constant outlet pressure under water hammer. Nonetheless, information about the regulating characteristics of these devices under such conditions in not yet available, and this becomes even more relevant now that pressure regulated CP&LM machines are operated with VRI with pulsing system discharges. The final phase of the experimental testing program required a method that would integrate both VRI and pressure regulating valves to simulate the response of the latter when operated with VRI technology. This is because in typical VRI equipped machines, VRI valves are installed upstream of pressure regulators such that their operational impacts are transferred or experienced by the regulators. The test method developed here integrated Stage 1 and 2 processes, but was preceded by a Stage 2 process. The idea developed here was to energise and pulse a VRI valve, and to transmit the impacts of any pressure and discharge variations onto a downstream pressure regulator. The VRI valve was installed on a tee piece with regulators in-line with the test apparatus. Data

collection and recording was set at a 10 kHz frequency, using the test method illustrated in Figure 3-9.

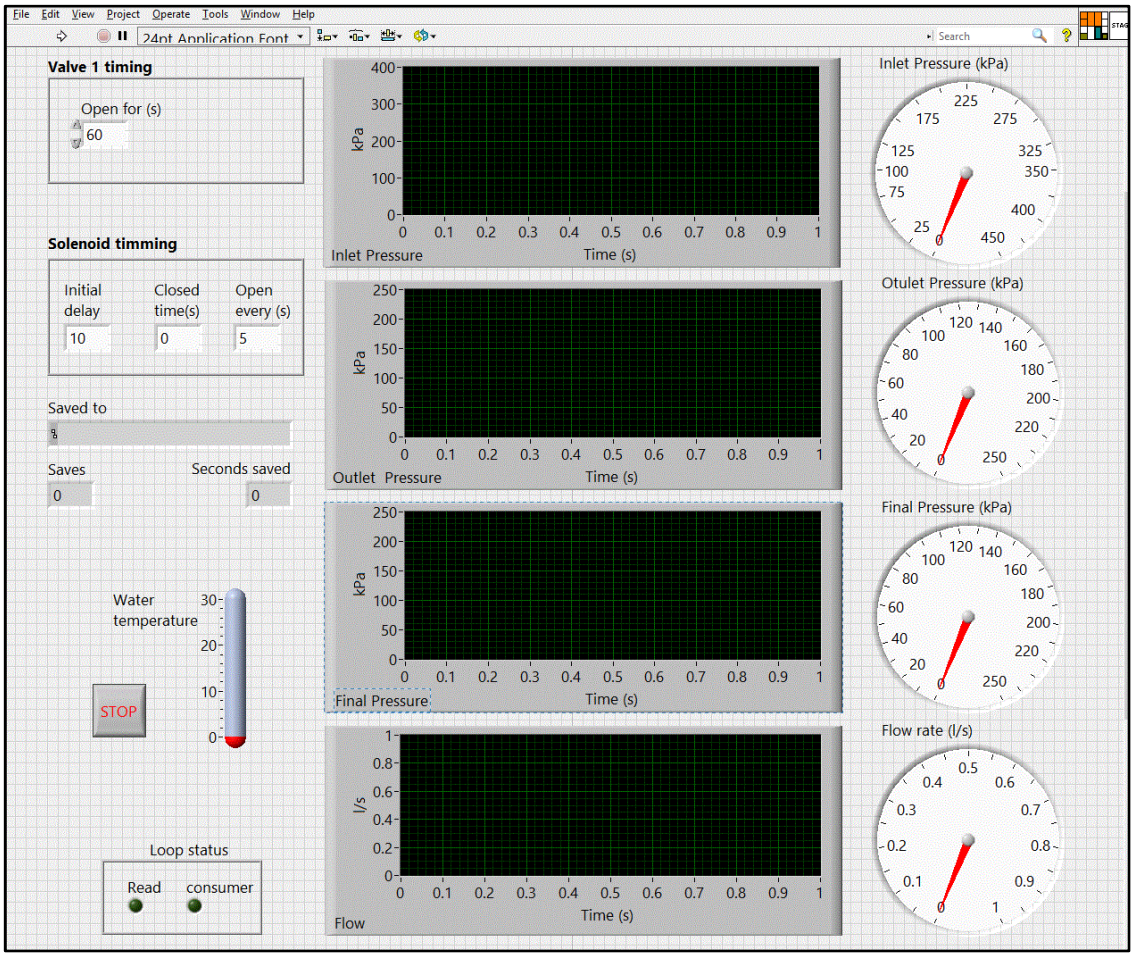

Figure 3-9: Stage 4 window for testing the response of pressure regulator performance to VRI pulsing

3.2.4 *Solenoid Valve Connection System*

The wiring of solenoid actuated VRI valves plumbed between two pressure sensing transducers in the test-rig, was achieved by using a 12 V relay board that was connected to a National Instruments 9481 DAQ module Figure 3-10. The relay board utilised DC current that was supplied from a 30 V DC regulated laboratory power supply. The positive and negative cables from the 30 V DC laboratory power supply were looped in the relay board to connect the cables supplying power to the electric solenoid in the VRI valve. The signal cables were connected from the DAQ module and relayed signals generated using the LabVIEW DAQ software to either open or close the valve. The control signal was defined as the duty-cycle of the valves through

the LabVIEW software interface and controlled the duration of opening and closing of the valves. The signal generated energised the solenoid and this maintained the valve in open position and it was de-energised to close. The description of the solenoid valve control signals in the LabVIEW program is described in more detail in Section 3.2.5.

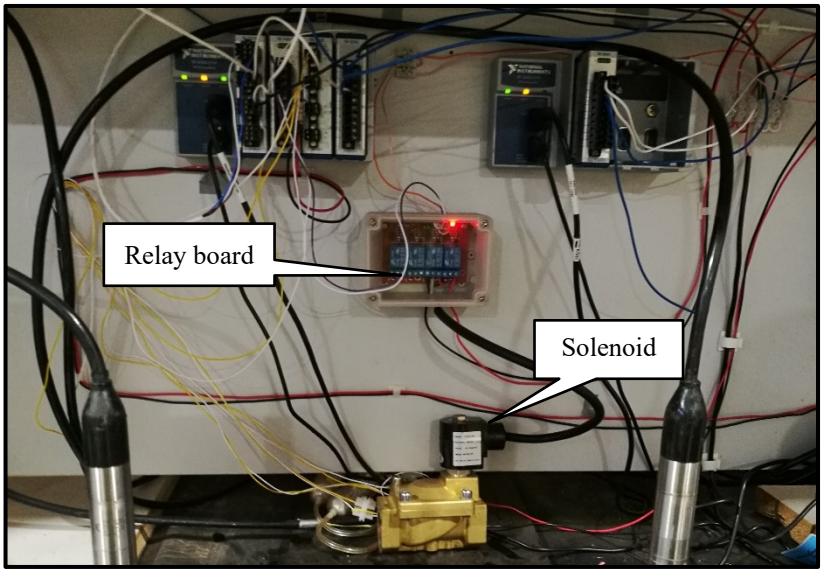

Figure 3-10: Connection of a VRI-iS solenoid valve to a relay board and a National Instruments (NI) DAQ module when air tested for pulsing

3.2.5 *Electronic Data Acquisition (DAQ) System*

This automatic electronic multi-function test apparatus employed a set of high-precision sensors (flow meter, upstream pressure transducer, downstream pressure transducer, and a resistance temperature detector). These electronic measuring devices were connected to, and controlled by a set of DAQ hardware modules mounted on two discrete National Instruments compact DAQ chassis providing voltage signals for the LabVIEW software (Figure 3-11). The specifications and measurement processes for these devices are discussed in Section 3.2.5.1 through to 3.2.5.3. The DAQ modules were each assigned specific sampling frequencies depending on the particular stage of testing, and the quality of data required (Section 3.2.3).

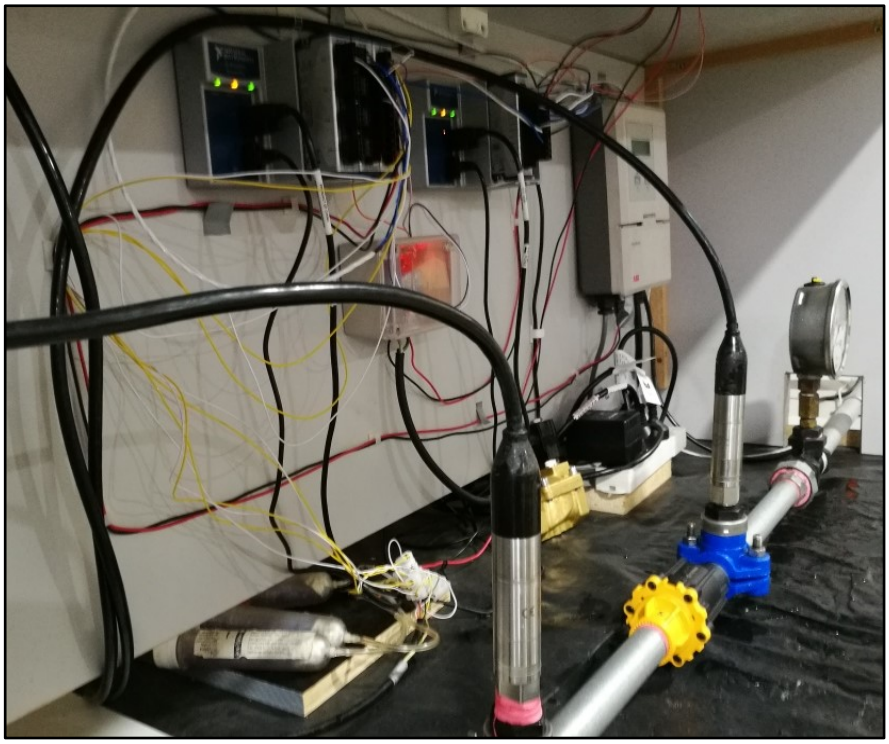

Figure 3-11: National Instruments DAQ modules mounted on compact DAQ chassis

Sampling rates during the Stage 1 testing phase were designed to sample at 1 kHz for 300 seconds, and record one second averages of the sampled data. Stage 2 testing had a continuous sampling frequency of 10 kHz and recorded the data as millisecond averages for 60 seconds immediately prior to solenoid valve closure. The high frequency used during this stage of testing was designed to capture the fast propagation of transient pressure waves when a solenoid is energized to close or open. Stage 3 testing permitted sampling of pressure regulator hysteresis when the valve moves from the fully-shut position to fully-open position, back to the fully-shut position controlled within a pre-set pressure range initiated in the main software window used for this testing phase. The sampling frequency was identical to Stage 1, except that measurements are recorded for a total duration of 180 seconds. However, for precise and complete characterisation of pressure regulator performance, other tests such as the minor loss and regulating accuracy are conducted using the Stage 1 process. The Stage 4 method was also configured with a 10 kHz frequency so as to characterise the response of pressure regulators when operating under the influence of VRI transients.

3.2.5.1 Discharge Measurement

Section 2.1.3 introduces the principles of discharge measurement which can be achieved by using a range of commercially available equipment. The flow meter used in this multi-function apparatus is a 15 mm nominal bore ABB Instrumentation MagMaster HA3 electromagnetic flow meter (serial number P/23730/1/1), capable of resolving flow rates with an accuracy of +/- 0.15% of full flow. This type of electromagnetic flow meter generates a magnetic field that is distorted in direct proportion to the velocity of the fluid and an induced voltage for measurement. With the known cross-sectional area, the discharge is computed using Equation 2.6. It was equipped with inlet and outlet flange fittings to enable the connection of 12.7 mm NPT (BSP) male connectors on both ends. The flow meter readings are displayed on the ABB digital transmitter, along with velocity. The ABB MagMaster flow meter had an analogue output of 4 to 20 mA linearly correlated from 0 to 0.9 L/s. However, a 467.7 Ohms Shunt resistor with a standard accuracy of 0.005 % was used to convert the 4 to 20 mA current output from the flow meter transmitter to the voltage required for the LabVIEW DAQ system, using the relationship expressed by Equation 3.1:

$$V_e = IR \tag{3.1}$$

where: V_e = voltage in Volts, I = current in Ampere, and R = resistance in Ohm.

This resistor was connected to a 4-channel National Instruments 9222 DAQ module which communicated voltage signals to LabVIEW. The voltage range was set at 0 to 10 V. The flow variation configured during testing using the automatic control of the LabVIEW software, was limited to 0.005 L/s. This band rate represents a 10 % to 0.8 % range for the lowest and highest flow rates tested. Mohr (2011) used a 10 % band rate which was controlled by a pair of levers for manual control of the throttling valves across the full range of tested flow rates.

3.2.5.2 Pressure Measurement

Pressure measurement is an integral part of testing any pressurised hydraulic system. A Bourdon gauge is commonly used to monitor and measure the amount of pressure

in the system. This type of device usually contains a metallic tube or diaphragm that flexes when fluid pressure rises. It is this flex or movement that is measured and transferred to a visual dial or some electronic data collection system, depending on the application and accuracy required. Electronic pressure measurement often uses pressure sensitive transducers (PST) which can be more accurate than other forms of pressure measuring devices such as Bourdon gauges. They contain strain gauges that sense the flex or displacement of a thin metallic diaphragm and transmit the measured fluid pressure as voltage signal that can be read by any electronic DAQ system.

This experimental apparatus was equipped with Druck PMP 4030 series pressure sensing transducers which were connected through 4 mm orifices using polyethylene metric tapping saddles designed according to ISO 13460-1:2015. The ISO standard requires that the diameter of pressure taps be between 3 and 6 mm for pipes with diameters of 50 mm or less and this apparatus was built using 19.05 mm galvanized steel piping. The pressure transducers output amplified voltage signals to a National Instruments 9263 DAQ module recording the pressure readings in LabVIEW as *.lmv* data files. The serial numbers for the Druck PMP 4030 series pressure transducers with an accuracy (non-linearity and hysteresis) of +/- 0.08% best straight line (BSL) are 1833125 and 1820216 respectively. The upstream pressure transducer, designated PT-1, was rated at 400 kPa while the downstream pressure transducer, PT-2 was rated at 250 kPa. The pressure transducers can withstand momentary over-pressure twice their rated pressure. Input supply voltage can be between 9 and 32 V DC. During testing, the open atmosphere side of the pressure transducers was vented with air that was passed through silica gel desiccant that was reconditioned through oven drying at 100 °C for 1 hour.

In the test apparatus, the pressure transducers were installed on the upstream and downstream side of the test specimen, and were supplied with voltage by a 30 V DC laboratory power supply. A minimum distance between the pressure taps and the specimen is required to avoid disturbance in pressure measurements caused by turbulence. Hence, the upstream pressure transducer was positioned at 2 pipe diameters from the test specimen, while the downstream transducer was positioned at

10 pipe diameters from the specimen (ISO 9644:2008). The elevation offset for the pressure transducers was measured, and was then used to raise pressure recordings, post-testing.

A pair of WIKI fluid damped 100 mm Bourdon pressure gauges with a reading accuracy of +/- 0.5 % were hydraulically coupled with the apparatus to aid in the manual control of the pressure in test-rig. Both pressure gauges had a maximum scale of 600 kPa, and they were installed on the upstream and downstream sides of the electronic pressure sensing transducers. An additional gauge with a maximum scale of 300 kPa was installed upstream of the butterfly valve on the inlet side of the entire test apparatus, to monitor and help maintain a constant stable supply pressure from the header tank.

3.2.5.3 Temperature Measurement

Temperature monitoring is important when conducting scientific experiments in hydraulic systems because it affects properties of the fluid such as density and viscosity. Figure 3-12 illustrates that the density of water decreases with an increase in temperature. However, the viscosity also tends to decrease when temperature increases. Recommendations within ISO Standard 9644:2008 state that temperature measurements should always be taken with any temperature sensing device of reasonable accuracy installed upstream of any throttling valves, and that water temperature should be maintained between 5 °C and 35 °C.

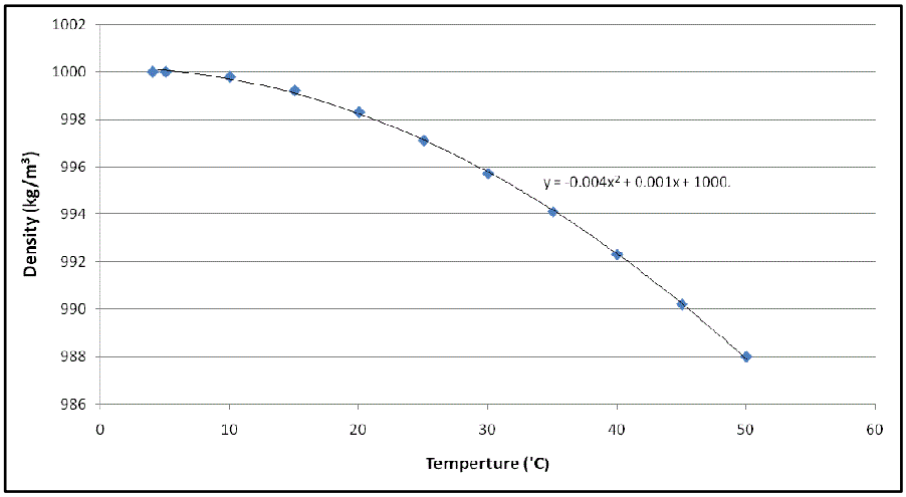

Figure 3-12: Relationship between temperature and density of water (Mohr, 2011)

Water temperature was measured in this test apparatus with an industrial insertion M12-PT100 RTD temperature sensor that was installed immediately downstream of the flow meter, and just upstream of the first automatic control valve at about 80 pipe diameters upstream from the first pressure transducer. This insertion RTD sensor was installed through a tee-piece fitting with its probe always submerged in the flowing water during testing. A 3 m insulated and jacketed M12CFM-T24SSPC-SFSR-FL cable with a straight socket connector was used to wire the RTD sensor to a National Instruments 9219 DAQ module. It measured the temperature via electrical resistance with the output signal placed into the National Instruments 9219 DAQ module, and the data recorded by the LabVIEW software. A temperature monitoring display was also provided in the LabVIEW software interface for the test-rig operator.

3.2.6 *Electronic Valve Control System*

The most critical components of this new automatic multi-function hydraulic test apparatus being developed are two electronically actuated control valves, one on the upstream side of the test specimen and a downstream throttling valve to control pressure head and discharge through the apparatus. This arrangement was first proposed by von Bernuth and Baird (1990) who observed in their experiments that the manual control of throttling valves could compromise the distribution of data points in pressure regulator outlet pressure hysteresis curve, thereby affecting the analysis and

results. They then hypothesized that automation of the throttling valves and data collection procedure would be able to generate closely spaced even spread data points to improve this pressure regulator performance characterisation process. Nevertheless, their work did not cover any scope of this automation process. The only work which is reported in the literature to have integrated automation, though only for automatic data collection is by Mohr (2011).

3.2.6.1 Specifications of the Test-Rig Automatic Control Valves

The initial configuration of the automatic multi-function hydraulic test apparatus employed a set of control valves that were electrically driven or controlled by Belimo NR24-3 actuators. These valves were previously used for manual control by Mohr (2011), through a bypass of the electronic control mechanism because they did not have feedback control voltage for high precision control. These actuators were later changed to LR24A-SR models (Figure 3-13), with feedback control to permit valve opening control using DC voltage. Each valve comprised two components; the main mechanical valve, and the electronic control actuator. The mechanical valves were typical ball valves equipped with an additional characterising disc positioned immediately upstream of the ball to enhance control over the flow passage size. The concave cross-section of the disc regulates flow with the ball movement such that any valve movement anywhere in the range of opening creates the same discharge change, and has a head loss coefficient K that is always equal to 1. This control mechanism also prevents initial turbulence in flow when the valve is opening.

Figure 3-13: Configuration of the Belimo LR24A-SR actuator with a ball valve equipped with a characterising disc in the test apparatus

The Belimo electronic control actuators provided electronic control to the valves through damper shafts that are connected to rotary manual knobs situated on top of the actuator housing and bolted down to the threaded female fittings of the main valve. The rotary manual knob would permit temporary and permanent disengagement of the gearing latch, therefore enabling switching between automatic and manual operational modes. The rotary angle of ball movement was a maximum of 90° with a corresponding run time of 90 seconds for the upstream valve and 80 to 110 seconds for the downstream valve from a fully-closed to a fully-open position. The response time (time taken for the control valve to respond relative to the time when a signal is created) for this type of Belimo valves was greater than 90%. The power and ground cables for the upstream valve was wired into a National Instruments 9481 DAQ module while those for the downstream control valve were wired to a National Instruments 9219 DAQ module. The signal wire was connected to a National Instruments 9263 DAQ module which received signals which were processed and then provided in the LabVIEW software for the user. The supply voltage for the Belimo valves could be 24 V AC/DC, but DC voltage was supplied for this test apparatus. Control voltage was set at 0 to 10 V DC with 1000 voltage steps between a fully closed and fully open valve position.

A precision orifice (orifice diameter = 9.72mm) installed on the downstream end of the apparatus was also used to provide additional control to the discharge and head through the apparatus.

3.2.6.2 Test-Rig Valves Control Algorithms

In order to execute the custom functions of test protocols designed for the novel automatic multi-function hydraulic test apparatus, an algorithm was needed. However, since the experimental sets were discrete, and that they required different test-rig configurations, separate algorithms had to be developed to achieve this experimentation process. Two different types of algorithms were written in the LabVIEW software code. The first code, was designed to continuously control the movement of the valves independently using the voltage steps, depending on whether the adjustment in flow is desired on the upstream or on downstream side of the test-rig. The code was configured to drive the valve for approximately 20 % of the opening duration, before any data could be recorded, because this percentage was tested experimentally and found to be a dead zone where no flow occurred regardless of the valve movement. This code was suitable for Stages 1, Stage 2, and Stage 4 Test Methodologies of the automatic multi-function test apparatus.

The second algorithm was designed and written specifically for the Stage 3 Test Methodology to characterise outlet pressure hysteresis on CP&LM pressure regulators. This code was written to control the movement of the upstream valve to open one step every two (2) seconds, while the LabVIEW DAQ system completes a check to determine if the flow is within a set tolerance band, before the downstream valve could automatically adjust to stabilise flow in cases when it is outside the tolerance band. The appropriate movement step duration was achieved through an iterative process undertaken between five (5) and one (1) second steps, in that sequence. The algorithms uses control voltage signals to automatically actuate a stepper-motor which drives the mechanical valves. The control voltage is set at 10 V with 1000 steps for each of the valves. This electronic movement of the test-rig control valves is controlled by using LabVIEW software toggle buttons which are designed

and placed on the dashboard. The detailed procedure of outlet pressure regulator hysteresis characterisation using this control valve algorithm is covered in Chapter 4.

Testing of the functionality of the control algorithms developed involved pressure head and discharge adjustments in the test apparatus. Table 3.1 shows the effects of the automated test-rig control valves on the pressure head and discharge, when there was no test specimen installed in the test apparatus.

Table 3-1: Electronic control valve's effect on pressure head and discharge in the automatic multi-function hydraulic test apparatus

		Resultant Discharge Effect	Resultant Inlet Pressure Effect	Resultant Outlet Pressure Effect
UPSTREAM VALVE	Opening	Increased	Increased	Increased
	Closing	Decreased	Decreased	Decreased
DOWNSTREAM VALVE	Opening	Increased	Decreased	Decreased
	Closing	Decreased	Increased	Increased

3.3 Summary

This chapter presented a proof of concept in the development and application of an advanced novel automatic measurement system for conducting hydraulic experiments. The automated experimental measurement apparatus integrates high precision sensing equipment and LabVIEW software graphical programming language as a platform for automation and data acquisition. It encompasses four different algorithms which are implemented as independent sub-models within the LabVIEW software interface. The first sub-model (Stage 1) offers capability to characterise the minor head loss for solenoid actuated VRI valves, sub-model 2 (Stage 2) offers capability to pulse and capture pressure wave transients from solenoid VRI valves, sub-model 3 (Stage 3) offers capability to characterise pressure regulator outlet pressure hysteresis, while sub-model 4 characterises the hydraulic response of CP&LM pressure regulators from

VRI transients. Sub-model 1 (Stage 1) also measures other pressure regulator performance characteristics such as, regulating accuracy, regulation curves, and static friction or minor head loss. Regression models were developed to produce pressure, discharge, and water temperature measurements from voltage and/or current signals obtained from sensing equipment. The appropriate test methods for utilising this novel system in the laboratory experimentation, to achieve the objectives of this research are presented in the Chapter 4.

4. DEVELOPMENT AND APPLICATION OF EXPERIMENTAL TESTING METHODOLOGY

4.1 Introduction

A detailed description of a novel system capable for automatic characterisation of the hydraulic performance of solenoid actuated VRI valves and pressure regulators used in CP&LM irrigation machines has been presented in the previous chapter. The present chapter discusses the development and application of a suitable testing methodology for implementing the new apparatus in the Engineering Hydraulics Laboratory (Z113), to achieve the experimental objectives of this research. Section 1.6 outlines the main objectives of the research. The suite of novel custom-built methodologies were developed through incremental alterations and calibration of the test apparatus to simulate field operations encountered by VRI machines equipped with pressure regulators. The ultimate goal was to commission a test procedure that is capable of producing accurate, repeatable and reliable results.

4.2 Types of Experimental Tests

The initial process in the development of the novel measurement techniques required prior identification of all datasets and possible experiments needed to be completed to address the objectives of this research. This exercise had already been implemented during the development phase of the automatic multi-function hydraulic apparatus, to arrive at the four discrete testing Stages designed in the LabVIEW computer program discussed in Section 3.2.3. The experiments that were planned for this unique extensive testing program were classified into two (2) broad categories, namely; (1) solenoid actuated (VRI) valve testing, and (2) pressure regulator performance testing, both for a range of nozzle discharge rates common under CP&LMs. There were a total of seven (7) different test types planned under these two broad experimentation categories. The set of experiments that were planned under Category 1 include (i) minor head loss testing, (ii) hydraulic transients testing during pulsing. The

experiments that were planned to be completed in Category 2 type of testing are (i) pressure regulation accuracy, (ii) pressure regulation curves, (iii) hysteresis on pressure regulator outlet pressure, and (iv) minor head loss. An additional set of different experiments were required to understand the impacts of VRI transients on pressure regulator performance, where the VRI valve and pressure regulator could be arranged so that the effects of valve pulsing on the pressure regulator can be measured. The detailed measurement procedures developed to accomplish each of these tests are discussed in Section 4.4, subsequent to a logical and scientific calibration of the automatic multi-function hydraulic test apparatus, as described in Section 4.3 below.

4.3 Calibration of Electronic Measurement Equipment

Before undertaking repeatable scientific measurements, a complete understanding of the accuracy, reliability, and limitations of the measuring equipment used is essential. This is critical in describing the quality, interpretation and application of measurement data. This research experimentation focused on the measurement of three main hydraulic parameters; pressure head, discharge, and water temperature. Calibration of the electronic measuring devices selected for the construction and utilisation of the automatic multi-function hydraulic measurement apparatus, such as the flow meter, pressure sensitive transducers, and temperature sensor were undertaken to ensure that highly accurate and repeatable measurements with small to negligible differences (high precision) were maintained throughout the experimental testing program. The sections below discuss the specifications and measurement capability as well as the calibration processes that were conducted for each of the electronic measurement equipment.

4.3.1 *Electromagnetic Flow Meter*

An ABB MagMaster electromagnetic flow meter used in the test apparatus was previously calibrated and certified before purchase by an accredited NATA flow testing and calibration facility. It had only been used once, prior to this research experimentation. Since the flow meter had a standard 4-20 mA current output signal, it was converted to an output voltage signal with a high quality Shunt resistor that

allowed LabVIEW DAQ to measure the discharge as voltage. Measurements were recorded from the LCD digital display of the flowmeter at approximately 0.1 L/s increments, between 0 and 0.92 L/s along with voltage readings taken using the LabVIEW DAQ software interface. The voltage was set at a maximum of 10 Volts in the LabVIEW software interface. It was validated manually by measurements taken using a FLUKE 115 TRUE RMS multimeter. To ensure that accurate flow readings were obtained during testing, the flow meter was electrically grounded using an appropriate earthing cable located at about 2 m from the laboratory test bench.

A volume balance method was used to validate the discharge readings of the ABB MagMaster electromagnetic flow meter, which were displayed on the digital LCD transmitter during testing. The procedure employed a 15 L water drum that was calibrated previously using a 1000 mL graduated plastic measuring cylinder (Appendix B). The time taken to fill this drum using the test-rig discharge when a pre-set flow rate of 0.2 L/s was tested, was recorded. The downstream end of the test-rig which is fitted with a precision orifice was modified to a 19.05 mm x 1 m clear garden hose to enable direct filling of the drum. Measurements were repeated five times and used to covert the volume to a discharge in L/s. An additional discharge of 0.35 L/s was set in the test-rig and a similar test procedure was applied. The average results obtained from this numerical computation were compared with the discharge obtained in the digital LCD display, with a maximum flow variation of 1.2 % obtained amongst readings. ISO 9644:2008 recommends a maximum permissible flow variation of 2 %. Therefore, with such an acceptable variation in flow, a linear regression model was fitted (Equation 4-1) to the data measured with the electromagnetic flow meter to calibrate the flow scale in the LabVIEW software and permit instantaneous digital flow measurements (Appendix B).

$$Q = 0.12V_e - 0.224 \qquad 4.1$$

where: Q = flow rate in L/s and V_e = voltage in Volts.

4.3.2 *Pressure Sensitive Transducers*

The electronic calibration of the Druck PMP 4030 series pressure sensitive transducers was undertaken using a Druck PV211 pneumatic pressure and vacuum hand pump connected to a digital pressure indicator (Druck DPI 802) as illustrated in Figure 4-1. The pressure transducer output voltage was set at 0 to 5 V. A series of trials were conducted to ensure that the threaded connections between the PV211 and pressure transducers were not leaking. To avoid compromising the quality of pressure readings, leak detection tests were conducted by applying a fixed amount of pressure on the pneumatic hand pump and releasing its arms to achieve stable and constant pressure values when no adjustments were made and that no pressure is bled from the test unit. Pressure measurements were taken at 10 kPa increments for both the 400 kPa and 250 kPa range pressure transducers.

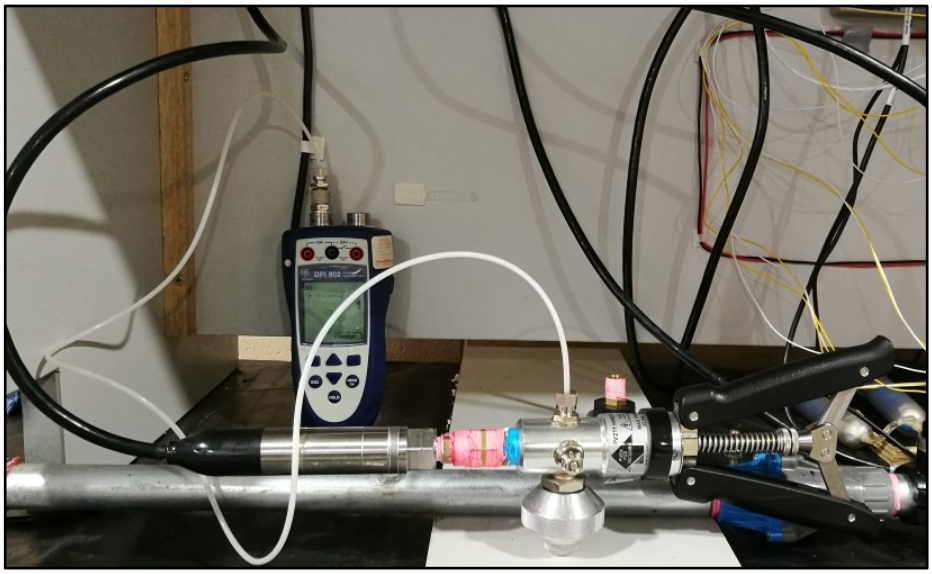

Figure 4-1: Calibration of pressure transducers using a Druck PV211 pneumatic pressure hand pump with a *Druck DPI 802*

Validation of the consistency and repeatability of the voltage and pressure readings obtained from the electronic pressure transducers calibrations were conducted by using the (1) pressure head from the constant header tank system and cross-examined using the WIKI fluid damped Bourdon gauges, and (2) by means of a portable high precision digital pressure indicator (Druck DPI 705) as shown in Figure 4-2, which is later referred to as the third pressure measurement option. The calibrations for the pressure transducers using the static head from constant header tank attempted to generate

equivalent voltage readings and used the separate linear regression models (Equation 4-2, 4-3, and 4-3) to convert these into pressure readings in LabVIEW. The first point of calibration for the upstream transducer had the downstream throttling valve fully opened, and the second point with the throttling valve fully closed to represent the maximum static head available upstream of the test specimen. The downstream pressure transducer was calibrated by establishing zero hydraulic head difference with the throttling valve completely closed. Under this condition, there was no flow through the solenoid valve as it was kept energised (opened) throughout the process to avoid creating a differential pressure upstream and downstream of the valve. A second hydraulic head difference was created by completely opening the downstream throttling valve. This condition provided the highest pressure differential point on the calibration curve.

The elevation offset of the pressure sensors were factored into the numerical computations of the resulting pressure readings. The voltage was measured using a FLUKE 115 TRUE RMS multimeter and correlated with the voltage readings obtained from LabVIEW. Both methods produced similar voltage results at the corresponding pressures. Linear regression models, each with $R^2 = 0.9999$ were then developed to calibrate the LabVIEW DAQ software (Appendix A).

$$P = 79.896V_e - 0.8426 \quad 4.2$$

$$P = 49.935V_e + 1.5407 \quad 4.3$$

$$P = 52.154V_e - 7.1416 \quad 4.4$$

where: P = pressure in kPa and V_e = voltage in Volts.

A third approach, numbered as 2 earlier, for validating the pressure transducer calibrations utilised a Druck DPI 705 that was connected through a pair of Schrader valves fitted on a tee piece from the test-rig piping, and one-quarter inch BSP and air-chuck fittings via an equal size clear tubing. The DPI 705 was connected to measure pressure readings immediately downstream of the pressure transducers when the constant header tank calibrations were undertaken during zero flow conditions.

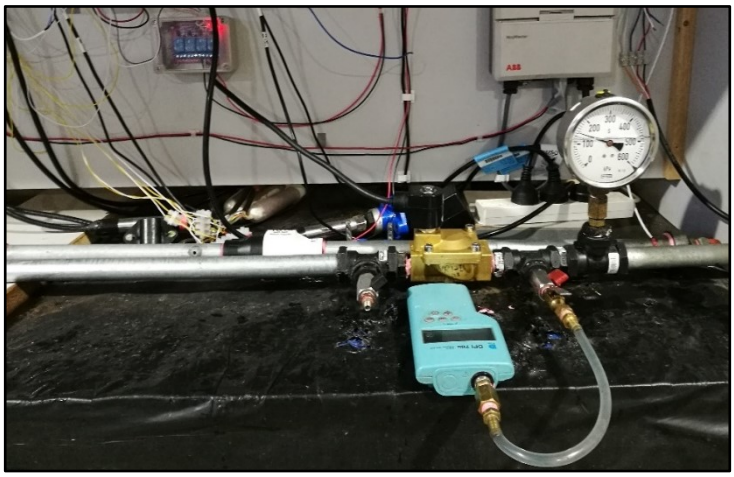

Figure 4-2: Calibration of static head from constant header tank using a Druck DPI 705 digital pressure sensor

4.3.3 *Resistance Temperature Detector*

The temperature (RTD) sensor was calibrated using a *Brannan* red spirit submersible thermometer with an accuracy of 0.5 °C that was dipped into a mixture of cold water and ice. To achieve this, the RTD sensor was removed from the test-rig and its probe immersed in the cold bath together with the tip of the red spirit thermometer. Once the temperature on the thermometer had reached 0 °C, a corresponding voltage reading was fixed in the LabVIEW software interface. Both instruments were then removed from the ice bath and their sensing tips immersed in the discharge at the downstream end of the apparatus for 120 seconds, to provide data used to develop a linear relationship between water temperature and the RTD output as interpreted by the LabVIEW DAQ system. The electronic control valves were both completely opened to prevent temperature rise due to friction and viscous energy dissipation during the calibration process.

4.4 Development of Testing Procedures

The development and application of the new test methodologies for the novel automatic test apparatus utilised LabVIEW software interface test Stages 1 to 4 inclusive, which are presented in Chapter 3 (Section 3.2.5). The rationale for the four (4) testing stages against a total of seven (7) different types of experiments, is due to the fact that some of the test stages could be easily modified to accomplish other experiment types, without having to write and package a completely new and different LabVIEW code for these tests. This will be explained in more detail in the different experimental procedures. The Stage 1 Test Method is designed to measure the minor head loss for VRI valves, Stage 2 Test Method is designed to measure the hydraulic transients generated by VRI valve pulsing, Stage 3 Test Method is designed to measure hysteresis in pressure regulator outlet pressure, and Stage 4 Test Method is designed to measure the hydraulic response of pressure regulators from the impacts of unsteady VRI transients. Each of these test methods required an independent and complete procedure which details the configuration of the main hydraulic apparatus, its integration with the specific LabVIEW software interface test protocol, as well as the necessary processes and/or adjustments of key components to arrive at the most accurate, repeatable and reliable measured data sets. These are discussed in detail under each of the specific test types below.

Preliminary measurements using these novel techniques proved that the test apparatus needed further improvements, especially for some experiments, to refine it to be capable of achieving all the study objectives. When all the modifications and improvements had been completed and calibrated, a second set of measurements was undertaken, and an extensive experimental testing program was commissioned utilising the test methods developed for each of the experimental sets.

4.4.1 *Measurements of Pressure Head Losses in VRI Valves*

The measurement procedure for determining the minor pressure head loss for VRI valves was developed using the LabVIEW Stage 1 Test Methodology (Section 3.2.3.1) described in Chapter 3 for the automatic multi-function apparatus. This LabVIEW test

protocol enabled the electric operation of VRI valves using a duty cycle, which could be manually inputted in LabVIEW using toggle buttons. This required the VRI valve to remain energised for the duration of the testing for normally closed (NC) valves, as opposed to normally open (NO) VRI valves. This was achieved by using a relay board that was kept powered by the DC laboratory power supply to maintain the VRI valve in an open position. This type of testing is novel because the ISO Standard 9644:2008 does not cover the hydraulic characterisation of electrically actuated irrigation control valves.

During the preliminary measurements for developing this test method, a single VRI valve was used. The test specimen was installed between the upstream and downstream pressure sensors, ensuring that no water was leaking. Entrapped air was removed from the test apparatus by manually opening the automatic control valves sequentially, after the butterfly valve from the header tank system was fully opened to flood water into the apparatus. The LabVIEW script was then started and a test discharge of 0.30 L/s entered into the input panel so that the automatic valve could continually adjust automatically and until the set-point discharge was achieved, or maintained through the apparatus. The valve movement always began with the downstream throttling valve opening by 20 %, before the upstream valve could begin to open and allow flow through the test specimen. When the desired test discharge is achieved and has stabilised, the LabVIEW DAQ system begins to save data, including the pressure upstream of the test specimen, the downstream pressure, control voltage, discharge, and water temperature. The last movement to control discharge was always maintained on the upstream test-rig control valve to ensure that the data being recorded was for a rising inlet pressure. The rationale for ensuring this type of control mechanism will be understood in more detail when describing measurements taken at unsteady-state conditions or when the inlet pressure was decreasing. This experiment was allowed to run for three (3) minutes, recording one (1) second averages of data at 1 kHz frequency. The same measurements were repeated five (5) times with flow and head closed off from the apparatus in between tests. Pressure difference analysis results were conducted and these produced similar results, highlighting the precision with which the automatic apparatus captured the data. The pressure difference across

the VRI valve was validated through measurements taken from the manual Bourdon gauges, with negligible differences when compared to the LabVIEW data.

When this test procedure was deemed to be appropriate for conducing minor head loss measurements for the valve, the minor head loss experiments for different valve brands, including more valve units, across the full range of nozzle flow rates, were conducted. Pressure head loss measurements conducted according to this type of setup are referred to as test bench pressure loss (ISO 9644:2008). The bench pressure loss measurements were taken successively in progressive steps to cover the entire range of nozzle flow rates from 0.05 to 0.70 L/s. When the VRI valve pressure loss tests had been conducted for up to the maximum discharge of 0.70 L/s successively, another set of measurements were taken with a decreasing discharge from 0.70 to 0.05 L/s. This approach was meant to verify the robustness and precision of the test-apparatus, or any performance characteristic difference on the valves when the measurements were taken differently. Care was always maintained to ensure that the last control movement was for the upstream test-rig valve to induce a rising inlet pressure. For the decreasing flow rates, this was achieved by controlling a discharge to a point slightly below the desired test discharge, so that the final adjustment from the control mechanism will be effected by the upstream valve, thereby generating a rising inlet pressure.

The minor head loss, h_m, attributable to the test specimen alone were obtained by correcting the total measured head loss by the losses due to friction in the piping system between the pressure transducers. Pipe friction losses were determined by replacing the test specimen with an equivalent size (19.05 mm) polyethylene coupling fitting which coupled the pipe sections between the pressure transducers. The assumption was that the fitting did not introduce any significant amount of head loss in the system. The test specimen minor head loss, h_m, was then computed using the following equation.

$$h_m = \Delta h + h_f \qquad 4.5$$

where: h_m is the VRI valve minor head loss, Δh_m is the total head loss, and h_f is the test section friction head loss.

The minor loss coefficient $K_{\_vri}$ for the tested VRI valves was determined from Equation 4.6, after converting flow rates into velocity heads through the VRI valves cross-sectional area.

$$K_{\_vri} = \frac{h_m}{V^2 / 2g} \qquad 4.6$$

4.4.2 *Investigation of Hydraulic Transients from VRI*

Test procedures for simulating the on-and-off pulsing of VRI valves under conditions similar to the normal field operations of VRI equipped CP&LM machines, to determine the effects of VRI pulsing on the pressure head and discharge of these systems, were developed using the Stage 2 Test Methodology (Section 3.2.3.2) of the automatic multi-function apparatus. These measurements were aimed at determining the occurrence of transient pressure head waves (water hammer) under VRI pulsing, and establish a measure of peak hydraulic head generated, how fast these transients are, and the potential impacts and risks they present to the operation and structural integrity of CP&LMs. This type of test procedure is novel and does not follow any particular standard. The development of hydraulic understanding around the unsteady performance of CP&LMs is the focus of this dissertation.

The test method was built by installing the VRI valve test specimen according to the test-rig configurations described below, and energising the VRI valve to remain open for a defined period under a particular test flow rate, before triggering the VRI valve test specimen to close while LabVIEW captured the high frequency dataset. The valve duty cycle was kept constant and equal to 50 %, with an ability to vary the on-and-off times over 60 seconds, which in this case was considered to be a cycle. The LabVIEW computer program enabled alternations of opening and closing times and data saving process during testing as previously described for this Stage 2 Test Method in Section 3.2.3.2. The transients were collected for discharge rates between 0.05 to 0.70 L/s. All measurements in this type of testing were measured at a frequency of 10 kHz, and were analysed according to the maximum observed pressure heads for corresponding discharges. However, the estimation of wave speeds, *c*, was not possible because the

test-rig was not designed to measure changes in velocity, or the traveling times of pressure waves between pressure transducers.

Two different types of VRI valve configurations were examined, one with the valve positioned on the horizontal plane and in-line with the test-rig piping, so that the effects of valve closures would be transferred upstream of the apparatus and be sensed by the upstream pressure transducer, PT-1. This set-up was denoted *Configuration A* (Figure 4-3). The second test set-up, *Configuration B* (Figure 4-4), had the VRI valve installed off a tee piece and positioned in a vertical arrangement so that the effects of pulsing could be distributed in both the upstream and downstream pipe sections from the VRI valve take-off. This type of VRI valve configuration is typical for VRI installation on commercial VRI machines. An additional piece of pipe equipped with a nozzle was connected through a goose-neck to maintain specific and constant discharge. A total of ten (10) separate tests for each of the two valve configurations were conducted each running for a period 60 seconds, with pulsing varied in between this duration. Table 4-1 below shows the durations of opening and closing times and the corresponding duty cycles, including initial delay times that were adopted for this testing of VRI valves. The results of preliminary transients testing demonstrated that the key parameter that influenced propagation of pressure wave transients was the initial time delay because it impacted flow and head stabilisation prior to the valve closure. The results also showed that the duration of valve closure had no significant impact on the test results, hence this duration was maintained between 5 and 10 seconds for this testing. It was also evident that multiple pulses did not affect the results, and this test methodology was then fixed between one and two pulsing frequencies.

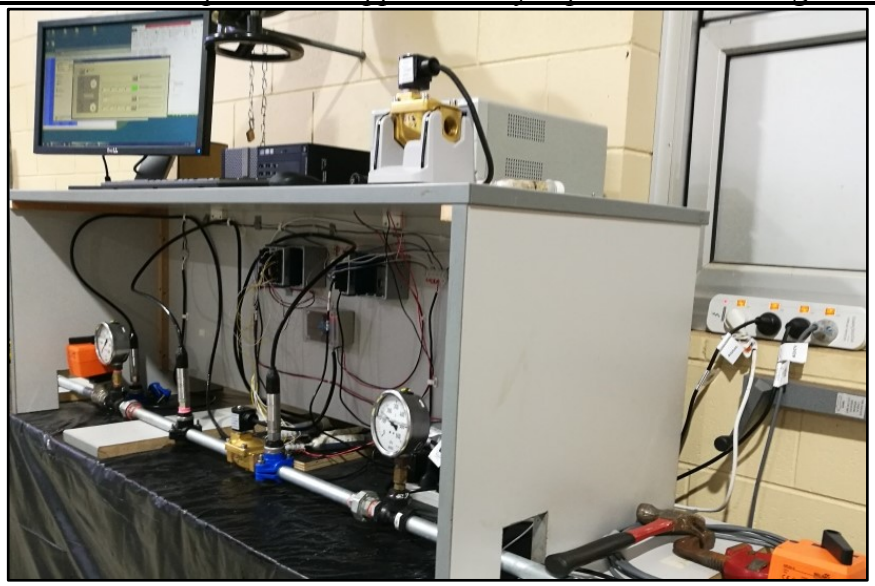

Figure 4-3: "Configuration A" of the VRI valve installation in the test apparatus

Figure 4-4: "Configuration B" of the VRI valve installation in the test apparatus connected to a 10 psi regulator via a gooseneck and fibre reinforced drop hose

Table 4-1: Frequencies and duty cycles used to test the solenoid actuated VRI valves

Test No.	Initial Time Delay (ON) (s)	OFF Time (s)	ON Time (s)	Duty Cycle (%)
1	5	5	5	50
2	10	5	5	65
3	15	5	5	75
4	20	5	5	80
5	30	5	5	85
6	5	10	5	35
7	10	10	5	50
8	15	10	5	60
9	20	10	5	65
10	30	10	5	75

Of critical importance in the fine-tuning of this hydraulic transient test procedure, was the response time from the moment a pulsing signal is generated by the LabVIEW software for the solid-state relays on the board to control the valve, and the actual time that the LabVIEW program could start recording data. When all measurements had been analysed and a relationship between flow rate and peak hydraulic head for the two study configurations had been developed, the procedure was adopted for extensive transient pressure wave testing. While the sequencing and modes of operation for VRI valves can be variable, especially on individual sprinkler controlled VRI CP&LMs, the scope of this work only focused on the effects of pulsing an individual valve, and does not cover the simultaneous effects from multiple valves.

4.4.3 *Operational Characterisation of Pressure Regulating Valves*

The test procedures for determining the functional characteristics of CP&LM pressure regulators were developed by installing a single regulator in the test stand, in accordance with Stage 1 and 3 test protocols, for a particular set of experiments, while maintaining a constant distance between the test specimen and the pressure sensors. The procedures being developed were designed to measure; (a) the ability of pressure regulators to maintain constant design outlet pressures as specified by their respective manufacturers, (b) the ability to maintain a constant outlet pressure with variable flow

rate at constant inlet pressure, (c) the ability to maintain constant outlet pressure with varying inlet pressure at constant flow rate (hysteresis), and (d) the amount of friction head loss through the pressure regulating devices. The range of nozzle flow rates used was also from 0.05 L/s to 0.70 L/s. Since the regulating mechanism of pressure regulators depends on the movement of the flow tube against a downward force generated by the mechanical spring, the position of the inlet pressure (rising or falling) to the regulator is of critical important because it determines the final regulator output pressure. Hence, all the pressure regulator performance tests, excluding hysteresis, were conducted with the inlet pressure rising as effected by the last opening or upward movement of the upstream test-rig control valve.

Nevertheless, to accurately measure the performance characteristics of the pressure regulating devices, a series of exploratory alterations in the configuration of the test apparatus were required for some experiment types of pressure regulator performance testing to provide test methodologies that could produce reliable results. The processes of developing these test methodologies using the LabVIEW Stage 1 and 3 Test Methods are discussed in the respective test sections below.

4.4.3.1 Regulation Accuracy

The test method for characterising the regulating uniformity of outlet pressure, or regulating accuracy, of pressure regulating valves, was developed using the LabVIEW Stage 1 Test Method. The single regulating valve used for this process was installed on the apparatus and a supply pressure equal to 1.5 times the declared pre-set pressure was applied with the inlet pressure rising, and at a corresponding flow rate equivalent to a reference velocity of 1.0 m/s as recommended by ISO 10522:1993. The flow rate corresponding to 1.0 m/s through the 19.05 mm valves was 0.3 L/s. Based on the declared pre-set pressures of the pressure regulator models intended for testing (Section 4.5.2), the following inlet pressures; 103.42 kPa for low pressure models, and 155.13 kPa for high pressure models were applied on the inlet or upstream end of the devices. Repetitions of this measurement process were conducted and data checked for consistency and deviation from the manufacturer stated pre-set pressure.

This test procedure was then adopted for testing all sampled CP&LM pressure regulators for outlet regulated pressure uniformity. This type of testing did not require any modifications to the apparatus. From the measurements obtained, the coefficient of variation, *CV*, was calculated according to Equation 4.7, which is:

$$CV = 100\frac{S_p}{p} \qquad 4.7$$

where: S_p = sample standard deviation of the regulated pressures (kPa), and p = mean regulated pressure of the sample (kPa).

Generally low *CV* values indicate proper quality control in the manufacturing process of the pressure regulating devices. The ISO Standard regards successful regulating accuracy to be achieved by pressure regulators that maintain outlet pressures within 10 % of the declared pressure setting.

4.4.3.2 ISO Standard Regulation Performance

ISO Standard 10522:1993 describes pressure regulator performance as the ability of the devices to maintain a constant outlet pressure with variable flow rate at constant inlet pressure, which is referred to as the regulation curve. The test procedure for measuring the regulation curve utilised the LabVIEW Stage 1 Test Method, where the selected pressure regulating valves, the low and high pressure models, were subjected to a range of inlet pressures at constant flow rates corresponding to velocities of 0.5, 1.0, 1.5, 2.0, and 2.2 m/s. These flow rates were equivalent to 0.15, 0.3, 0.43, 0.57, and 0.63 L/s for the 19.05 mm low pressure models, and up to 0.7 Ls for the high pressure models. The three inlet pressures applied for each of the flow rates were 1.5 times the pre-set pressure, 0.8 times the nominal pressure, and the inlet pressure set at the middle of the regulation range as recommended by the ISO Standard 10522:1993, ensuring a rising inlet pressure. Thus, the low pressure model was evaluated at 103.42 kPa, 515 kPa and 355 kPa, while the high pressure model was evaluated at 155.13 kPa, 550 kPa, and 400 kPa. From the measured data, graphs of regulated pressure as a function of flow rate were plotted for each model representing the three different pressure settings.

These experiments were repeated six (6) times for 300 seconds each, and data was recorded at 1 kHz.

After sample size selection (Section 4.5.2), the low pressure models for Brands X, Y, and Z were then evaluated at the same inlet pressures 103.42 kPa, 515 kPa and 355 kPa, while the high pressure models of the same brands were evaluated at 155.13 kPa, 550 kPa, and 400 kPa. From the measured data, graphs of regulated pressure as a function of flow rate were plotted for each model representing the three different pressure settings, as described above.

4.4.3.3 Hysteresis in Pressure Regulation Curves

The most important tests that needed to be conducted on pressure regulators were to determine the regulator outlet pressure as a function of inlet pressure, for constant flow rate, capturing the outlet pressure hysteresis. This type of testing represents the unsteady performance of pressure regulators when CP&LMs experience changes in supply head and discharge due to hydraulic conditions such as, elevation changes, fluctuations in groundwater tables, and VRI pulsing. Junior et al. (2018) conducted a study where the regulated pressure was evaluated as a function of inlet pressure at constant flow rate without factoring hysteresis. Regulator outlet pressure hysteresis is important for low pressure systems, and should be taken into account when evaluating or modelling regulator performance under varying inlet pressure and flow rates, which are often experienced by the devices when operated under unsteady conditions. Pressure regulator hysteresis testing for this study required automated continuous movement of the upstream automatic valve to generate rising and falling inlet pressures to the regulators, to record hysteresis in outlet pressure at different constant flow rates. ISO Standard 10520:1993 suggests that hysteresis tests should be undertaken at pressure increments of 50 kPa, a traditional approach which has been implemented previously by von Bernuth and Baird (1990), Mohr (2011), and Junior et al. (2018). The principal aim of this work was to automate this process to simulate in-field conditions for regulators when CP&LMs traverse undulating fields, when groundwater tables fluctuate, and when VRI valves pulses on-and-off. As a requirement to ensure that the results were reliable and repeatable, a novel, involved,

and tediously repetitive test method was developed. The Stage 3 Test Methodology (Section 3.2.3.3) and criteria in LabVIEW program was designed specifically for this series of testing. Figure 4-5 below shows the results of the application of the automatic test procedure when measuring pressure regulator outlet pressure hysteresis from the header tank system.

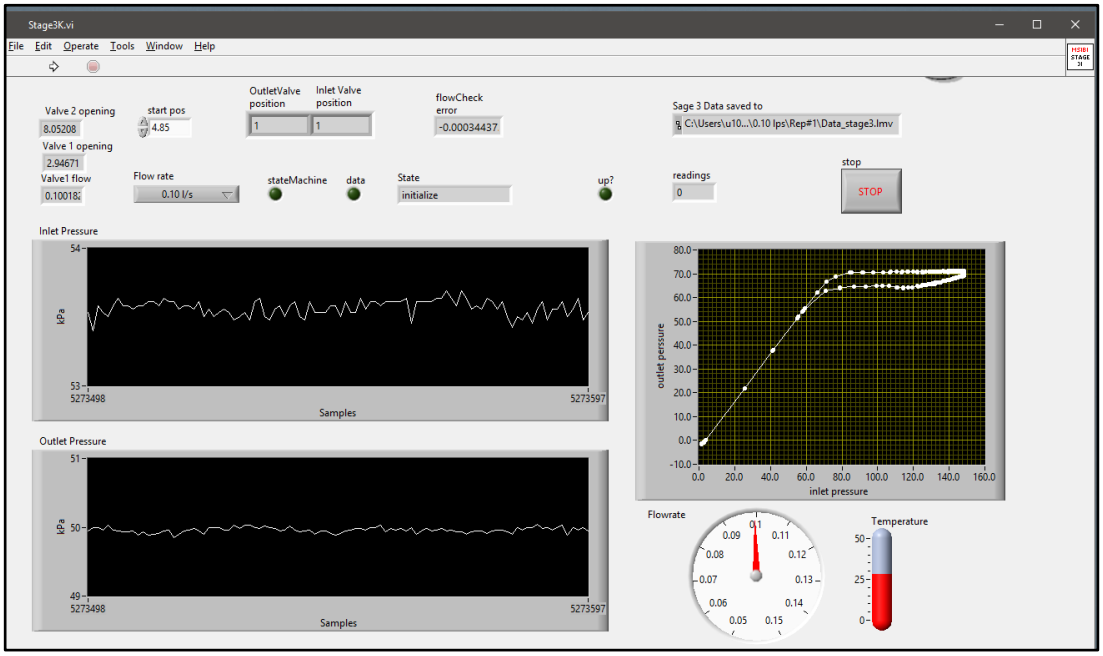

Figure 4-5: Pressure regulator outlet pressure hysteresis measured from the low head supplied by the header tank system, using the automatic test procedure in Stage 3

One of the main objectives of this work is to be able to develop an appropriate mathematical model which describe pressure regulator performance more accurately for a majority of modern low pressure CP&LMs, taking into account outlet pressure hysteresis. In this case, the total pressure head supply from the constant header tank system (Section 3.2.1) was not sufficient. The maximum inlet pressure required for this type of testing was 300 kPa, which is around the highest pressure usually received by pressure regulators near pivot points or LM carts. To meet these test requirements, a booster pump was coupled to raise the head. However, when the high pressure pump was introduced, it was no longer possible to control small incremental steps in inlet pressure, to obtain smooth data points across the hysteresis curve with the test-rig control valve automation. This system worked successfully for the simple procedures described in ISO tests because the 50 kPa increments could be adjusted manually to fix the pressure points throughout the entire curve. Hence, multiple approaches needed

to be trialled to solicit the most appropriate technique for automatic characterisation of pressure regulator outlet pressure hysteresis, so that the test procedure could yield a high density of data points spread across the hysteresis curve.

Modification of Valve Control Mechanism

The LabVIEW code for automating the movement of the upstream control valve relative to the downstream throttling valve to control head and discharge in the test-rig was initially written based on movement in two (2) seconds time steps as described in Section 3.2.6. The LabVIEW program would calculate the flow error, and transmit a signal to the downstream throttling valve to re-adjust the flow rate to be within a pre-defined flow rate band (tolerance), before test data is recorded and this process is restarted. This procedure worked flawlessly during testing under low head supply from the header tank system. When the pressure head was increased to 30 m with the auxiliary pump, it created significantly larger steps between data points such that it was very difficult to characterise hysteresis. The modulation of the test-rig electronic control valves was not great at this high inlet head. Therefore, the movement step duration (time-step) for the control valve was then reduced to one (1) second with a slight improvement in the measured data, though they remained unsatisfactory. This indicated that the test procedure limitations were outside the valve control algorithm, hence further modifications in the test-rig were still required to successfully complete automated pressure regulator outlet pressure hysteresis characterisation.

Pressure Head Reduction with Orifice Plate

A comprehensive and analytical hydraulic investigation was undertaken to reduce the total dynamic head into the apparatus to be as close as possible to the required 30 m of head, when the pump and header tank produced a total head of 65 m. A set of orifice plates with diameters of 4, 6, 8, and 10 mm were designed and fabricated in the Mechanical Workshop located at USQ. The orifice plates were each installed between the flow meter and the upstream test-rig control valve, immediately before the temperature sensor, to cover the range of flow rates to be tested. The idea was to introduce a significant head loss before the upstream test-rig control valve, since it was unable to generate this effect. Measured data using the installed orifice plates did not

yield any positive improvements, as the flow rate into the apparatus became compromised with small diameter plates. The data also exhibited large steps in outlet pressure hysteresis for the higher flow rates due to significant input head, and could not complete the entire regulation curve (Figure 4-6). Head reduction into the apparatus was insignificant. This outcome necessitated further investigations in the modification of the test-rig to enable the characterisation of pressure regulator outlet pressure hysteresis.

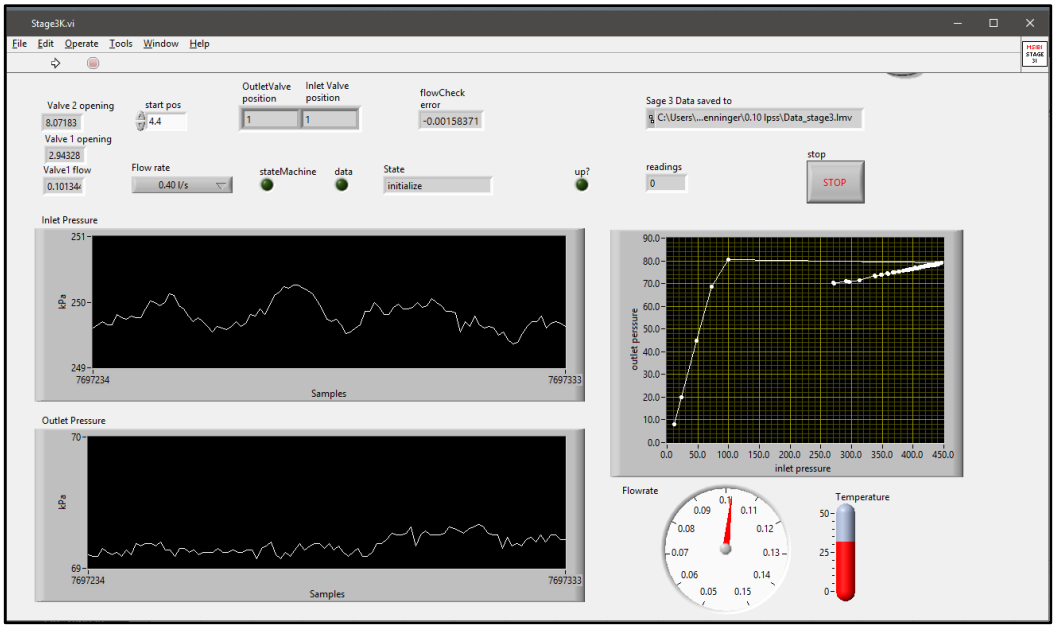

Figure 4-6: Big steps in regulator outlet pressure hysteresis data points when significant head is supplied to the test apparatus

Pressure Head Reduction with Flow Bypass

Another attempt to dissipate or reduce the total head supplied to the test-apparatus incorporated a bypass system from the pump discharge using a 19.05 mm equal tee and an equal size manual control valve. The tee piece was installed in such way that the straight sections of the tee were parallel to, and connected the pump discharge and the supply line into the apparatus. The tee section was connected to a bypass line that was controlled by the manual gate valve, and discharged excess flow into the concealed underground gutters which channelled water back to the underground tank. During testing, flow into the apparatus was regulated by continuous adjustment of the gate valve so that when low flow rates were being tested, the flow through the bypass system could be increased. Similarly, the bypass flow was reduced when the desired flow rate in the apparatus was close the maximum test flow rate. Although there was

a slight improvement in pressure regulator hysteresis measurements taken using this approach, especially in the falling limb of the hysteresis curve, they were still not satisfactory given the large step size between data points in the rising limb of the hysteresis curve (Figure 4-7). It was either, the flow control mechanism adjustment in the bypass was not very precise due to human error, or the combination of head reduction relative to the test flow rate were not sufficient. Hence, further ideas were still required to improve the hysteresis characterisation process.

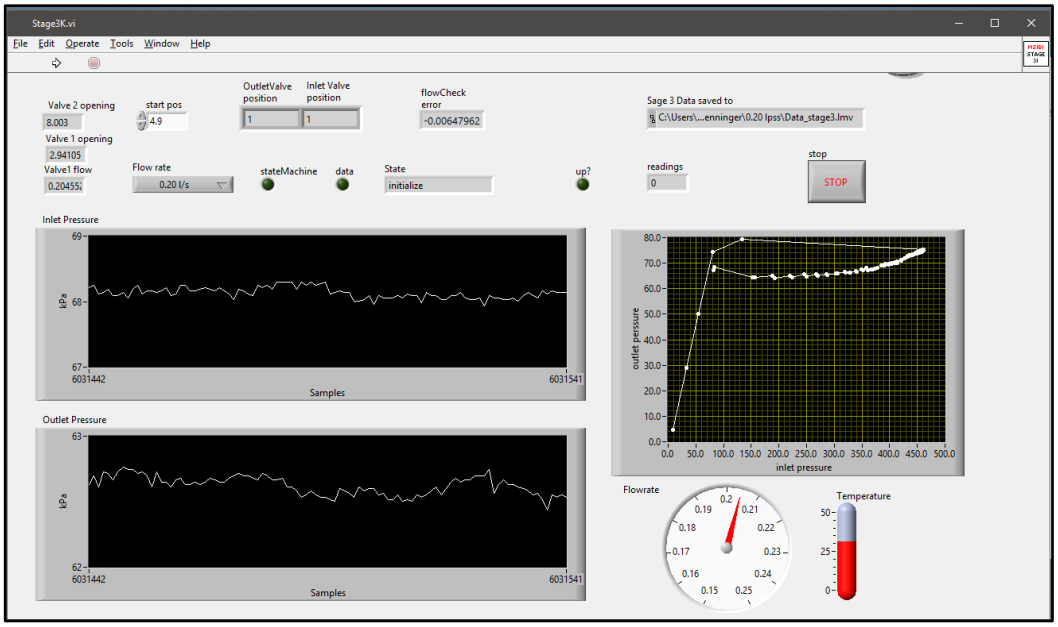

Figure 4-7: Pressure regulator outlet pressure hysteresis testing showing significant steps especially on the rising limb of the hysteresis curve when a significant head is supplied to the test apparatus

Pressure Head Reduction with Jet Pump

A different approach involving the coupling of a Jet pump in the test apparatus to provide a better control of discharge and head reduction was employed. The jet pump used was a DAB Jet 100 Max that was directly and closely coupled to a single-phase 0.75 kW 2-pole electric motor. The jet pump had a flow range of 0.4 to 3.3 m^3/h at 46 to 24 m head. This discharge corresponded with the maximum discharge of 0.92 L/s that was calibrated on the LabVIEW DAQ software and ABB electromagnetic flow meter, although the maximum test flow rate for pressure regulators was below this set point. The idea was that when coupled to the positive suction head of 16 m supplied by the header tank system, the total head available at the maximum discharge could still meet the maximum head of 30.6 m (300 kPa) required for pressure regulator

hysteresis testing. This pump was equipped with a pressure switch which enabled switching off when the pressure threshold was above a particular setting. Measurements with this type of pump did not yield any improvements in the pressure regulator outlet pressure hysteresis curve as inlet head was still high and maintained irregular data points in the curve.

Direct Suction from Underground Tank

Since the booster pump had capacity adequate to deliver the required head alone, including friction losses, the constant head supply tank was by-passed so that the pump would supply discharge directly from the underground storage using a 50 mm flexible corrugated polyethylene suction pipe (Figure 4-8). The suction lift from the reservoir was 4 m. The discharge line was a 25 mm diameter nylon reinforced clear hose of 20 m length, as the position of the underground tank was remote from the test apparatus. The substantial drop in head at the test-rig to 40 m from this configuration also did not improve outlet pressure hysteresis characterisation test result resolution.

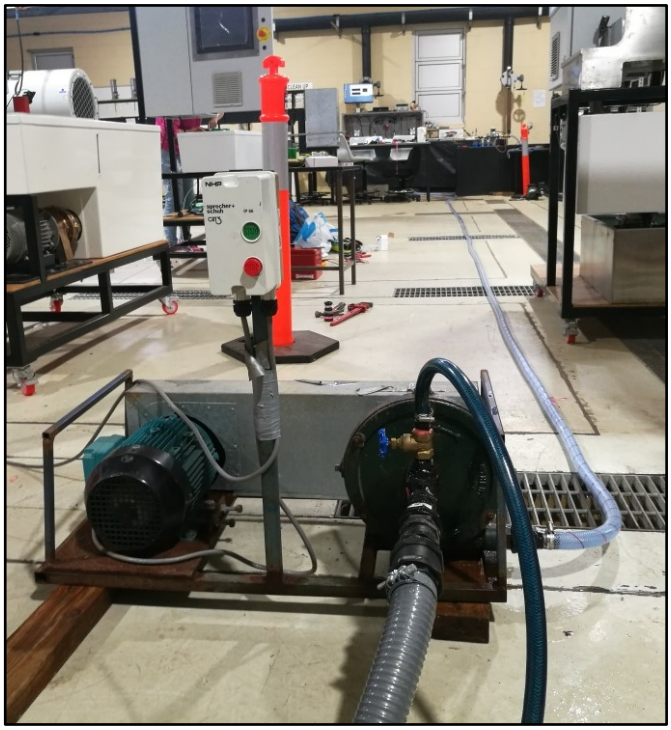

Figure 4-8: Southern Cross pump connected and running from underground storage tank

An additional approach to test the effect of a further reduction in head was tested by replacing the Sothern Cross pump with a jet pump as shown in Figure 4-9. However, the measurement outcome was still not satisfactory. Hence, from these tedious exploratory tests, it was evident that the upstream automatic valve controlled by LabVIEW was not able to achieve the required necessary control and further upstream primary modulation was needed.

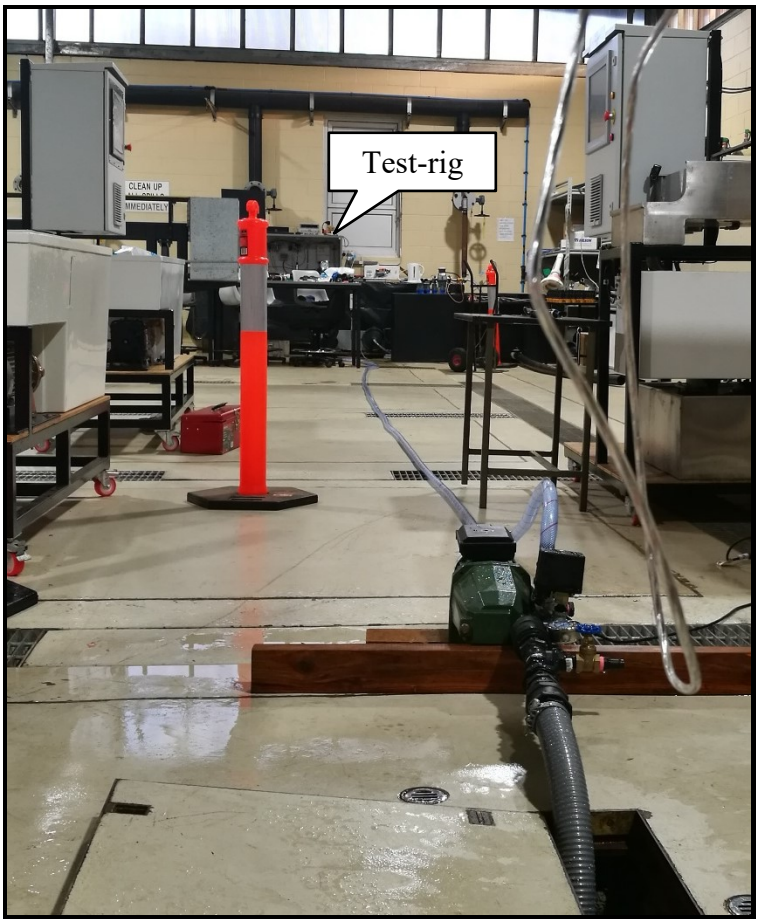

Figure 4-9: DAB Jet 100 Max pump connected and running from underground storage tank

Simulation of Flow Modulation with Gate Valve

After a series of tedious and time consuming trials, it was evident that new and better strategies were needed to accomplish small incremental supply head steps for satisfactory outlet pressure hysteresis characterisation. A 19.05 mm gate valve was installed on the pump discharge to achieve additional complementary modulation of pressure head and discharge. Measured data showed that there was a slight improvement in control, and that the spread of captured data points provided a clear

depiction of outlet pressure hysteresis. This achievement was a step improvement towards the realisation of automatic characterisation of pressure regulator hysteresis. The main challenges were the inability of the gate valve to generate smooth flow control, and maintain a particular opening position for the required experimental repetitions. Nonetheless, this flow rate modulation procedure proved beneficial in providing ideas for improved test-rig control, to yield good experimental results.

Flow Modulation with Needle Valve

An in-line throttling needle valve with an internal diameter of 19.05 mm was purchased and installed in place of the upstream gate valve for manual precision control of pressure and flow rate from the pump. The model was DV16V with a maximum working pressure of 41,369 kPa (6000 psi). It was equipped with a graduated rotating knob and a coded spindle (Vernier) to permit accurate control of flow during testing. This new valve was opened slowly to pass flows which were approximately 5 % higher than each required test flow rate. The LabVIEW program controlling the automatic movement of the other control valves in the test-rig was initiated with input of the desired test flow rate. During each experiment, care was required to ensure continuous opening of the needle valve to maintain an adequate flow through the test apparatus and prevent excessive opening of the upstream automatic valve to allow more flow. Measurements were taken at 1 kHz between 0.1 and 0.60 L/s using 0.1 L/s increments to enable future modelling of the results, as discussed in Chapter 6. Unlike the small test durations lasting for as little as 60 seconds and up 300 seconds for the other types of experiments, the test durations for regulator outlet pressure hysteresis varied between 720 seconds (12 minutes) for flow rates equal or close to 0.6 L/s, and 2160 seconds (36 minutes) for flow rates equal or close to 0.1 L/s, subject to the movement step duration of the test-rig control valves over the 1000 voltage steps each.

Extensive testing of the regulator outlet pressure at varying inlet heads and constant discharge across a nozzle flow range appropriate for CP&LM irrigation machines, was undertaken on all sampled pressure regulators of the low and high pressure models for the X, Y, and Z brands. Four units for the low pressure models and four units for the

high pressure models for each of the X, Y, and Z brands were selected for automatic hysteresis testing. This resulted in a total sample of 24 pressure regulator units tested. Figure 4-10 shows one set of regulator outlet pressure hysteresis testing outcomes with pressure data points on the hysteresis curve measured during the continuous movement of automatic test-rig control valves when augmented with modulation of pressure and discharge from the needle valve at the upstream of the test apparatus. A variation in the distribution of outlet pressure data points in the hysteresis curve was noticed (Figure 4-11), especially with increase in discharge due to the resultant vibration of the mechanical spring inside the devices. However, the results were still acceptable and the measurement procedure was adopted for the experimental hydraulic characterisation of pressure regulator outlet pressure hysteresis.

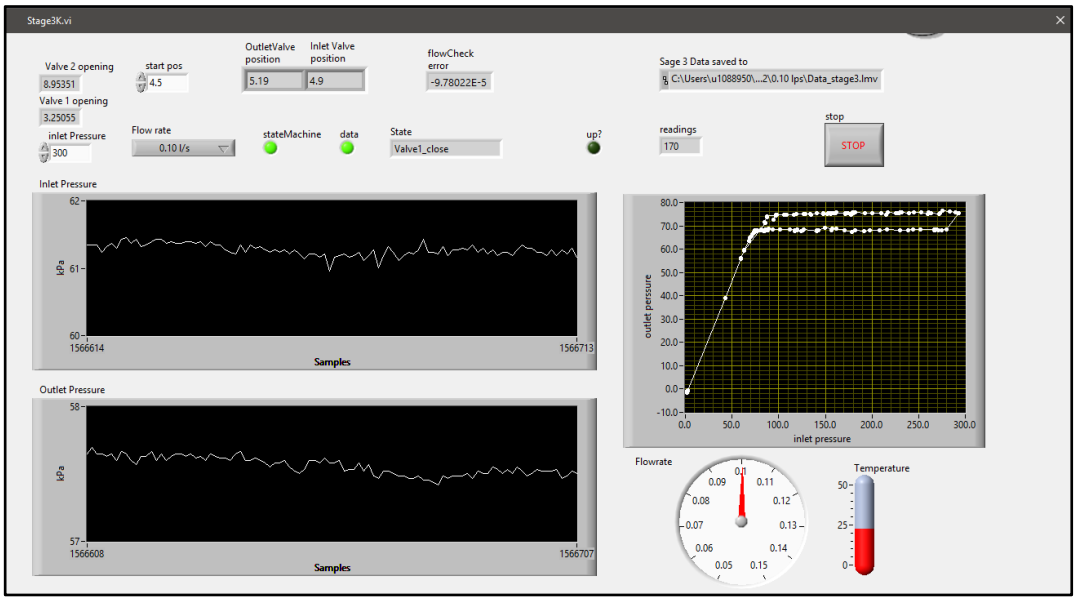

Figure 4-10: LabVIEW Stage 3 window showing outlet pressure hysteresis testing at 0.1 L/s with flow modulation using a needle valve for a low pressure regulator model

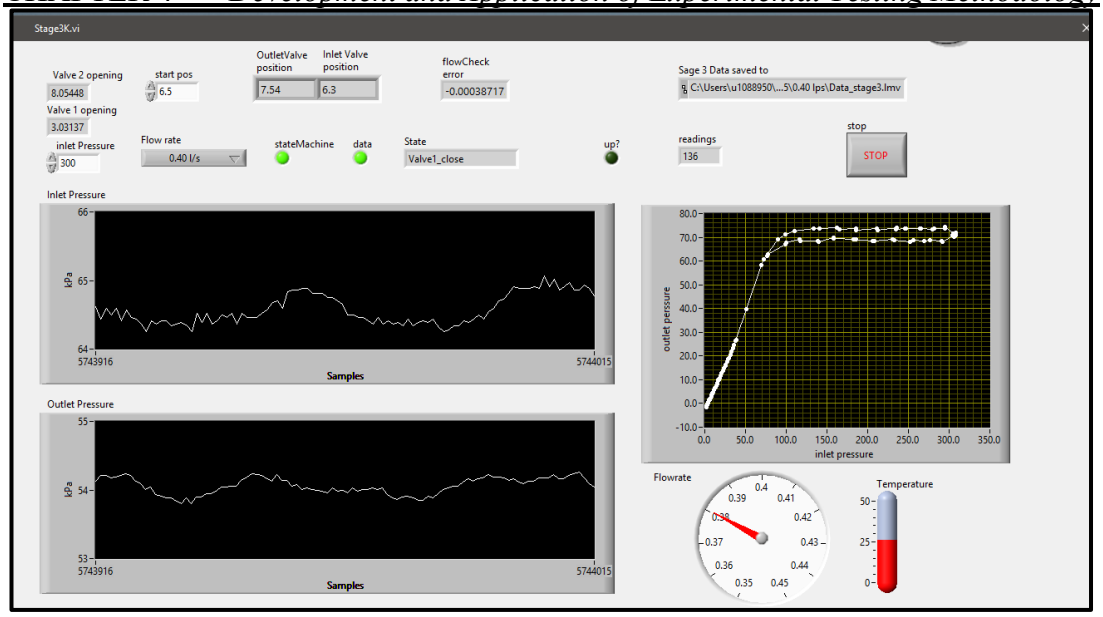

Figure 4-11: LabVIEW Stage 3 window showing a variation in the distribution of data points at 0.4 L/s for the same pressure regulator tested in Figure 4-10.

4.4.3.4 Pressure Head Losses

CP&LM pressure regulators function by automatically modulating the open cross-sectional area to generate a variable head loss through the displacement of the flow tube upstream and downstream to counteract force imbalances between back-pressure and a mechanical spring. Therefore, the head loss through the devices is bounded within the variable head loss, and a static friction head loss due to the inherent flow passage. Measuring the static component of friction head loss requires that the flow tube be frozen or locked in a stationary position, a process which required the tested units to be disassembled and the spring removed. To achieve this, electrical PVC conduit of 17 mm internal diameter was cut into sections and fitted inside the internal casing of the pressure regulator. The PVC section was used to encase the flow tube and maintain it in a neutral fixed position when pressurised flow occurred. The X and Z pressure regulator brands were tested using the same procedure, because they could easily be di-assembled with Phillip head screws and Allen key head screws, respectively. Measurements taken with a Digital Vernier Calliper with 0.01 mm accuracy showed that the flow tubes for both brands, and for both low and high pressure models were not of equal dimensions, hence sections of PVC were cut between 22 and 33 mm, at 1 mm increments to identify the most suitable length that could maintain the flow tube at its neutral position without any leaks. This approach

differs from Mohr (2011) who used a high-strength non-stretch fishing line that was glued on the internal wall of the flow tube, and passed through the discharge end of the regulator and test rig piping and nozzle, where it was loaded with weights to restrict movement.

Once the regulators were re-assembled, they were installed in the test-rig as previously described. The Stage 1 Test Methodology and the related LabVIEW program was used for this series of tests. This experiment was allowed to run for three (3) minutes, recording one (1) second averages of data at 1 kHz frequency, as described in Section 4.4.3.1, except for the test duration. The minor pressure loss measurements for the pressure regulators were conducted with discharge and head closed off from the apparatus in between tests. The pressure loss data then was analysed to establish the magnitude of head loss in static or immovable pressure regulators.

A different approach was employed for the determination of static minor head loss for Y brand pressure regulators because they did not use any easily removable material in their assembly mechanism. The lower casing of selected units was cut-away on the upstream section which had latching grooves that clamped the bottom section to the upper casing of the device. The cut-away section was maintained at approximately 180° of the whole body of the device so that the other remaining half could assist when re-assembling the valve for testing. When the spring was removed and all components were repositioned, a combination of IRWIN Quick-Grip and stainless steel adjustable hose clamps were used to hold and tighten the valve to prevent leaks as shown in Figure 4-12. This arrangement worked flawlessly when high flow rates and inlet heads were tested. Figure 4-13 shows the initial arrangement that was trialled which could only work for flow rates of up to 0.30 L/s at relatively low input heads. The requirement of a downstream valve to control discharge and pressure in the test-rig was evident in this test. This type of tests required modification of the test-rig to enable the pressure regulator installation on the downstream end of the apparatus. The Druck DPI 705 pressure transducer kit with Schrader valves and air chuck fittings was used to take pressure loss readings on the upstream and downstream side of tested regulators.

Figure 4-12: Set-up of manufacturer Y pressure regulator during minor head loss testing at Z113 Hydraulics Laboratory

Figure 4-13: Set-up of manufacturer Y pressure regulator during low head testing

4.4.4 *Measurements of Impacts of VRI Transients on Pressure Regulator Performance*

A test procedure for investigating the impacts of VRI induced pressure wave transients on pressure regulator performance was achieved by integrating the VRI valve and pressure regulator test configurations into a system that could enable the effects of pulsing to be experienced by the regulator. This was a novel test procedure. The Stage

2 Test Methodology in LabVIEW was capable of controlling the instantaneous opening and closing of solenoid valves, and two VRI valve configurations had been investigated. To induce a transient, test *Configuration B* was used with the test pressure regulator installed downstream through a tee piece, which was also coupled to the VRI valve, so that the hydraulic impact of VRI on-and-off pulsing could be received at the inlet of the tested pressure regulator. Equal diameter nozzles were used on the terminal downstream ends of the tee-piece pipelines, to control the discharge through the VRI valve and the pressure regulator. The LabVIEW input parameters for VRI valve opening and closing durations, including delay times, were defined, and the "Start" button clicked to initiate each experiment, once the upstream main supply valve was fully open. Measurements were taken at 10 kHz for a three second duration to enable interpretation of the response of pressure regulator outlet pressure to fast transients.

When all the test procedures had been developed and validated, and were deemed appropriate for extensive testing, the next stage was to determine the appropriate number of samples or test units and repetitions required to complete the comprehensive characterisation of VRI valves and pressure regulators. Section 4.5 below discusses the scientific processes employed to accomplish this requirement.

4.5 Sample Size Selection for Experimental Units

Statistical procedures are available to help determine appropriate sample sizes that could effectively describe performance, provided the sampled units are representative of current production for a particular brand, model or population. A good sample size helps to draw accurate inferences and validity about the total population. In manufacturing engineering, the statistical variation is used to delineate the variability that exist among individual units of a particular product manufactured in the same production line. However, to be able to characterise and separate this variation, the test procedure variation which is bounded within the variation of an individual units or devices must be known. Previous studies have shown that the appropriate number of samples required to characterise manufacturing variability is unknown. It is not known whether testing as few as three, 25, or as many as 500 samples will give a good

indication of this variability. It is worth noting though that the number of VRI valves and pressure regulators can be generally in the order of hundreds depending on the (i) size of CP or LM machine and sprinkler spacing, and (ii) magnitude of field variability and desired level of VRI management.

von Bernuth and Baird (1990)and Bralts et al. (1981) proposed that the number of units and repetitions depend upon the performance of the device, when a fixed confidence interval on the parameter being estimated is desired. In the few reported studies on pressure regulator performance, von Bernuth and Baird (1990)tested only five units, Mohr (2011) tested 16 units from a total sample of 88 units, and Junior et al. (2018) tested only three. Fraisse et al. (1995) tested as few as two irrigation control valves to characterise their performance. Hence, to mathematically estimate the appropriate sample size requires that initial tests be conducted on a few devices and the data processed statistically before the total sample calculated is subjected to the same test conditions.

The Normal Model, which is sometimes referred to as the Standard Normal Distribution is a commonly used statistical tool to describe and analyse datasets. It originates from the *Central Limit Theorem* which states that "The mean of a random sample has a sampling distribution whose shape can be approximated by the Normal model, i.e. the larger the sample, the better the approximation will be". Figure 4-14 shows a graphical representation of the Normal Distribution Model. In the normal distribution, a *z*-score is used to describe the number of standard deviations a data point is from the mean. Generally, one standard deviation away from the mean contains 68 % of the distribution, two standard deviations contains 95 %, and three standard deviations contains 99.7 %. This is sometimes referred to as the 68-95-99.7 rule (Ryan, 2013). The *z*-score is mathematically expressed by Equation 4.8.

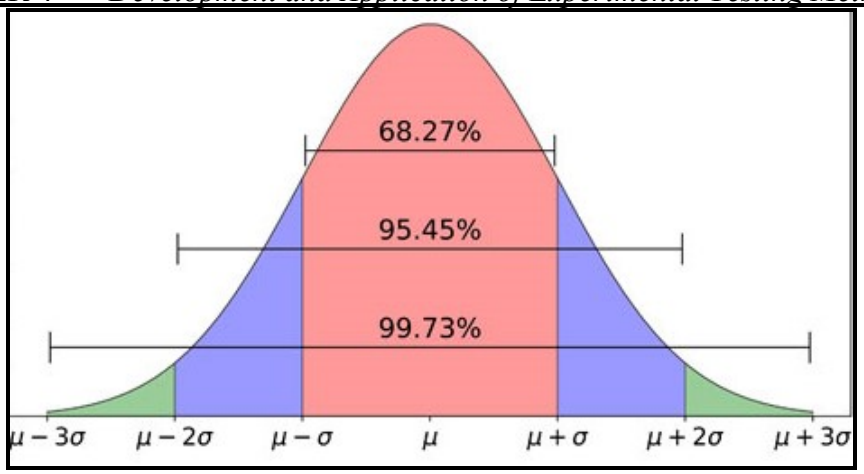

Figure 4-14: The Normal Distribution Model showing the 68-95-99.7 rule

$$z = \frac{y - y_{mean}}{\sigma} \qquad 4.8$$

where: z is the z-score, y is the observational point, μ is the mean and σ is the standard deviation.

Equation 4.8 allows the numerical computation of the z-score which gives a measure of how far away from the mean a particular data point is. It does not include the sample size from which the mean is calculated. A suitable equation which permits the determination of sample size, n, while accounting for the measure of standard deviations from the mean is Equation 4.9,

$$z = \frac{\bar{y} - y_{mean}}{\frac{\sigma}{\sqrt{n}}} \qquad 4.9$$

which when rearranged to Equation 4.10 (Ryan, 2013), gives:

$$n = \left(\frac{\sigma}{\frac{\bar{y} - y_{mean}}{z}} \right)^2 \qquad 4.10$$

where: $\overline{y}$ is the population or theoretical mean, y_{mean} is the mean and n is the sample size.

Once measurements on the sampled units have been conducted, the next step is to separate the variation between individual units (variance between treatments) and the experimental error or variation due to experimental measuring apparatus (variation within treatments), using analysis of variance (ANOVA) (Turner and Thayer, 2001). It is used to split observed aggregate variability found in a data set into systematic and random errors. To do this, the test statistic F-ratio is calculated as a quotient of the treatment mean square error (MSTR) and error means square (MSE),

$$F_{ratio} = \frac{MSTR}{MSE} \tag{4.11}$$

where,

$$MSTR = \frac{SSTR}{k-1} \tag{4.12}$$

and,

$$MSE = \frac{SSE}{n-k} \tag{4.13}$$

with: n as the total number of pieces of sample data and k denotes the population being sampled, while the treatment sum of square (SSTR) is calculated by Equation 4.14 and the error mean square (MSE) is calculated by Equation 4.15.

$$SSTR = n_1(x-x)2 + n_2(x2-x)2 + \ldots + n_k(xk-x)2 \tag{4.14}$$

$$MSE = (n_1-1)s21 + (n_2-1)s22 + \ldots + (n_k-1)s2_k \tag{4.15}$$

The final stage of the statistical process is to decide on a significance level, where the critical value (F_{ratio}) is taken from the F-distribution. If the test statistic is greater than

the critical value, the null hypothesis is rejected, and for a test statistic less than the critical value the null hypothesis is accepted.

In some cases, non-probabilistic sampling techniques such as purposive sampling are used to determine the sample size. In this case, the researcher uses their own judgement, usually of practical nature to determine the elements and quantity of samples to be used in an experiment. This method has the advantages of time and cost saving because it prevents the inclusion of unnecessary samples which might not have additional value to the results, or when financial capital limits the use a large sample size. An example of purposive sampling is a case of television (TV) reporters stopping certain individuals on the street in order to ask their opinions about certain political changes. The TV reporter has to apply certain judgment when deciding who to stop on the street to ask questions, otherwise it would be the case of random sampling technique. Fraisse (1994) applied this technique when selecting the number of solenoid valves for laboratory testing to modify a LM for variable water applications.

In this research, the actual number of samples and tests needed to adequately describe the hydraulic performance of VRI valves and CP&LM pressure regulators were determined using two types of sampling techniques, and then applying the statistical treatment discussed above. Purposive sampling methods were used to determine the number of solenoid valves needed for the experiments, as implemented previously by Fraisse (1994). Only the sample sizes for pressure regulators were calculated using the random sampling technique. The rationale for using two different sampling techniques was due to equipment cost, and the time required to complete all test types for all irrigation valves, especially pressure regulating valves. VRI valves were relatively expensive when compared to pressure regulating valves, and the latter required considerable test time, and particular manual care to successfully complete testing to obtain results.

Three units of manufacturer X, Y, and Z regulators (Section 4.5.2) for both low and high pressure models were randomly selected. The valves were inspected without

disassembly to ensure there were no foreign materials that could block or compromise flow passage. They were installed in the test apparatus, one at a time and tested for leaks. Before any testing could occur, air was removed from the apparatus by gradually opening the valves from the upstream automatic control valve all the way to the downstream valve with the main supply butterfly valve fully open to let water into the test-rig. Inlet pressures equal to 1.5 times the pre-set pressures for the low pressure, 103.4 kPa, and high pressure models, 155 kPa was applied at a flow rate equal to 0.3 L/s. This flow rate is equivalent to a reference velocity of 1 m/s as recommended by ISO Standard 9644:2008. Each pressure regulator unit was tested three (3) times (repetitions) for a duration of 300 seconds using the Stage 1 method of the automatic multi-function apparatus. Flow through the test-rig was closed between repetitive tests of each pressure regulating valve, by closing water supply through the butterfly valve once each test was completed, and reopening it slowly before the next test began a few minutes later. This allowed the spring mechanism in the pressure regulating valves to reset to a neutral position, rather than begin tests with it already displaced.

The outlet pressures from the tested pressure regulator units were analysed using the statistical criteria described in the first part of this section. Based on the statistical results, Table 4-1 below shows the total number of pressure regulators needed to be tested to successfully describe their performance. This implies that if time and capital were not limiting, a significantly larger number of pressure regulating valves than that recorded in Table 4-3, would be needed to correctly characterise performance. The total number of actual VRI valves and pressure regulating valves finally tested are those shown in Table 4-2 and 4-3. Nevertheless, the studies reporting on pressure regulator performance (von Bernuth and Baird, 1990, Mohr, 2011, Junior et al., 2018) tested only a few units and cited the issue of time constraints.

Table 4-2: Statistical number of pressure regulating valve units to be tested for common Brands used with CP&LMs

PRV Brand	X		Y		Z	
PRV Model	Low Pressure	High Pressure	Low Pressure	High Pressure	Low Pressure	High Pressure
No. of Units	96	97	97	97	97	98

Measurements of minor pressure head loss in each VRI unit for Manufacturer A were also conducted three times for a duration of 300 seconds using the Stage 1 method of the automatic multi-function apparatus. The same range of nozzle flow rates discussed previously were used in this type of testing. The data was processed to determine the extent of variation between individual tests, in order to decide on the number of repetitions required to accurately describe performance. These experiments were designed to establish a measure of test procedure variation on the results. The results showed that the test procedure and test apparatus did not introduce any significant variation among tests, and therefore it was necessary to characterise variation between experimental units. This outcome therefore limited the repetitions to a maximum of three in the experimental program. Significant variations were observed between individual units of VRI valves and pressure regulators. The following sections, Section 4.4.1 and 4.4.2, present the specifications, types, and actual number of experimental units tested in this research, including the criteria used to denote these units for reference and interpretation in subsequent chapters of this thesis.

4.5.1 *Solenoid VRI Valves*

The VRI valves tested in this study were 2-way, pilot operated solenoid valves that are produced by the irrigation industry for VRI applications. Some were normally closed (NC) types and required 12 V DC to operate, while the rest were normally open (NO) types of solenoid valves. The solenoid VRI valves selected were purchased from local Australian irrigation suppliers. Due to the hypothesis made by this research around the uncertainty of performance of VRI equipment, the valve selection process adopted a strategic approach (purposive sampling technique) and more of an exploratory nature to arrive at the final total number of brands and number of units eventually tested.

To achieve this, preliminary testing of a single valve unit for the most common brand was undertaken before additional units could added in the sample size. The results of initial testing brought immediate concern regarding the performance of the valve, or whether the results were due to the performance of the automatic test apparatus. Hence a set of experiments were designed to verify the repeatability and regularity of operation of more valve units for the same brand. The exploratory process then

incorporated other VRI valve brands which are also used in industry, as shown in Table 4.2. The discretional use of alphabetical codes to represent valve brands or manufacturers was meant to prevent endorsement by the author and conflict of interest, given the uncertainty of performance characteristics in the laboratory settings.

Table 4-3 – Tested solenoid actuated VRI valves and their main characteristics

Manufacturer	No. of Tested Units	Nominal Size (mm)	Operating Pressure (kPa)	
			Minimum	Maximum
A	2	19.05	50	1560
B	4	19.05	-	-
C	2	19.05	-	-

4.5.2 *CP&LM Pressure Regulators*

The most commonly used pressure regulator brands to control nozzle discharge in CP&LM irrigation machines are described in detail in Section 2.5.5.2. Two pressure regulator brands that are used in Australian machines were selected for the study, along with an additional new brand that is being trialled in the Mediterranean and American regions. The models of CP&LM pressure regulators that were selected for this study are 68.95 kPa (10 psi) and 103.42 kPa (15 psi), where the former was denoted “low pressure” model, and the latter denoted “high pressure” model, respectively. These models are common in Australian CP&LM irrigation machines because of high energy tariffs, whereas in American machines the high pressure models can be 155 kPa (20 psi) or more due to the affordability of energy. While the 41.4 kPa (6 psi) model is the lowest available in the manufacturing series of CP&LM pressure regulators, its application in industry has recently been withdrawn anecdotally for performance related issues, amongst other factors.

The selected units of pressure regulator brands common for Australian CP&LMs were purchased from local irrigation suppliers. However, no attempt was made to verify if the purchased lot was representative of current production. The units of the new

pressure regulator brand were provided free of charge, and were shipped from Austria to Australia by the manufacturer. The specifications of the pressure regulators are summarised below, using the same criteria used in Section 4.4.1.

Table 4-4 – Tested CP&LM pressure regulators and their specifications

PRV Brand	PRV Model (Pressure)	No. of Tested Units	Inlet/ Outlet Sizes (mm)	Maximum Operating Pressure (kPa)	Discharge Range (L/s)
X	Low	15	19.05	-	0.03 – 0.63
	High	15	19.05	-	0.03 – 0.76
Y	Low	10	19.05	827	0.03 – 0.95
	High	10	19.05	930	0.03 – 0.95
Z	Low	15	19.05	830	0.03 – 0.88
	High	15	19.05	900	0.03 – 1.07

4.6 Data Analysis

Detailed numerical solution schemes and algorithms were developed in MS Excel 2016 to interpret the separate and different datasets developed from the novel experiments described in this chapter. The electronic experimental data from this research was recorded and stored in *.lmv* data files. This data was used to calculate the minor head loss for solenoid actuated VRI valves, including the empirical determination of minor loss coefficients for the valves to aid in VRI hydraulic system design and management. The data from the experiments was also used to calculate the relative magnitudes of hydraulic heads generated by pressure wave transients from pulsing VRI valves to infer their impacts on CP&LMs hydraulics. The data was also used to determine the pressure regulating characteristics of the most common pressure regulators used with CP&LMs around the world, as well as the development of a mathematical model for describing the hydraulic performance of pressure regulating valves in unsteady conditions experienced by these machines. The data from the experiments were also used determine the impacts of VRI transients on the regulating accuracy of CP&LM pressure regulators.

4.7 Summary

This chapter presented the development of a novel testing methodology that is designed specifically for implementing the novel automatic multi-function hydraulic measurement apparatus, to characterise the hydraulic performance of VRI valves and CP&LM pressure regulators. The tedious and time consuming incremental processes and adjustments undertaken to refine the test apparatus to the most ideal combinations of configurations, and test procedures are presented. The chapter also covers the statistical processes employed to attain the actual number of test samples, number of tests, and tests duration for each of the hydraulic experiments that were planned. Finally, the analytical techniques applied on the separate datasets measured to provide the results that addresses the main objectives of this research are also discussed.

5. EXPERIMENTAL RESULTS AND ANALYSIS

5.1 Introduction

It has been expressed throughout the discussions in previous chapters that this research is concerned with the hydraulic characterisation of solenoid actuated VRI valves and pressure regulators used in CP&LM irrigation machines. The principal aim is to develop hydraulic modelling techniques that can permit or simplify the hydraulic re-design processes required when retrofitting and managing VRI machines. This chapter presents the results and separate analyses of the different datasets obtained from the extensive laboratory experimental testing program conducted according to the requirements, criteria, and methodologies developed in Chapter 4 for the novel automatic multi-function hydraulic measurement apparatus described in Chapter 3.

In order to accomplish all the experimental tests needed to address the objectives of this research, a total of 4,608 hours were dedicated in the Engineering Hydraulics Laboratory (Z113) for the design, construction, testing, refinement, and calibration of the novel automatic multi-function hydraulic measurement apparatus, including the significant testing and extensive characterisation of solenoid VRI valves and CP&LM pressure regulators. The results of each of these experimental tests are presented in the following sections.

5.2 Pressure Head Losses through VRI Valves

The determination of pressure head loss through VRI valves was a means of establishing the magnitude of head loss generated by these valves, and the impacts on total system head for VRI equipped CP&LM irrigation machines. Such information is critical for understanding the hydraulic performance of these machines when operating without the VRI on certain portions of the field, or prior to pulsing. However, before proceeding with the extensive characterisation of VRI valve head loss, accuracy measures were implemented to ensure the results were repeatable and reliable. This

rigorous process had been explored extensively in Chapter 3 and 4 to ensure the LabVIEW automatic DAQ system was capable of producing good results. The techniques applied to minimise errors and measurement variability as a result of the automatic DAQ system is well explained in these chapters. The other potential sources of variability relate to the accuracy of the sensing equipment. The non-linearity and hysteresis of the Druck PMP 4030 pressure sensing transducers is claimed at +/- 0.08% best straight line (BSL).

Figure 5-1 and Figure 5-2 presents the distribution of inlet and outlet pressure data points for a test duration of 180 seconds at 1 kHz measuring frequency. The samples for this test duration in each transducer is equal to 1800 samples or data points. The variation of pressure data points measured from the pressure transducers is within 2 kPa, for both inlet and outlet pressure transducers. Figure 5-3 is a graphical presentation of the two pressures when measured on both the upstream and downstream sides of the VRI valve. This process of interpreting the average deviation of pressure data from the specified measured parameters was meant to develop an appropriate method of handling this variability over such large amounts of datasets from the LabVIEW DAQ system, to enable the determination of the minor head loss for the VRI valves. Several tests were conducted to verify this spread for a couple of different pressures and flow rates and the results showed that the average deviation from a pre-set pressure can be maximum of 2 kPa.

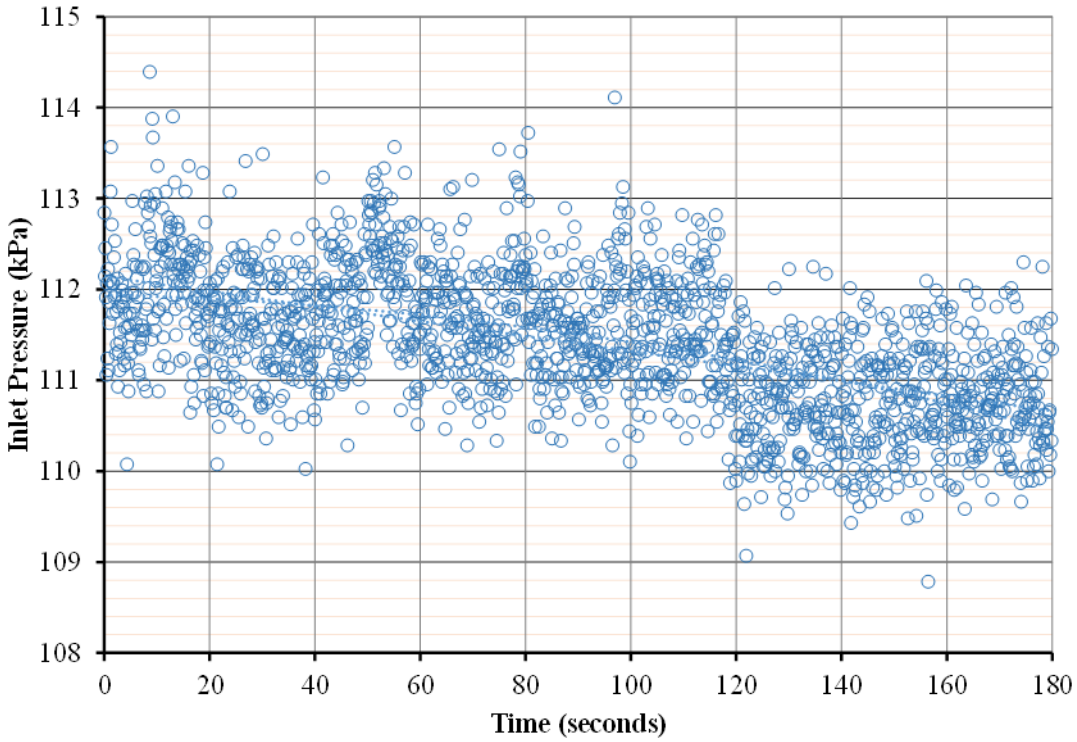

Figure 5-1: Distribution of pressure data points measured by the upstream pressure transducer at 1 kHz frequency

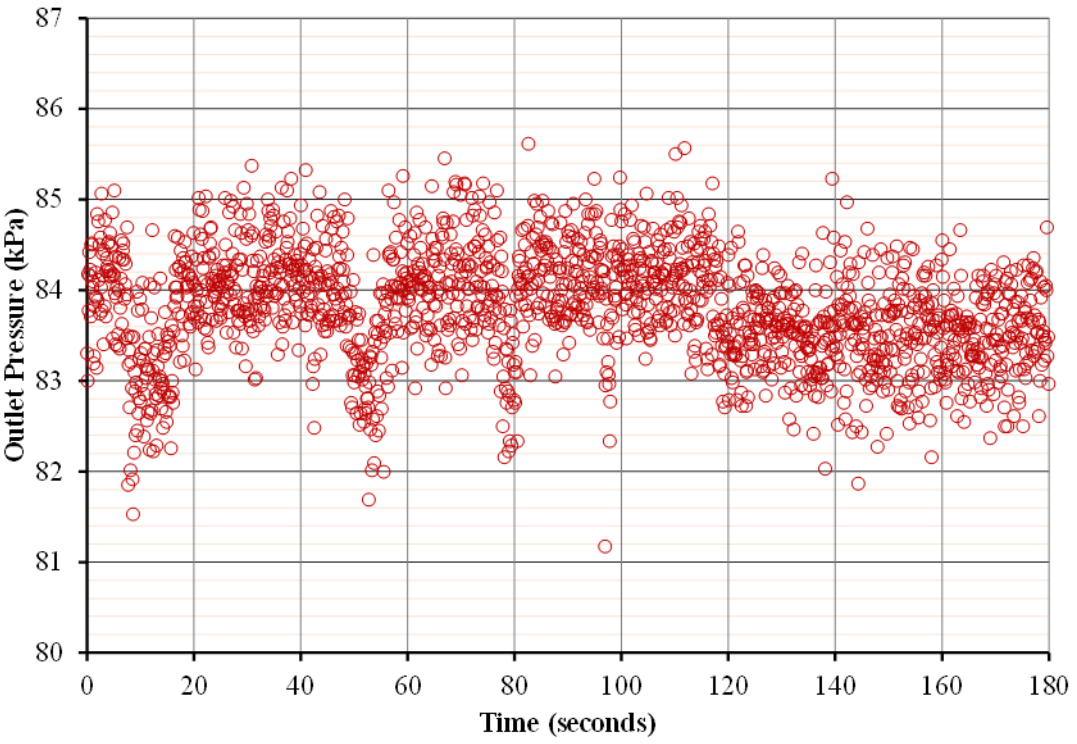

Figure 5-2: Distribution of pressure data points measured by a downstream pressure transducer 1 kHz frequency

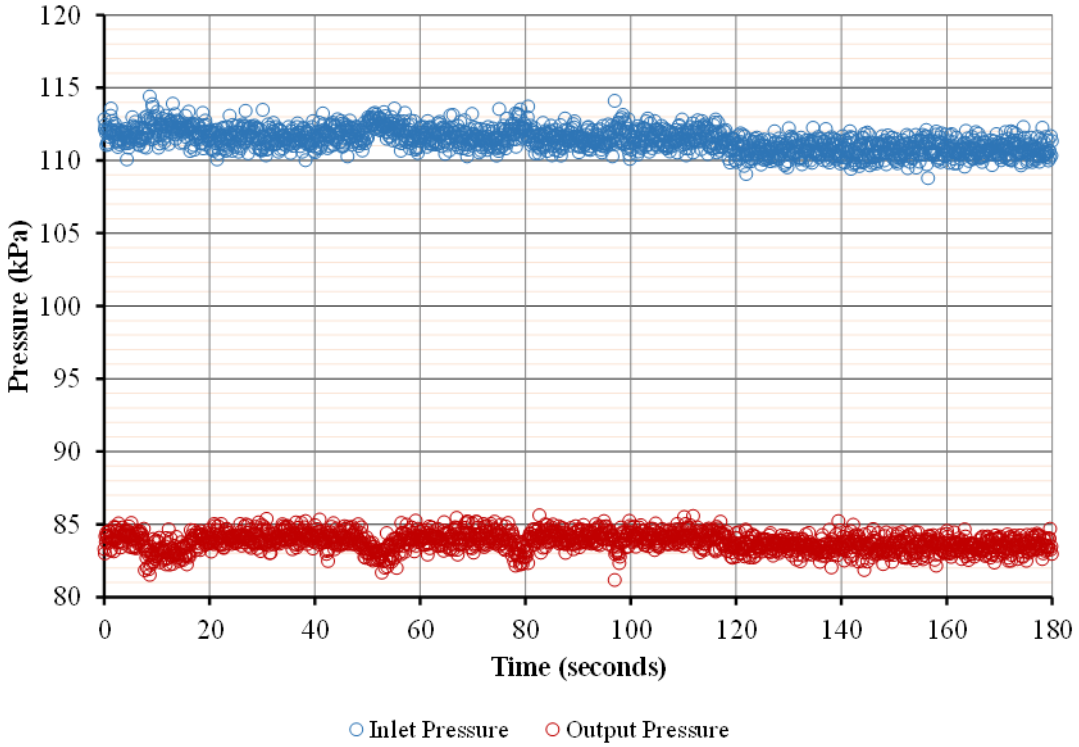

Figure 5-3: Pressure data points for the upstream and downstream pressure transducers at 1 kHz frequency

Preliminary measurements of the minor head loss carried out at the median and highest nozzle flow rates of 0.30 and 0.63 L/s for the Manufacturer A type of VRI valve, indicated that a substantial amount of head loss was occurring through these valves. The results obtained from this testing raised immediate concerns over the additional head loss created by VRI on CP&LMs, as well as the impacts on machine hydraulics and overall water applications. As a result, a decision was made to test an additional valve of the same model and manufacturer. The results from these two types of Manufacturer A VRI valves, when subjected to identical test conditions, were not significantly different. However, commercially available solenoid valves that are commonly used with VRI in industry (Table 4-2) are not similar in both design and manufacture, and it is known that this has a potential to cause differences in performance. Consequently, all the VRI valves presented in Table 4-2 were tested.

The results of minor head loss for the tested VRI valves of Manufacturer A, B, and C are presented in Figure 5-4 through to Figure 5-12. During testing, the measurements were conducted with pressure readings measured in kPa and flow rate in L/s. The

horizontal axes in the results presented represent flow rate while the vertical axes represent pressure head loss in m head of water. An exploratory approach was undertaken to determine the maximum flow rates above the test flow limit of 0.63 L/s and the corresponding pressure head losses through the respective VRI valves. The results of this approach are represented by the data points with the highest flow rates in the head loss-discharge curves. One hundred and forty-four (144) experimental tests were completed to determine the minor pressure head losses for the three VRI valve manufacturers examined in this research. Eighteen tests were completed for each VRI valve unit across the six different discharges investigated, with each test replicated three times. The minor head loss measurements were conducted with the test-rig connected to the constant head water supply, although some validation tests during the calibration stage of the test-apparatus were conducted with the apparatus connected to a booster pump. It was established that there was no difference between the minor head loss results between the constant header tank and the booster pump. The high inlet pressures during this type of experiments did not cause any difference in the resultant minor head loss, except for a corresponding increase in the downstream outlet pressure, and vice versa. Since the experiments were completed in different times of the year with seasonal differences in temperature, the measurements were checked for any significant variations due to water temperature reduction which might have affected the results due changes in water viscosity. This quality check was necessary because of the potential seasonal temperature fluctuation in the underground water storage supplying the header tank system in the Z113 Hydraulics Laboratory. It was found that the change in water temperature from about 30 °C in summer to about 17 °C in winter caused a difference of less than 1 kPa in pressure readings.

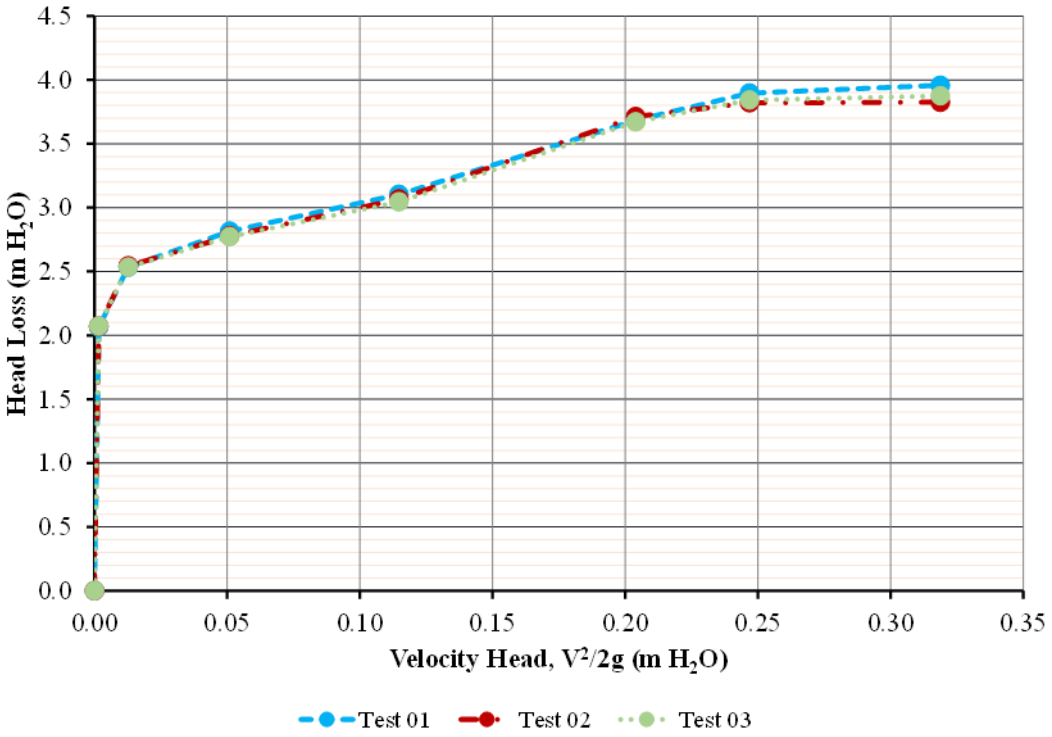

Figure 5-4: Minor head loss for Manufacturer A No. 01 type of VRI valve across a CP&LM nozzle flow rate

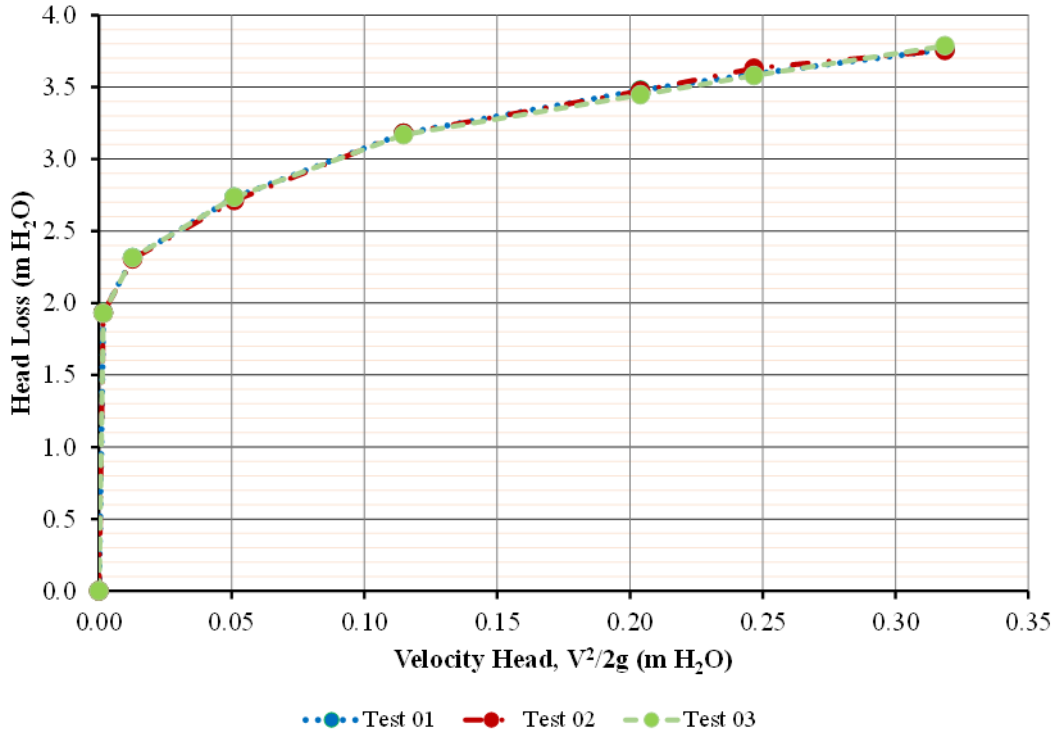

Figure 5-5: Minor head loss for Manufacturer A No. 02 type of VRI valve across a CP&LM nozzle flow rate

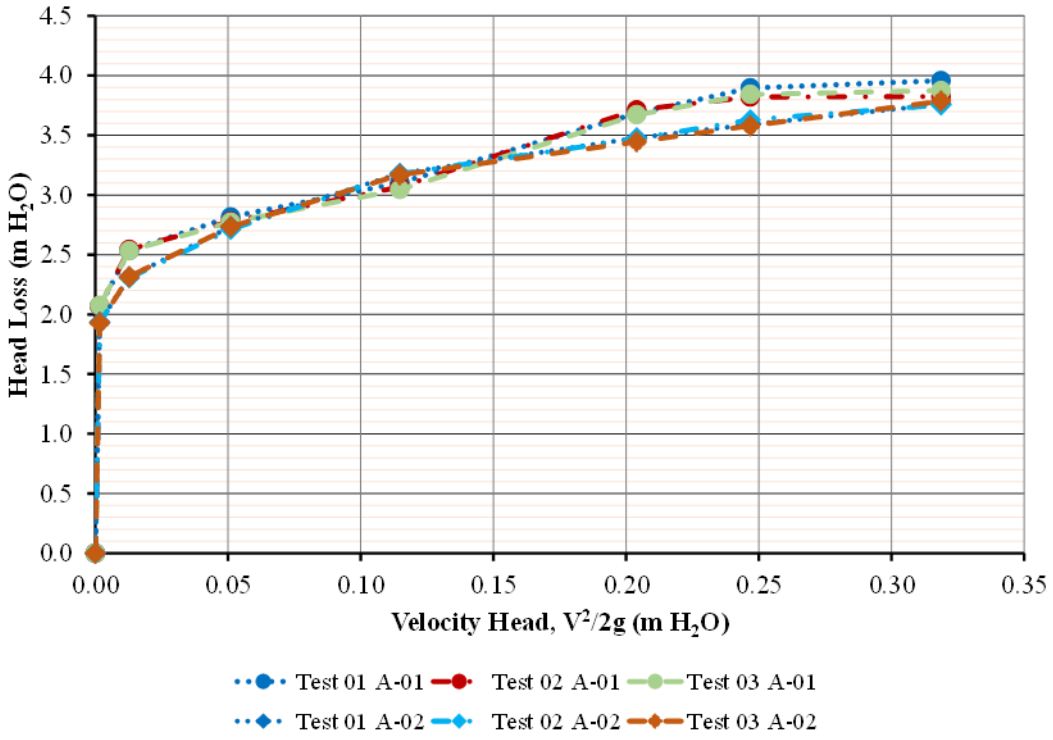

Figure 5-6: Comparison of minor head losses for No. 01 and 02 types of Manufacturer A VRI valves

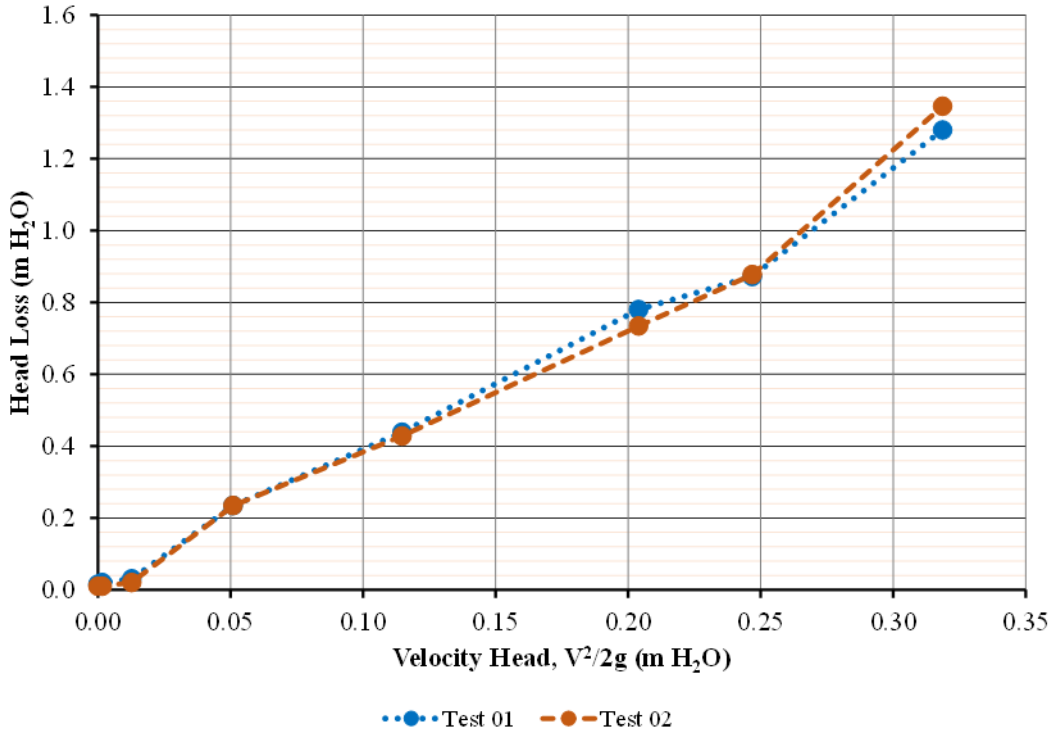

Figure 5-7: Minor head loss for Manufacturer B No. 01 type of VRI valve across a CP&LM nozzle flow rate

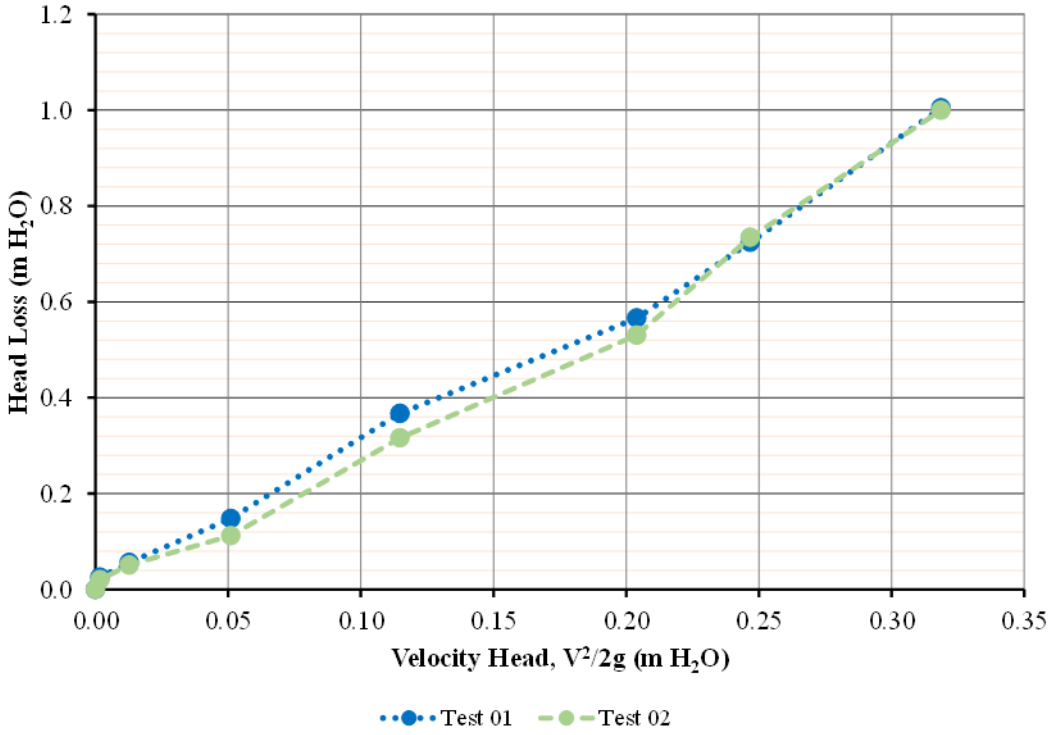

Figure 5-8: Minor head loss for Manufacturer B No. 02 type of VRI valve across a CP&LM nozzle flow rate

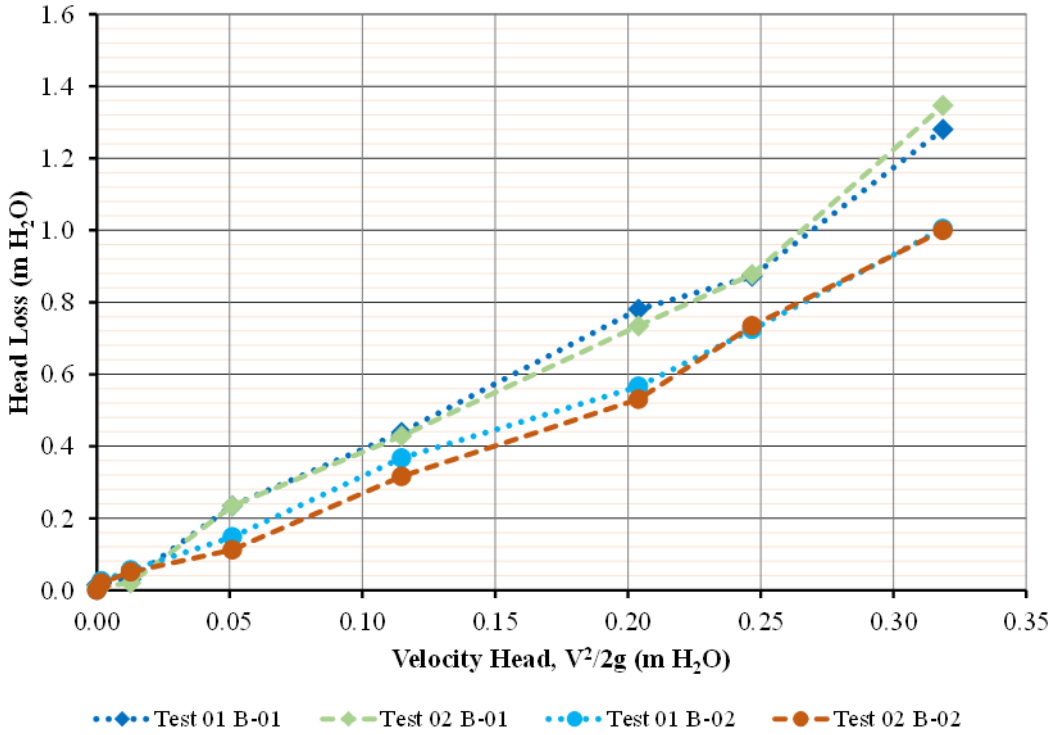

Figure 5-9: Comparison of minor head losses for No. 01 and 02 types of Manufacturer B VRI valves

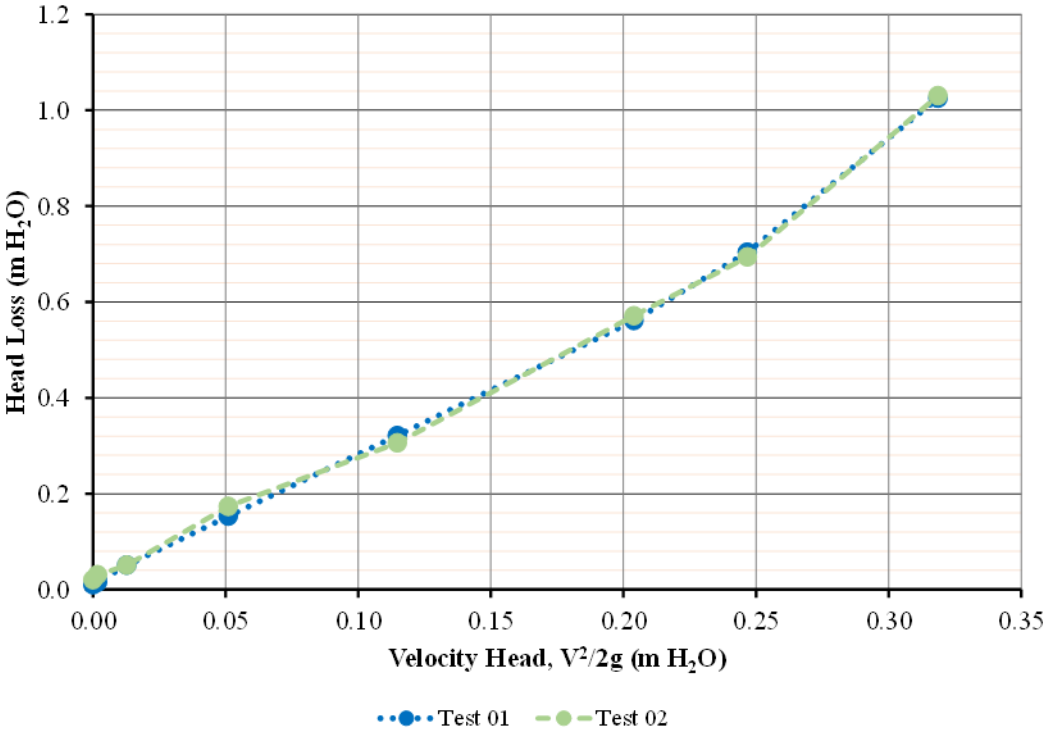

Figure 5-10: Minor head loss for Manufacturer C No. 01 type of VRI valve across a CP&LM nozzle flow rate

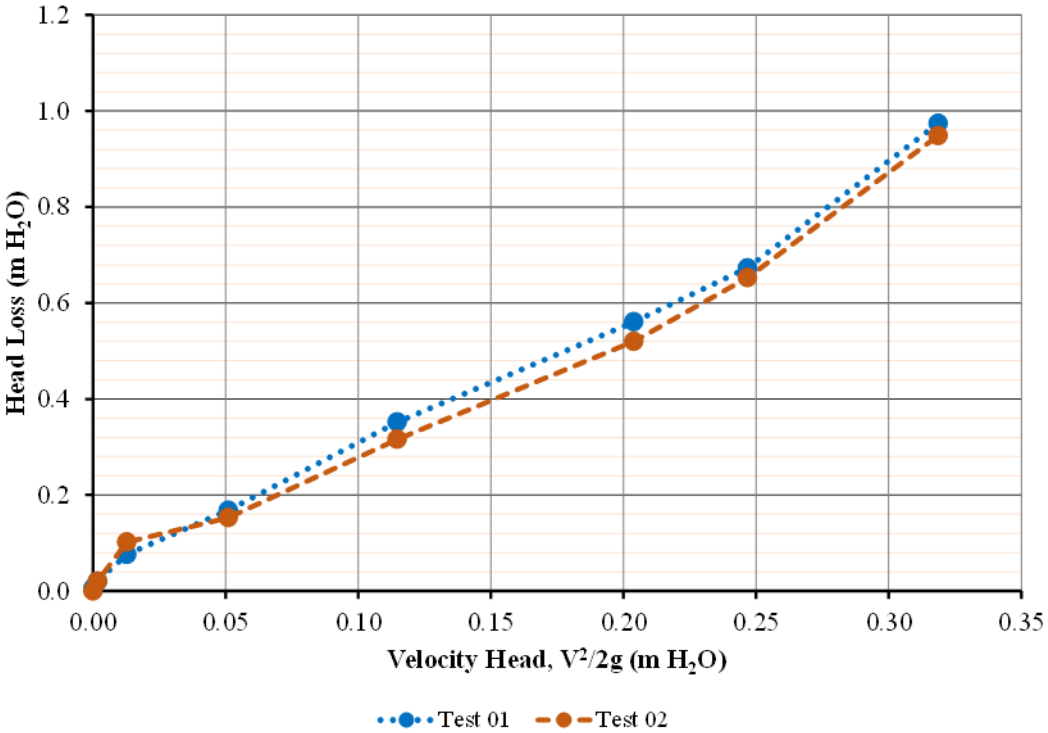

Figure 5-11: Minor head loss for Manufacturer C No. 02 type of VRI valve across a CP&LM nozzle flow rate

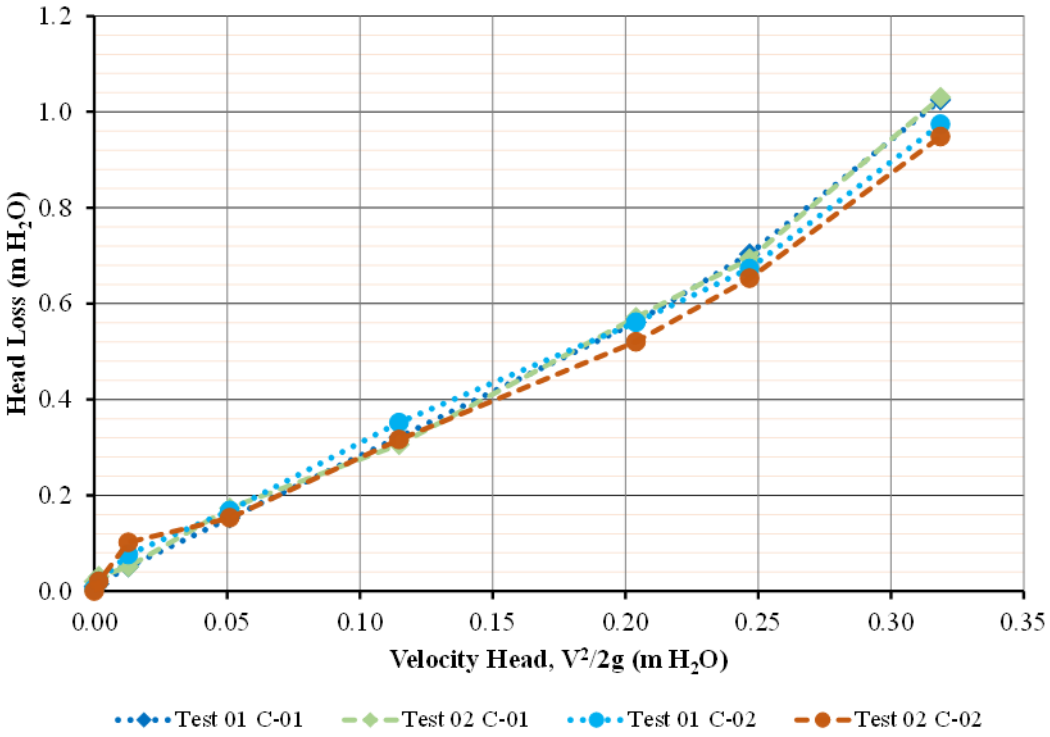

Figure 5-12: Comparison of minor head losses for No. 01 and 02 types of Manufacturer C VRI valves

The minor head losses for Manufacturer A types of VRI valves (Figure 5-4) were significantly higher than the head losses for Manufacturer B and C types of VRI valves (Figure 5-7 and Figure 5-10) across the full range of the same flow rates. The head losses measured through Manufacturer A type of VRI valve varied from a minimum average of 2.0 m head for a discharge of 0.05 L/s, to a maximum of 3.8 m head for a discharge of 0.63 L/s. The head loss increased to 4.0 m head when the discharge through the valve increased to 0.68 L/s. In the case of Manufacturer B VRI valves, the minimum measured pressure head loss was 0.03 m head for a discharge of 0.05 L/s, rising to 0.8 m head at 0.63 L/s. The head loss increased to 1.2 m head at the discharge of 0.75 L/s. The head loss measured for Manufacturer C type of VRI valves varied from 0.02 m head loss at 0.05 L/s to 0.7 m head loss at 0.63 L/s. The head loss was 1.0 m head when the discharge through the valve was 0.75 L/s. As expected, low discharges cause low head drops across the valves and this head loss increases with an increase in discharge. The head losses for Manufacturers B and C VRI valves did not differ significantly, both between samples of the same type of valve, and between manufacturers. One important observation is that the head loss for Manufacturer A valves varies considerably, and is consistently higher than the head loss for B and C

valves across the full range of flow rates tested. For an initial discharge of 0.05 L/s, the head loss is 1.2 m higher than the maximum head losses for the maximum discharges for valves manufactured by B and C. Results from different test techniques provided similar outcomes. It is my opinion therefore, that this considerable difference is caused by a significant physical difference in construction, as the diaphragm for Manufacturer A valves could only allow a maximum discharge of 0.68 L/s in the test-rig, while Manufacturers B and C had a maximum discharge of 0.75 L/s, despite all valves having a nominal 19.05 mm internal diameter.

5.3 Calculation of Minor Loss Coefficients for VRI valves

To mathematically derive the minor loss coefficient, K, for the VRI valves, the pressure loss results from the experiments in Section 5.2 were converted to m head of water with corresponding discharge converted to velocity head in m head of water. This is because head loss through valves is approximated to be proportional to the velocity head and the minor loss coefficient, as represented by Equation 2.16. Since Manufacturer A VRI valves had significantly higher head losses (maximum 4.0 m head), coupled with non-linearity of data points at the lowest to medium discharges, additional discharges were tested to enable the determination of a relationship between discharge and head loss data. Figure 5-13 shows the minor head loss for VRI valves when additional flow rates were incorporated in the test results.

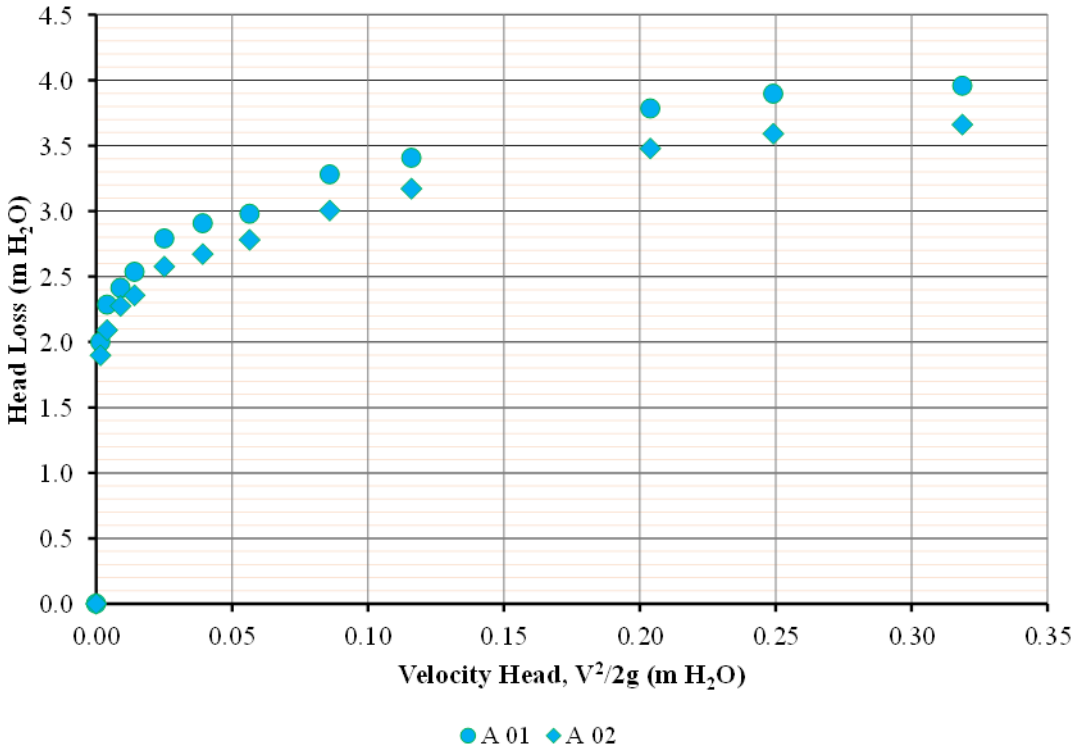

Figure 5-13: Minor head loss for Manufacturer A type of solenoid actuated VRI valves when additional flow rates have been incorporated in the testing

The results of velocity head and pressure head loss were plotted, with the horizontal axes representing velocity head, while the vertical axes represented head loss as shown in Figure 5-14. A linear regression model was then fitted in the minor loss data for the three VRI valve brands as shown in Figure 5-14. This relationship shows that the head loss through Manufacturer A valves is 4 times the velocity head, while that of Manufacturers B and C are 3 times the velocity head. From the results, it is evident that the head losses for Manufacturers B and C are almost identical at lower velocity heads, and will only differ slightly with higher velocity heads. The measured units of Manufacturer A VRI valves also show some variation in head loss which implies the existence of manufacturing variability. The results of the minor head loss testing for the VRI valves demonstrate that retrofitting VRI technology on CP&LM laterals increases the amount of total head loss in the system. The magnitude of the loss through the VRI valves array is estimated using Equation 2.16 for the different valve brands, where the minor loss coefficients, *K*, derived in Figure 5-14 are used for each of the manufacturer brands. The equation is then re-written into Equation 5.1 to represent the minor loss coefficient for the individual valve brands tested. The brands

B and C have the same minor loss coefficient while manufacturer A has a separate minor loss coefficient.

$$h_{m-vri} = K_{\_vri} \frac{V^2}{2g} \qquad 5.1$$

where: $h_{m\text{-}vri}$ = minor loss for a solenoid VRI valve (m head), and $K_{\_vri}$ = minor loss coefficient for a solenoid VRI valve (dimensionless)

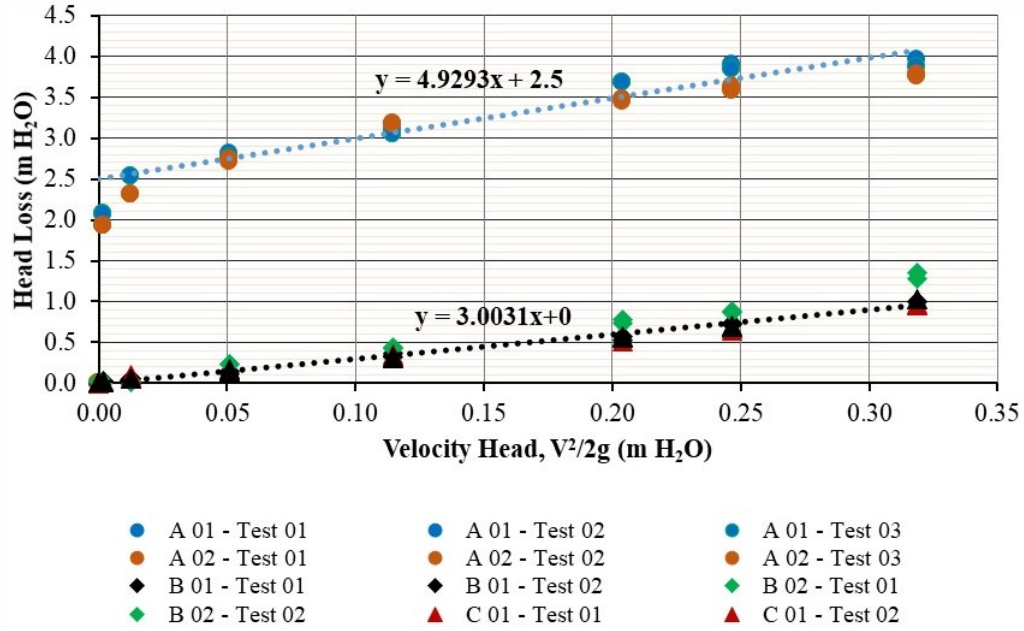

Figure 5-14: Minor loss coefficients *K* for the Manufacturers A, B and C types of solenoid VRI valves commonly used with CP&LMs

The magnitudes of these minor loss coefficients and the corresponding minor head losses across the CP&LM nozzle discharge implies the significance of reviewing the total pressure loss equation for designing these irrigation machines to incorporate the minor head loss component for VRI valves. Therefore, a modified version of the pressure loss equation for CP&LM laterals is proposed for the hydraulic design of VRI CP&LMs, and this is discussed in Section 5.4 below.

5.4 Modification of Total Pressure Loss Equation for VRI CP&LMs

The total pressure head loss through a CP or LM irrigation machine is summarised and calculated using Equation 2.23 as discussed previously in Section 2.4.4 in Chapter 2. This mathematical expression is a direct summation of all pressure head losses that occur in the lateral of the machine. However, based on the VRI valves pressure loss results and minor loss coefficients developed for the solenoid valves commonly used in VRI machines in industry, the VRI minor loss term, $h_{m\text{-}vri}$, (Equation 5.1) proposed above is for inclusion to the total pressure loss equation for CP&LMs. This term represents the additional minor head loss from VRI valves when designing VRI machines and will be used to review the total system pressure head, to justify any necessary adjustments in the hydraulic system for VRI CP&LM irrigation machines. This head loss component is important when VRI machines are irrigating portions of a field uniformly where the system discharge is at its peak or highest as opposed to when a couple of sprinkler heads are pulsed off when VRI operation is in effect.

The improvement in the total pressure loss equation is desirable because not all VRI machines will pulse sprinklers for the entire irrigation cycle but will do so for a proportion of time when the system is approaching or irrigating portions of the field that has been pre-programmed to receive proportional amounts of the total depths being applied by the VRI machine. The proposed modification to the total pressure loss equation for VRI CP&LM laterals result in a new version of a pressure loss equation as shown below.

$$h_l = h_f + h_{\Delta e} + h_s + h_r + h_m + h_{m-vri} \qquad 5.2$$

The modified total pressure head loss equation is an initial breakthrough towards an appropriate hydraulic re-design for VRI machines. When factoring the VRI valve minor head loss in the total head loss of a standard machine that is later retrofitted with VRI technology, shows that there are some potential improvements required in the overall hydraulics of the irrigation system especially in the pumping plant. The impact of the additional VRI valves minor head loss on CP&LMs retrofitted with this

technology is demonstrated using an experimental CP that was used for irrigation research at USQ, as shown in Figure 5-15 below.

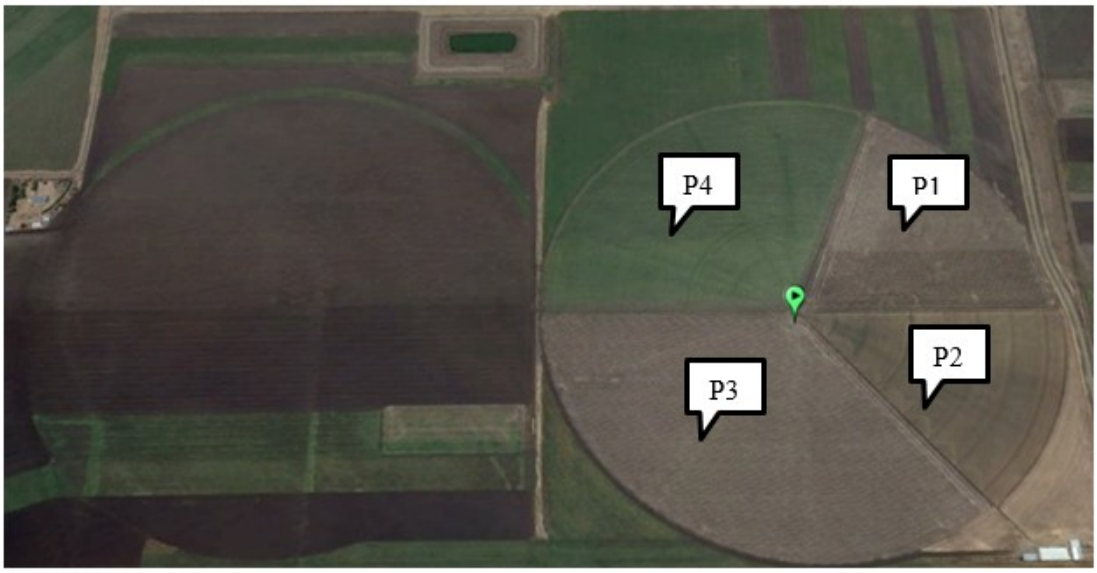

Figure 5-15: The VRI CP irrigated cotton field (right) in Southern Queensland showing the different VRI irrigated blocks

5.4.1 *Specifications of the Experimental CP*

The experimental CP is a seven span machine that irrigates a total area equal to 50 Ha. The CP is a Valley machine that is manufactured by Valmont Irrigation. The first span is 38.7 m long, with spans two to seven inclusive equal to 57.3 m, and a 12 m overhang. This machine is designed for a system flow rate equal to 45.2 L/s at a corresponding centre pressure head of 16.5 m (23.4 psi) and a system in-line end pressure equal to 10 m head (14.2 psi). Water supply is groundwater using a large submersible pump that is fitted in a deep bore. The submersible pump is controlled by a variable frequency drive (VFD) using a feedback loop that is incorporated in the water supply system to maintain about 14 PSI end pressure. The sprinkler package of the CP is a Nelson S3000Y (Nelson Irrigation Corporation, Australia) rotating spray plate sprinklers (RSPS) that is operated and maintained at 7.0 m (68.95 kPa or 10 psi) by Nelson pressure regulators. The sprinkler package has a total of 186 3TN nozzles of 26 different diameters ranging from 2.8 to 7.3 mm. The spacing between nozzles is constant and equal to 2.15 m. The first nozzle is installed at 8.04 m from the pivot point while the last nozzle is positioned at 394.23 m from the pivot point. The nozzles are located at approximately 2.0 m from the soil surface using a semi-rigid plastic drop

hoses. The VRI system that is retrofitted in this CP is a Valley VRI-iS and is operated on sections of the field from a Valley Pro2 control panel with mobile phone connection through an AgSense Commander VP system. The VRI system uses manufacturer A (Section 4.5.1) type of solenoid valves to control individual sprinkler discharges.

5.4.2 *Additional VRI Minor Head Loss to Total CP Head Loss*

Assuming that the CP machine described in Section 5.4.1 above was operating on a level field with zero slope, the difference in pressure head, 6.5 m (16.5 m – 10 m) between the centre pad and the last sprinkler at the overhang at the end of the machine would be a result of friction head loss in the lateral pipe and losses thorough fittings, bends and pressure regulators. However, it is very uncommon to have a CP that is operating in such perfect conditions. The total head loss would be expected to include the elevation profile of the irrigated field which occurs when the machine is irrigating an area with the highest elevation relative to the centre of the CP machine. The lateral supply line pressure threshold is important for pressure regulators as they require a minimum inlet pressure for regulation to occur. The actual inlet pressure head and the regulation processes are explained in the pressure regulator performance results in Section 5.6. Manufactures use a minimum 3.5 m head above the pre-set pressure for regulation to occur, although the results of pressure regulator performance in this research showed that regulation can occur slightly below this head. However, his hydraulic concept shows that pressure regulators located towards the end of the CP may have their performance compromised as only 3.0 m of head would be available to operate the 10 psi model pressure regulators.

$$h_l = 16.5m = h_f + h_{\Delta e} + h_s + h_r + h_m \qquad 5.3$$

The additional head loss from VRI valves in this machine at 4.0 m at higher discharges for the VRI valve manufacturer A, will increase the total head loss from 16.5 to 20.5 m (Equation 5.4). This means that the total dynamic head (TDH) of the system will increase and would necessitate reviewing the capacity and adequacy of the pump towards meeting this new additional head. The minor head loss from the VRI valves is approximately 25 % of the total head loss through the machine. This outcome is important in the design of VRI machines because the current irrigation design

principles assume that minor losses (which is predominantly the losses in valves), are limited to a maximum 10 % of the system's total pressure head loss. The magnitude of the minor head loss in VRI valves justifies the need for modifying the total pressure loss equation used in CP&LM irrigation design to a better version for the design of VRI CP&LMs. The additional VRI minor head loss is incorporated into the original standard equation by adding the minor loss term for VRI valves which is represented by Equation 5.1, to produce Equation 5.4.

$$h_l = 20.5m = h_f + h_{\Delta e} + h_s + h_r + h_m + h_{m-vri} \qquad 5.4$$

5.5 Analysis of Hydraulic Transients from VRI Pulsing

The novel investigation of the propagation of hydraulic transients from VRI pulsing was undertaken using Manufacturer A type of solenoid actuated VRI valves, from the experimental test-rig Configurations A and Configuration B, as described in Section 4.5.2 (Figure 4-3 and Figure 4-4). The flow rates used were identical to those tested in Section 5.2 (however from 0.05 to 0.7 L/s). However, before pulsing the VRI valve and measuring the transients propagated, an investigation of the unsteadiness of the water supply in the test apparatus was undertaken to establish the magnitude of oscillations generated from the header tank supply and oscillations generated by the booster pump. The measurements were conducted using the upstream pressure transducer located a few pipe diameters from the VRI valve. The idea was to enable the delineation of these oscillations in the transients' measurements. Figure 5-16 and Figure 5-17 shows the results of the unsteadiness of the water supply into the test apparatus at 0.63 L/s. It is evident that the oscillations in both the header tank supply and booster pump are very small, within 0.2 kPa which is about 0.02 m head. Therefore it will not be construed that these pressure oscillations will affect the propagation of pressure wave transients in the VRI pulsing simulation experiments as they will be invisible at the relative small scales used to show transients.

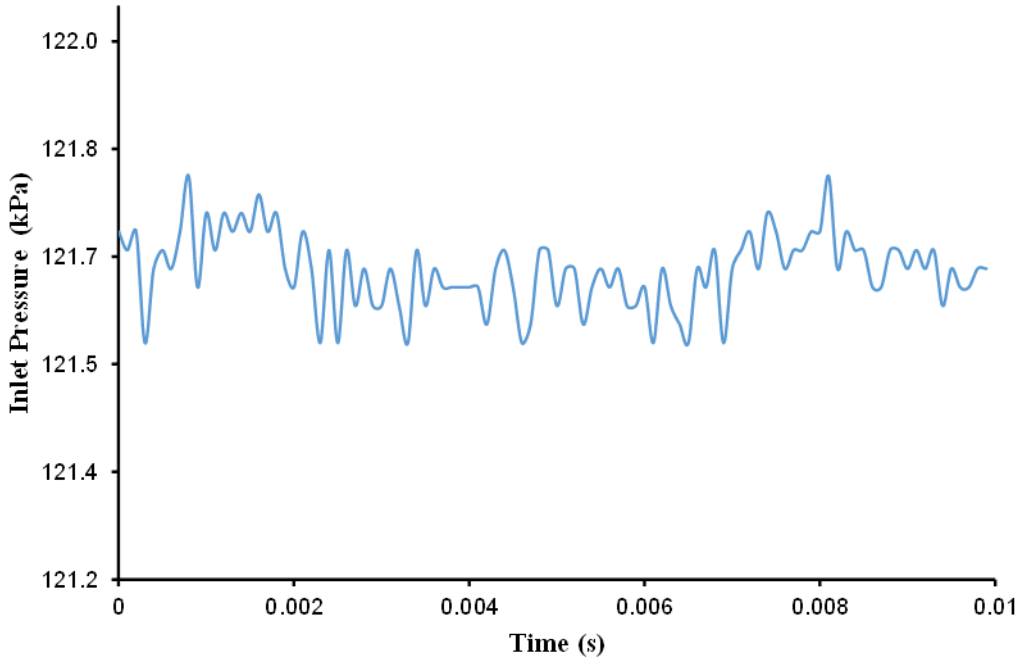

Figure 5-16: Oscillations in the test apparatus created by water supply from header tank at 0.63 L/s

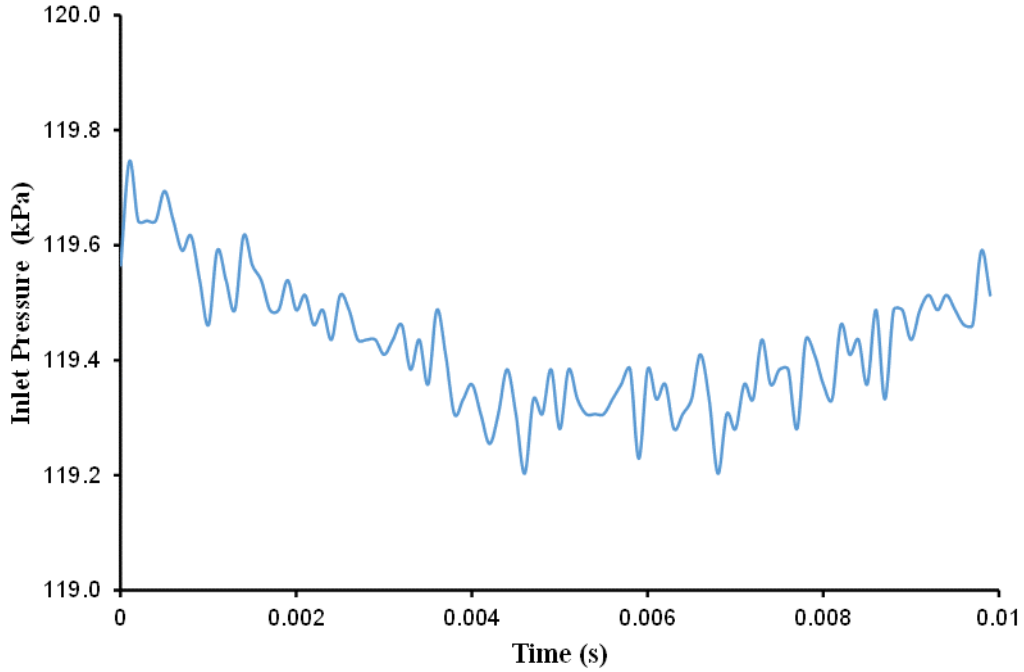

Figure 5-17: Oscillations in the test apparatus created by the Sothern Cross booster pump at 0.63 L/s

The simulation of VRI pulsing and measurement of the transients created was first conducted with Configuration A as described in Chapter 3 and Chapter 4. The initial

set of experiments were completed with an approximately 6 m of flexible pipe on the upstream of the test apparatus when supplied from the header tank water supply system. The transient pressures collected from the upstream pressure sensing transducer for a specific pre-set duty cycle, and the calculated hydraulic head for each flow rate are summarised in Table 5-1. The maximum hydraulic head increases from about 1.1 times of the inlet pressure head at the lowest flow of 0.05 L/s to about 2.4 times at the maximum flow rate of 0.7 L/s. The maximum available head in the test apparatus was measured to be approximately 14 m when there was additional friction and velocity head losses in the 6 m x 20 mm flexible hose.

Table 5-1: Maximum hydraulic head created from VRI valve pulsing at Configuration A of the test apparatus with a long flexible connecting hose

Flow rate (L/s)	Velocity (m/s)	Inlet Head (m)	Max Head (m)	Head Rise Factor
0.05	0.2	14	15	1.1
0.15	0.5	14	17	1.2
0.30	1.0	14	22	1.6
0.43	1.5	14	30	2.1
0.57	2.0	14	32	2.3
0.63	2.2	14	34	2.4
0.70	2.5	14	34	2.4

From the above measurements, it was observed that there was potential dampening of the transients generally escaping into the upstream section of the flow meter where the 6 m flexible hose was connecting the test apparatus and the header tank system. Therefore, the flexible hose length was reduced to only about 1.5m in total to enable the connection of the water supply system and the test apparatus. A second series of tests were then completed and the results obtained are summarised in Table 5-2. The difference in the magnitudes of hydraulic head created is large for these flow rates between the two setups of the upstream connection. This shows that the flexible hose was dissipating a significant proportion of the transients induced by the pulsing solenoid valve. The maximum hydraulic head increases from about 1.1 times of the inlet pressure head at the lowest flow of 0.05 L/s to about 3.1 times at the maximum flow rate of 0.7 L/s. The inlet head increased to about 15 m when the long flexible hose was reduced, indicating that it created approximately 1 m head loss in the test system.

Table 5-2: Maximum hydraulic head created from VRI valve pulsing at Configuration A of the test apparatus with a minimum flexible connecting hose

Flow rate (L/s)	Velocity (m/s)	Inlet Head (m)	Max Head (m)	Head Rise Factor
0.05	0.2	15	16	1.1
0.15	0.5	15	22	1.5
0.30	1.0	15	29	1.9
0.43	1.5	15	33	2.2
0.57	2.0	15	37	2.5
0.63	2.2	15	42	2.8
0.70	2.5	15	46	3.1

The graphical representation summary of the maximum hydraulic heads created from the transients with long and short hose connections are shown in Figure 5-18.

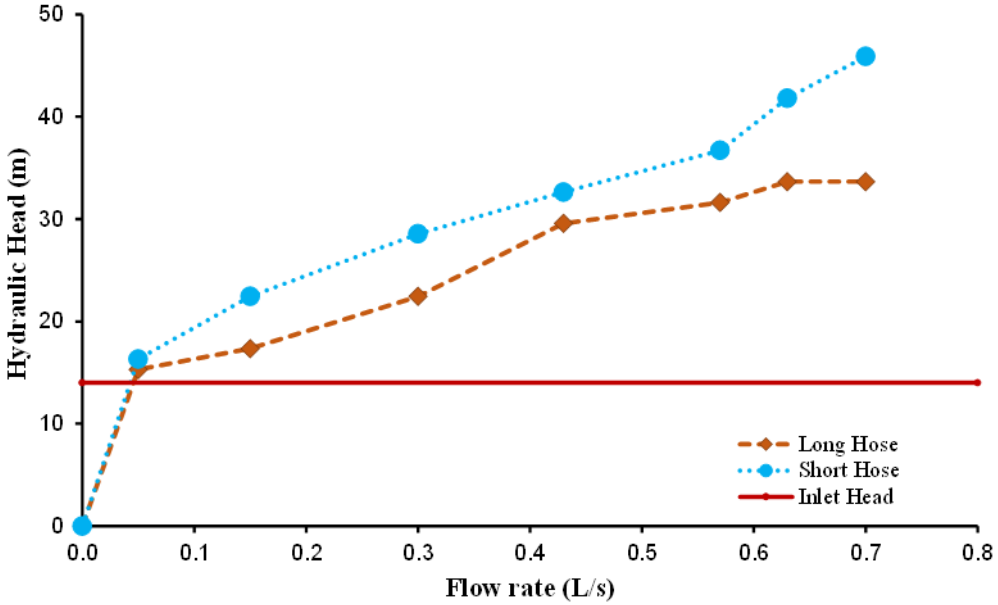

Figure 5-18: Comparison of maximum hydraulic head measured using Configuration A with long and short flexible hose connections

Figure 5-20 through to Figure 5-21 shows the graphical output of the original measurements in kilopascals of some of the results presented in Table 5-2. These maximum pressures are significantly different between flow rates below and above the 0.3 L/s threshold. They increase with an increase in flow and the pressure waves occur for a few seconds after which the pressure attains its original near steady state condition. From the pulsing experiments, it was observed that the differences in maximum pressures created can only be established when the test apparatus is supplied from the constant header tank water supply system. The tests conducted using the

booster pump as explained in the section below did not produce any significant variations in the maximum pressure generated when the solenoid valve was pulsed off. Instead the maximum head is nearly constant at approximately 70 m (690 kPa).

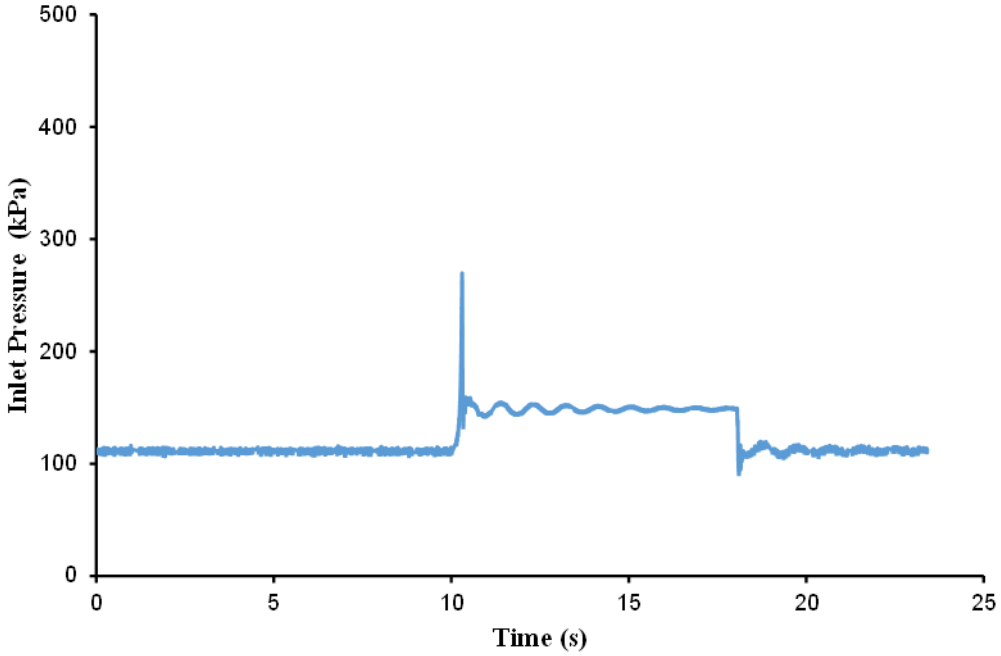

Figure 5-19: Pressure wave transient propagation at 0.3 L/s when test apparatus is supplied from the header tank system

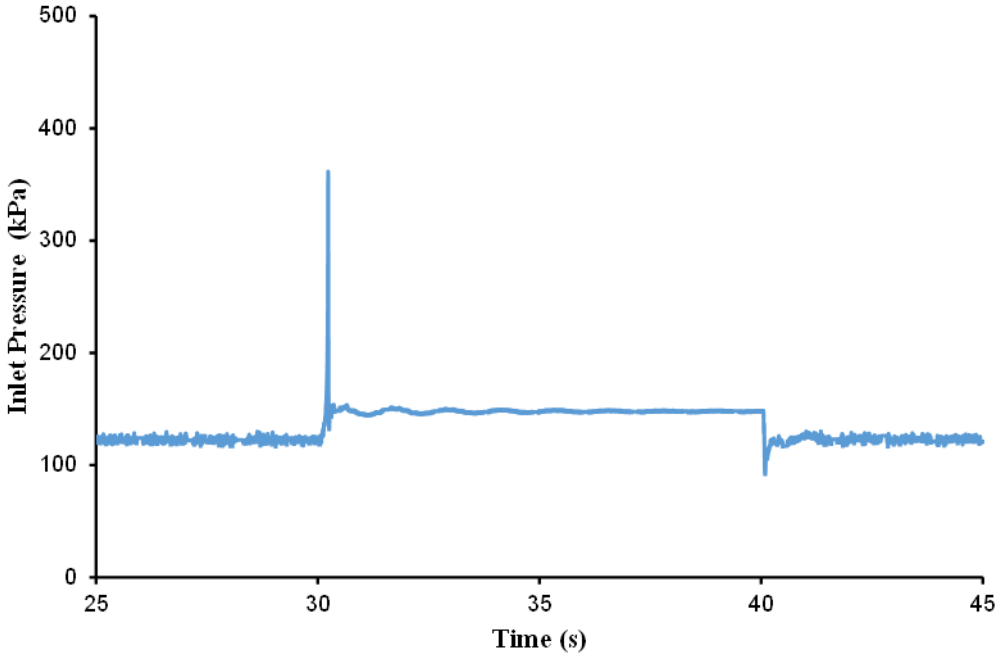

Figure 5-20: Pressure wave transient propagation at 0.63 L/s when test apparatus is supplied from the header tank system

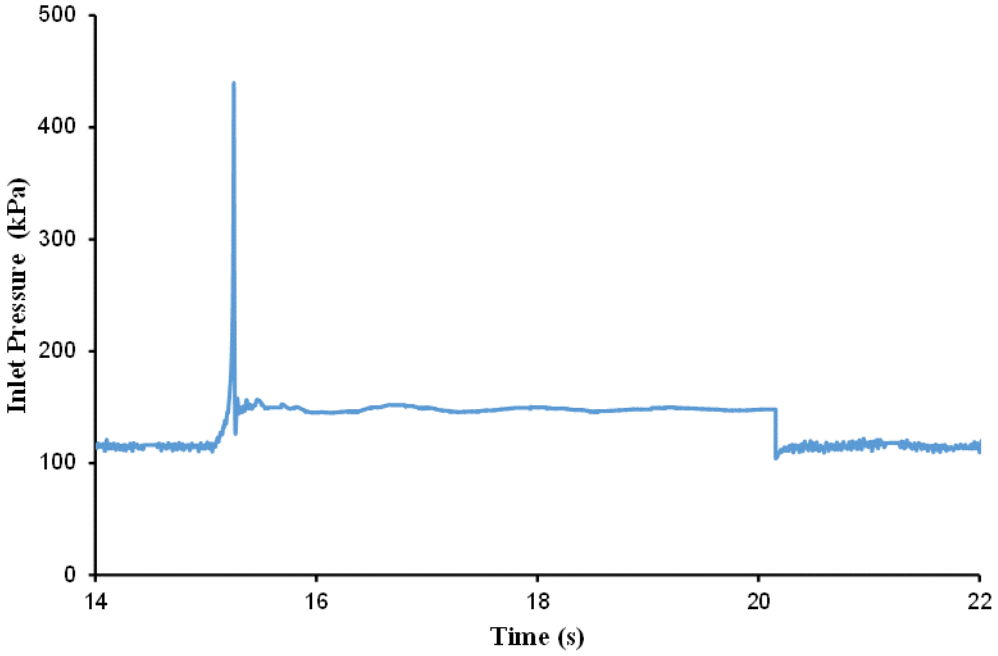

Figure 5-21: Pressure wave transient propagating at 0.70 L/s when test apparatus is supplied from the header tank system

Figure 5-22 and Figure 5-23 below shows transient pressures collected from both pressure transducers at corresponding flow rates and similar test conditions. The pressure wave increases to approximately 450 kPa in this case. However, it was observed that the magnitude of the transient is influenced by the amount of time the flow stream is allowed to pass before the next pulse is created, apart from the flow rate. The transients at the highest flow rate region (0.43 to 0.7 L/s) create sub-atmospheric pressures at the downstream transducer while the transients produced from the lower flow rates (0.05 to 0.3 L/s) had positive pressures. Negative pressures can sometimes be excessive and introduce transient cavitation. The pressure waves propagated when Configuration B of the test apparatus was used are represented by Figure 5-23. In this case, the pressure wave propagates equally in both directions of the VRI valve and is the reason the inlet and outlet pressures are following the same pattern (Figure 5-23) as opposed to the results shown in Figure 5-22. This type of VRI valve configuration is the most common for VRI systems in industry.

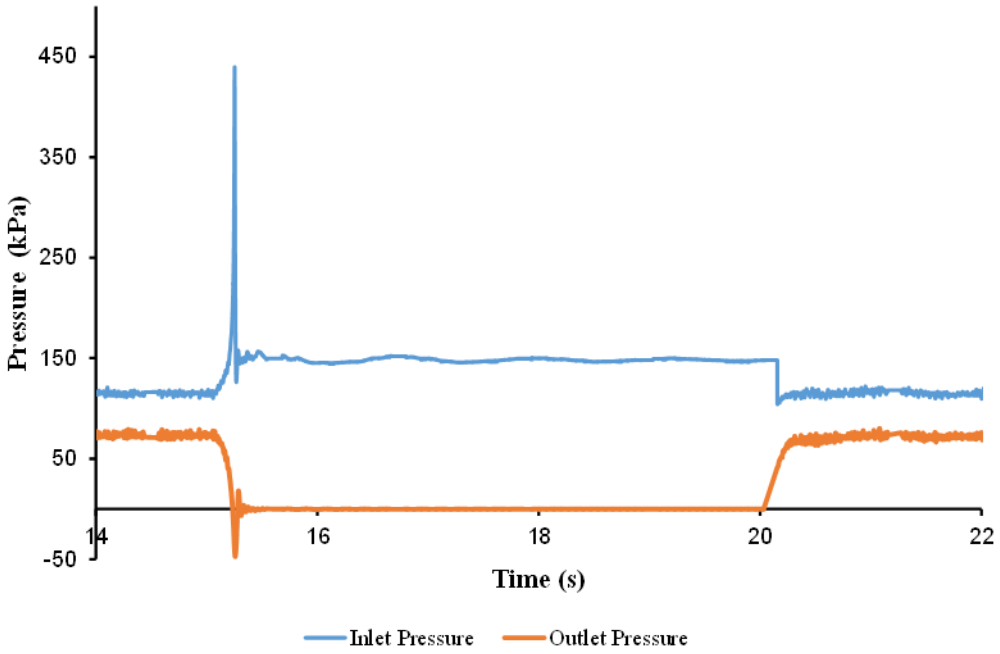

Figure 5-22: Transient pressures measured on both transducers on the upstream and downstream sides of the VRI valve at 0.70 L/s

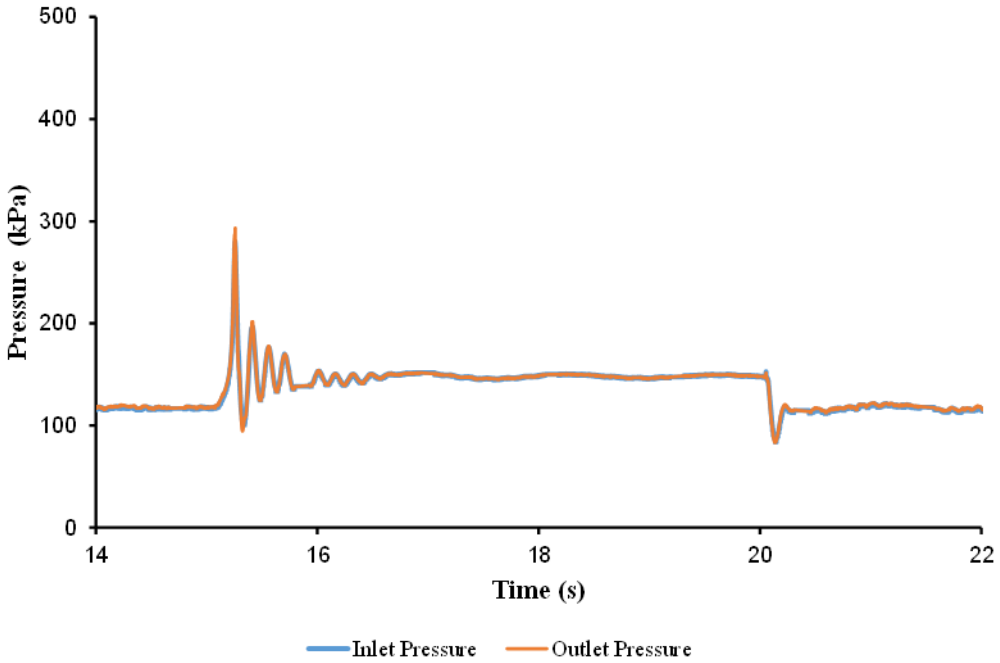

Figure 5-23: Propagation of transient pressure waves when measured using Configuration B of the test apparatus at 0.70 L/s

Transient pressures collected when the test apparatus was coupled to a booster pump for higher pressure testing using Configuration A are represented in Figure 5-24 for the upstream pressure transducer, and Figure 5-25 for both pressure transducers. The

results show that the maximum hydraulic pressure is greatest and is approximately 690 kPa or 70 m for each test.

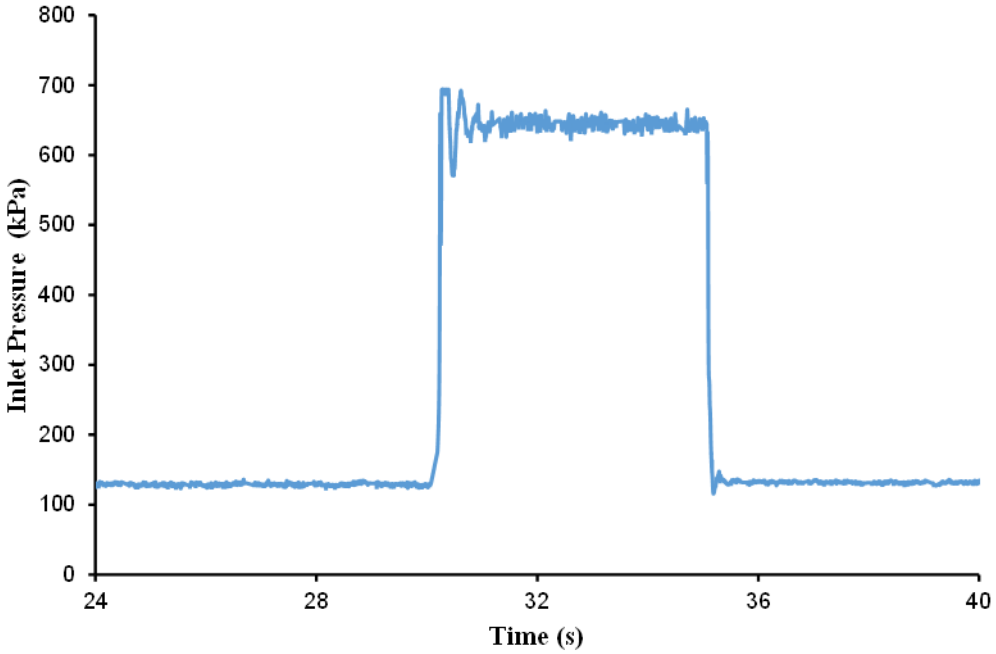

Figure 5-24: Pressure wave transient propagation at 0.63 L/s using Configuration A of the test apparatus when connected to a booster pump

The response of the downstream pressure is different amongst Configurations A and B. It reduces to zero and further below atmospheric pressure when the transient is generated at Configuration A due to the valve closure restricting any flow movement to the downstream section of the apparatus (Figure 5-25).

The downstream pressure response in Configuration B follows the same positive direction as the upstream pressure, as it is the case for the constant header tank supplied tests. However, it only rises to a certain limited percentage of the total maximum upstream pressure rise as opposed to having the same magnitude in the header tank tests (Figure 5-23). Figure 5-26 shows that the downstream pressure rises to about 420 kPa at 0.63 L/s, and is observed rising to 435 kPa at 0.7 L/s. This is a significant increase from the measurements obtained with the constant header tank supply at identical flow rates with the same test Configuration B (290 kPa at 0.7 L/s). Based on a fixed inlet pressure equal to 150 kPa maintained between these two tests using a control valve installed between the pump and flow meter, it was discovered that the pressure head increase factors are within the order of 1 as shown in Table 5-3.

Table 5-3: Maximum hydraulic head created from VRI valve pulsing at Configuration B of the test apparatus with a minimum flexible connecting hose

Flow rate (L/s)	Velocity (m/s)	Inlet Head (m)	Max Head (m)	Head Rise Factor
0.05	0.2	15	35	2.3
0.15	0.5	15	36	2.4
0.30	1.0	15	37	2.5
0.43	1.5	15	40	2.7
0.57	2.0	15	42	2.8
0.63	2.2	15	43	2.9
0.70	2.5	15	44	3.0

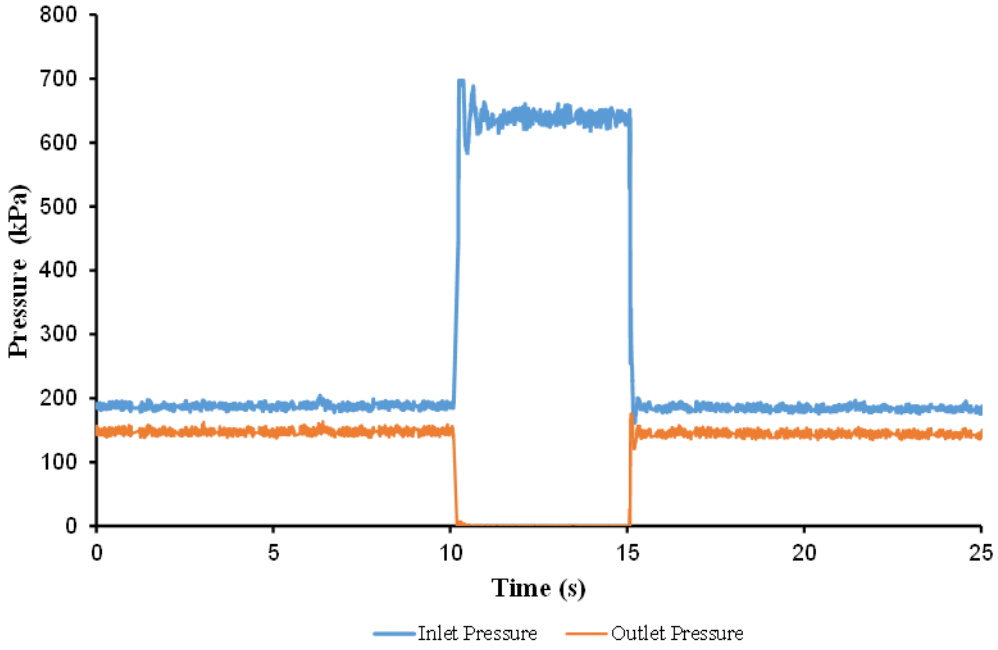

Figure 5-25: Transient pressures measured at 0.63 L/s on both the upstream and downstream transducers using Configuration A when connected to a booster pump

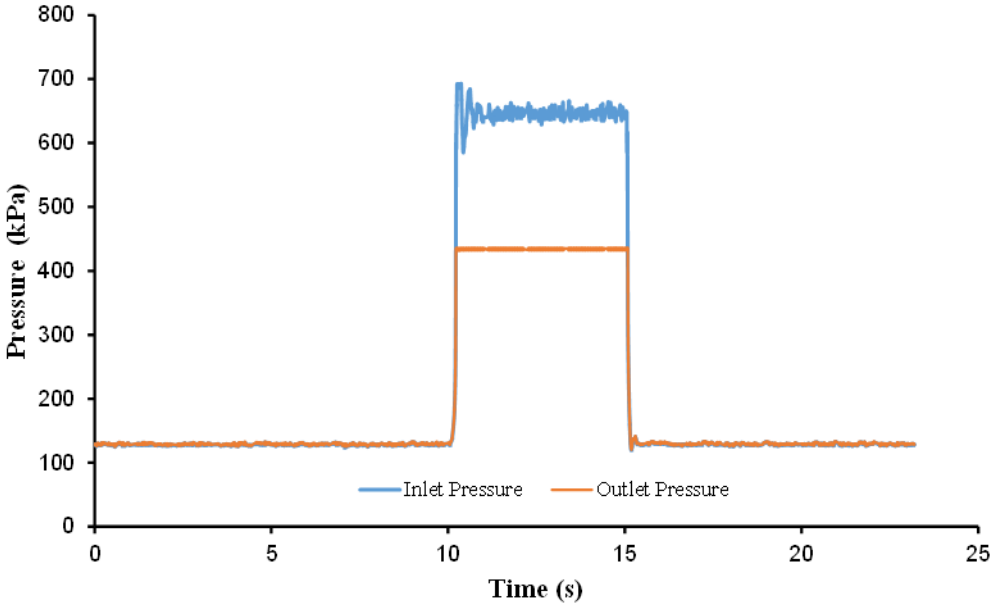

Figure 5-26: Propagation of transient pressure waves at 0.63 L/s when Configuration B of the test apparatus is connected to a booster pump

The transient pressures measured from these types of experiments were also compared against a set of numerically analysed dataset using Joukowsky principles (Equation 2.8 and Equation 2.9) on the same flow rates and pipe rig properties (wall thickness and internal diameter) to determine the maximum potential increase in water velocity. Theoretical modulus of elasticity for the steel pipe used and the modulus of elasticity of water at the testing temperatures were employed to estimate the wave celerity *c* which was found to be 1,403 m/s. Equation 2.8 was then rearranged and simplified to Equation 5.5 to predict the changes in velocity. The results of the hydraulic analysis when using the measured pressure head changes are illustrated in Table 5-4, Table 5-5, and Table 5-6 . The temporary change in water velocity is approximately 0.1 m/s across the flow rates for the header tank tests and is 0.2 m/s for the booster pump tests. These resultant velocity increase are responsible for the sudden rise in the pressure head measured.

$$\Delta V = \frac{\Delta H x g}{c} \qquad 5.5$$

Table 5-4: Maximum water velocities calculated from Joukowsky equation using measured parameters and a calculated wave speed c = 1,403 m/s for the long hose connection to the header tank for Configuration A

Flow rate (L/s)	Velocity (m/s)	Inlet Head (m)	Max Head (m)	Δ Head (m)	Δ Velocity (m/s)
0.05	0.2	14	15	1	0.2
0.15	0.5	14	17	3	0.5
0.30	1.0	14	22	8	1.1
0.43	1.5	14	30	16	1.6
0.57	2.0	14	32	18	2.1
0.63	2.2	14	34	20	2.3
0.70	2.5	14	34	20	2.6

Table 5-5: Maximum water velocities calculated from Joukowsky equation using measured parameters and a calculated wave speed c = 1,403 m/s for the short hose connection to the header tank for Configuration A

Flow rate (L/s)	Velocity (m/s)	Inlet Head (m)	Max Head (m)	Δ Head (m)	Δ Velocity (m/s)
0.05	0.2	15	16	1	0.2
0.15	0.5	15	22	7	0.6
0.30	1.0	15	29	14	1.1
0.43	1.5	15	33	18	1.6
0.57	2.0	15	37	22	2.2
0.63	2.2	15	42	27	2.4
0.70	2.5	15	46	31	2.7

Table 5-6: Maximum water velocities calculated from Joukowsky equation using measured parameters and a calculated wave speed c = 1,403 m/s for the short hose connection to a booster pump for Configuration B

Flow rate (L/s)	Velocity (m/s)	Inlet Head (m)	Max Head (m)	Δ Head (m)	Δ Velocity (m/s)
0.05	0.2	15	35	20	0.3
0.15	0.5	15	36	21	0.7
0.30	1.0	15	37	22	1.2
0.43	1.5	15	40	25	1.7
0.57	2.0	15	42	27	2.2
0.63	2.2	15	43	28	2.4
0.70	2.5	15	44	29	2.7

5.6 Hydraulic Performance of CP&LM Pressure Regulators

As mentioned previously (Section 4.4.2), the tested pressure regulators from the three manufacturers were denoted X, Y, and Z for both low pressure (10 psi) and high pressure (15 psi) models. The results of the extensive laboratory testing of the operational characteristics of CP&LM pressure regulators are presented in the following sections.

5.6.1 *Pressure Regulation Accuracy*

The hydraulic characterisation of the regulating accuracy of CP&LM pressure regulators was an attempt to verify the ability of the devices to produce or deliver the design output pressures to the nozzle as specified by their respective manufacturers. Replication tests were first performed on one unit of each of the three manufacturers to determine if there were variations in outlet pressure. The flow rate was set at 0.3 L/s and 110 kPa of supply pressure for the three replicate tests. The results showed that the regulator outlet pressure measurements for the three replicates for each manufacturer were not significantly different (maximum 0.01%). The regulation accuracy test results for the CP&LM pressure regulator brands most commonly used in industry are shown Table 5-7. The results from this 240 tests show that in general, the regulator output pressures are different from the pre-set pressure specified for each of the brands. Notably, the mean measured regulated pressure for manufacturer X was below the nominal pre-set pressure, while the means for manufacturers Y and Z were significantly higher than the regulator pre-set pressure specified by the manufacturers for both low and high pressure models.

The deviation for manufacturer X pressure regulators was -3.9 % (-2.67 kPa) for the low pressure models and -5.3 % (-5.5 kPa) for the high pressure models. The deviation of the mean regulated pressure for manufacturer Y regulators was 9.3 % (6.43 kPa) for the low pressure models while the high pressure models had a mean deviation of 7 % (7.19 kPa), which is the highest test result variation across all the three pressure regulator brands. The manufacturer Z regulators had a mean deviation of 6.1 % (4.24

kPa) for the low pressure models and 1.3 % (1.29 kPa) for the high pressure models, respectively.

Table 5-7: Pressure regulating accuracy of CP&LM pressure regulators conducted at a reference velocity of 1 ms^{-1}.

PRV Manufacturer	X		Y		Z	
PRV Model (Pressure)	Low	High	Low	High	Low	High
Declared pre-set pressure (kPa)	68.95	103.42	68.95	103.42	68.95	103.42
Mean regulated pressure (kPa)	66.28	97.92	75.38	110.61	73.18	104.71
Standard deviation of regulated pressures (kPa)	0.44	1.67	0.60	0.70	0.66	0.45
Coefficient of variation (%)	0.7	1.71	0.8	0.6	0.9	0.4
Deviation between mean regulated pressure and declared pre-set pressure (kPa)	-2.67	-5.50	6.43	7.19	4.24	1.29
Deviation between mean regulated pressure and declared pre-set pressure (%)	-3.9	-5.3	9.3	7.0	6.1	1.3

PRV – pressure regulating valve

The ISO Standard 10522:1993 specifies the average deviation of regulated pressure for a sample of ordinary pressure regulators should not exceed 7 % of the declared pre-set pressure, which would be 4.8 kPa and 7.2 kPa, respectively, for the low and high pressure models. From the experimental results, it is evident that all the pressure regulator models tested met the criteria stated by the ISO Standard, except for the low pressure model of manufacturer Y pressure regulators. Nonetheless, all these pressure regulator brands were classified as direct acting-ordinary pressure regulators because they consisted of a conical tapered water passage or flow tube that automatically induce a variable head loss to maintain a relatively constant pressure at the outlet under varying pressures and discharges. The manufacturer Y pressure regulators exhibited significantly higher deviations, as the high pressure model also presented the maximum allowable mean deviation of 7 %.

The coefficient of variation (CV) for all three pressure regulator manufacturers X, Y, and Z were lower than the limit of 10 % usually recommended by ISO Standard 10522:1993. Manufacturer X pressure regulators had a CV of 0.7 % for the low pressure model and 1.7 % for the high pressure model. Manufacturer Y had a CV of 0.8 on the low pressure model, and 0.6 % for the high pressure model, while manufacturer Z had 0.9 % for the low pressure model and 0.4 % for the high pressure model. These CV values are correlated to the standard deviation of the regulated pressures for manufacturers X, Y, and Z pressure regulators, which are all under 1 standard deviation from the mean except for the high pressure model for manufacturer X regulators. The very low CV values demonstrate that the regulator outlet pressures were nearly similar for each model of the tested units, which indicate proper quality control in the manufacturing process of pressure regulating devices.

5.6.2 *Pressure Regulation Curves*

Pressure regulating curves for the manufacturers X, Y, and Z CP&LM pressure regulators were plotted using the data obtained from ninety (90) tests conducted according to the experimental measurement processes described in Section 4.5.3.2. These types of tests were conducted to determine the magnitude of regulator outlet pressure reductions due to increase in head loss, as caused by varying flow rate through the devices. The graphs of the regulating curves were plotted using two different approaches. The first set of graphs shows the regulator outlet pressure as a function of supply pressure at constant discharges, while the second set of graphs shows the flow rate as a function of the regulator outlet pressure at a constant supply pressure for three different set pressures, as recommended by ISO Standard 10522:1993. It is can be established from the results that the regulator outlet pressure is largely influenced by supply pressure and discharge from the devices. The regulated pressure tends to increase with increases in supply pressure up to a certain threshold and then declines further.

Figure 5-27 and Figure 5-28 represent outlet pressures for two units of the 10 psi model X pressure regulator. There is a slight increase in outlet pressure when inlet pressure increases up to about 400 kPa at the same flow rate. The pressure reduces again slightly

below the pressure measured at 1.5 times the nominal set pressure for the devices. The influences of flow rate on outlet pressure is also demonstrated by the decline in pressure as flow rate increases from 0.15 to 0.63 L/s. However, it is evident that the outlet pressure is not always following the same pattern with increases in inlet pressure and discharge as shown by the regulated pressures for 0.63 L/s at the higher inlet pressures. The outlet pressure variation across the discharge tends to increase with increase in supply pressure.

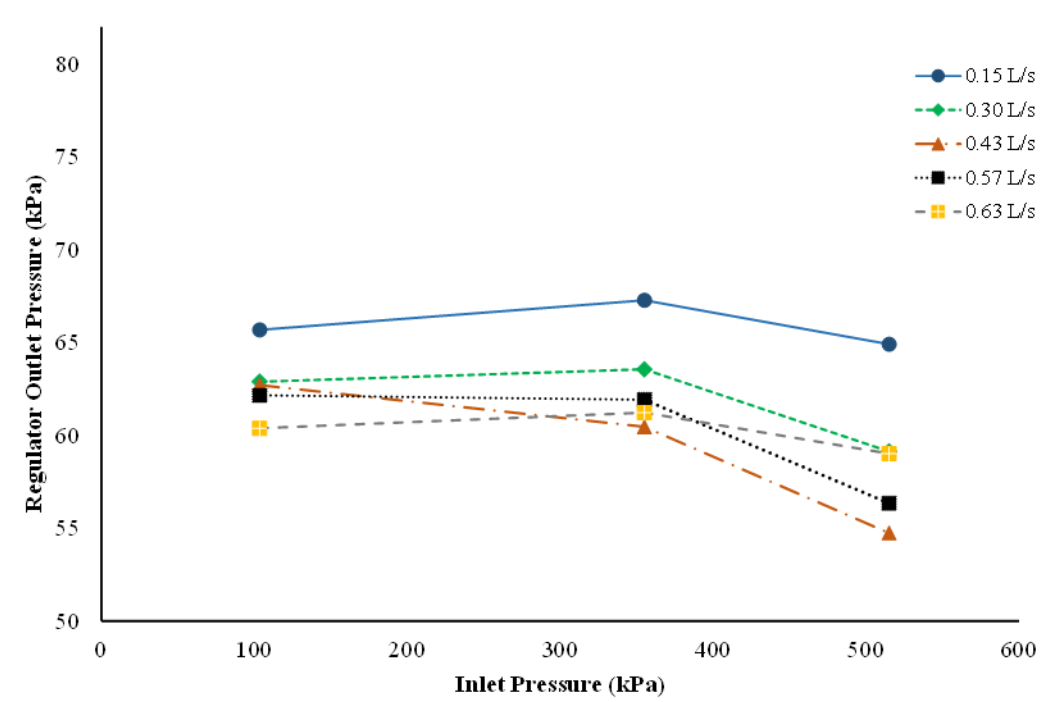

Figure 5-27: Regulation curve for a 10 psi X - #01 pressure regulator showing a decline in the regulated pressure with increase in discharge

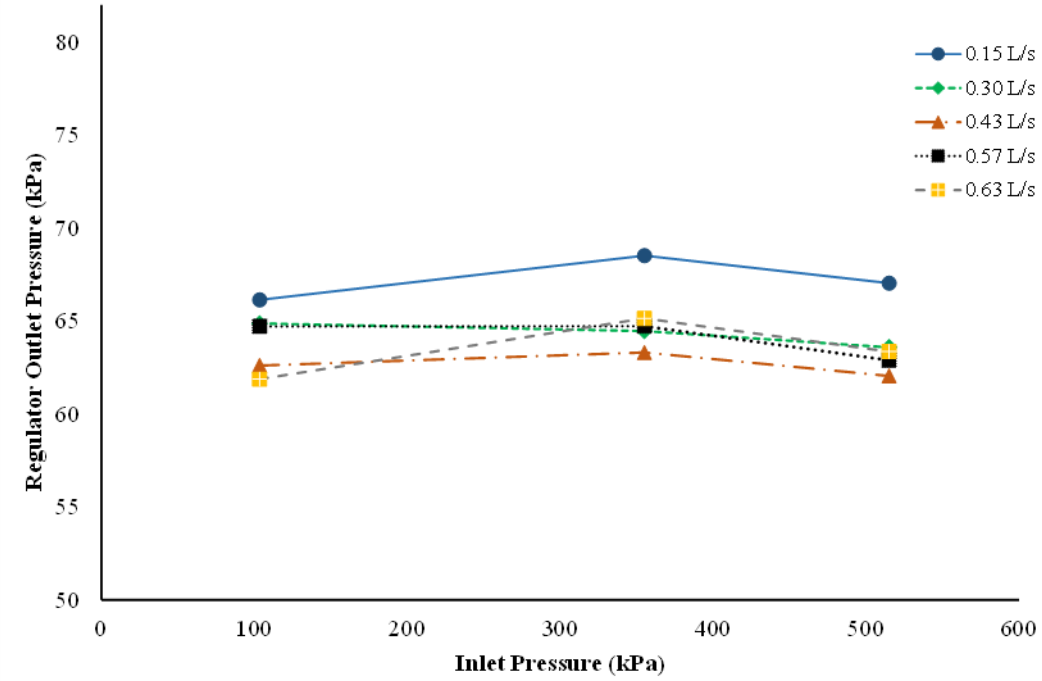

Figure 5-28: Regulation curves for a 10 PSI X - #10 pressure regulator showing a decline in the regulated pressure with increase in discharge

Figure 5-29 illustrates the combined performance of the two units of the tested X type of pressure regulators. The results show that the units are not entirely operating similar and this could be attributed to a testing conditions which might displace the flow tube momentarily, thereby resulting into a different outcome in the outlet pressure. In this type of test, care was always ensured that the measurements were taken when the supply pressure is increasing, and this was achieved by the upstream control valve.

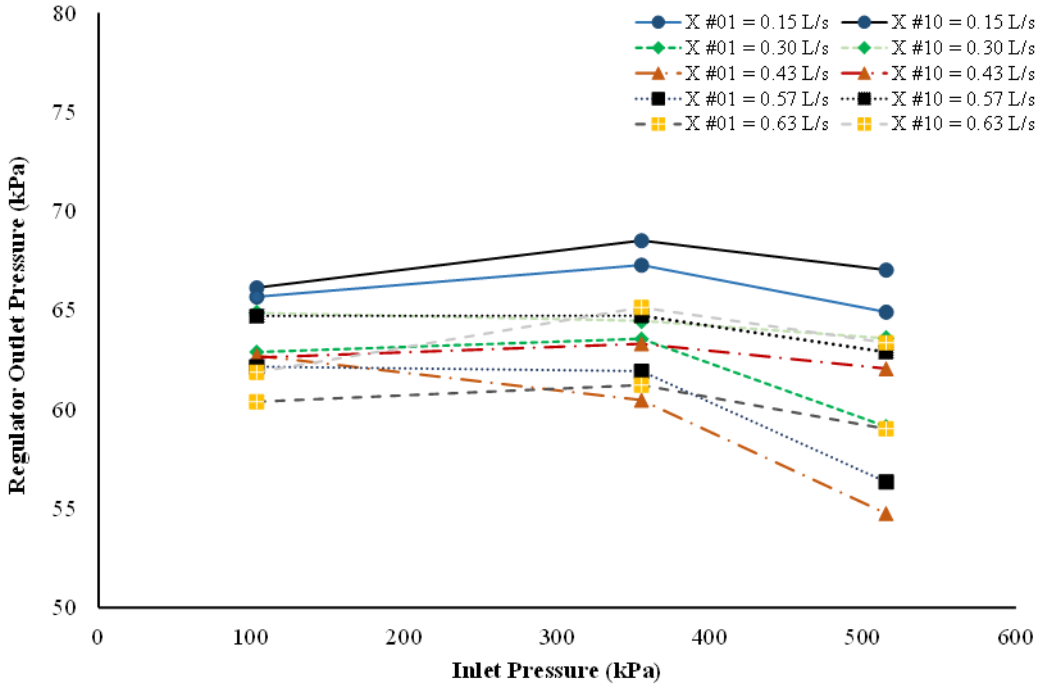

Figure 5-29: Regulation curves for the 10 PSI X - #01 and X - #10 pressure regulators

The performance of the high pressure (15 psi) regulators was different under the same hydraulic testing conditions (Figure 5-30 and Figure 5-31). The X-#01 had outlet pressures decreasing slightly from the 103 kPa to 400 kPa inlet pressure across the flow rates tested. The outlet pressures were generally about 95 kPa at 0.15 L/s and 94 kPa and these inlet pressures respectively. It declined from 91 kPa to about 90 kPa at the maximum flow rate equal to 0.63 L/s. The variation in the regulated pressures increased significantly as inlet pressures increased. At an inlet pressure of 550 kPa, the outlet pressure ranged from 97 kPa for the low flow rate down to 88 kPa at the highest flow rate. Of note is that all the regulated pressures were below the nominal pressure rating of the device as specified by the manufacturer. However, the X-#10 performed differently exhibiting a much wider variation in the regulated pressures between individual flow rates. The variation is large between the lowest flow rates up the median flow rate after which the pressures become very closely tight to each other with increase in flow rate. The performance comparison amongst the two pressure regulator units is shown in Figure 5-32.

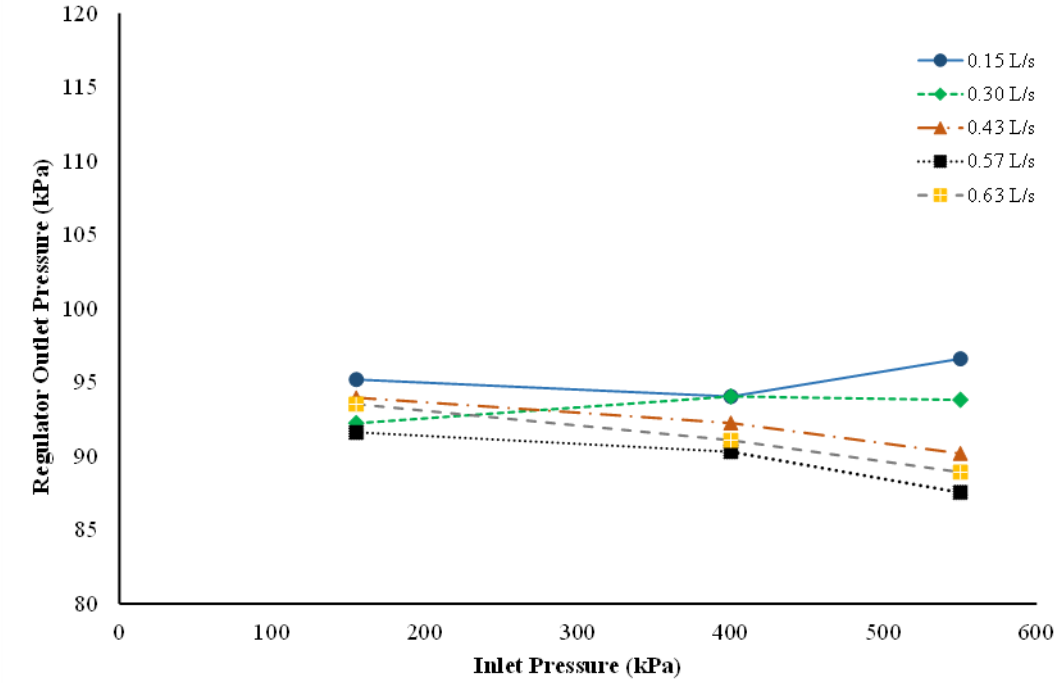

Figure 5-30: Regulation curve for a 15 PSI X - #01 pressure regulator showing a decline in the regulated pressure with increase in discharge

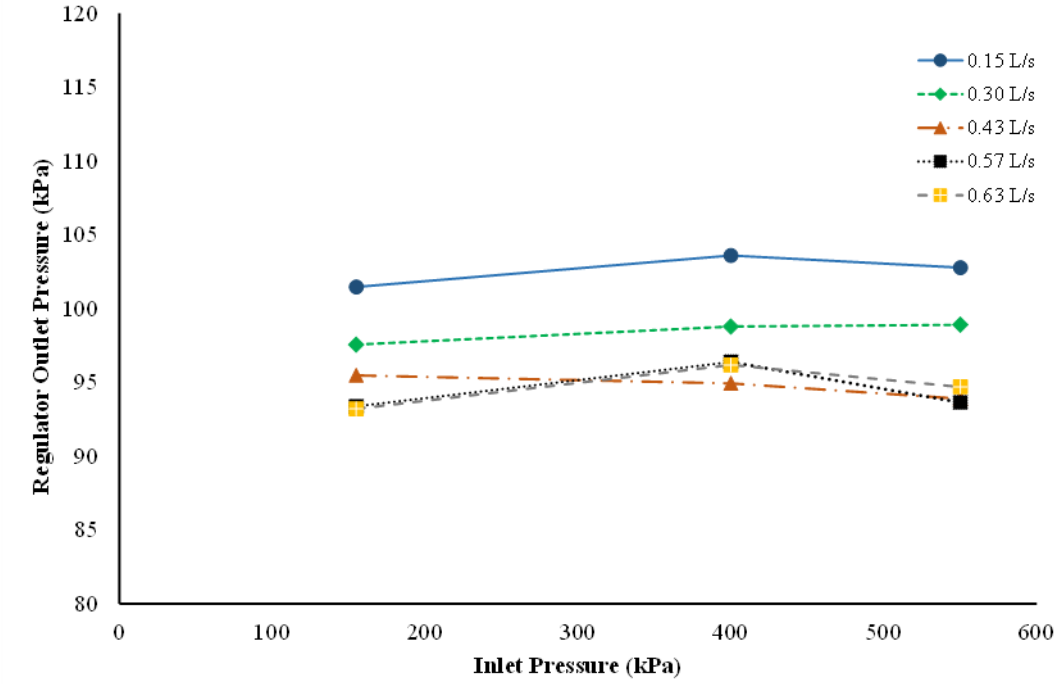

Figure 5-31: Regulation curve for a 15 PSI X - #10 pressure regulator showing a decline in the regulated pressure with increase in discharge

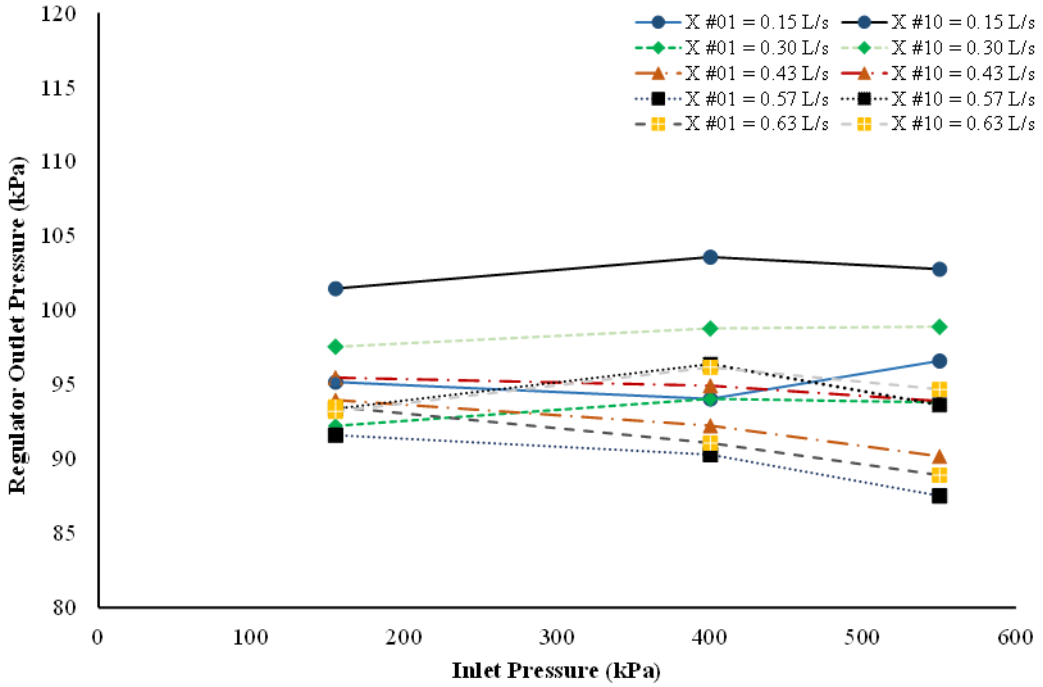

Figure 5-32: Regulation curves for the 15 PSI X - #01 and X - #10 pressure regulators

The regulated pressures as a function of flow rate at specific constant inlet pressures for the low pressure brand of Y regulators are illustrated in Figure 5-33 through to Figure 5-35.

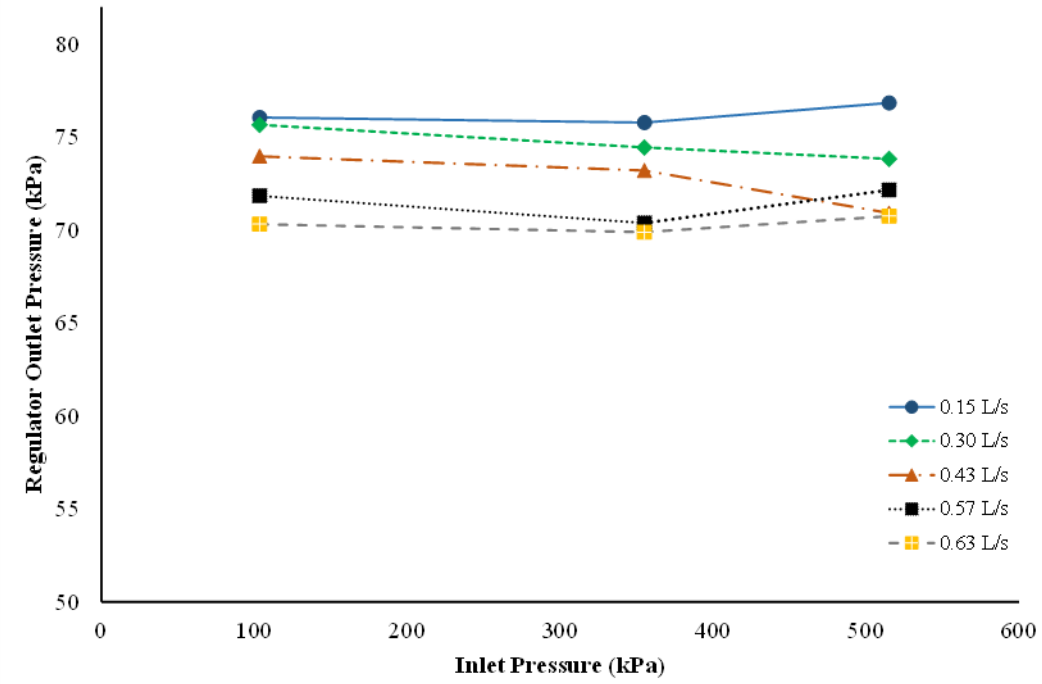

Figure 5-33: Regulation curve for a 10 PSI Y - #01 pressure regulator showing a decline in the regulated pressure with increase in discharge

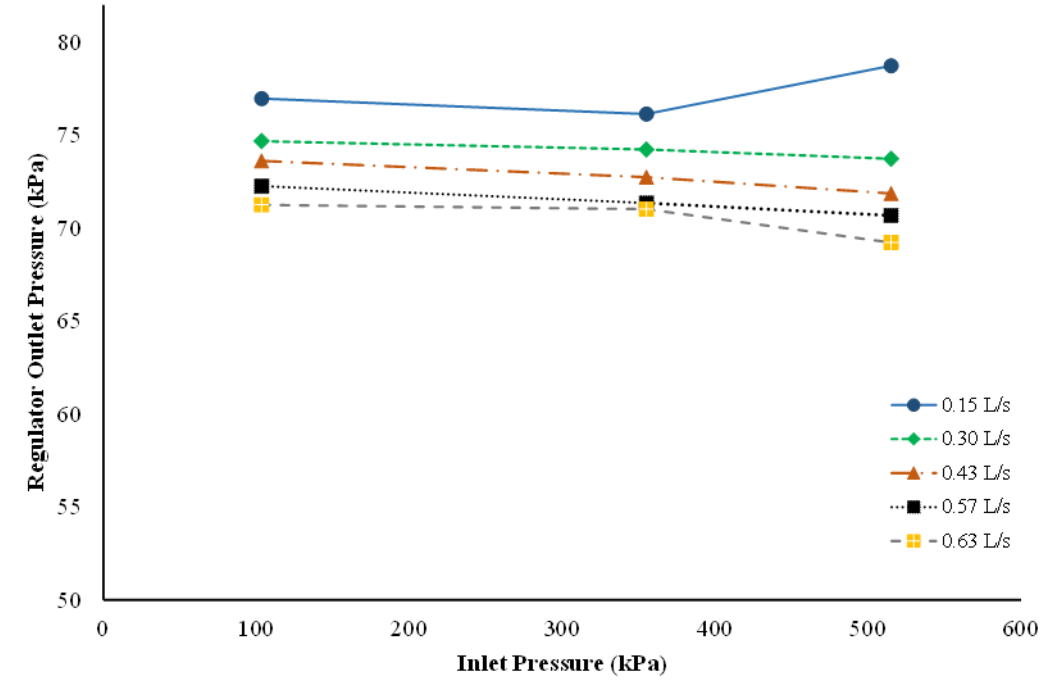

Figure 5-34: Regulation curve for a 10 PSI Y - #10 pressure regulator showing a decline in the regulated pressure with increase in discharge

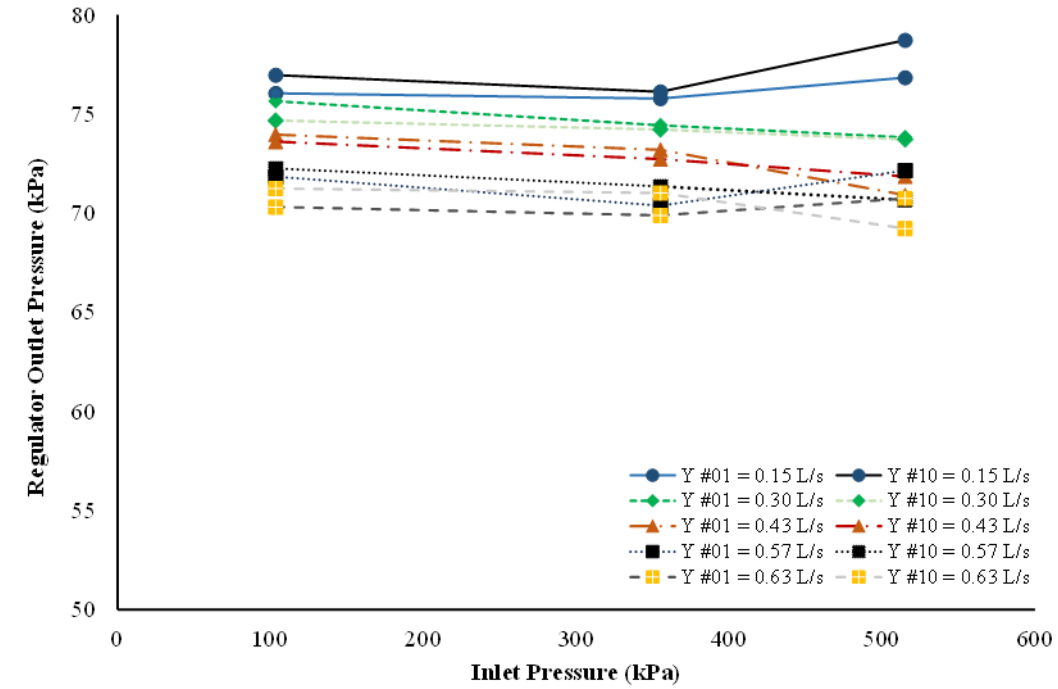

Figure 5-35: Regulation curves for the 10 PSI Y - #01 and Y - #10 pressure regulators

The regulating performance for the high pressure models of the Y brand of pressure regulators is represented in Figure 5-36 to Figure 5-38.

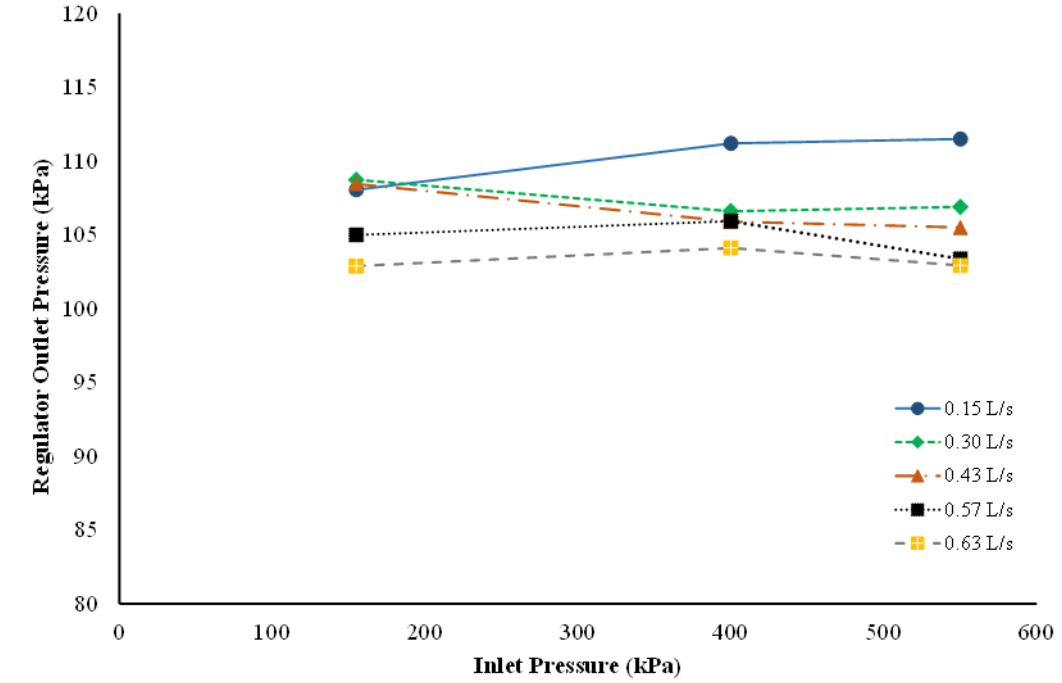

Figure 5-36: Regulation curve for a 15 PSI Y - #01 pressure regulator showing a decline in the regulated pressure with increase in discharge

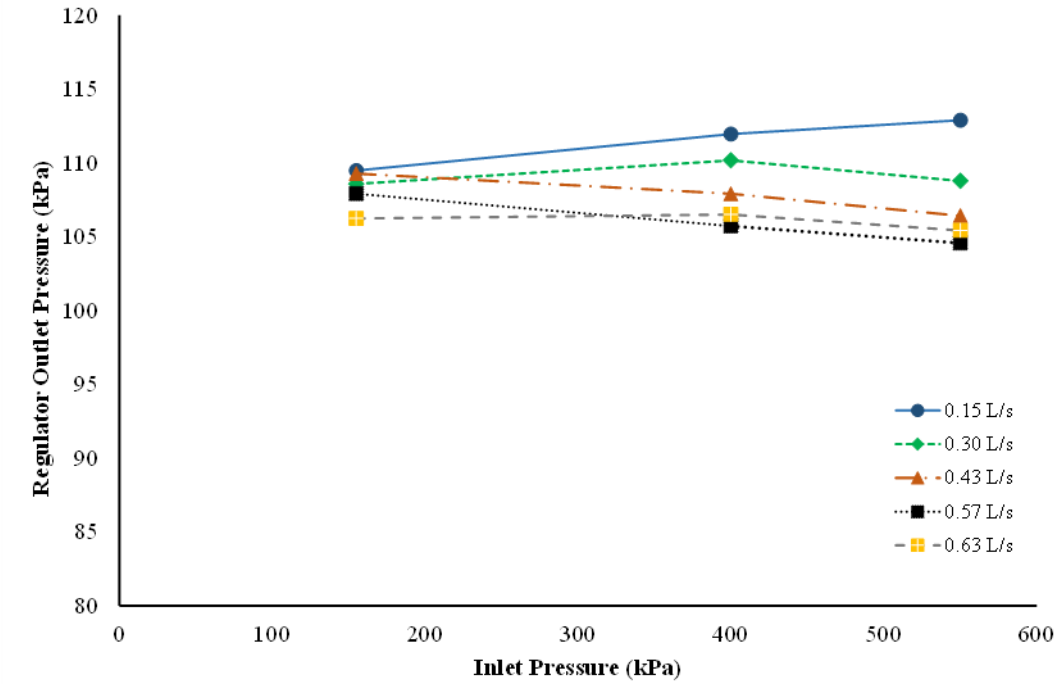

Figure 5-37: Regulation curve for a 15 PSI Y - #10 pressure regulator showing a decline in the regulated pressure with increase in discharge

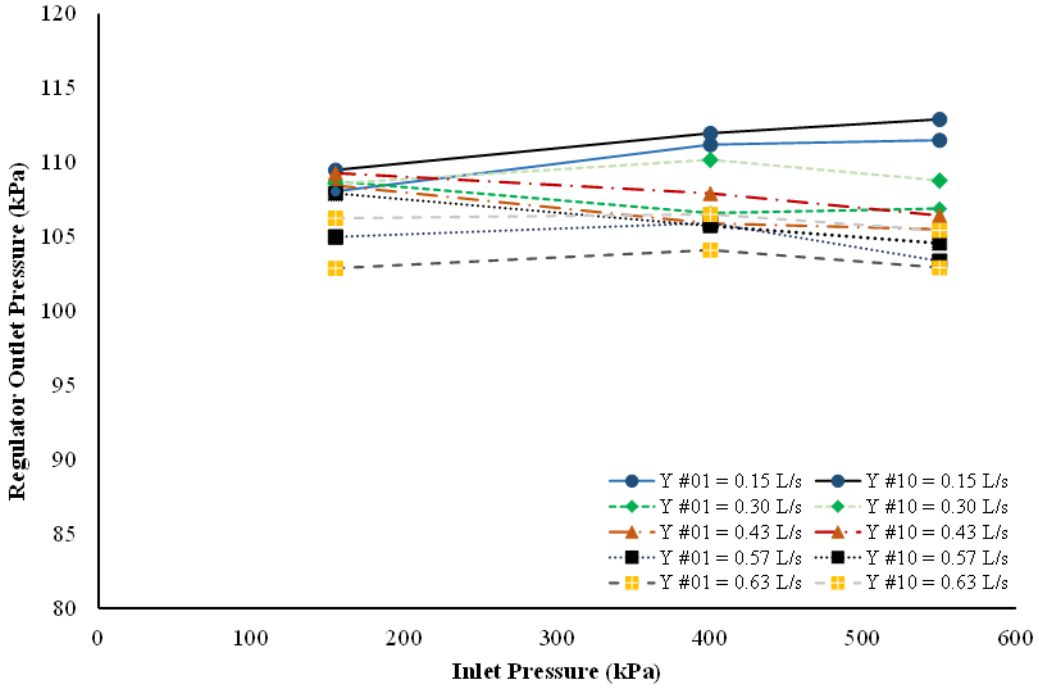

Figure 5-38: Regulation curves for the 15 PSI Y - #01 and Y - #10 pressure regulators

The performance of the Z brand low pressure regulators is shown the figures below. It is apparent from the results that the spread amongst individual data points is very small in this brand. As inlet pressure increases, this small spread in outlet pressure is further reduced. This is likely attributed to increase in drag force with higher flow which holds the flow area wide open, thus resulting to higher regulator outlet pressures.

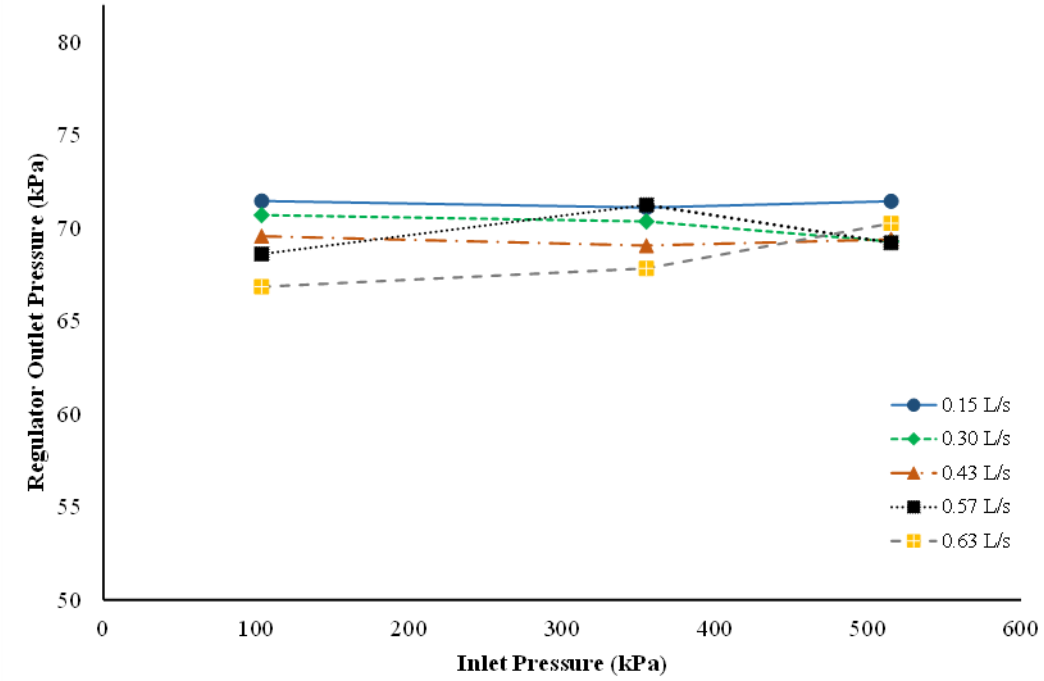

Figure 5-39: Regulation curve for a 10 PSI Z - #01 pressure regulator showing a decline in the regulated pressure with increase in discharge

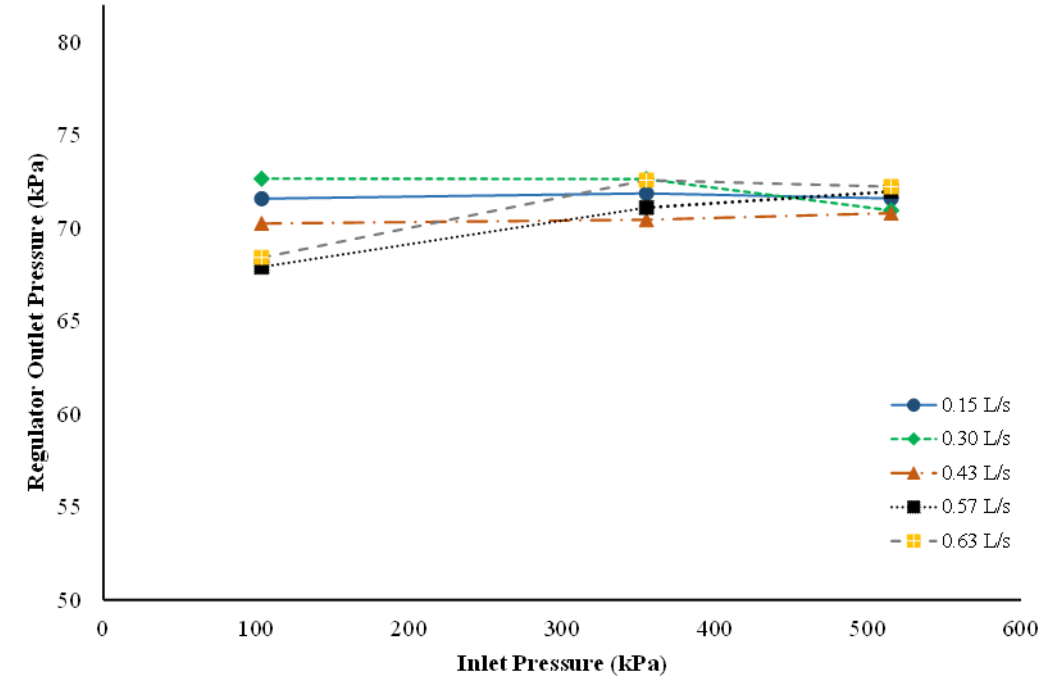

Figure 5-40: Regulation curve for a 10 PSI Z - #10 pressure regulator showing a decline in the regulated pressure with increase in discharge

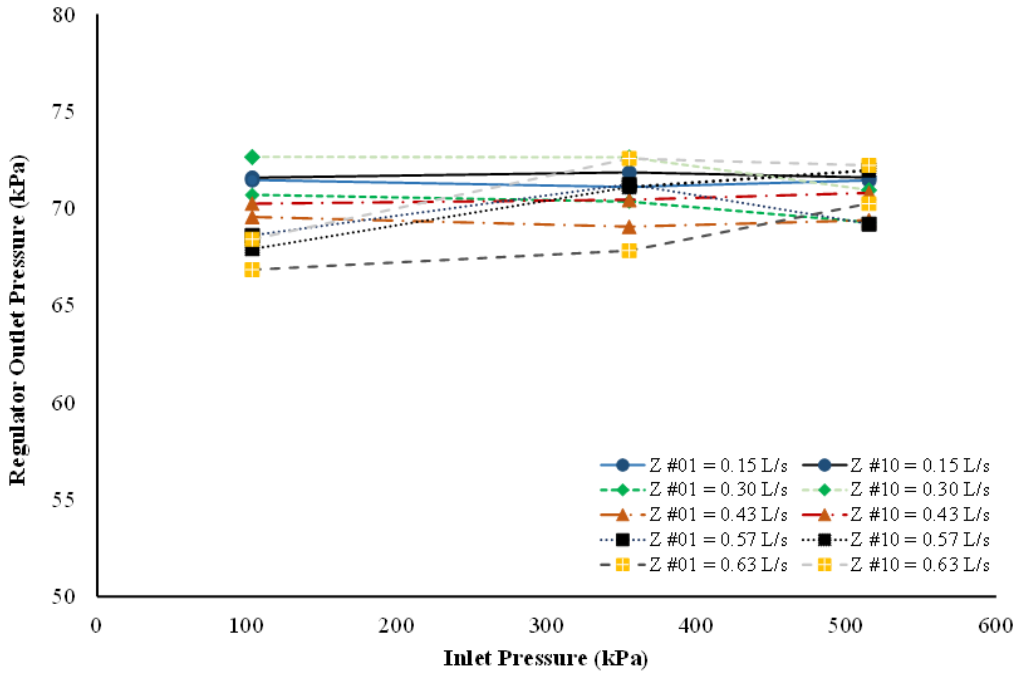

Figure 5-41: Regulation curves for the 10 PSI Z - #01 and Z - #10 pressure regulators

Figure 5-42 through to Figure 5-44 shows the results of Z high pressure regulator models demonstrating a contrary performance from the low pressure models where the tightness of outlet pressures across flow rates is generally inverse. The regulated pressures vary with higher inlet pressures more like the X and Y regulators presented above.

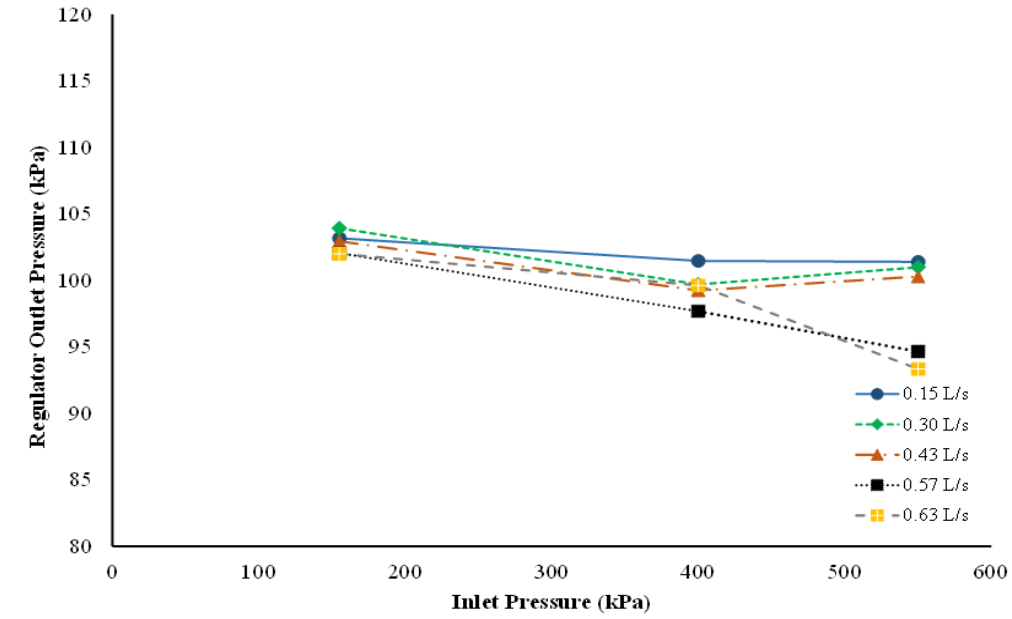

Figure 5-42: Regulation curve for a 15 PSI Z - #01 pressure regulator showing a decline in the regulated pressure with increase in discharge

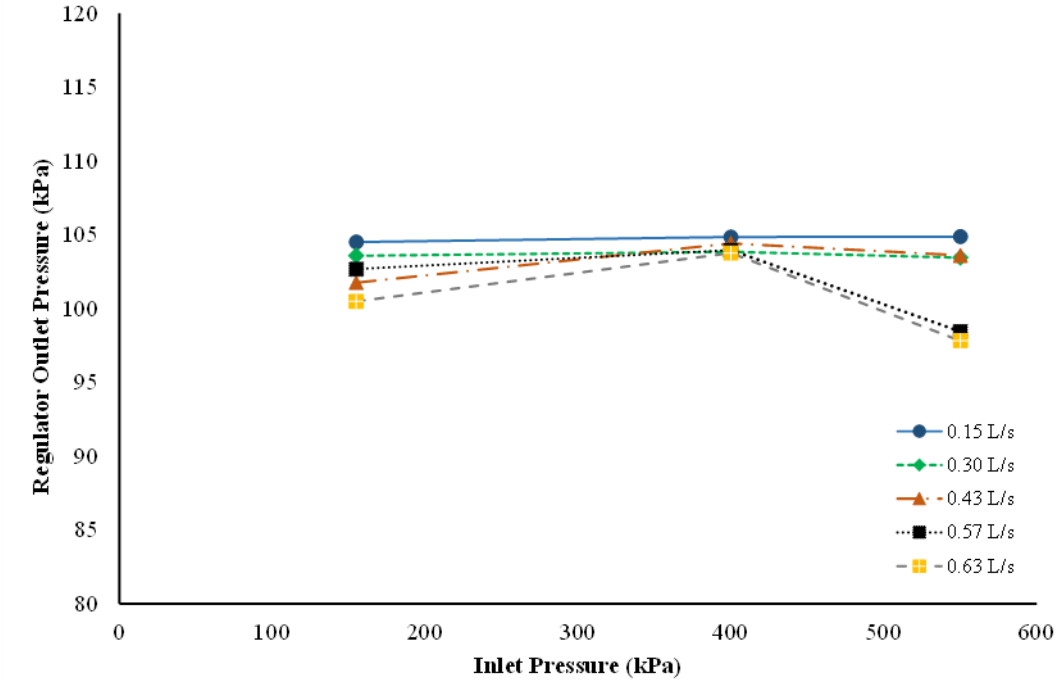

Figure 5-43: Regulation curve for a 15 PSI Z - #10 pressure regulator showing a decline in the regulated pressure with increase in discharge

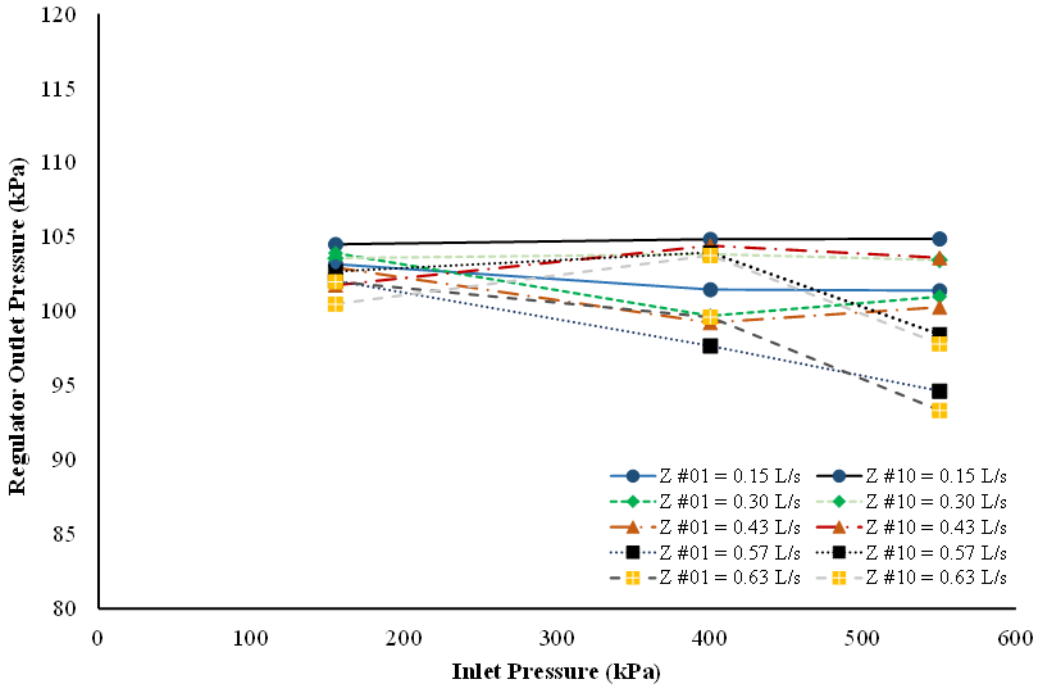

Figure 5-44: Regulation curves for the 10 PSI Z - #01 and Z - #10 pressure regulators

The same regulation performance curves for the tested flow rates at the three different inlet pressures are presented in the following graphs for the same units of the X, Y,

and Z pressure regulators. This time, the outlet pressures are plotted against flow rate to determine the spread of the regulated pressure with increase in flow rate. It can be observed that the two units of the X type of regulator brand on both low and high pressure models are not performing identical especially as the inlet pressure increases to 515 kPa (Figure 5-45 to Figure 5-50). However, a general trend is that the regulated outlet pressure is slightly higher at 0.15 L/s although below the nominal set pressure for the models. It decreases gradually as the flow rate increases to the maximum 0.63 L/s across the three inlet pressures supplied.

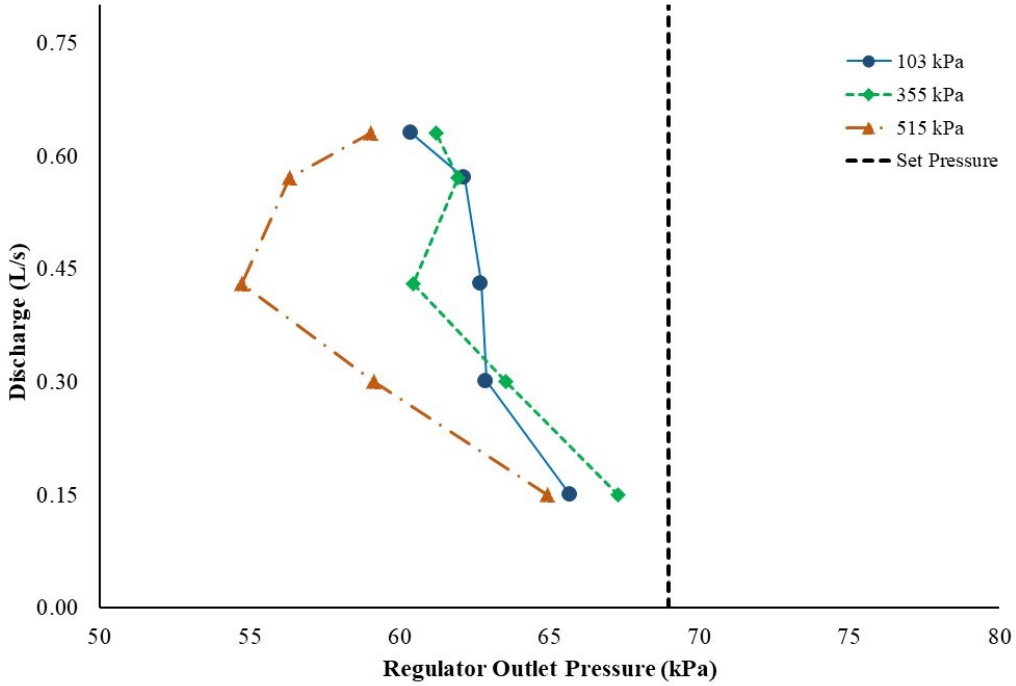

Figure 5-45: Regulation curve for the 10 PSI X - #01 pressure regulator showing regulating tolerance across a range of input pressures

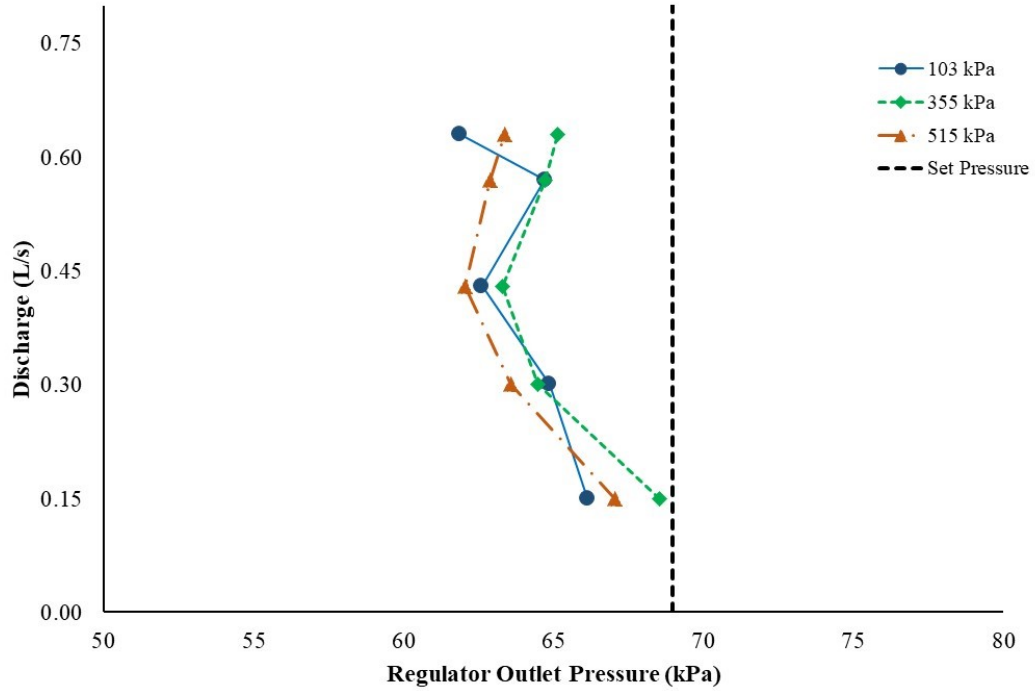

Figure 5-46: Regulation curve for the 10 PSI X - #10 pressure regulator showing regulating tolerance across a range of input pressures

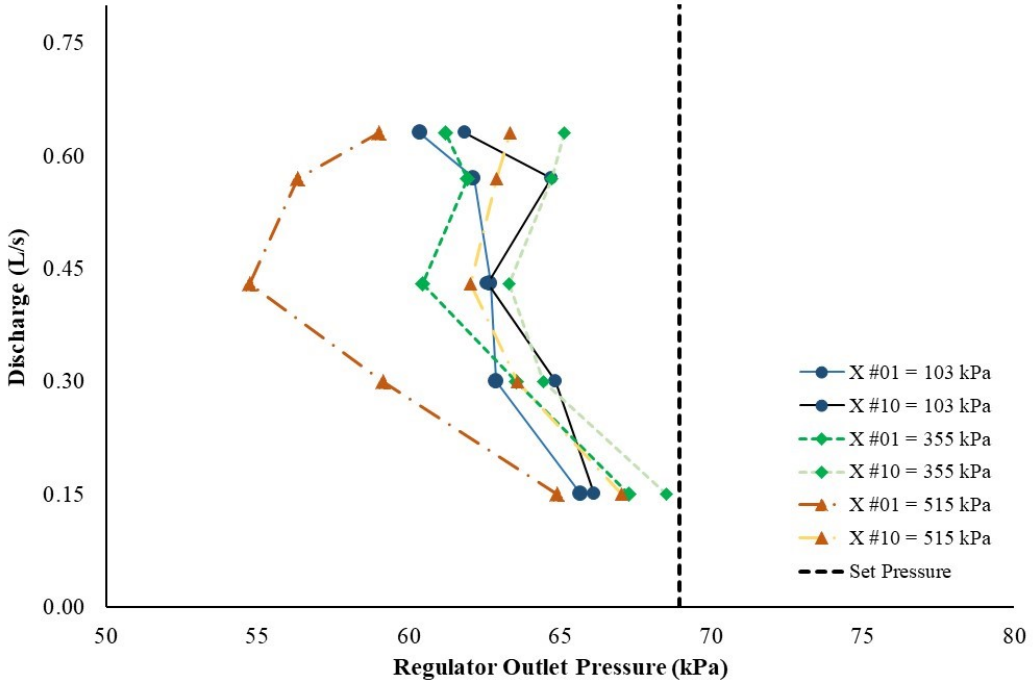

Figure 5-47: Pressure regulating tolerance for the 10 PSI X - #01 and X - #10 pressure regulators

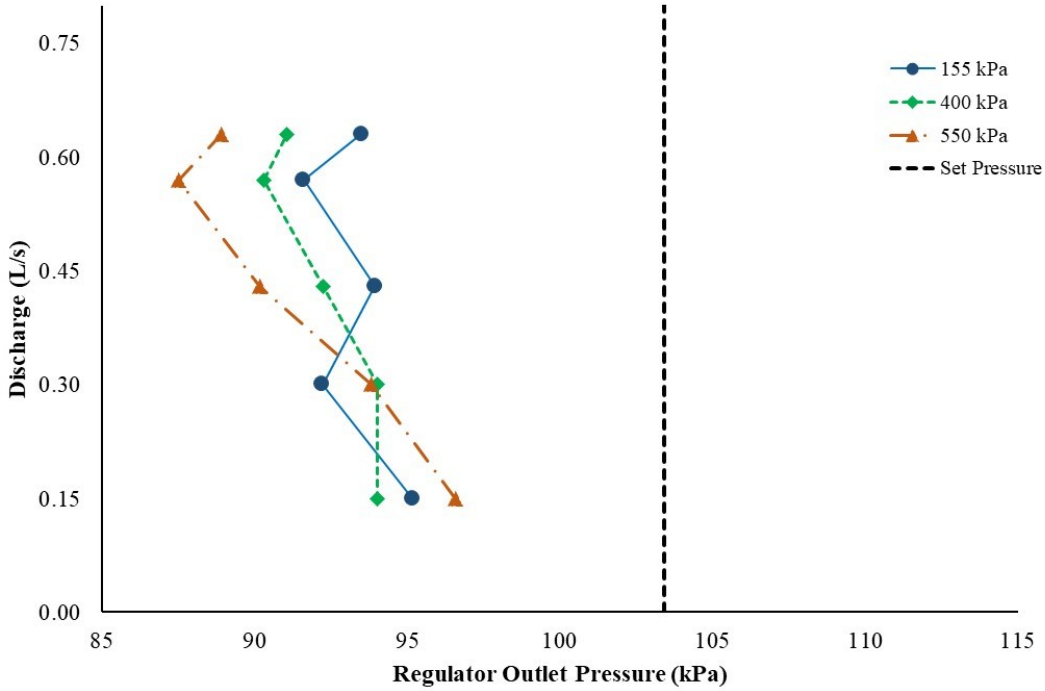

Figure 5-48: Regulation curve for the 15 PSI X - #01 pressure regulator showing regulating tolerance across a range of input pressures

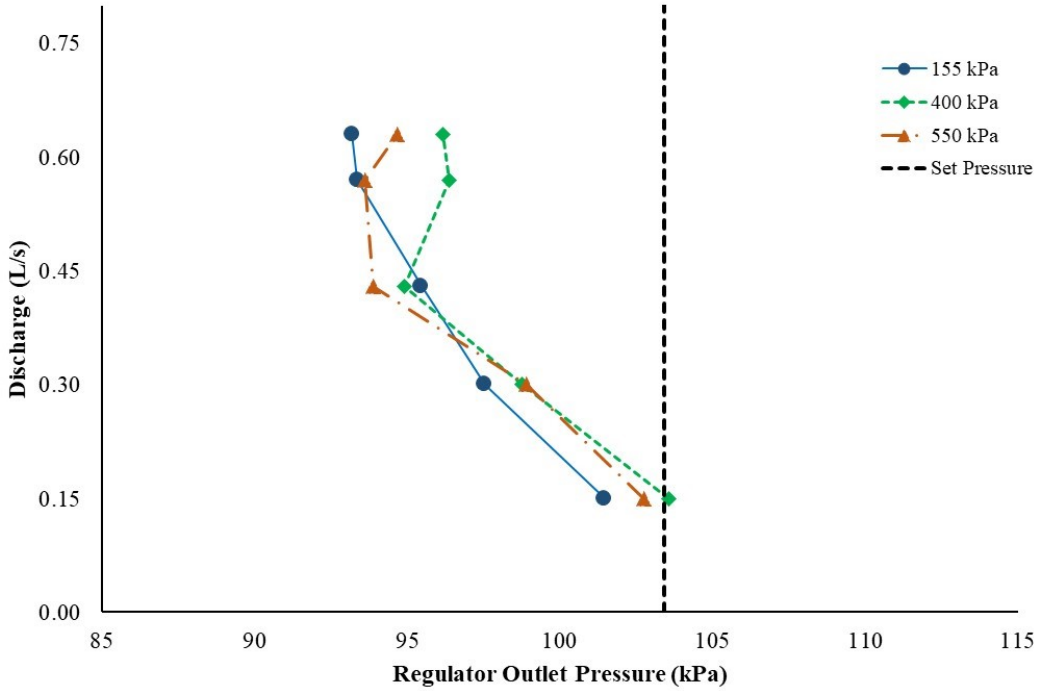

Figure 5-49: Regulation curve for the 15 PSI X - #10 pressure regulator showing regulating tolerance across a range of input pressures

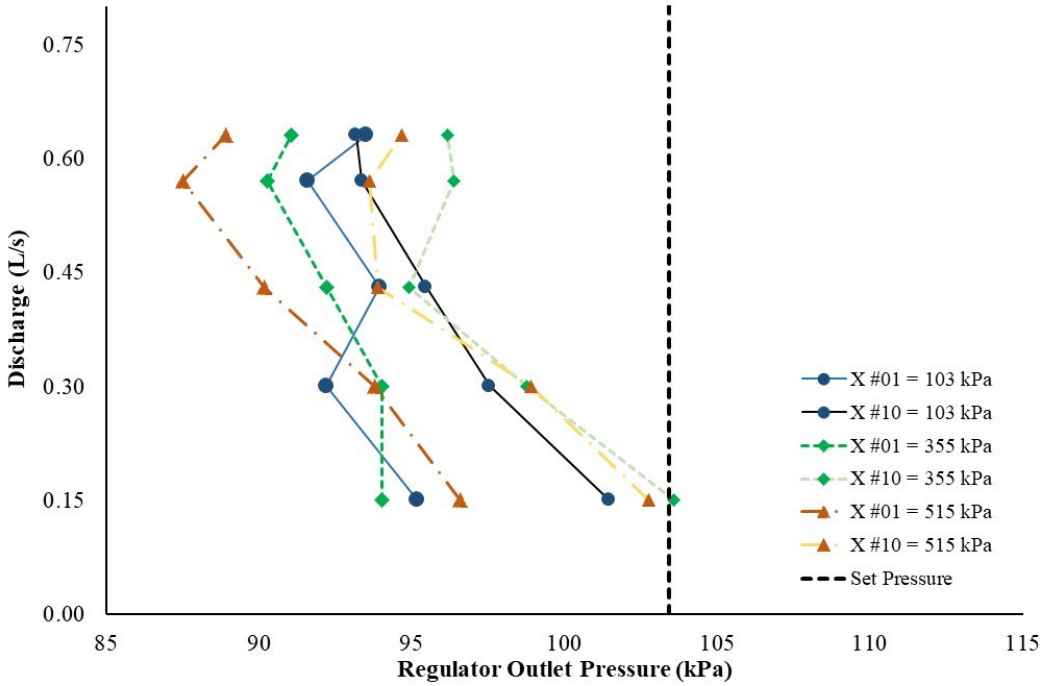

Figure 5-50: Pressure regulating tolerance for the 15 PSI X - #01 and X - #10 pressure regulators

The regulated outlet pressures for the different flow rates at the three inlet pressures for the Y pressure regulator brand are shown in Figure 5-51 to Figure 5-56. The regulated pressures are generally above the nominal set pressure for both the low and high pressure models of manufacturer Y regulator. The outlet pressures decrease as flow rate increases to 0.63 L/s regardless of the inlet pressure magnitude.

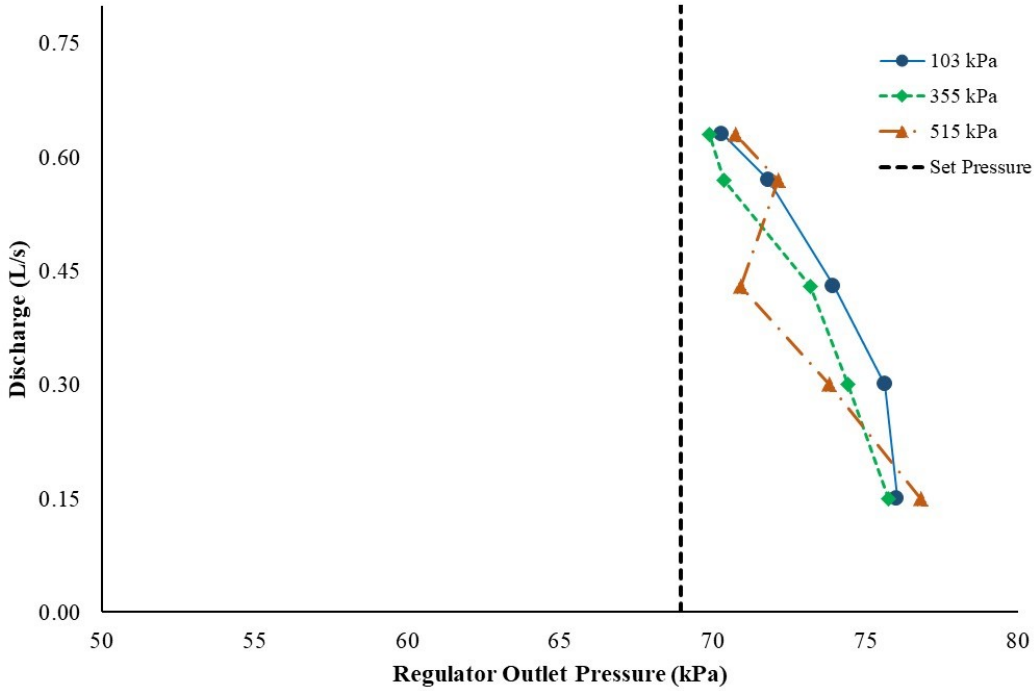

Figure 5-51: Regulation curve for the 10 PSI Y - #01 pressure regulator showing regulating tolerance across a range of input pressures

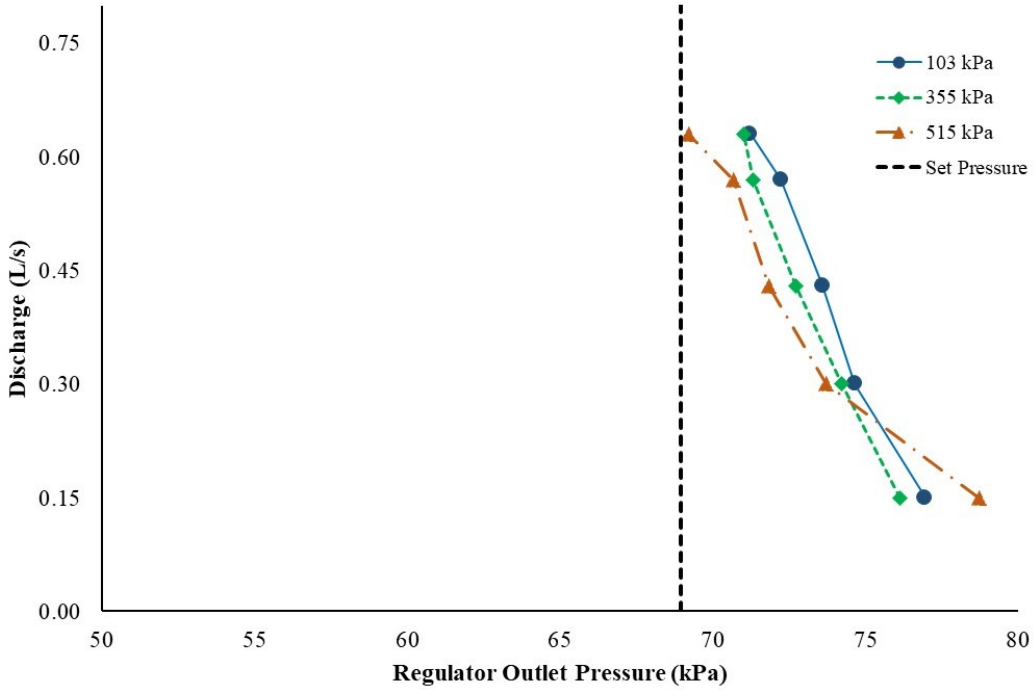

Figure 5-52: Regulation curve for the 10 PSI Y - #10 pressure regulator showing regulating tolerance across a range of input pressures

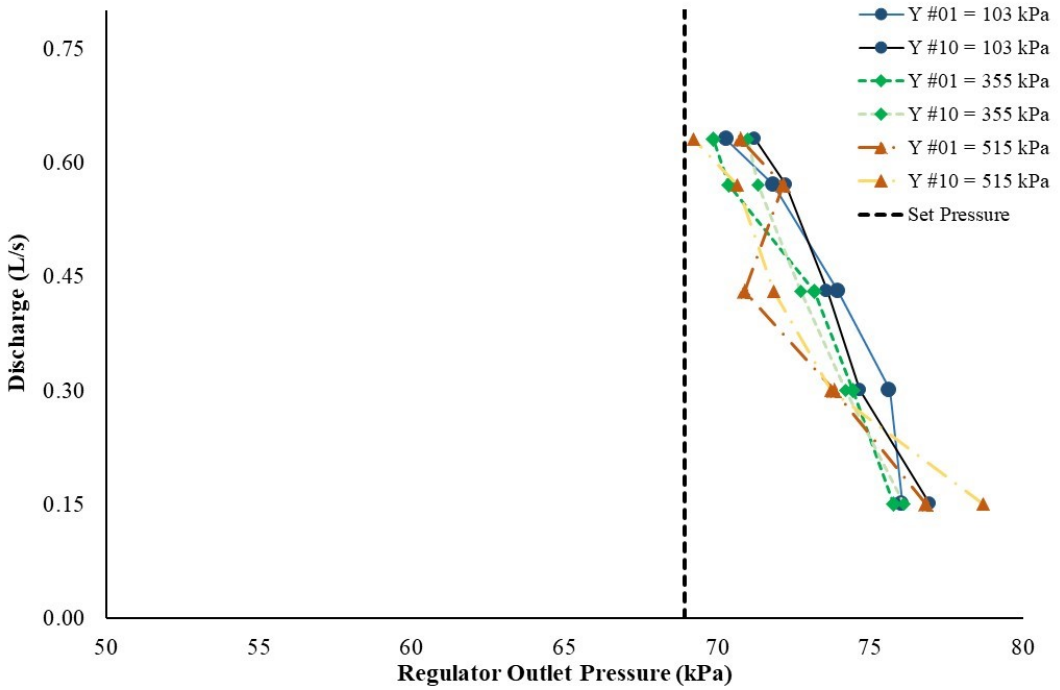

Figure 5-53: Pressure regulating tolerance for the 10 PSI Y - #01 and Y - #10 pressure regulators

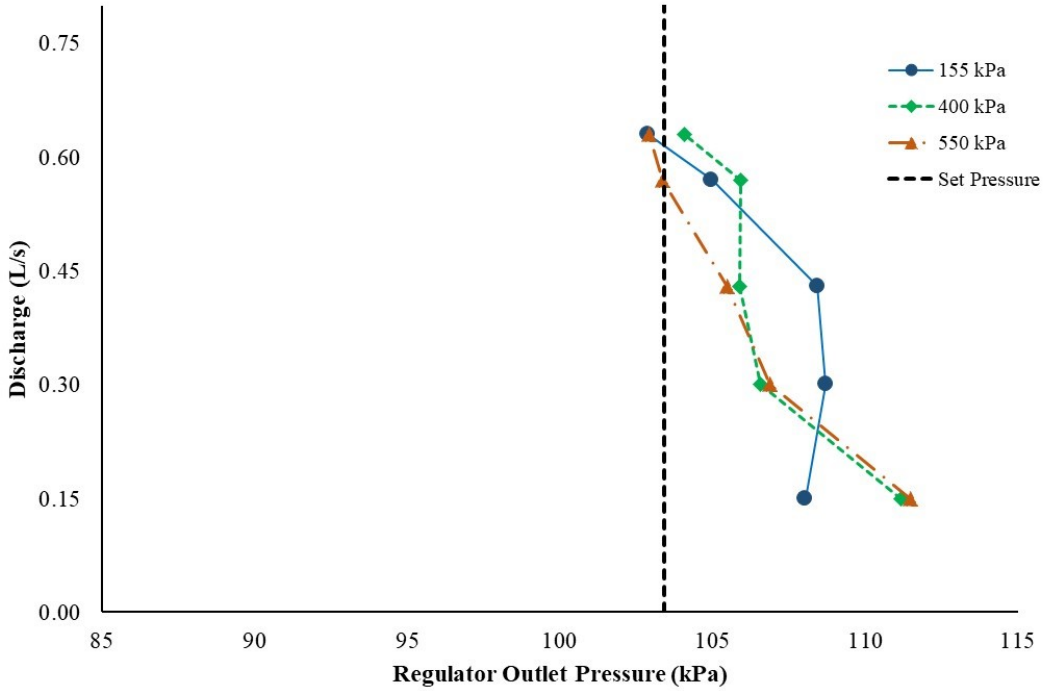

Figure 5-54: Regulation curve for the 15 PSI Y - #01 pressure regulator showing regulating tolerance across a range of input pressures

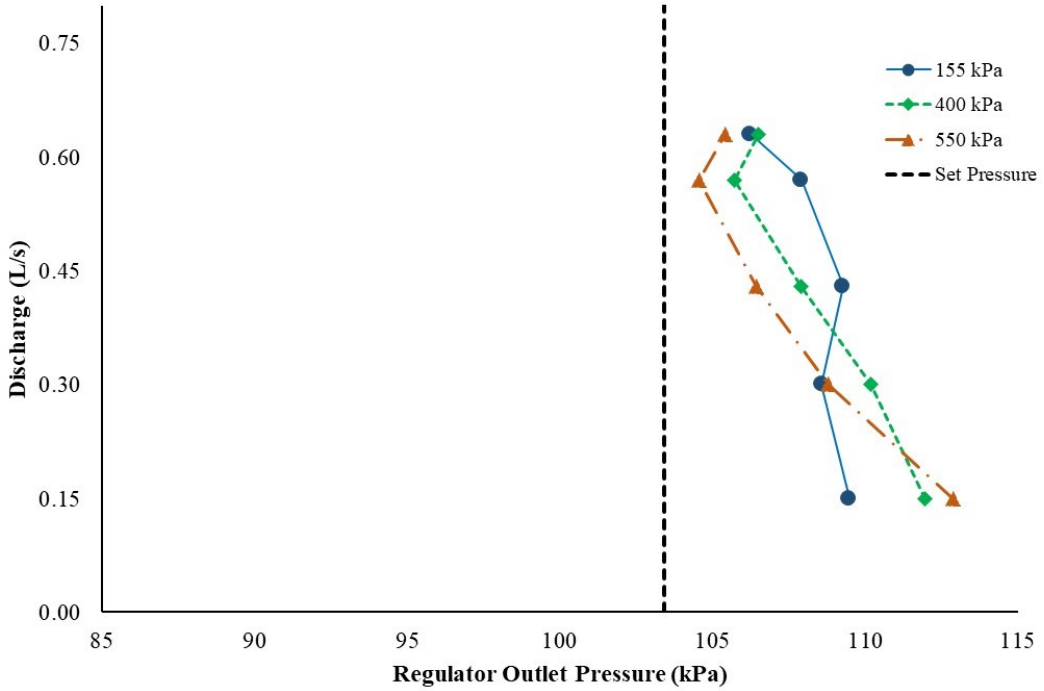

Figure 5-55: Regulation curve for the 15 PSI Y - #10 pressure regulator showing regulating tolerance across a range of input pressures

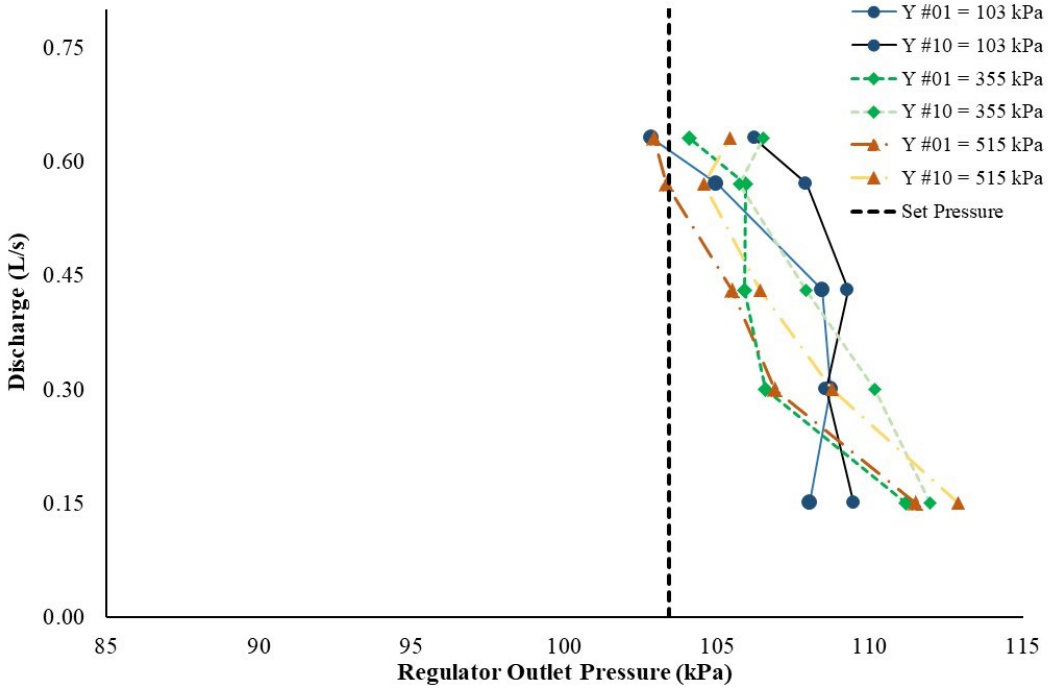

Figure 5-56: Pressure regulating tolerance for the 15 PSI Y - #01 and Y - #10 pressure regulators

The regulated pressures across the tested nozzle flow rates for the Z pressure regulator manufacturer, of both the low and high pressure models are shown in Figure 5-57 to

Figure 5-62. A similar trend is observed with the reduction in the regulated pressures as flow rate increases. This s despite the increase in inlet pressure. The unique observation in the performance of the Z pressure regulators is that the variation amongst individual tested units is small and the data points are closely spaced to each other. However, the regulated pressures are still above the nominal pressure rating of the models tested at the lower flow rates, but will fall slightly below this nominal pressure setting at the maximum tested flow rate.

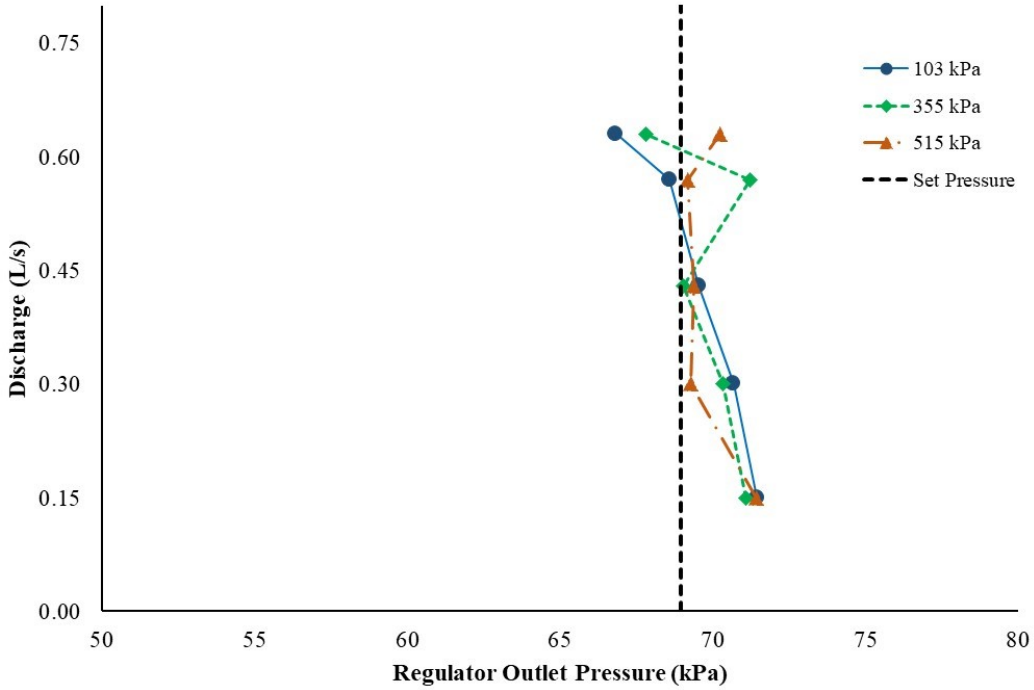

Figure 5-57: Regulation curve for the 10 PSI Z - #01 pressure regulator showing regulating tolerance across a range of input pressures

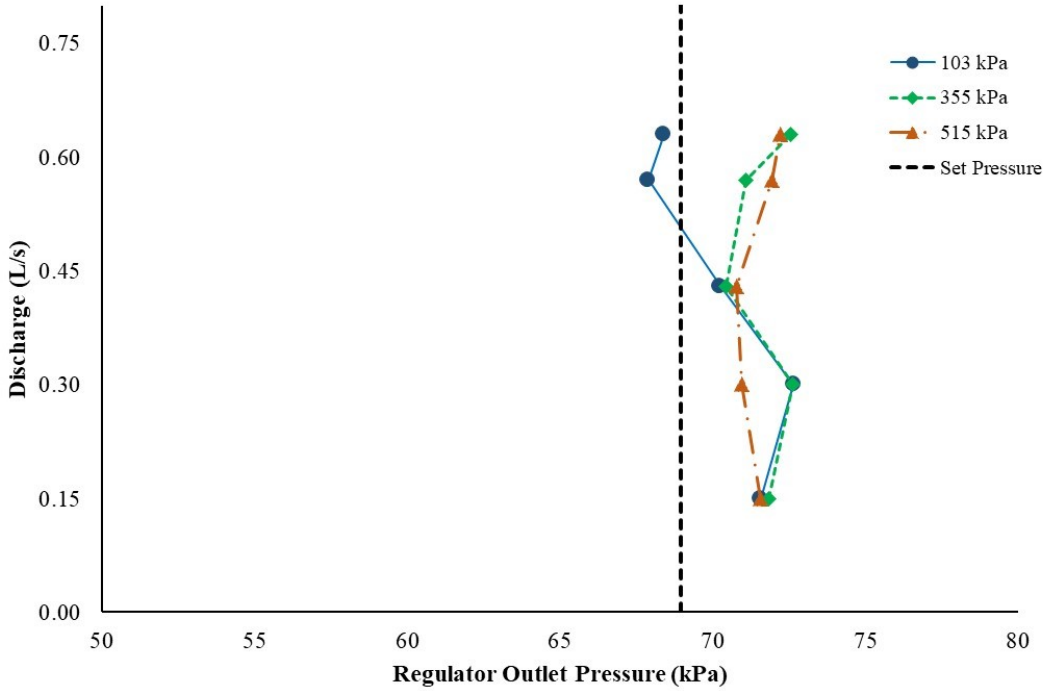

Figure 5-58: Regulation curve for the 10 PSI Z - #10 pressure regulator showing regulating tolerance across a range of input pressures

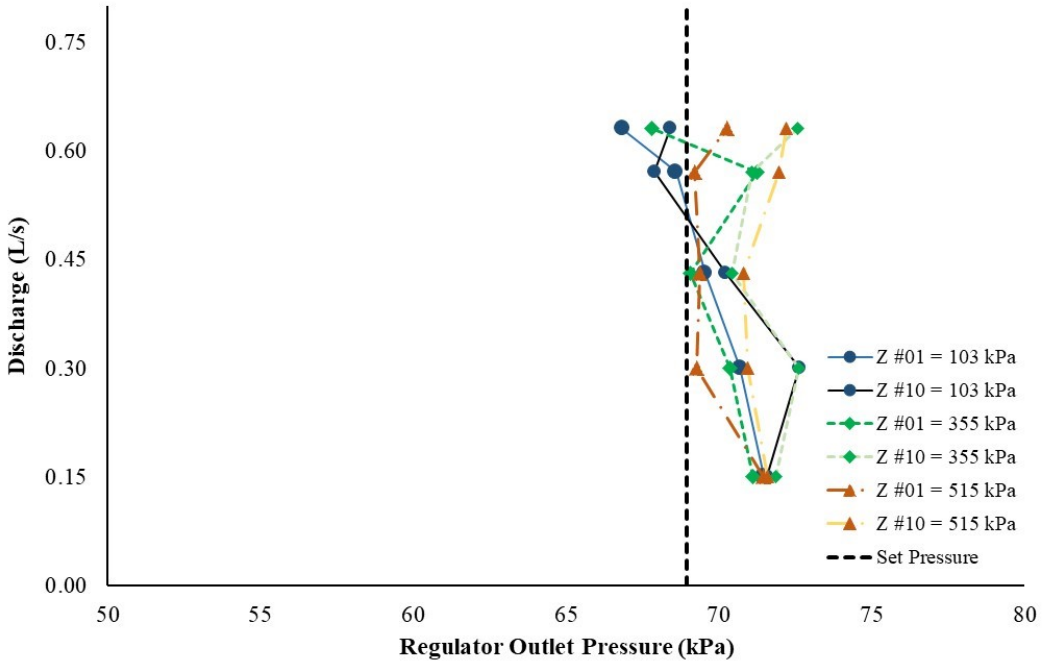

Figure 5-59: Pressure regulating tolerance for the 10 PSI Z - #01 and Z - #10 pressure regulators

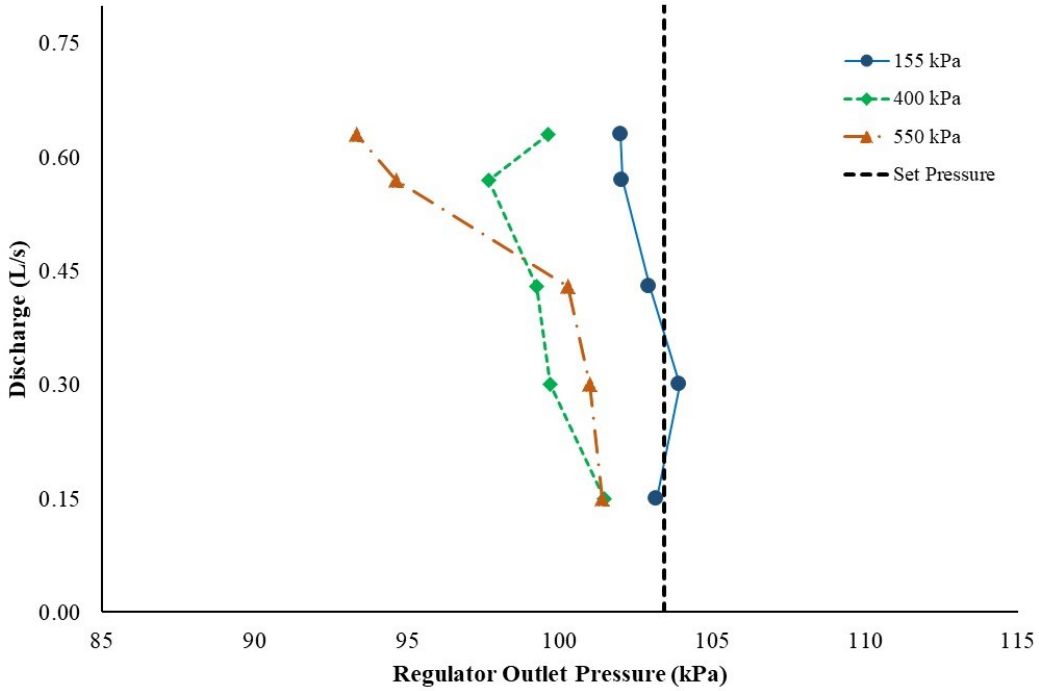

Figure 5-60: Regulation curve for the 15 PSI Z - #01 pressure regulator showing regulating tolerance across a range of input pressures

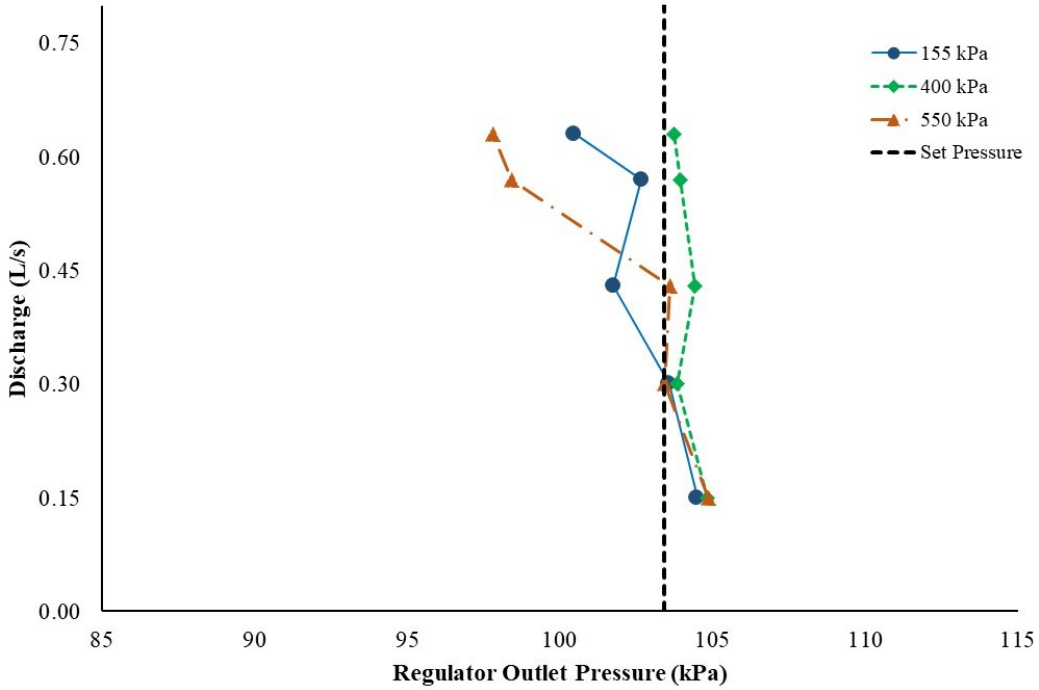

Figure 5-61: Regulation curve for the 15 PSI Z - #10 pressure regulator showing regulating tolerance across a range of input pressures

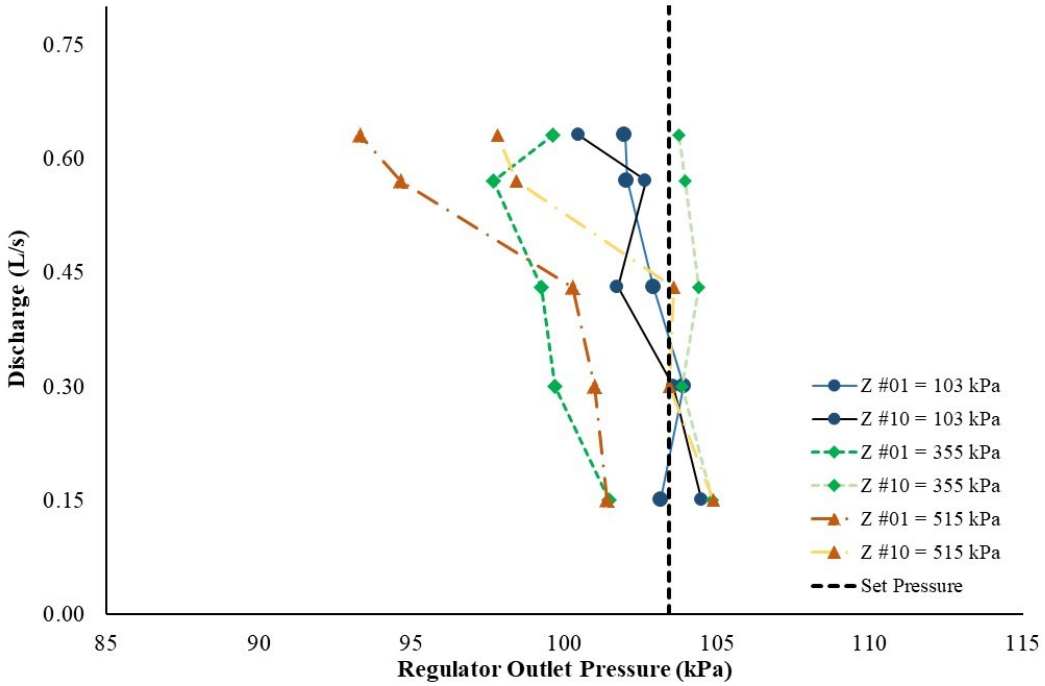

Figure 5-62: Pressure regulating tolerance for the 15 PSI Z - #01 and Z - #10 pressure regulators

The regulation curves and regulating tolerances for the low and high pressure X, Y, and Z pressure regulators were plotted together are shown Figure 5-63 through to Figure 5-66 below. It can be established from this combination that the Y and Z regulator manufacturers are performing at least above and close to the nominal set pressures stated by the manufacturers, while the X brand is generally performing below the nominal set pressures. On the low pressure models, the Y and Z are very close to the nominal pressure setting but the Y brand is somehow higher while the Z brand is operating tightly close to this setting. The high pressure models are however different in that there is a clear difference in regulating performance between the Y and Z brands, which Z still regulating very close to the set pressure while the Y brand is regulating fairly higher than the manufacturer setting. This performance results demonstrate the superiority of the Y and Z brands over the X regulator brand. Overall, the average deviation from the nominal set pressures is calculated to be 7 % lower for X, 7 % higher for Y, and 1 % higher for the Z regulators. This indicates the regulating accuracy of the regulators under steady flow conditions. The performance of the regulators in unsteady varying inlet pressures that causes hysteresis in the regulator outlet pressures is covered in Section 5.6.5.

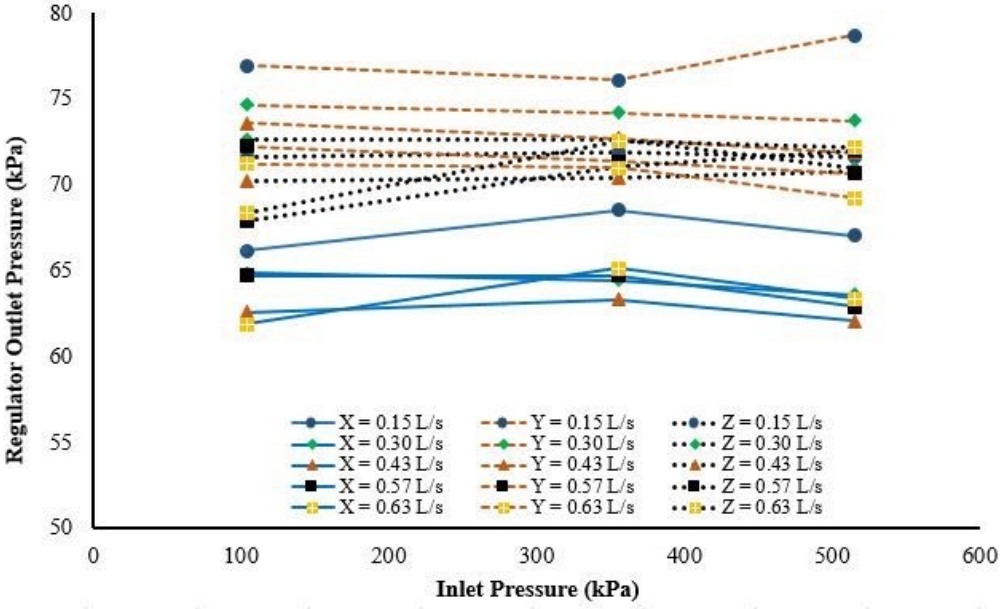

Figure 5-63: Comparison of regulation curves for all 10 PSI X, Y, and Z pressure regulators

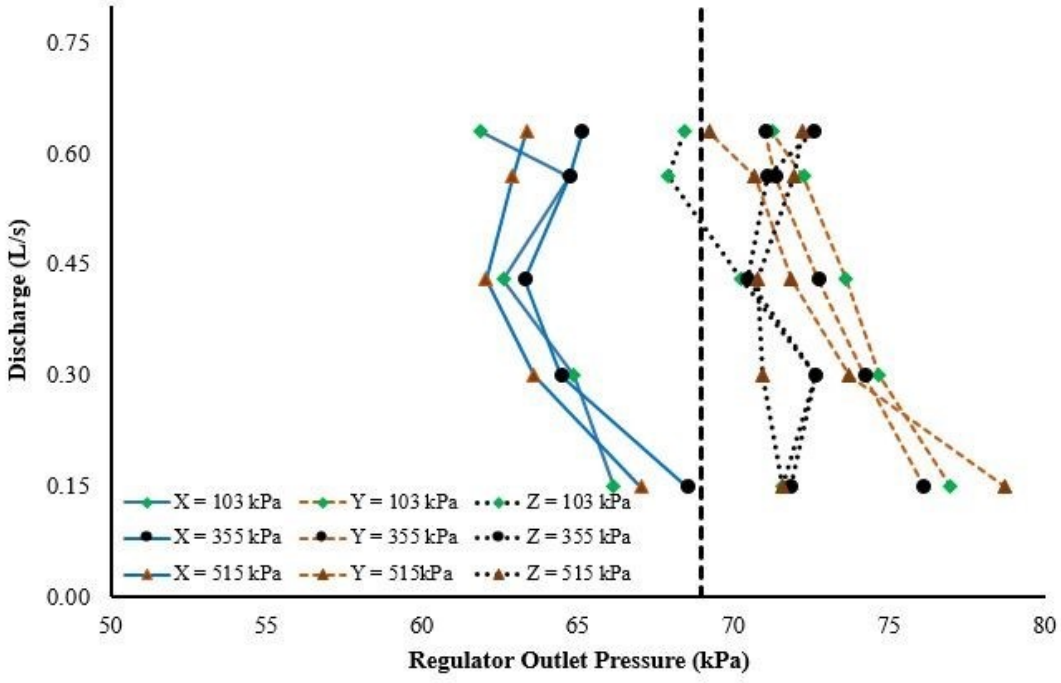

Figure 5-64: Comparison of the regulating tolerances across a range of input pressures for the 10 PSI X, Y, and Z pressure regulators

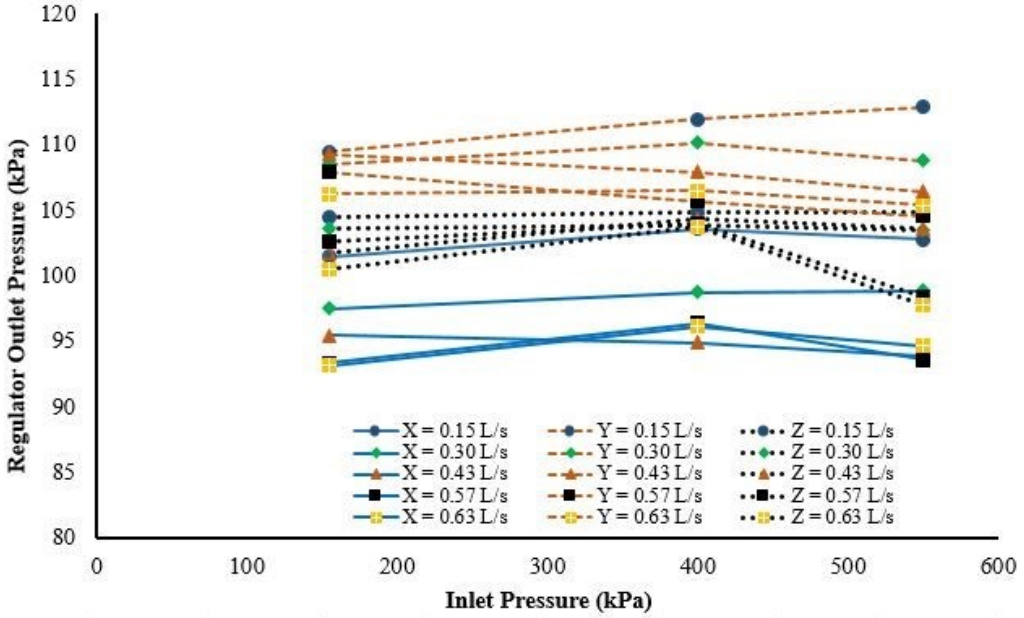

Figure 5-65: Comparison of regulation curves for all 15 PSI X, Y, and Z pressure regulators

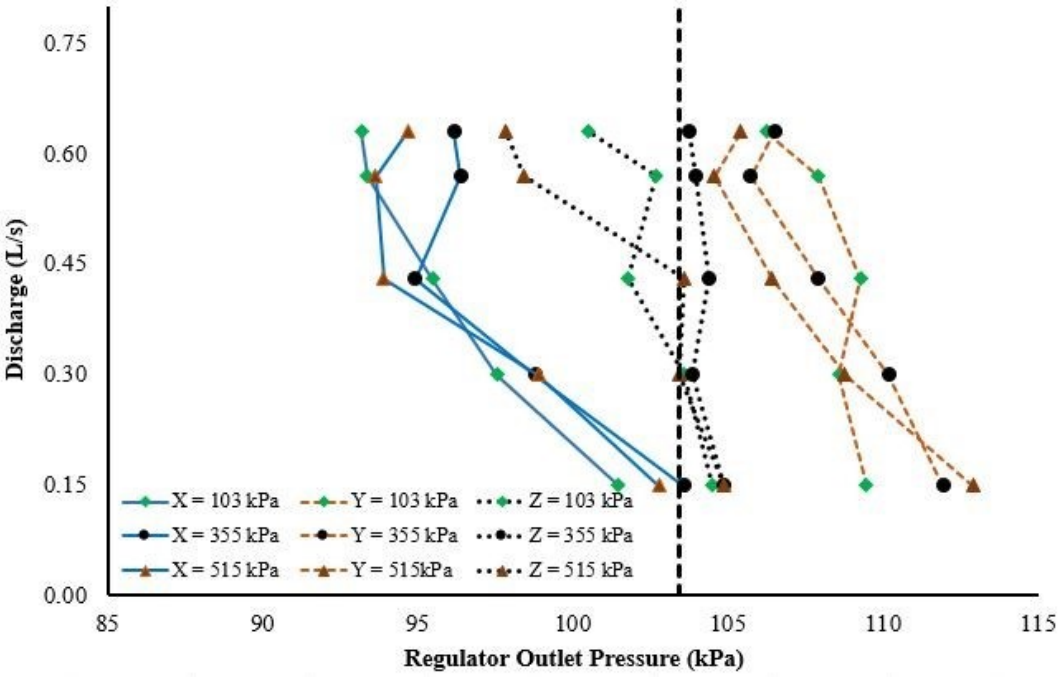

Figure 5-66: Comparison of the regulating tolerances across a range of input pressures for the 15 PSI X, Y, and Z pressure regulators

5.6.3 *Minor Head Losses through Pressure Regulators*

The minor pressure head loss testing of the X, Y and Z pressure regulators was carried out for a total of one hundred and eight (108) tests using the test criteria described in

Section 4.4.3.4 in Chapter 4. In these experiments, the flow tube was maintained at a stationary position to prevent any head loss in the devices that could result from other processes other than friction due to flow passage through the tube. The mechanical spring was taken out of the pressure regulator units selected for this type of testing. Figure 5-67 through to Figure 5-69 shows the results of the minor head losses measured from the low pressure models of the three brands of pressure regulators under investigation. The graphical presentation of the minor loss through the X type of pressure regulator shows that the loss is not consistent amongst tested units although they all have a linear relationship. There is a linear increase in head loss difference from < 1.5 % to about 30 % between the lowest and highest values of minor head loss at the lower and higher velocity head. However, the minor head loss is consistent amongst tested units for the Y and Z pressure regulators. The minor head losses are higher for the Z pressure regulators, followed by X pressure regulators, with the lowest obtained for the Y pressure regulator units. The differences in the minor head losses for the three low pressure regulator brands is graphically illustrated in Figure 5-70. The differences in maximum flow capacities for the pressure regulator brands is manifested in the last data points in the graph where the minor head losses are corresponding to different velocity heads.

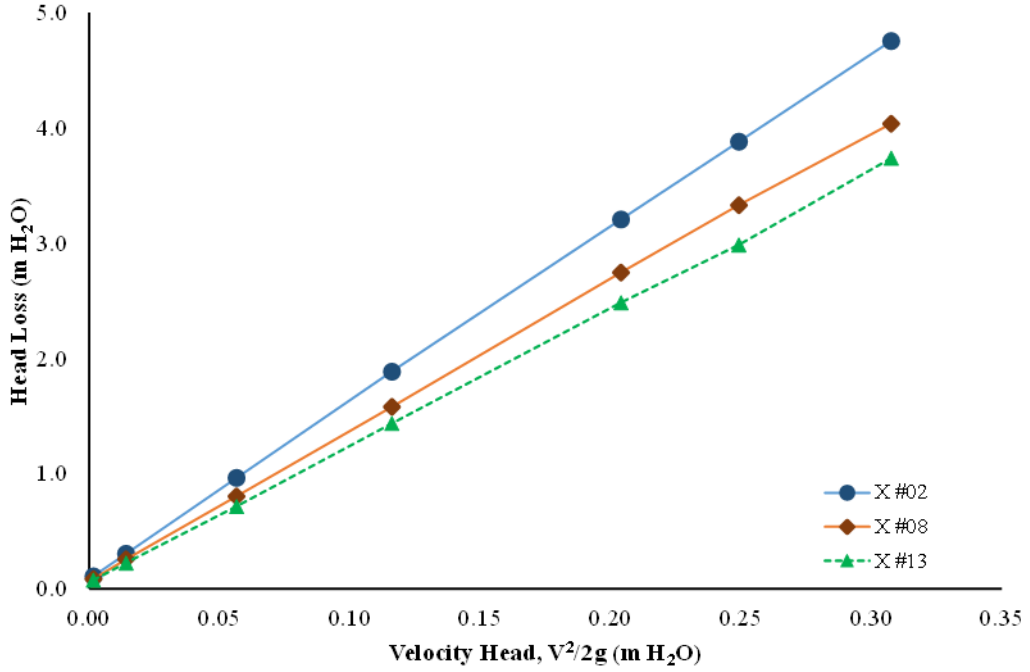

Figure 5-67: Minor head loss for the units of the X 10 PSI type of pressure regulators

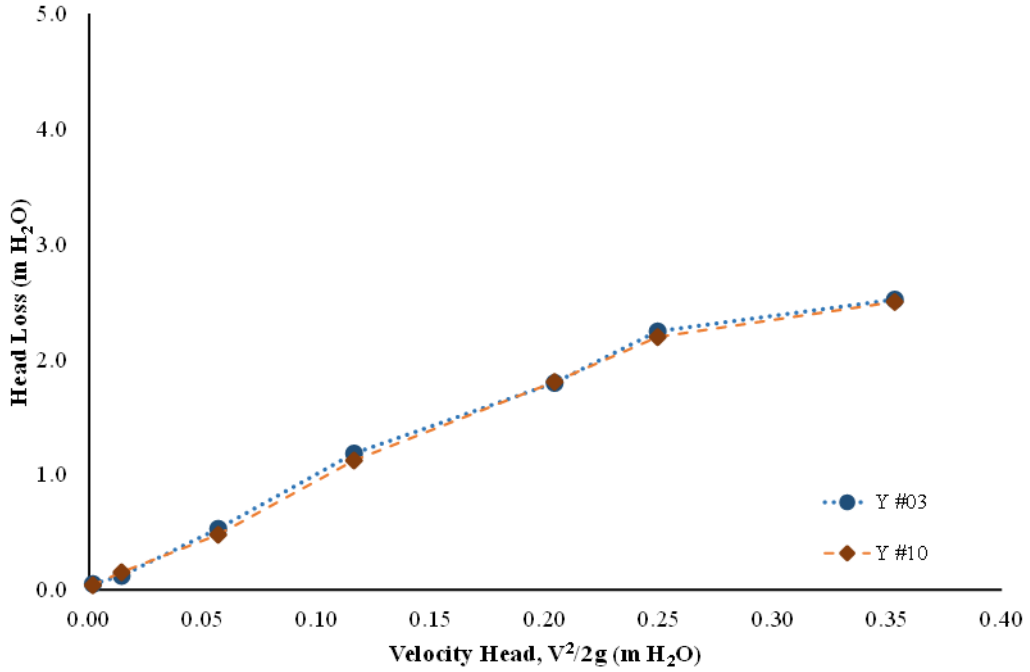

Figure 5-68: Minor head loss for the units of the Y 10 PSI type of pressure regulators

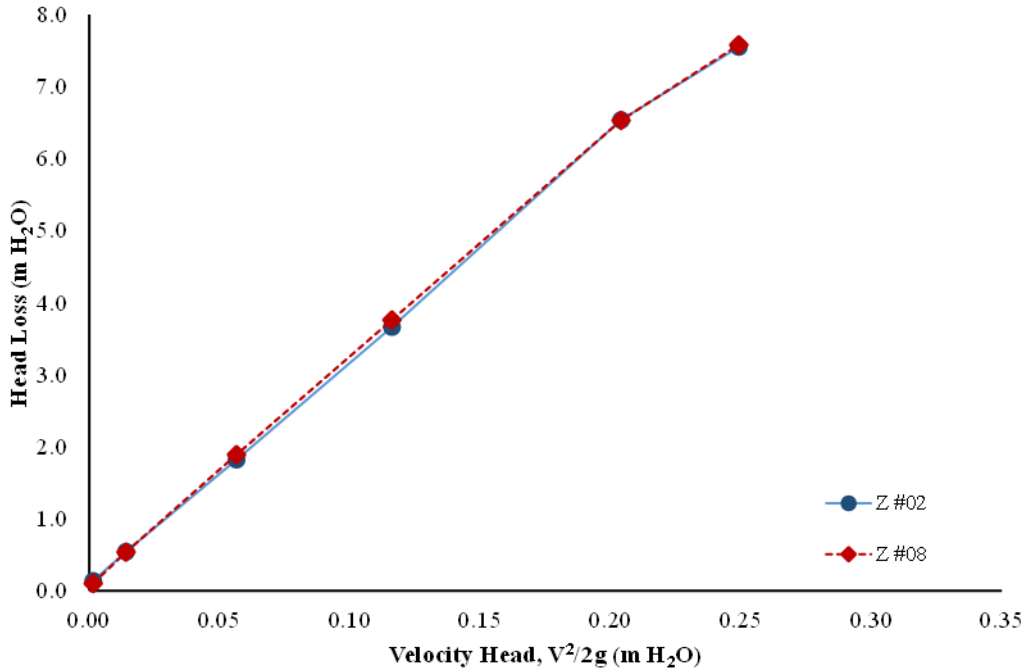

Figure 5-69: Minor head loss for the units of the Z 10 PSI type of pressure regulators

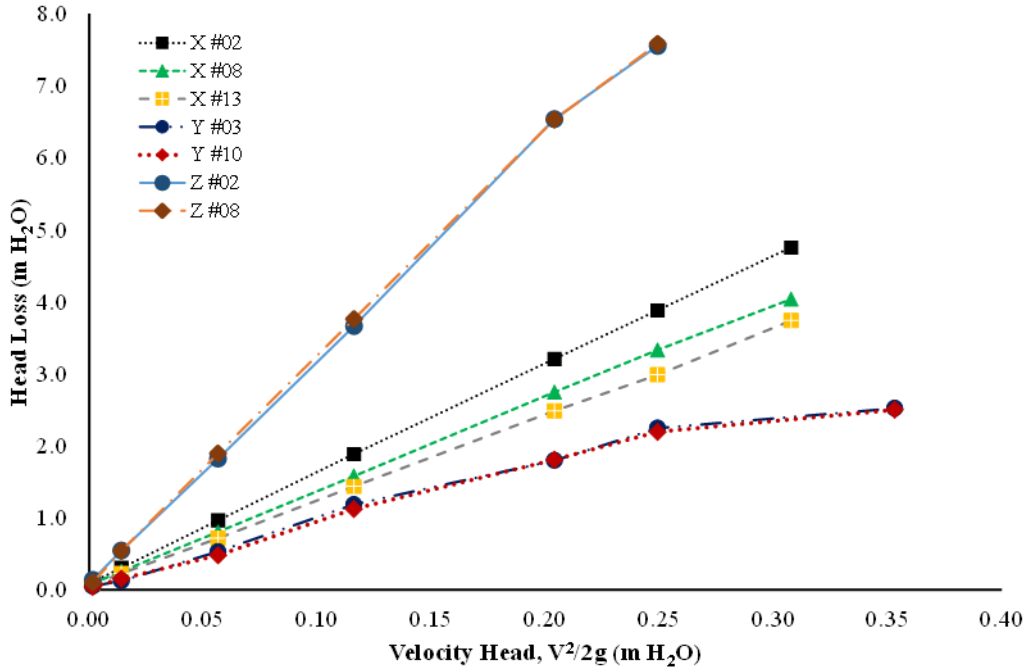

Figure 5-70: Minor head loss for all the X, Y, and Z 10 PSI type of pressure regulators

The results of the minor head loss testing for the high pressure models of the X, Y and Z pressure regulators are presented in Figure 5-71 through to Figure 5-73. The loss through the X type of pressure regulator increases linearly across the majority of flow rates as represented by velocity head and drops slightly at the highest flow rate. The differences in pressure loss data points is also evident in the high pressure model although the spread is smaller than in the low pressure units. The minor pressure loss amongst the tested units of the Y and Z pressure regulators is relatively similar across the flow rates tested, and they take a nearly identical form as the low pressure models. It also evident that the minor head loss magnitudes is highest for the Z pressure regulators, followed by X regulators and lowest for the Y pressure regulators. This trend is similar to the hydraulic performance obtained for the low pressure model pressure regulators. The minor pressure head loss comparison for the X, Y and Z pressure regulators is illustrated in Figure 5-74.

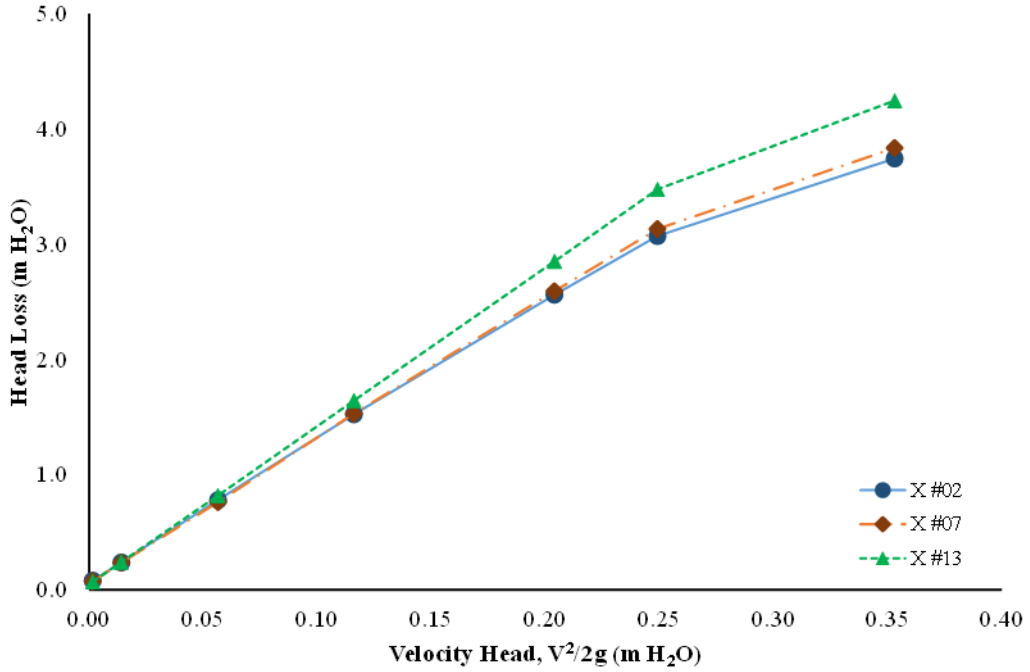

Figure 5-71: Minor head loss for the tested units of the X 15 PSI type of pressure regulators

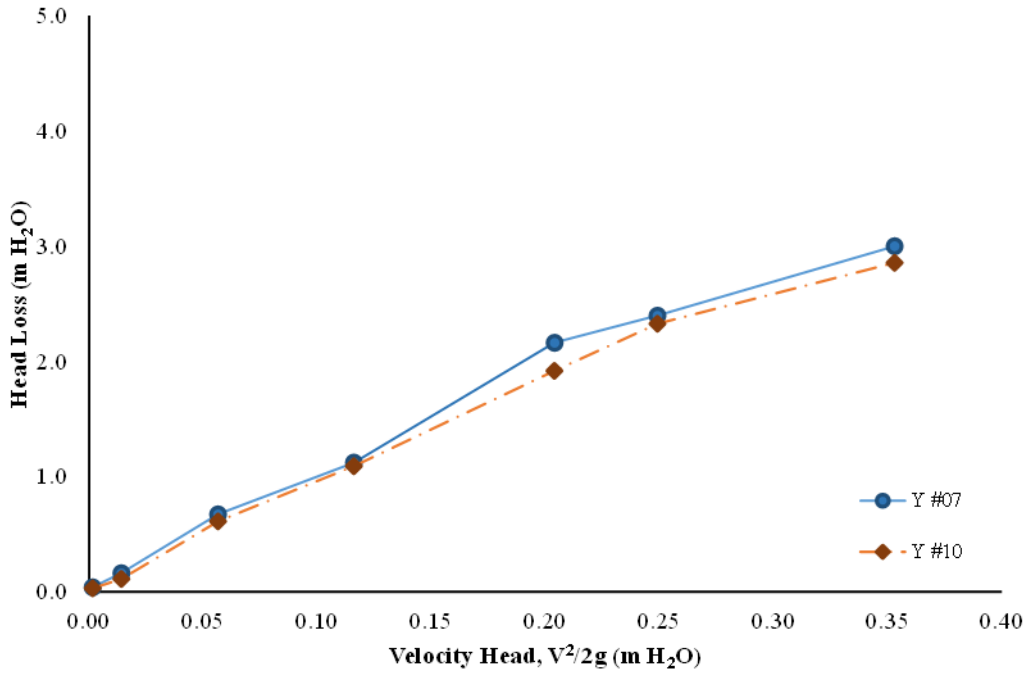

Figure 5-72: Minor head loss for the tested units of the Y 15 PSI type of pressure regulators

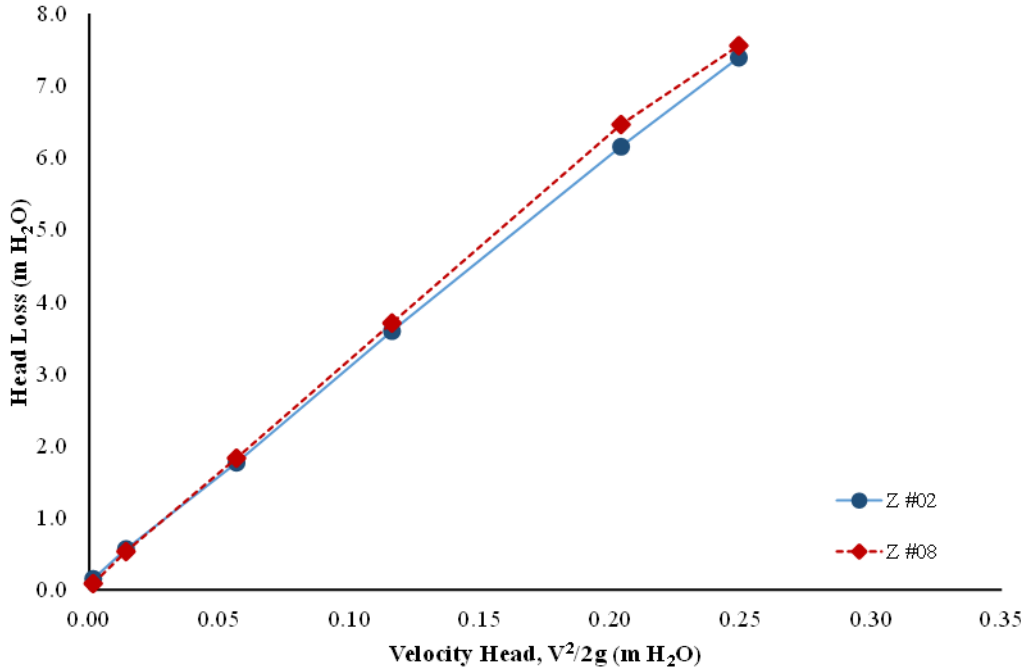

Figure 5-73: Minor head loss for the tested units of the Z 15 PSI type of pressure regulators

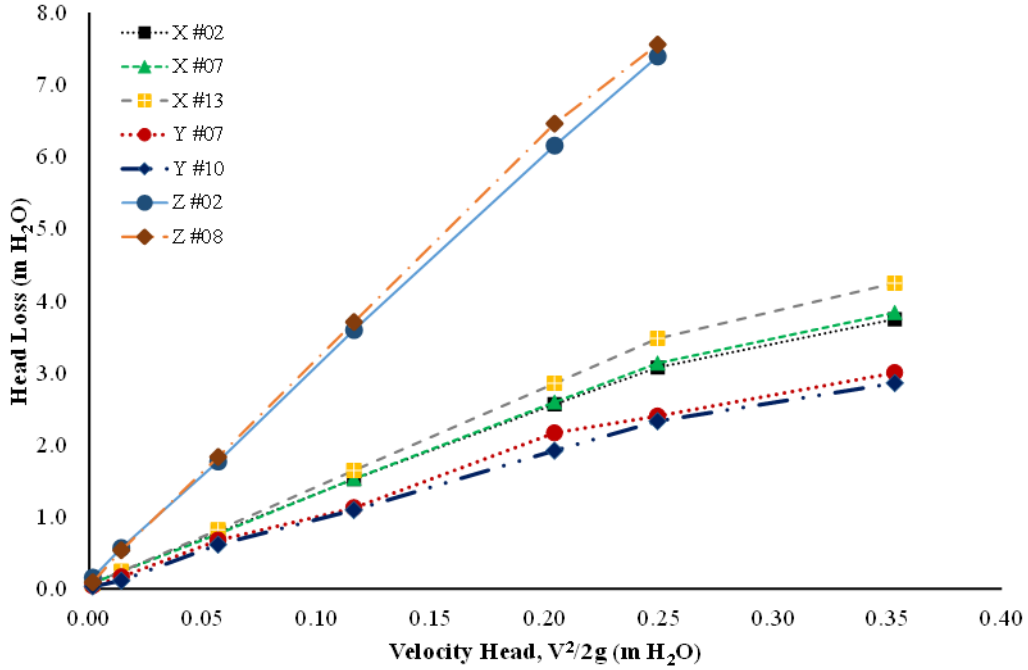

Figure 5-74: Comparison of minor head losses for all the X, Y, and Z 15 PSI types of pressure regulators

The minor head losses for the different pressure regulator brands when compared between the low and high pressure models as shown in Figure 5-75, Figure 5-76, and Figure 5-77. A noticeable difference in head loss between the low pressure and high

pressure models for the X brand pressure regulator exist, especially at the highest flow rates represented by the higher velocity heads in the graph. The difference is highest for the X regulators, followed by the Y regulators and with the smallest difference found within the models of the Z pressure regulators. These results are independent and contrary to the actual head losses generated by each of the three pressure regulator brands, where the highest loss is obtained from the Z regulators, followed by the X regulators, and the lowest head loss obtained in the Y pressure regulators.

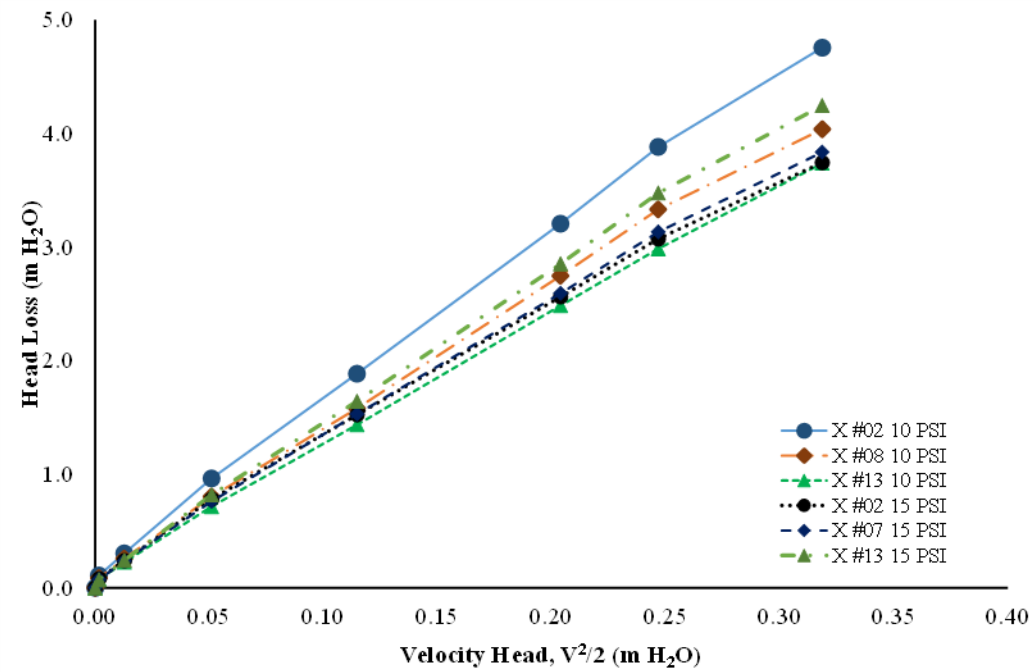

Figure 5-75: Comparison of minor head losses between the 10 and 15 PSI models of the X type of pressure regulator brand

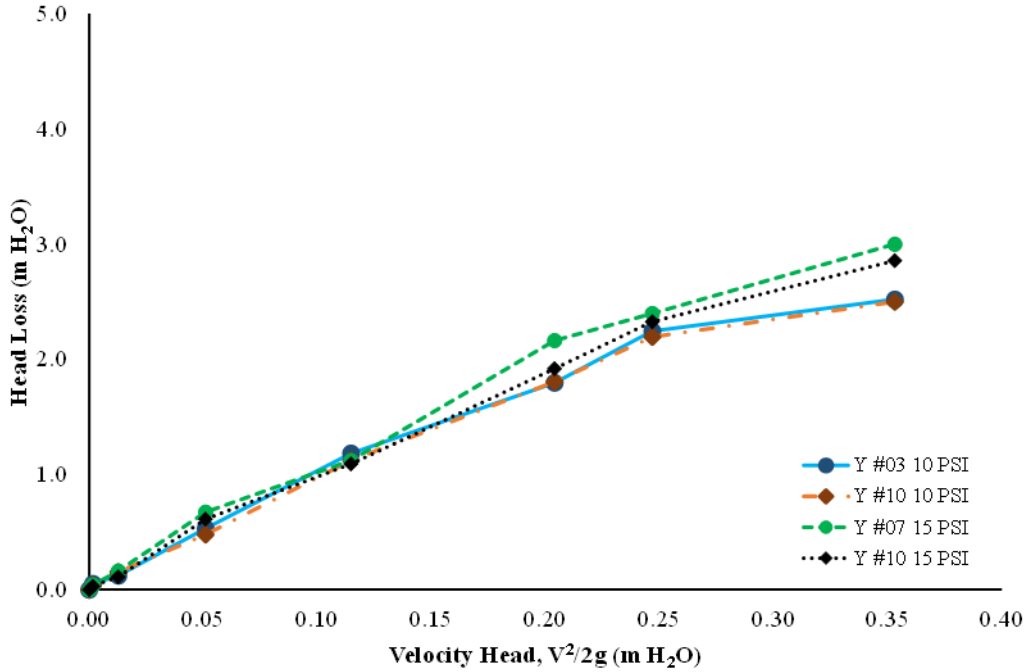

Figure 5-76: Comparison of minor head losses between the 10 and 15 PSI models of the Y type of pressure regulator brand

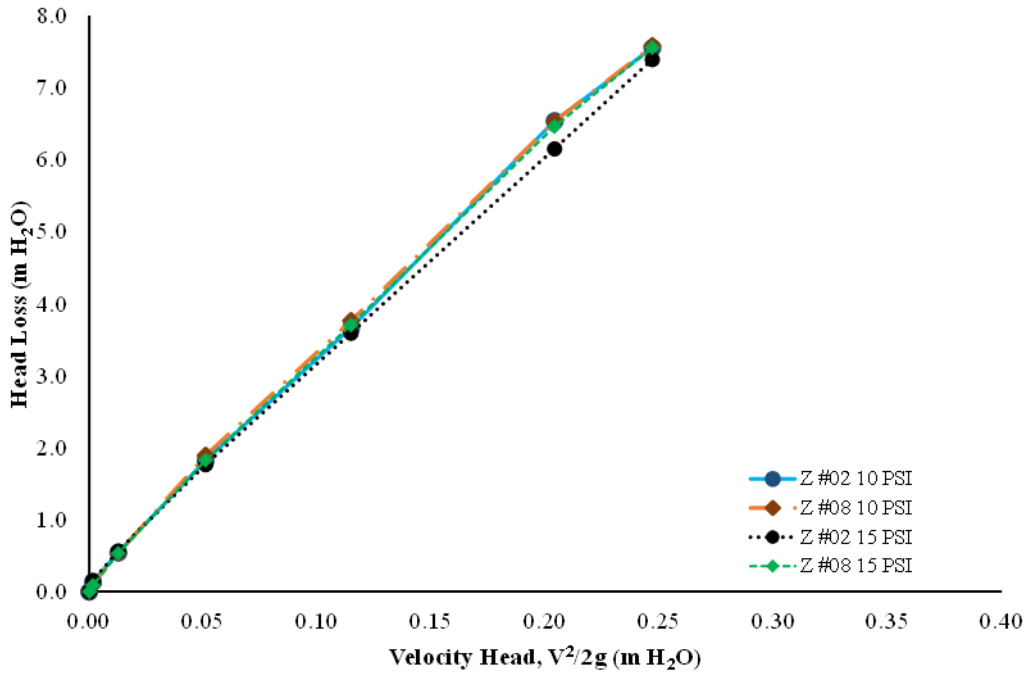

Figure 5-77: Comparison of minor head losses between the 10 and 15 PSI models of the Z type of pressure regulator brand

5.6.4 *Calculation of Minor Loss Coefficients for Pressure Regulators*

The minor loss coefficient, *K,* for the tested pressure regulators is derived using a criteria similar to that discussed in Section 5.3 for determining the minor loss coefficients for VRI valves. The minor pressure head loss results in Section 5.6.3 obtained from the non-regulating test conditions of the pressure regulating valves with the flow tube maintained in a stationary position is used in the calculations. It is evident, however, that there is no significant difference in head loss between the low pressure and high pressure regulator models. This implies that any differences between the models has to do with the design of the mechanical spring which brings about the differences in set pressures. The negligible differences in the minor head loss results for both the low and high pressure models therefore suggest that a unit minor loss coefficient can be calculated for each of the three different brands using the minor loss data from the two pressure models. Nonetheless, it must be noted that the results for the X pressure regulator models are heteroscedastic especially on the high discharge region. A test for this heteroscedasticity or spread was however, not completed due to the large number of tests needed to be completed for all the pressure regulators. Figure 5-78, Figure 5-79 and Figure 5-80 shows the mathematical equations developed for describing the minor loss coefficients for the X, Y, and Z pressure regulators. The equations all have a coefficient of determination (R^2) greater than 98 % implying the accuracy and suitability of the loss coefficients in estimating the minor head loss through pressure regulators.

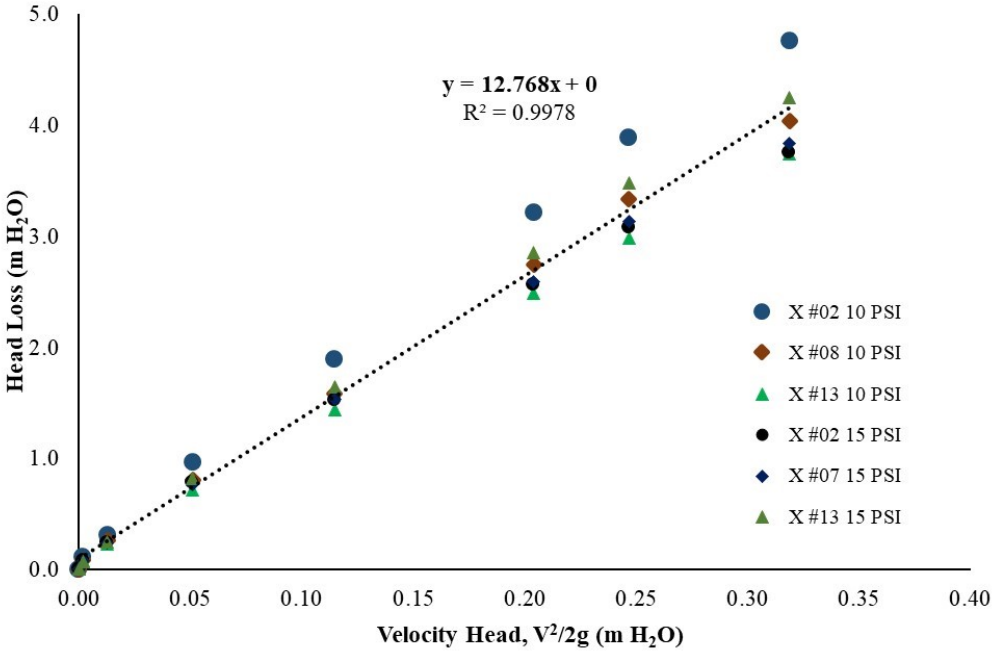

Figure 5-78: Minor loss coefficient *K* for the X type of pressure regulator brand

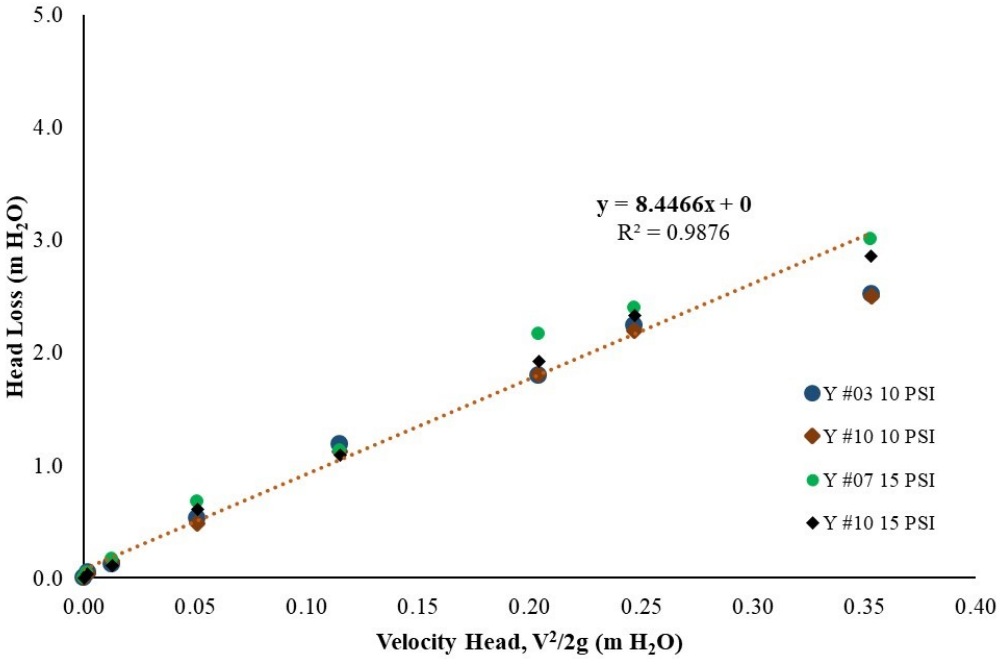

Figure 5-79: Minor loss coefficient *K* for the Y type of pressure regulator brand

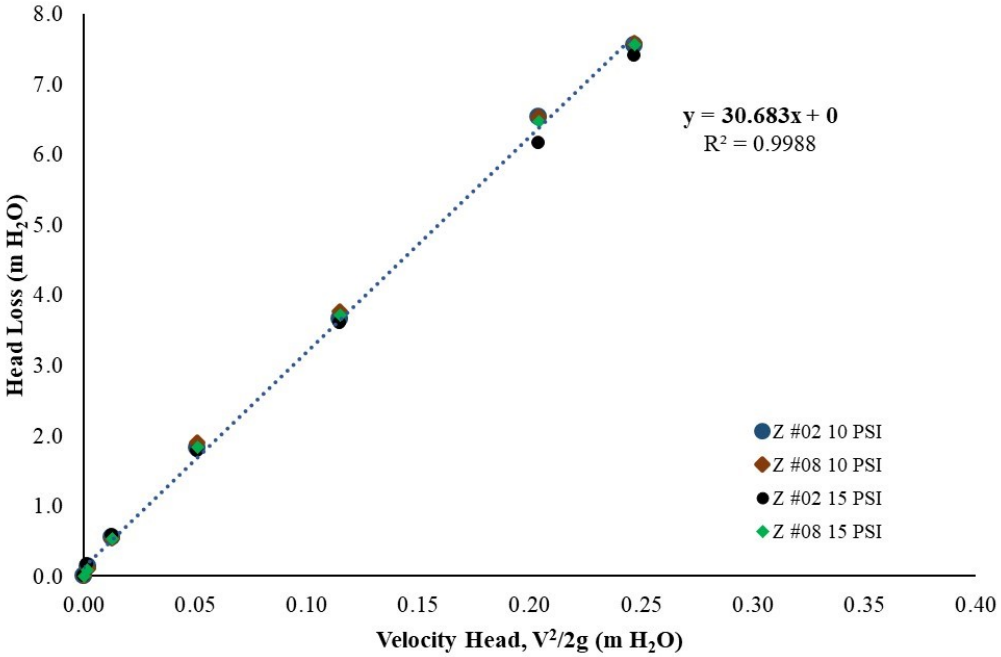

Figure 5-80: Minor loss coefficient *K* for the Z type of pressure regulator brand

5.6.5 *Pressure Regulator Outlet Pressure Hysteresis*

Section 4.5.3.3 outlines the novel procedure developed for characterising pressure regulator outlet pressure hysteresis, through rigorous alterations of, the test-rig control valves algorithm, and the actual configuration of the test-apparatus. The results of pressure regulator outlet pressure hysteresis for the X, Y, and Z CP&LM pressure regulators obtained from a total of one hundred and forty four (144) tests are presented in this section. Figure 5-81 and Figure 5-82 attempts to replicate the results of pressure regulator outlet pressure hysteresis obtained by Mohr (2011) and Junior et al. (2018). The authors obtained regulator outlet pressure hysteresis results by testing the devices at 0.30 L/s when inlet pressure varied by 50 kPa increments to a maximum test pressure (~800 kPa) and back to zero pressure using manually controlled throttling valves, as shown in Figure 5-83.

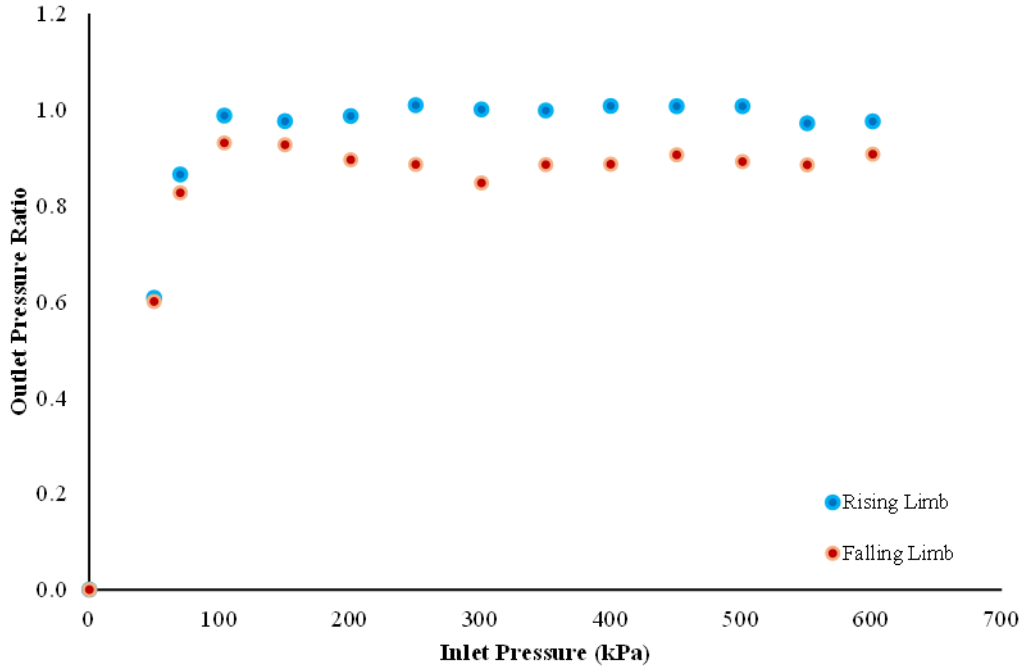

Figure 5-81: Hysteresis envelope for the X type of low pressure regulator model measured at 0.30 L/s

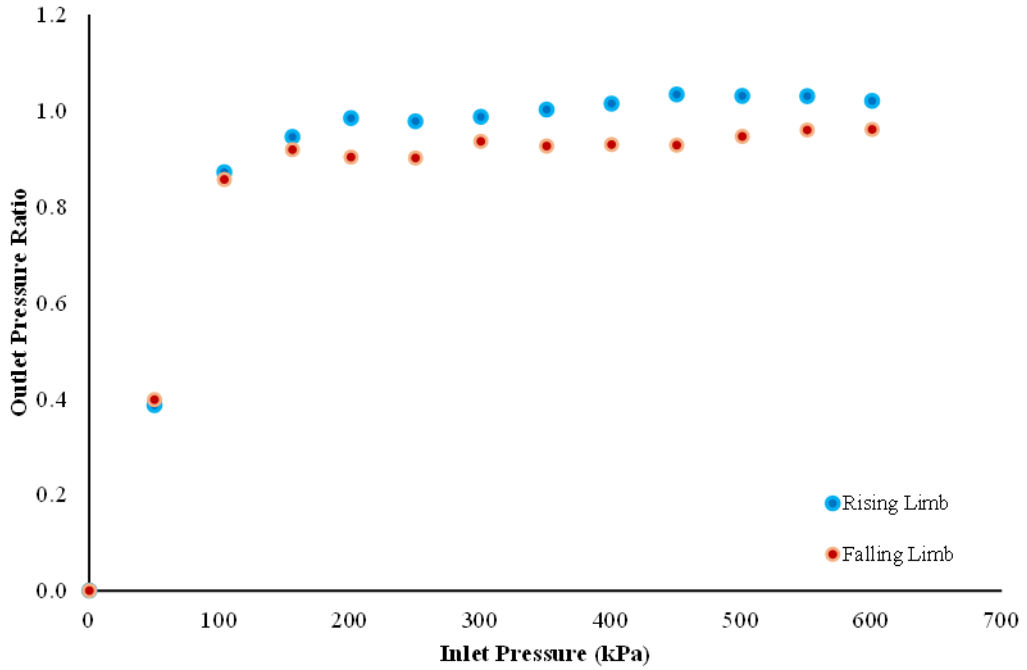

Figure 5-82: Hysteresis envelope for the X type of high pressure regulator model measured at 0.30 L/s

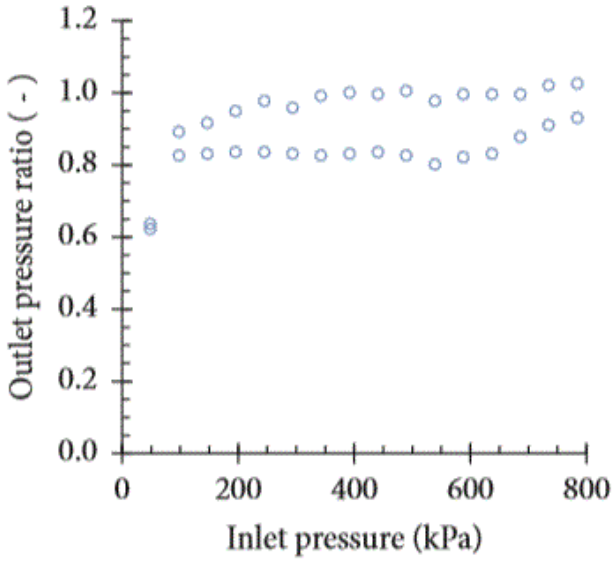

Figure 5-83: Hysteresis envelope for a pressure regulator model tested by Junior et al. (2018)

Pressure regulator outlet pressure hysteresis testing in this research was conducted with inlet pressure increments occurring automatically with a constant discharge to simulate field performance of the devices using the novel testing procedures developed in Chapter 3 and Chapter 4. The flow rates used in these experiments ranged between 0.1 to 0.6 L/s, at 0.1 L/s increments. The maximum pressure limit was set at 300 kPa as opposed to the replication tests above. The idea was to develop a pressure regulator performance dataset that represents practical conditions of modern low pressure CP&LMs. The measurements were taken at 1 kHz frequency. The results of the regulator outlet pressure hysteresis curves for the low pressure models tested are illustrated in Figure 5-84 through to Figure 5-92 where the x-axis represent the supply pressure and y-axis is the output pressure ratio which is calculated as a ratio of actual outlet pressure to the regulator set pressure. The set pressure for the low pressure models is 68.95 kPa and 103.42 kPa for the high pressure regulator models. The hysteresis curves or hysteresis envelopes for the high pressure models of pressure regulators are shown in Figure 5-93 through to Figure 5-101.

It can be seen from Figure 5-84 to Figure 5-86 that the regulated pressures between the flow rates tested from 0.1 to 0.6 L/s, are at least close to the regulator set pressure when inlet pressure is rising for the low pressure X pressure regulator model. The regulator outlet pressures falls below the set pressure when inlet pressure is falling

which is a clear depiction of the characteristic performance of the devices when utilised to regulate sprinkler heads for CP&LM machines operating in variable topography. The disparity amongst outlet pressure data points is quite significant below the regulator set pressure for this type of regulator between the rising and falling inlet pressure limbs.

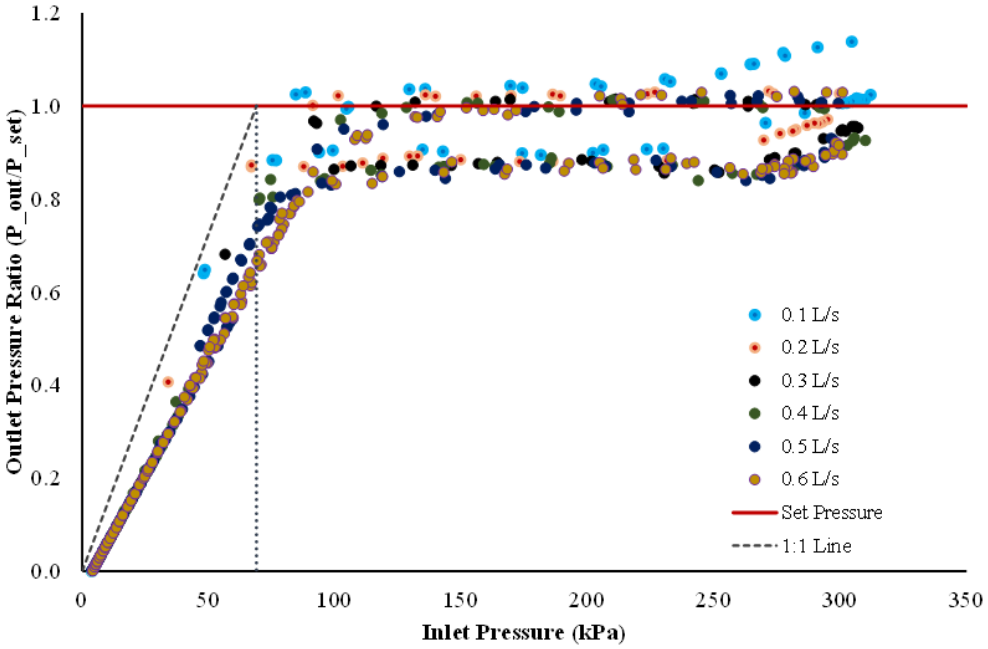

Figure 5-84: Outlet pressure hysteresis envelopes for a low pressure X - #06 regulator at a discharge range of 0.1 to 0.6 L/s

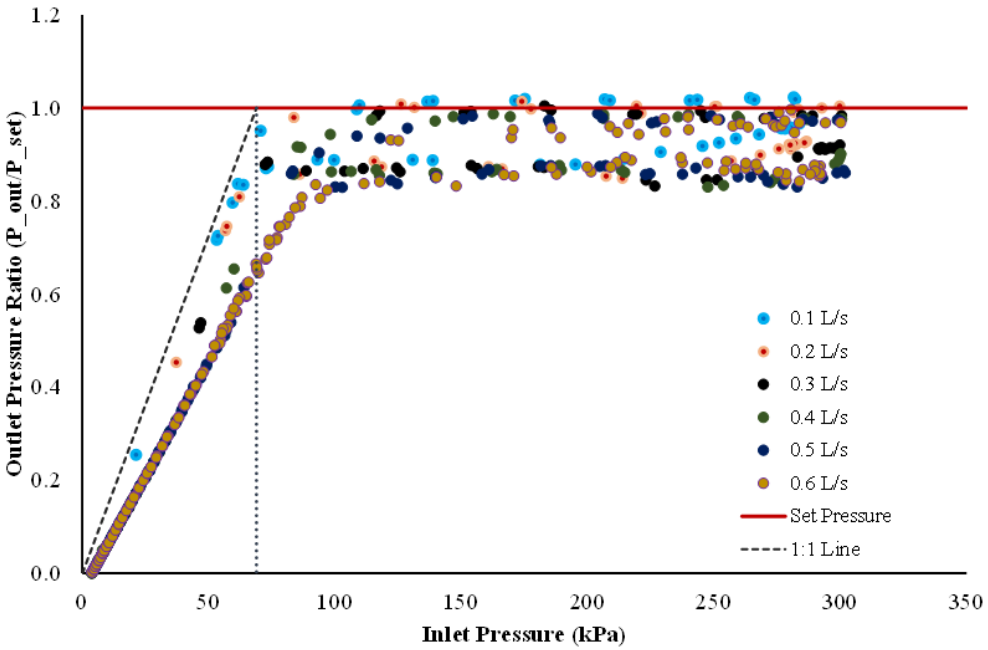

Figure 5-85: Outlet pressure hysteresis envelopes for a low pressure X - #10 regulator at a discharge range of 0.1 to 0.6 L/s

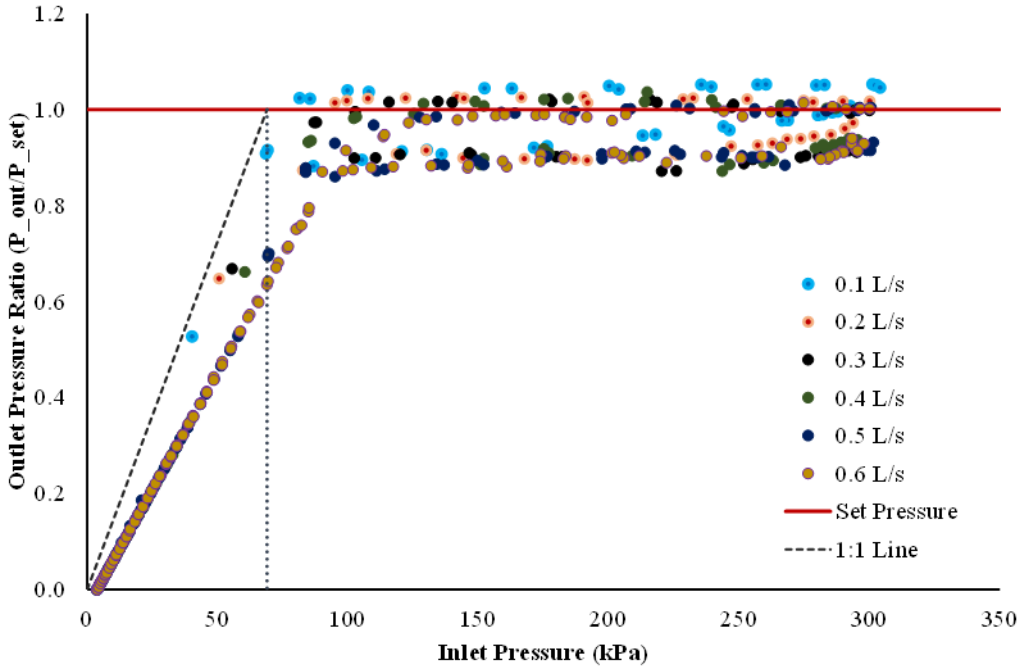

Figure 5-86: Outlet pressure hysteresis envelopes for a low pressure X - #14 regulator at a discharge range of 0.1 to 0.6 L/s

The regulated pressures for the tested units of low pressure Y pressure regulator model are at least above the regulator set pressure at the tested flow rates when inlet pressure is both in the rising and falling limbs. However, there is still a regulating performance difference amongst the three tested units as shown in Figure 5-87 through to Figure 5-89. The Y-#01 regulator is tracking slightly below the set pressure point when inlet pressure is falling for a majority of flow rates while the Y-#07 and 09 are at least equal to the set point when inlet pressure is falling. The disparity amongst outlet pressure data points is quite significant above the regulator set pressure for this type of regulator between the rising and falling inlet pressure limbs.

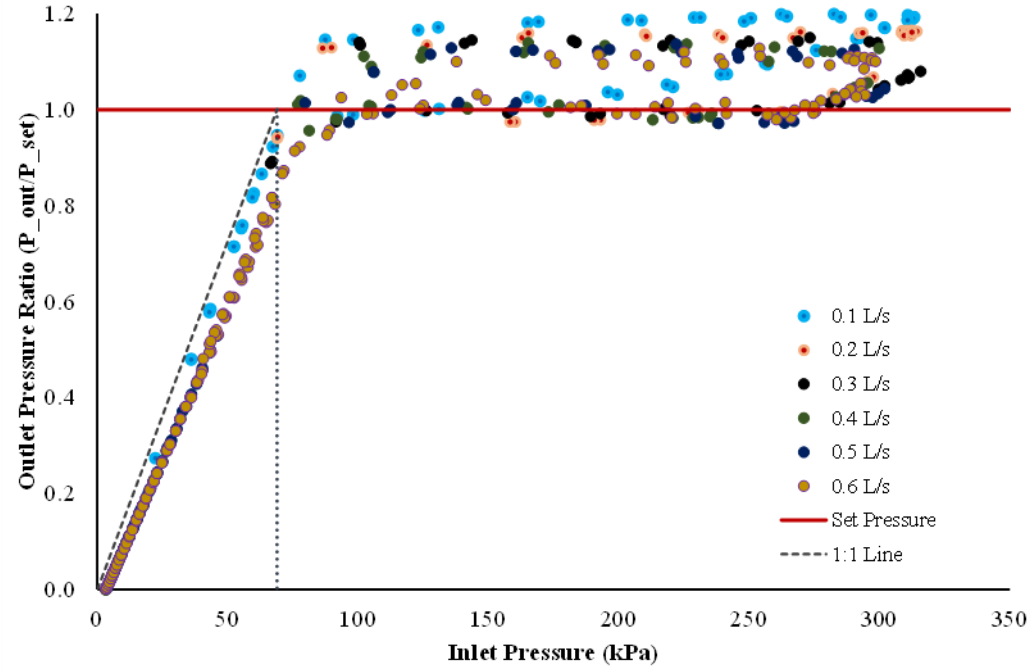

Figure 5-87: Outlet pressure hysteresis envelopes for a low pressure Y - #01 regulator at a discharge range of 0.1 to 0.6 L/s

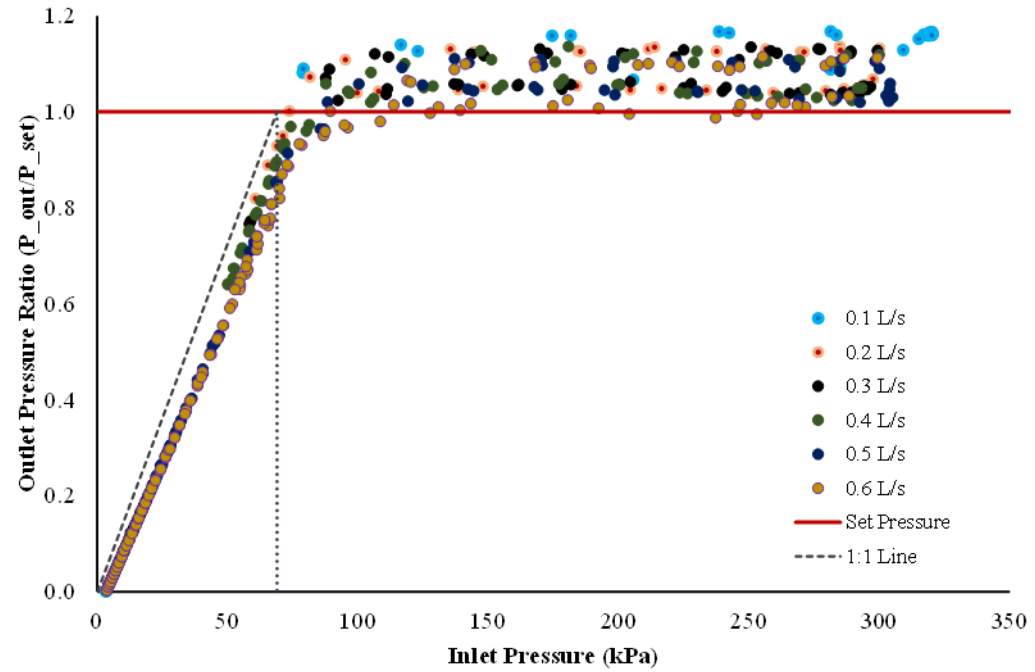

Figure 5-88: Outlet pressure hysteresis envelopes for a low pressure Y - #07 regulator at a discharge range of 0.1 to 0.6 L/s

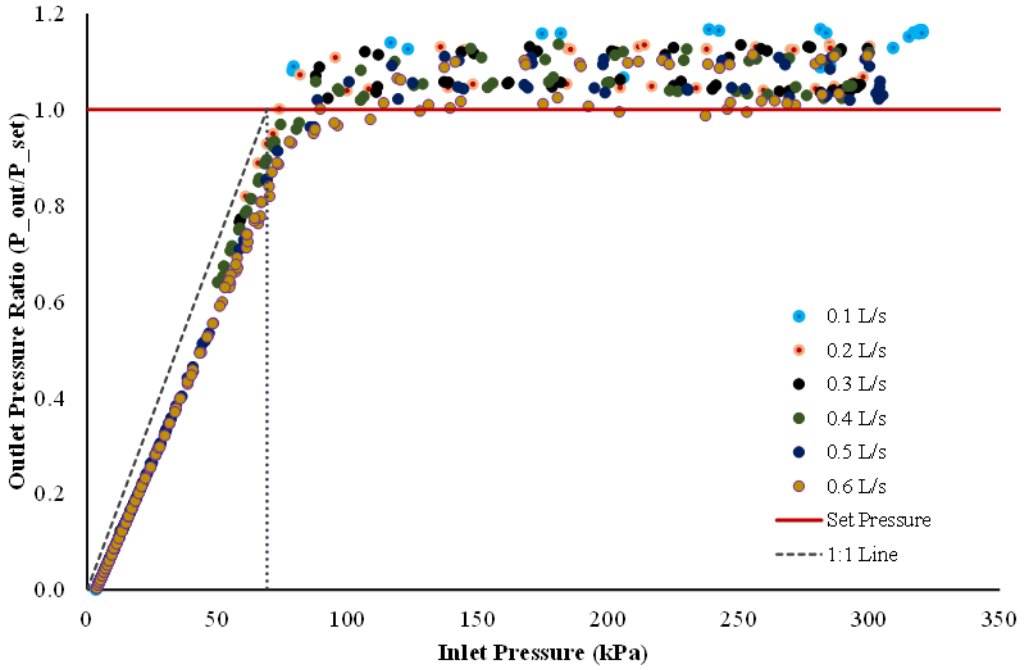

Figure 5-89: Outlet pressure hysteresis envelopes for a low pressure Y - #09 regulator at a discharge range of 0.1 to 0.6 L/s

The regulated pressures for the tested units of low pressure Z pressure regulator model are above the regulator set pressure at the tested flow rates when inlet pressure is in the rising limb and falls slightly below when inlet pressure is tracking a falling limb. This type of regulator performs very close to the set pressure as shown in Figure 5-90 through Figure 5-92. The Z-#09 regulator is tracking slightly below the pressure set point when inlet pressure is falling for a majority of flow rates while the Z-#05 and 15 units are at least equal to the set point when inlet pressure is falling.

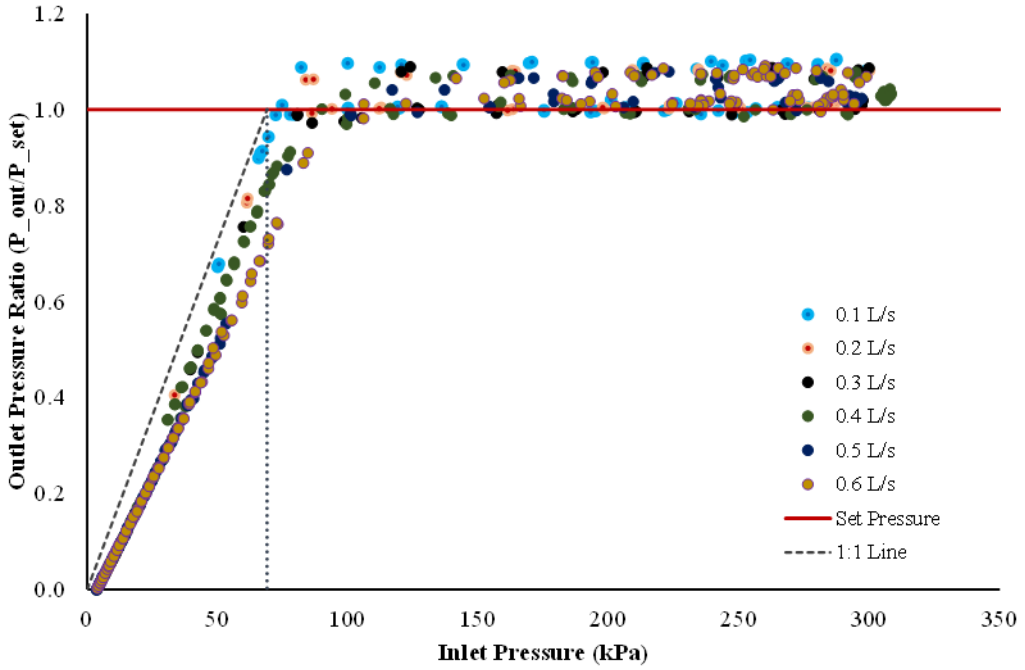

Figure 5-90: Outlet pressure hysteresis envelopes for a low pressure Z - #05 regulator at a discharge range of 0.1 to 0.6 L/s

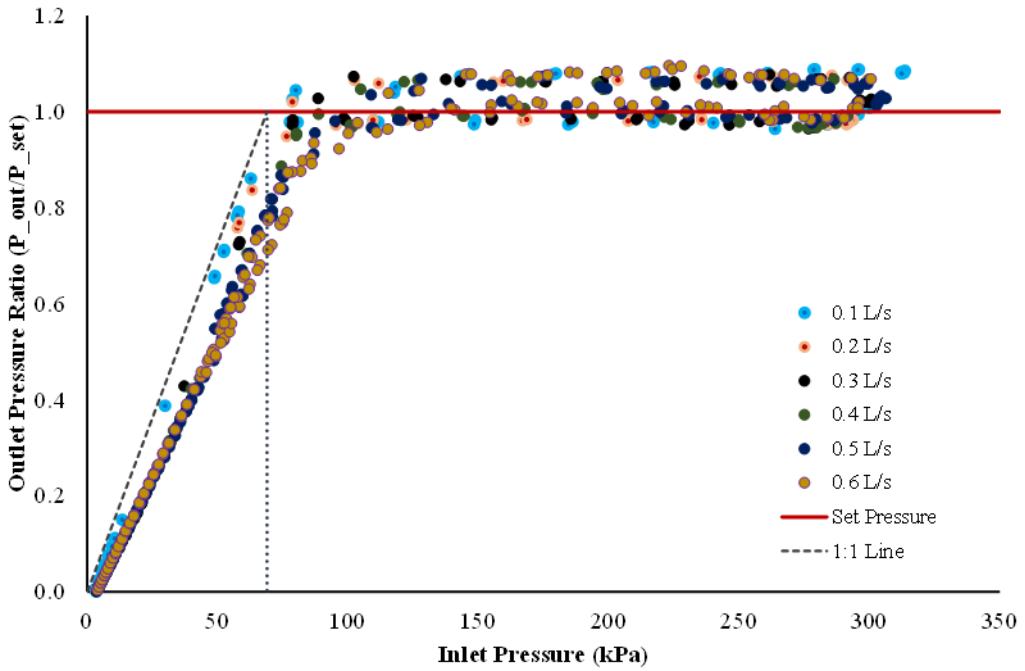

Figure 5-91: Outlet pressure hysteresis envelopes for a low pressure Z - #09 regulator at a discharge range of 0.1 to 0.6 L/s

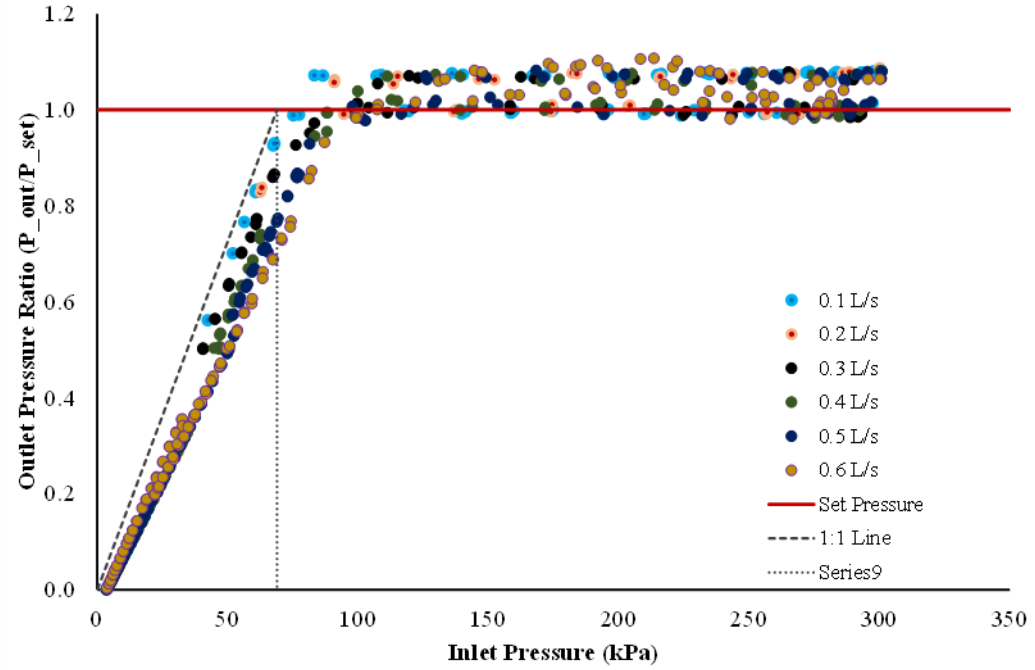

Figure 5-92: Outlet pressure hysteresis envelopes for a low pressure Z - #15 regulator at a discharge range of 0.1 to 0.6 L/s

Figure 5-93 through to Figure 5-101 represent the hysteresis envelopes or the pressure regulation curves for the high pressure (15 psi) regulators for the investigated X, Y, and Z manufacturer brands. The X brand of pressure regulators have outlet pressure data points spread away from the 1:1 line in the non-regulating segment of the hysteresis curve, which implies that they have a much narrow or smaller regulation range when compared to the Y and Z pressure regulators. They generally have their regulated outlet pressures around the manufacturer set pressure when inlet pressure is on the rising limb (Figure 5-93 and Figure 5-95). However, a much lower result than the regulator set pressure is observed for the X-#07 (Figure 5-94) regulator when inlet pressure is increasing. This shows that different units of pressure regulators of the same brand and model can perform very differently under identical test conditions, which could be attributed to manufacturing variability, or the flow tube movement not in the same position for the different units when tested. A significant amount of vibration and noise production was observed from the devices at the highest flow rates tested, but this was controlled by the pair of electronic control valves before data logging took place.

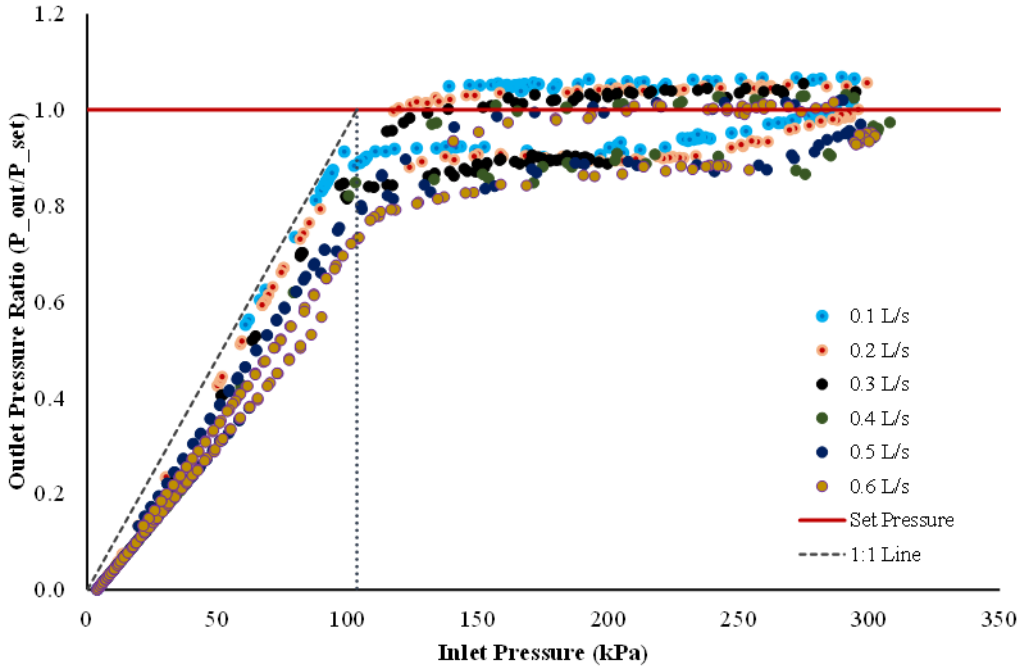

Figure 5-93: Outlet pressure hysteresis envelopes for a high pressure X - #03 regulator at a discharge range of 0.1 to 0.6 L/s

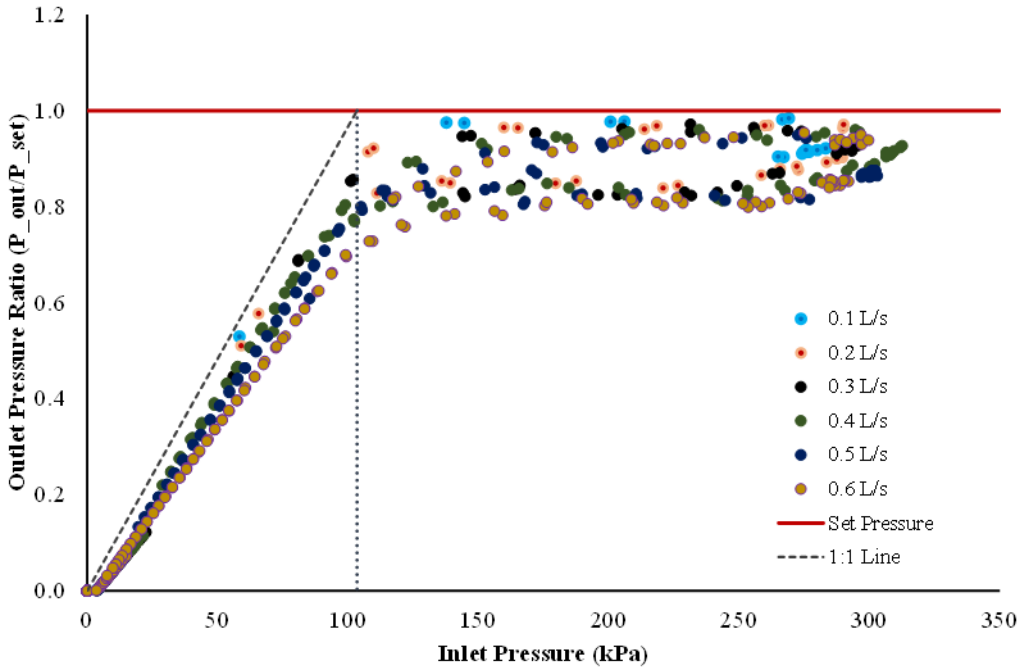

Figure 5-94: Outlet pressure hysteresis envelopes for a high pressure X - #07 regulator at a discharge range of 0.1 to 0.6 L/s

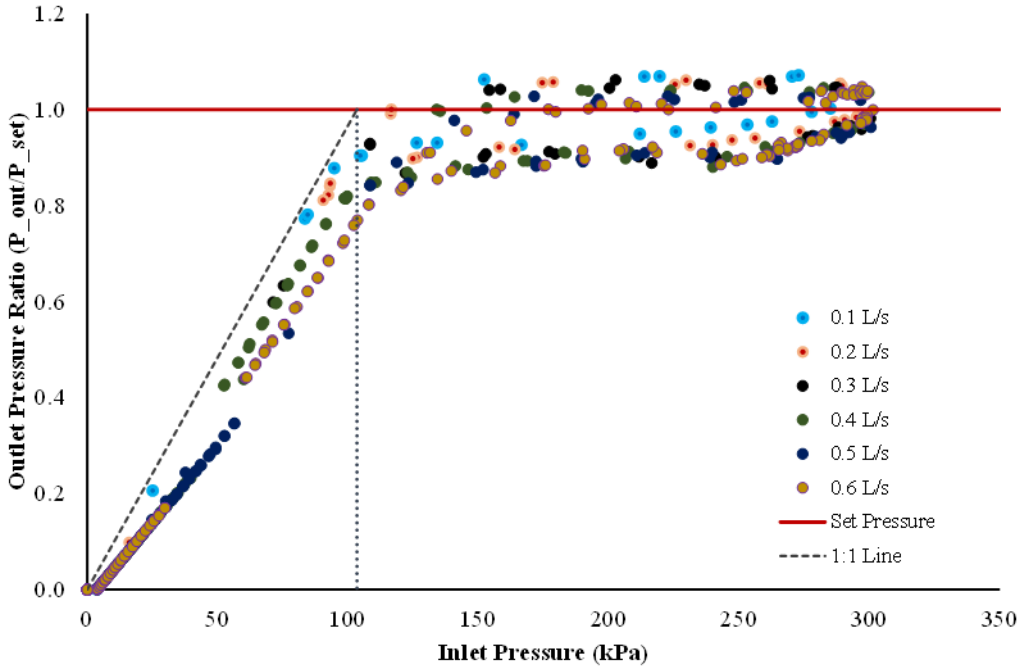

Figure 5-95: Outlet pressure hysteresis envelopes for a high pressure X - #12 regulator at a discharge range of 0.1 to 0.6 L/s

The Y brand of regulators are performing on average very close to the manufacturer set pressure (Figure 5-96, Figure 5-97, and Figure 5-98). The outlet pressure is above the nominal set pressure for the units tested across the different flow rates when the inlet pressure is on the rising limb of the regulation curve. They track below the set pressure when inlet pressure is on the falling limb. These pressure regulators are performing very close to the 1:1 line in the non-regulating segment of the hysteresis curve. This means that the head loss due to friction on the devices is not significant. Figure 5-98 however, exhibited a unique performance result where both the regulator outlet pressures are above the nominal set pressure across all tested flow rates when the inlet pressure is both on the rising and falling limbs. This is a clear indication of the performance difference amongst unit to unit of a particular pressure regulator brand or model.

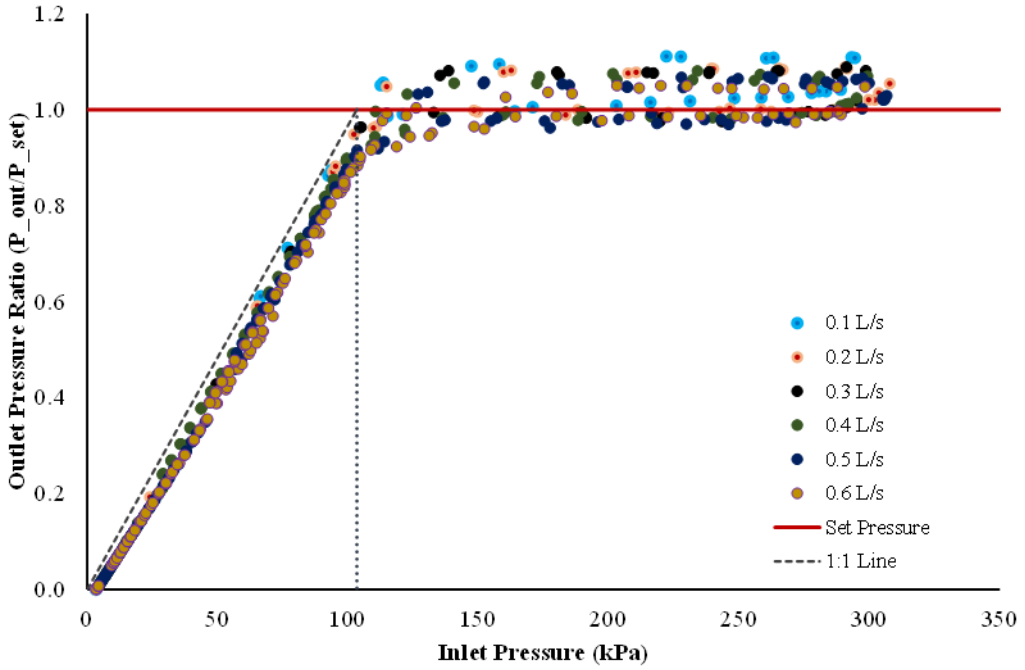

Figure 5-96: Outlet pressure hysteresis envelopes for a high pressure Y - #01 regulator at a discharge range of 0.1 to 0.6 L/s

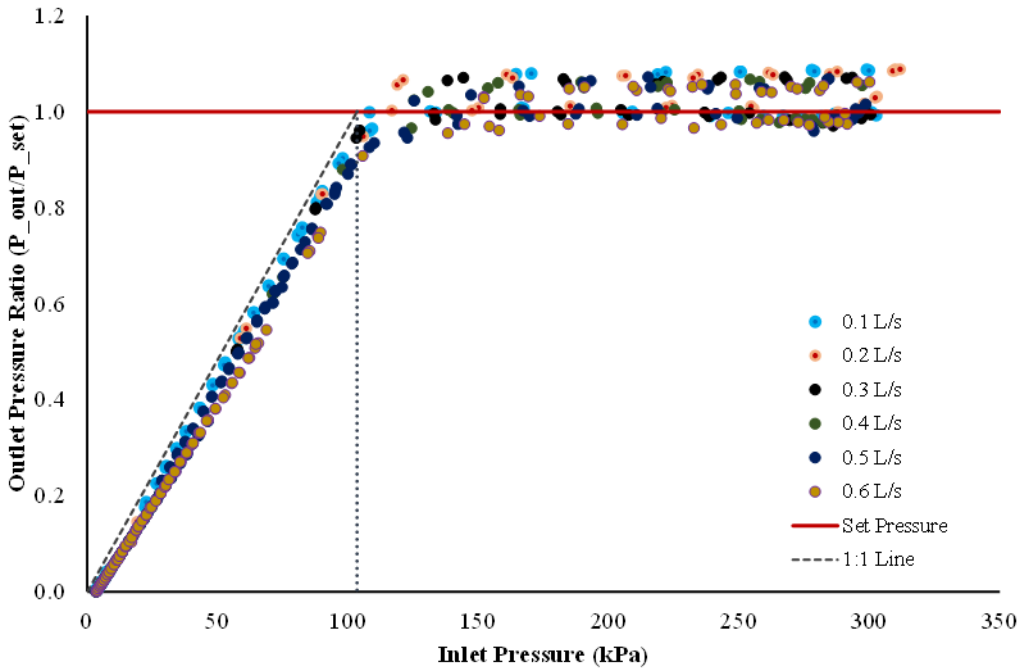

Figure 5-97: Outlet pressure hysteresis envelopes for a high pressure Y - #03 regulator at a discharge range of 0.1 to 0.6 L/s

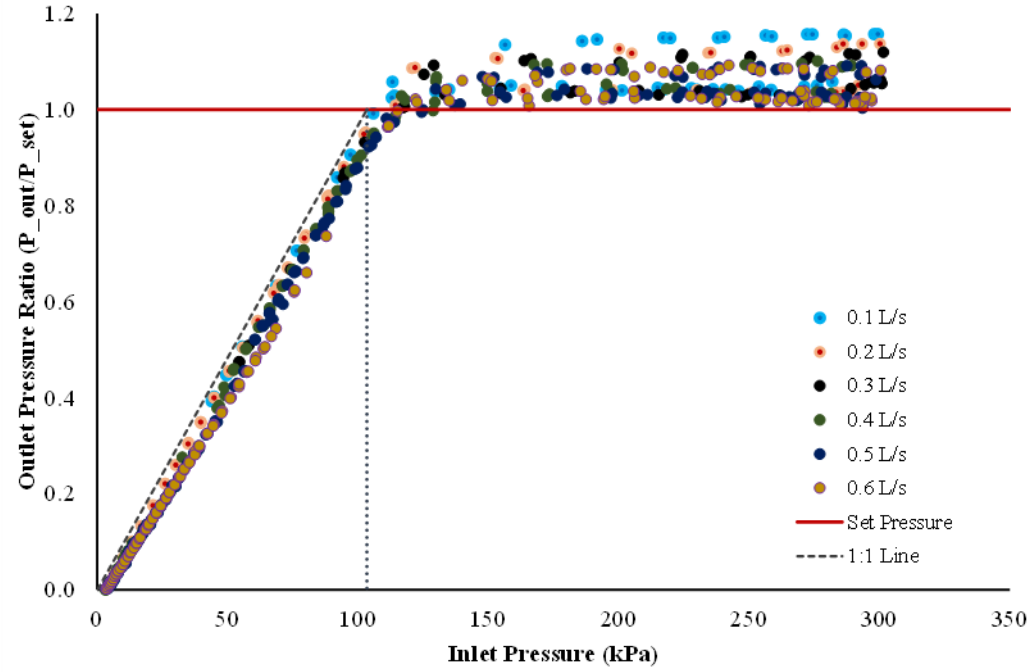

Figure 5-98: Outlet pressure hysteresis envelopes for a high pressure Y - #09 regulator at a discharge range of 0.1 to 0.6 L/s

The performance of the Z brand set of pressure regulators is illustrated in Figure 5-99, Figure 5-100, and Figure 5-101. A remarkable outcome from this type of pressure regulators is that they produce regulated pressures that are very tightly close to the nominal set pressure for the low pressure (10 psi) model, regardless of the direction of the supply pressure. It is still evident though that the outlet pressures reduce with an increase in discharge. The Z brand pressure regulators are however characteristic to significant head losses as shown in the data points along the 1:1 line in the non-regulating segment. These results have been validated with the high head losses obtained in the minor loss measurements when the flow tube was frozen. There is also less variability in the performance results of the three units tested in this type of pressure regulator. Like in the case of the X and Y regulators, there was a lot of vibration and noise production from the devices at the highest flow rates tested.

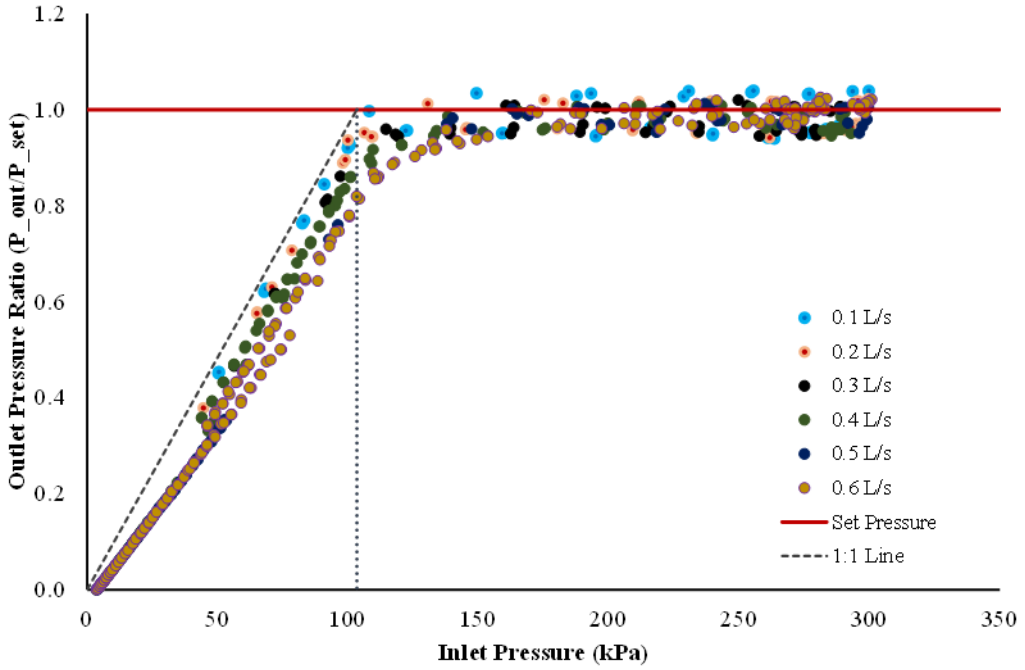

Figure 5-99: Outlet pressure hysteresis envelopes for a high pressure Z - #03 regulator at a discharge range of 0.1 to 0.6 L/s

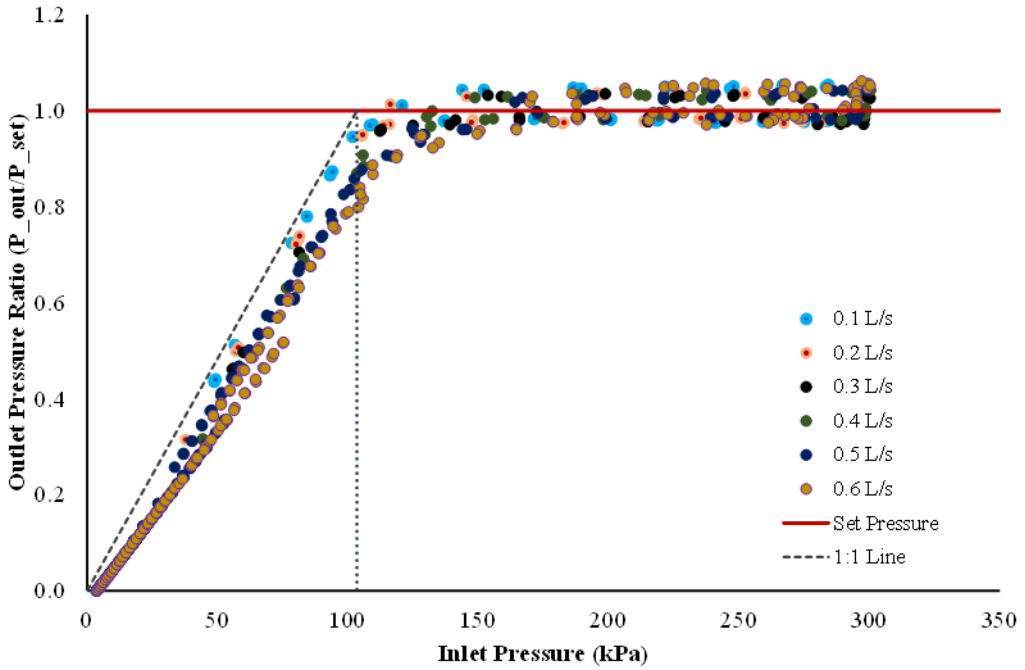

Figure 5-100: Outlet pressure hysteresis envelopes for a high pressure Z - #06 regulator at a discharge range of 0.1 to 0.6 L/s

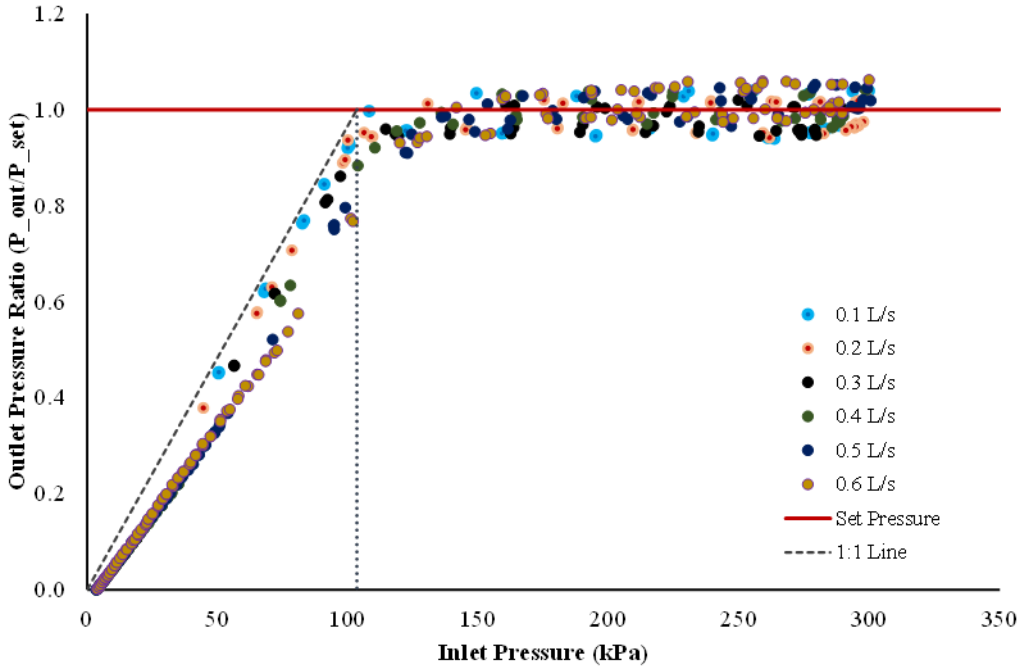

Figure 5-101: Outlet pressure hysteresis envelopes for a high pressure Z - #09 regulator at a discharge range of 0.1 to 0.6 L/s

5.6.5.1 Effects of Discharge on Regulator Hysteresis Performance

To enable the calculation of the deviation of outlet pressure hysteresis from the regulator set pressures with variation in flow rate amongst tested pressure regulators, the hysteresis envelopes were amplified as shown in the sample Figure 5-102 through to Figure 5-107. This deviation amongst tested pressure regulator brands and models is important in the description of the pressure regulator mathematical model developed in Chapter 6.

Figure 5-102 shows the regulator outlet pressures against the set pressure. The regulated pressures are generally below the set pressure except for regulated pressures measured at 0.1 L/s and rising inlet pressure limb. The variation between tested flow rates (0.1 to 0.6 L/s) is about 6 kPa when inlet pressure is rising and about 4.5 kPa when inlet pressure is falling for the low pressure X type of pressure regulator. The maximum deviation from the set pressure at the highest flow rate when inlet pressure is rising is about 5 kPa. The deviation from the set pressure at the minimum flow rate when inlet pressure is falling is 8 kPa rising to 12 kPa at 0.6 L/s. The outlet pressure regulator varies about 11 kPa between the rising and falling pressure regimes at 0.1

L/s. It varies by 6 kPa between the rising and falling pressure regimes at 0.6 L/s. The average deviation from the regulator set pressure at the rising limb is 4 kPa and this is assumed to be corresponding to the median flow rate. The average deviation from the set pressure at the falling pressure limb is 10 kPa.

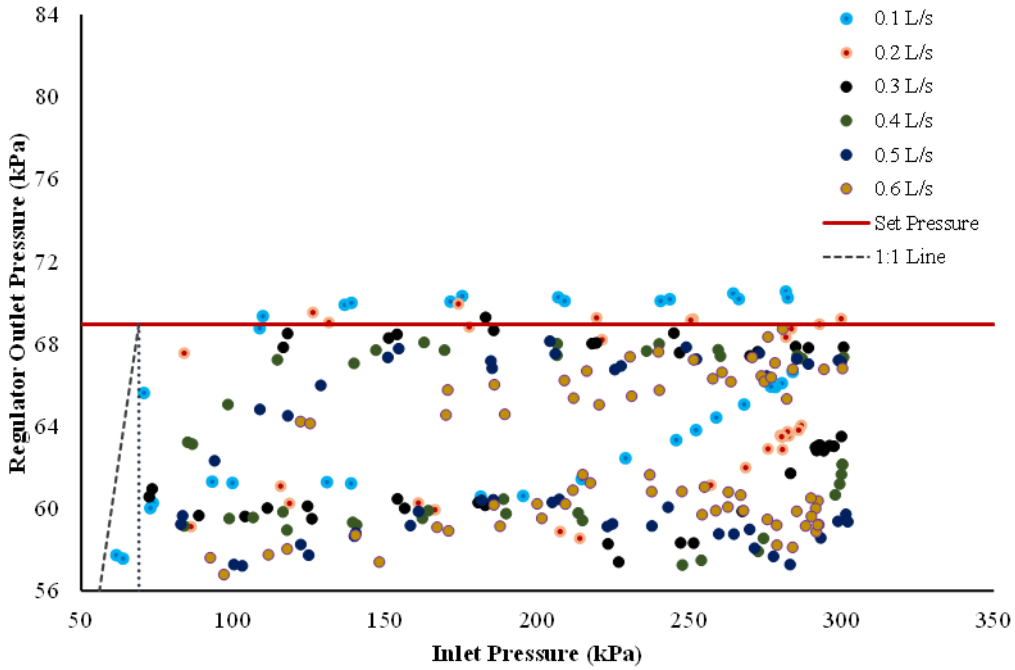

Figure 5-102: Exploded hysteresis envelopes for the low pressure X - #10 regulator at a discharge range of 0.1 to 0.6 L/s

The variation in outlet pressure for the low pressure model Y pressure regulator (Figure 5-103) is about 4.5 kPa between the lowest and highest flow rate when inlet pressure is rising. The difference is 4 kPa when inlet pressure is falling. The regulated pressure for this type of regulator is generally above the set pressure regardless of whether the inlet pressure is rising or falling. The maximum deviation from the set pressure in this model is obtained from the lowest flow rate at a rising inlet pressure and is about 12 kPa, which reduces with an increase in flow rate to 6 kPa at 0.6 L/s. The regulated pressure tracks the set pressure when inlet pressure is falling at the highest flow rate and is 4 kPa above the set pressure at the lowest flow rate. The average deviation from the regulator set pressure at the rising limb is 8 kPa and this corresponds closely to the median flow rate. The average deviation from the set pressure at the falling pressure limb is 4 kPa.

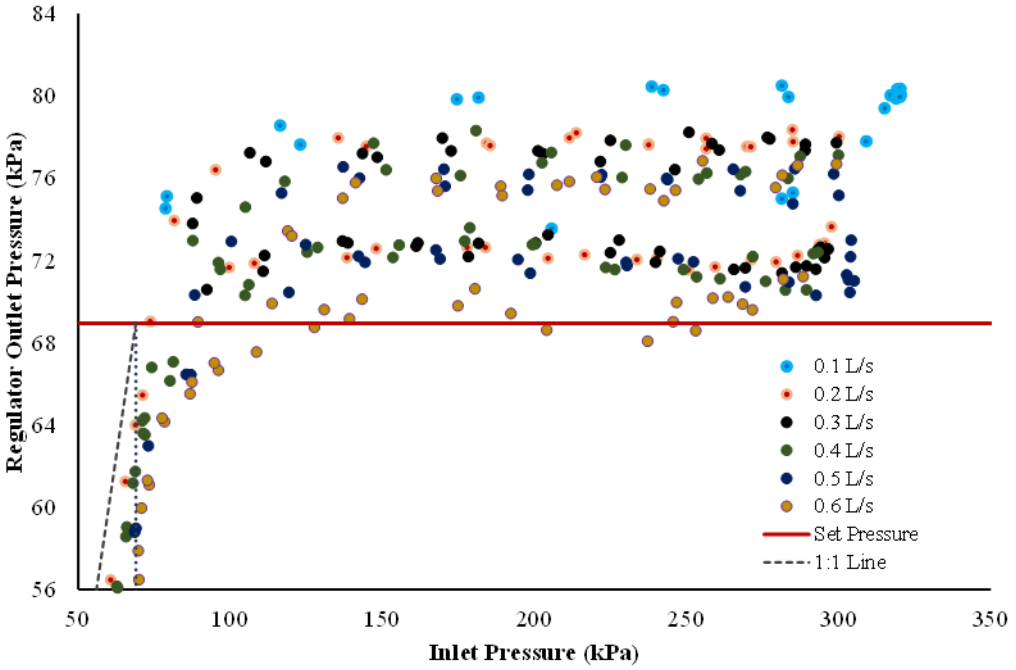

Figure 5-103: Exploded hysteresis envelopes for the low pressure Y - #09 regulator at a discharge range of 0.1 to 0.6 L/s

Figure 5-104 shows the regulated pressures for the Z low pressure regulator model at the same tested flow rates between 0.1 to 0.6 L/s. The regulated pressures are also generally higher or at least tracking slightly below the regulator set pressure. The maximum difference in regulated pressures from the set pressure is obtained in the lowest flow rate and is about 7 kPa above the set pressure. The difference in the regulated pressure between 0.1 and 0.6 L/s when inlet pressure is rising is 3 kPa and is also about 3 kPa with a falling inlet pressure limb. The average deviation from the regulator set pressure at the rising limb is 5 kPa and this corresponds closely to the median flow rate. The average deviation from the set pressure at the falling pressure limb is about 1 kPa. The lowest regulated pressures at the falling pressure limbs is also about 1 kPa below the set pressure.

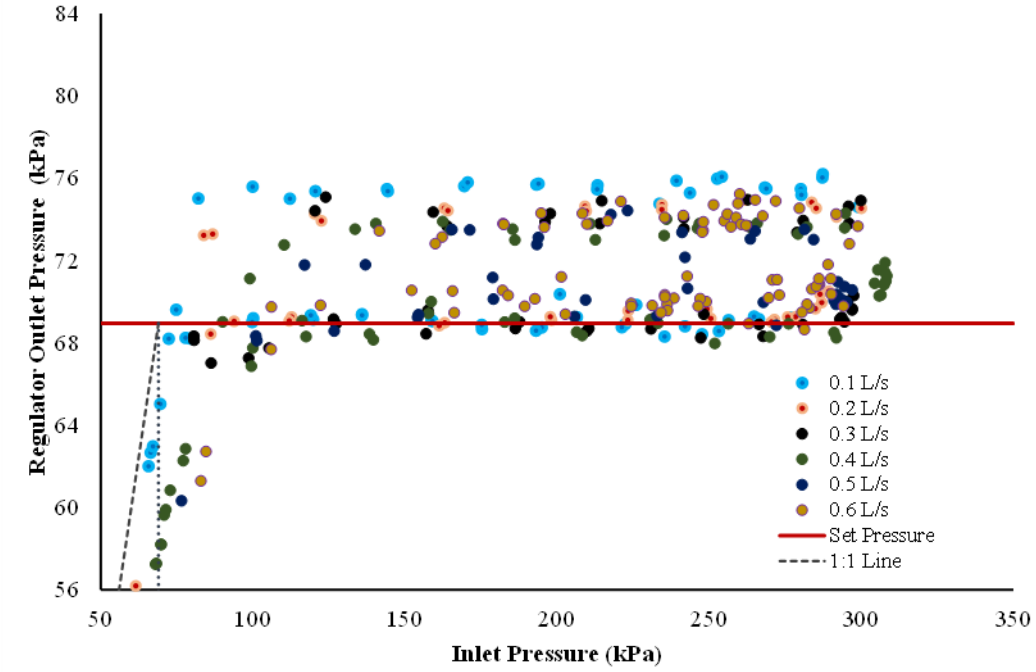

Figure 5-104: Exploded hysteresis envelopes for the low pressure Z - #05 regulator at a discharge range of 0.1 to 0.6 L/s

The disparity of regulator outlet pressures for the high pressure X regulator model is distributed above the regulator set pressure when inlet pressure is rising and falls below the set pressure when inlet pressure changes to a falling pressure limb (Figure 5-105). The maximum deviation from the set pressure in this type of pressure regulator is on the highest flow rate when inlet pressure is falling, and this is equal to about 13 kPa. The difference in the regulated pressure between 0.1 and 0.6 L/s when inlet pressure is rising is 7 kPa and is also about 7 kPa with a falling inlet pressure limb. The average deviation from the regulator set pressure at the rising limb is 4 kPa and this corresponds closely to the median flow rate of 0.3 L/s. The average deviation from the set pressure at the falling pressure limb is about 10 kPa.

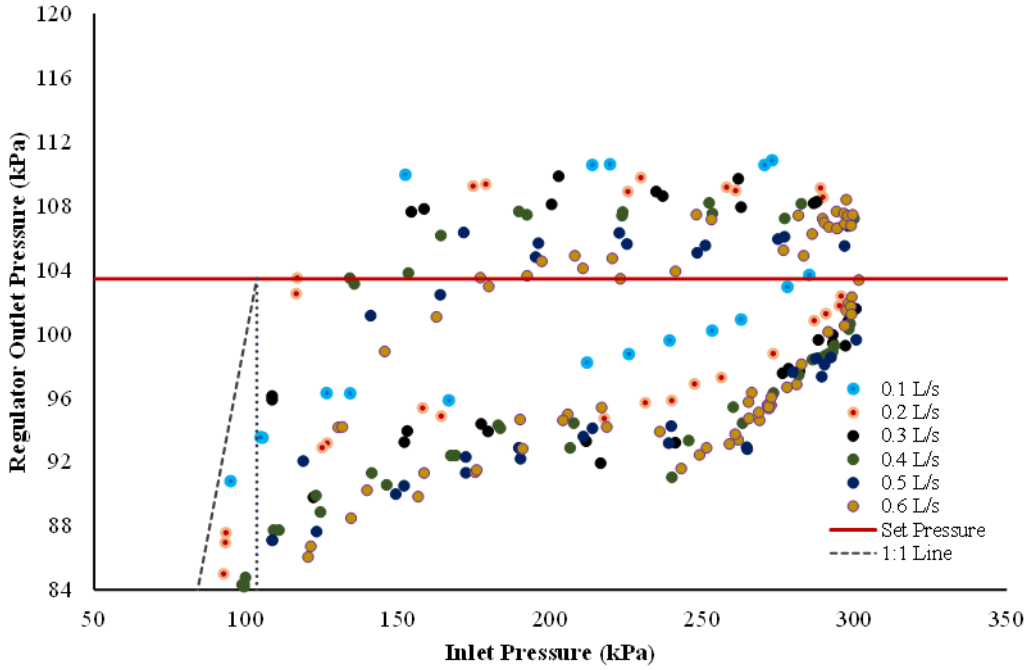

Figure 5-105: Exploded hysteresis envelopes for the high pressure X - #12 regulator at a discharge range of 0.1 to 0.6 L/s

Figure 5-106 shows the distribution of regulated pressures above the set pressure of the high pressure Y pressure regulator model both in the rising and falling pressure limbs between the tested flow rates. The maximum deviation from the set pressure is found to be 15 kPa on the lowest flow rate when inlet pressure is rising. The smallest difference is about 2 kPa which is obtained from the highest flow rate when inlet pressure is falling. The average deviation from the regulator set pressure at the rising limb is 5 kPa and this corresponds closely to the median flow rate of 0.3 L/s. The average deviation from the set pressure at the falling pressure limb is about 10 kPa.

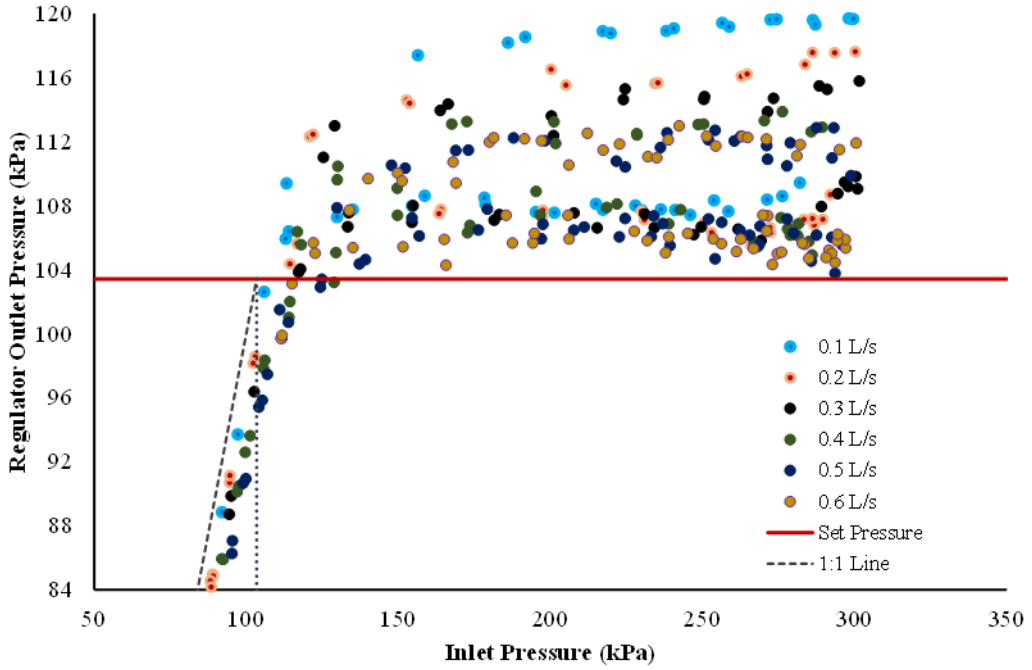

Figure 5-106: Exploded hysteresis envelopes for the high pressure Y - #09 regulator at a discharge range of 0.1 to 0.6 L/s

Regulated pressures for the high pressure Z pressure regulator model are shown in the figure below and are distributed very close to the set pressure in both the rising and falling pressure limbs. The maximum deviation in this pressure regulator model is found on the lowest flow rate and in both rising and falling pressures limbs. The difference in outlet pressures between the flow extremes tested is 11 kPa when the inlet pressure is rising and falling. The maximum deviation from the set pressure at the lowest flow rate is about 4.5 kPa when inlet pressure is rising. These regulated pressures are above the set pressure for the device. The deviation when inlet pressure is falling for the same flow rate is 6 kPa and is below the regulator set pressure. The average deviation from the regulator set pressure at the rising limb is 2 kPa and this corresponds closely to the median flow rate of 0.3 L/s. The average deviation from the set pressure at the falling pressure limb is about 4 kPa.

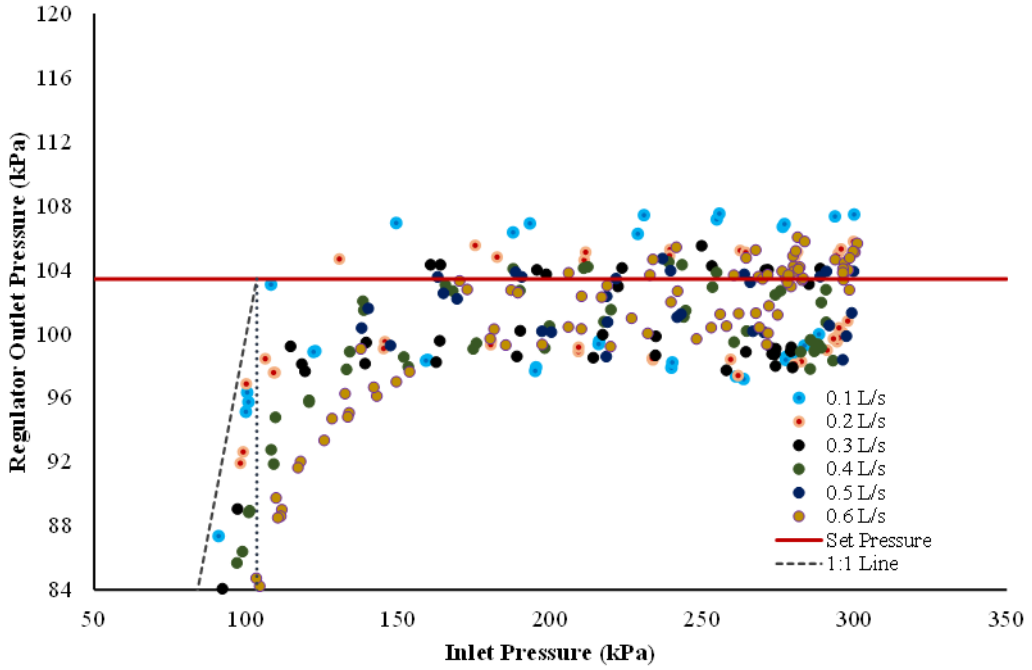

Figure 5-107: Exploded hysteresis envelopes for the high pressure Z - #03 regulator at a discharge range of 0.1 to 0.6 L/s

5.6.5.2 Effects of Differences in Pressure Regulator Units on Regulation Performance

The effects of unit to unit differences amongst pressure regulator performance was tested using a number of selected regulator units all through single flow rate. The idea was to establish the regulating accuracy and consistency of a particular models (low pressure 10 psi and high pressure 15 psi) of pressure regulating valves when operating on a CP& LM irrigation machine. These tests attempted to demonstrate the manufacturing variability that existed amongst the batch of pressure regulators for each model, which impact on regulation performance. Comparisons of the results obtained from tests conducted at 0.3 L/s and 0.6 L/s on three selected units of both the low pressure and high pressure models are illustrated in Figure 5-108 through to Figure 5-119. The regulating performance differences are observed amongst the tested units of each model and tend to be more significant with increases in discharge. The tested units of the low and high pressure models perform nearly identical to each other at 0.3 L/s, except for the inherent differences that have already been identified for the X, Y, and Z manufacturer brands. However, it is evident that the tested units of the X brand vary significantly at 0.6 L/s, followed by the Y brand, and last but not least which is the Z brand with a very tight band even at the highest flow rate.

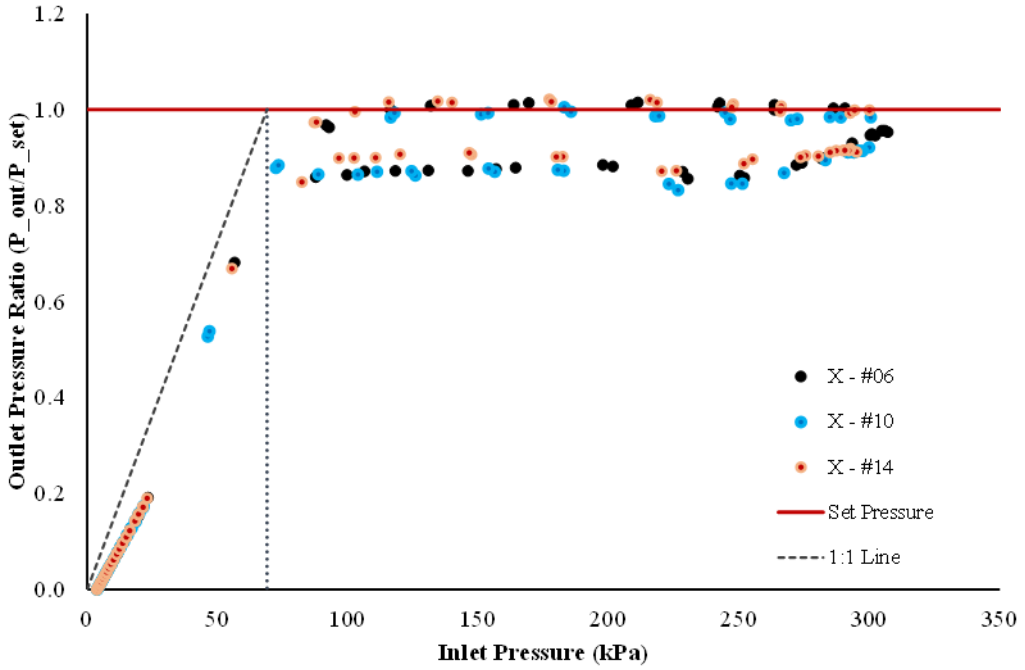

Figure 5-108: Comparison of X low pressure regulator hysteresis envelopes tested from three different units at 0.3 L/s

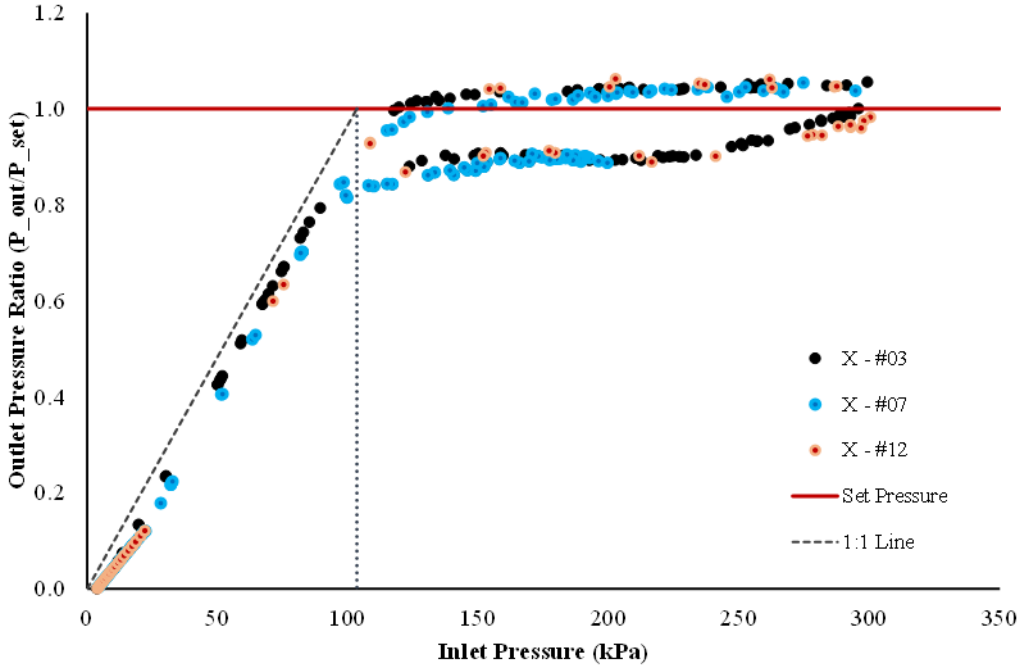

Figure 5-109: Comparison of X high pressure regulator hysteresis envelopes tested from three different units at 0.3 L/s

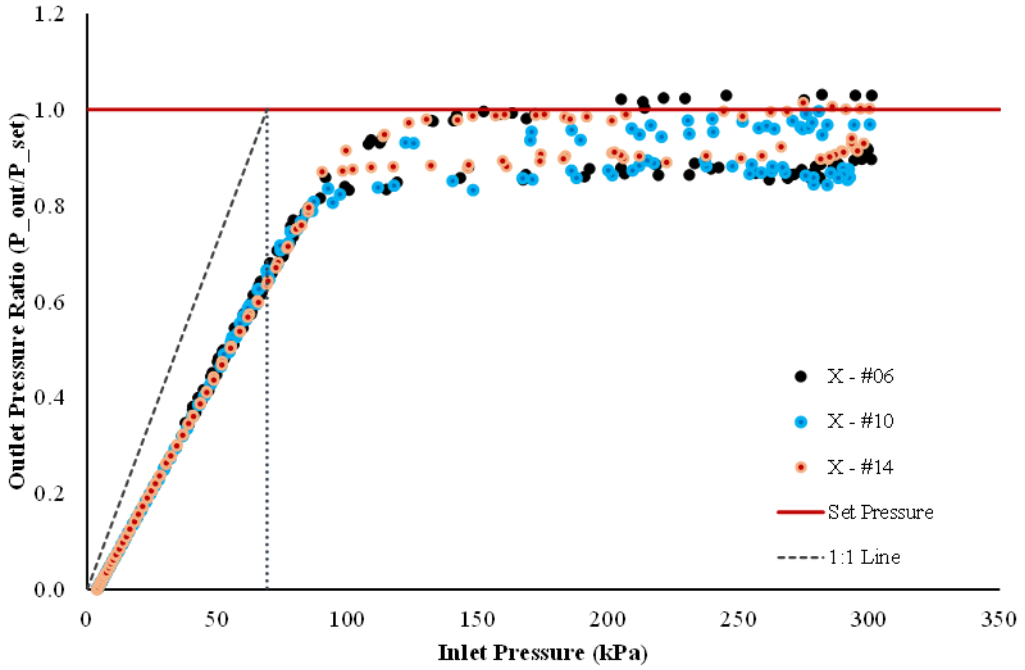

Figure 5-110: Comparison of X low pressure regulator hysteresis envelopes tested from three different units at 0.6 L/s

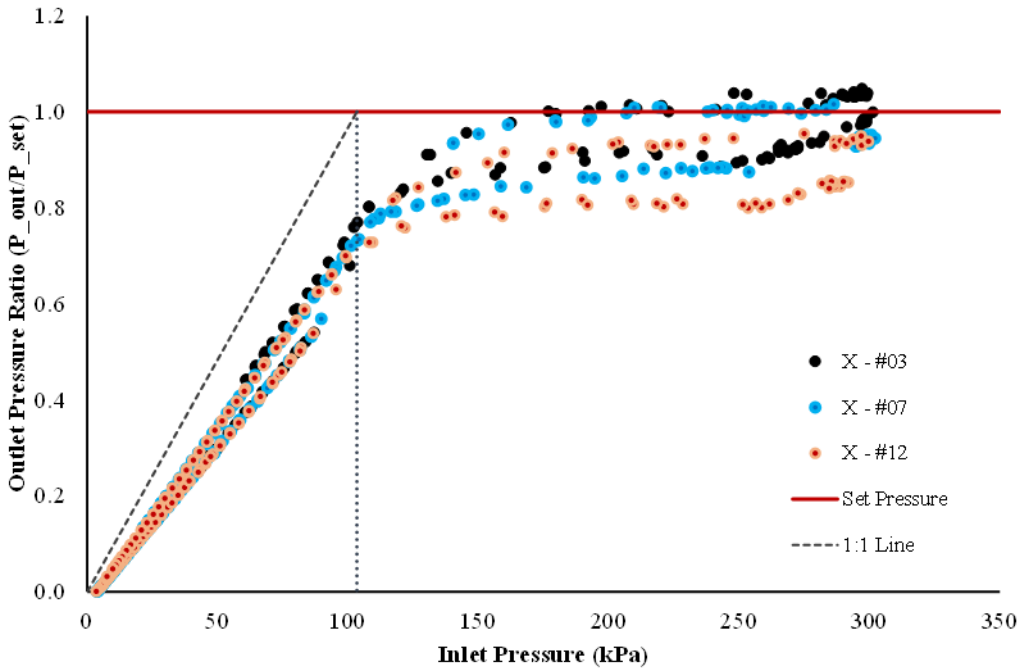

Figure 5-111: Comparison of X high pressure regulator hysteresis envelopes tested from three different units at 0.6 L/s

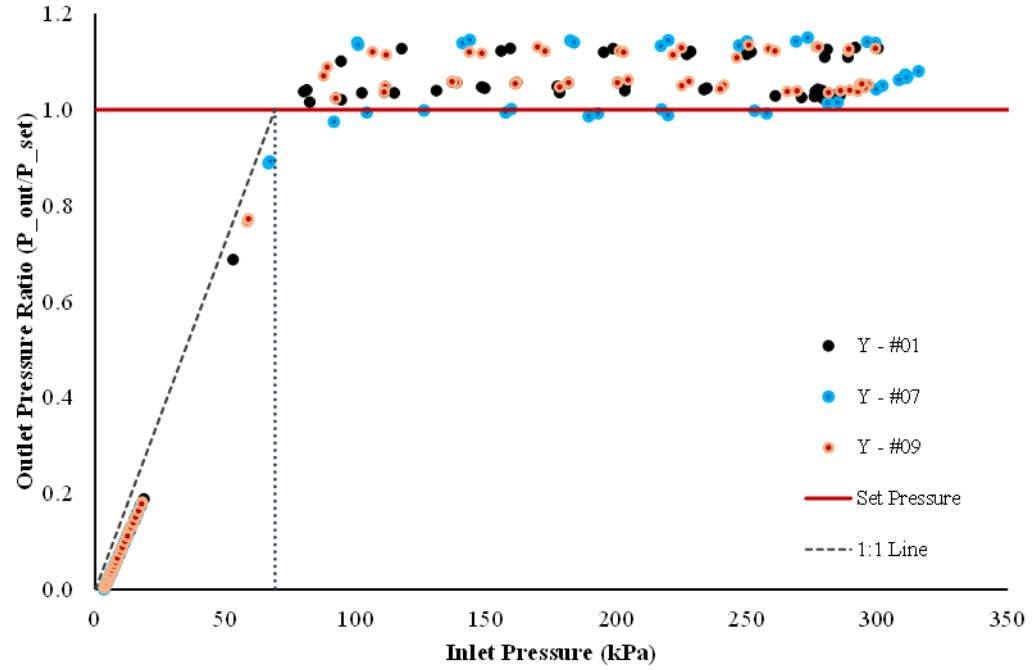

Figure 5-112: Comparison of Y low pressure regulator hysteresis envelopes tested from three different units at 0.3 L/s

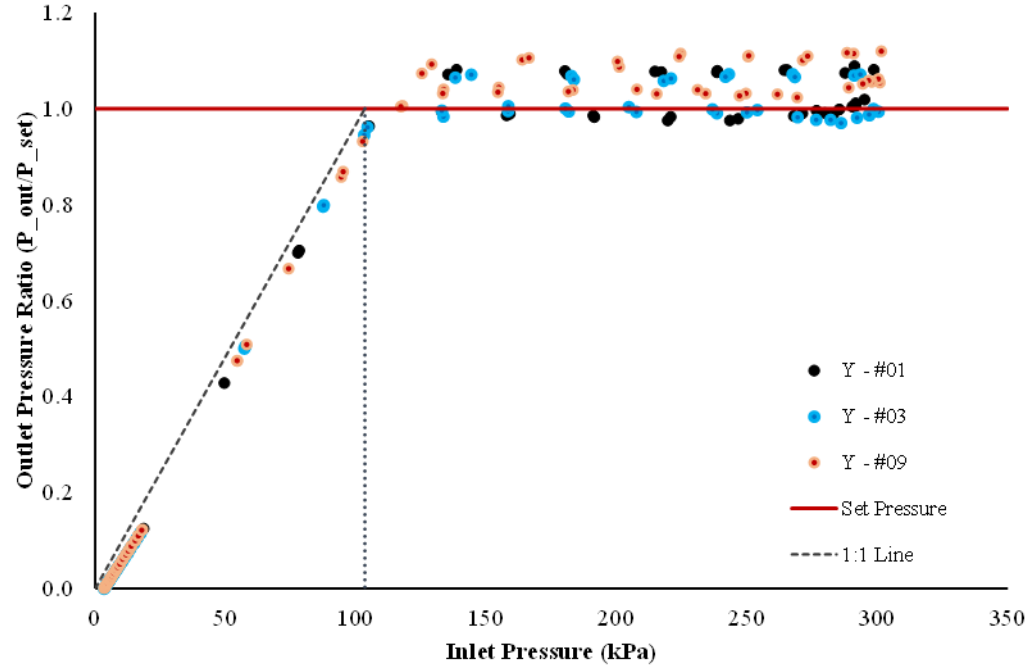

Figure 5-113: Comparison of Y high pressure regulator hysteresis envelopes tested from three different units at 0.3 L/s

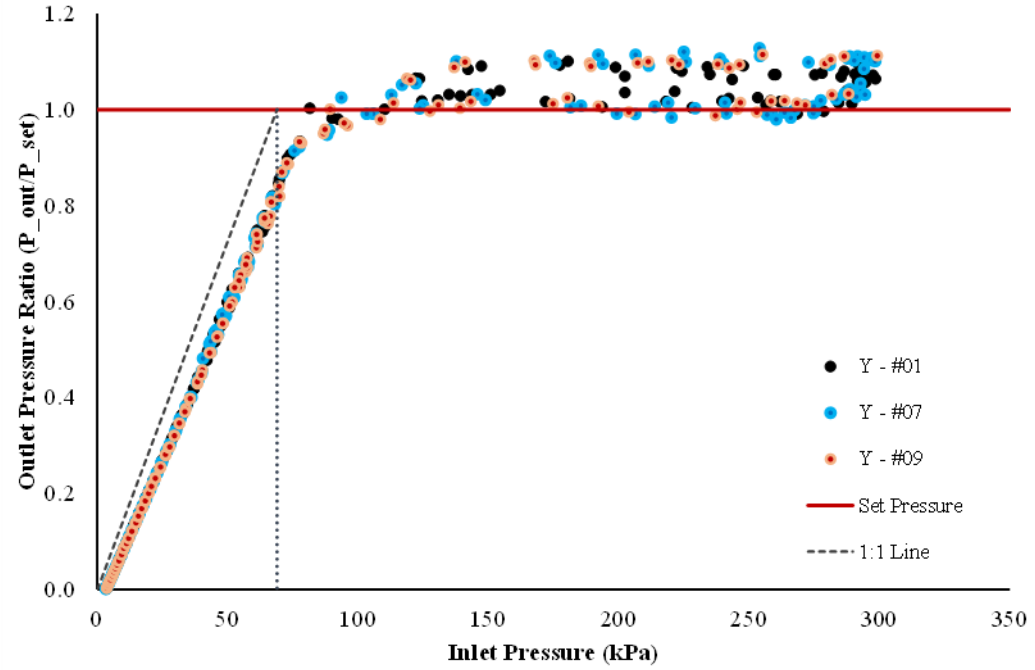

Figure 5-114: Comparison of Y low pressure regulator hysteresis envelopes tested from three different units at 0.6 L/s

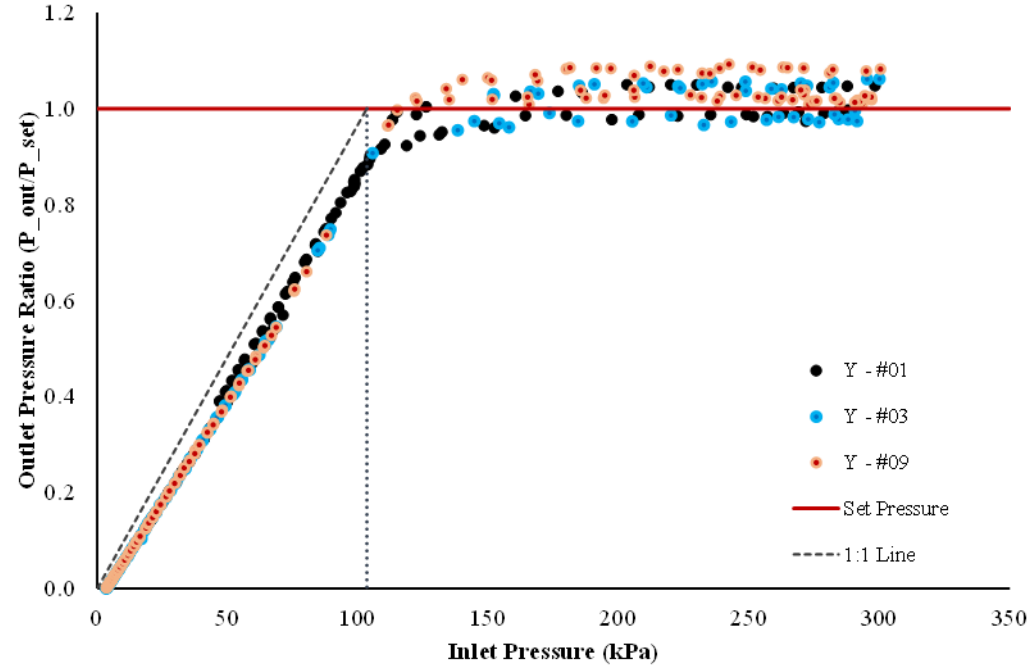

Figure 5-115: Comparison of Y high pressure regulator hysteresis envelopes tested from three different units at 0.6 L/s

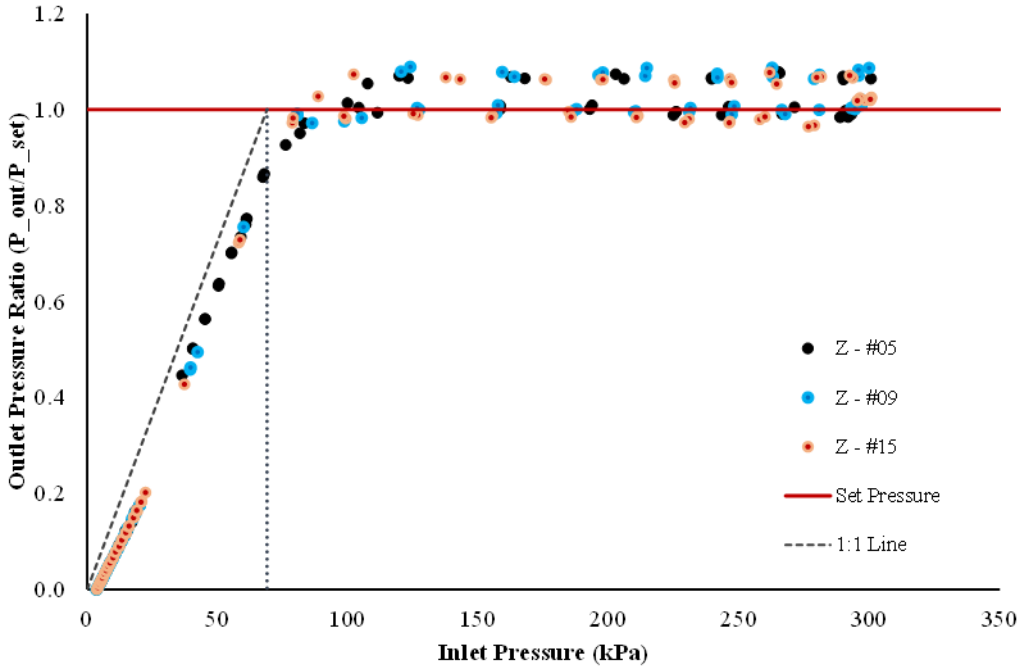

Figure 5-116: Comparison of Z low pressure regulator hysteresis envelopes tested from three different units at 0.3 L/s

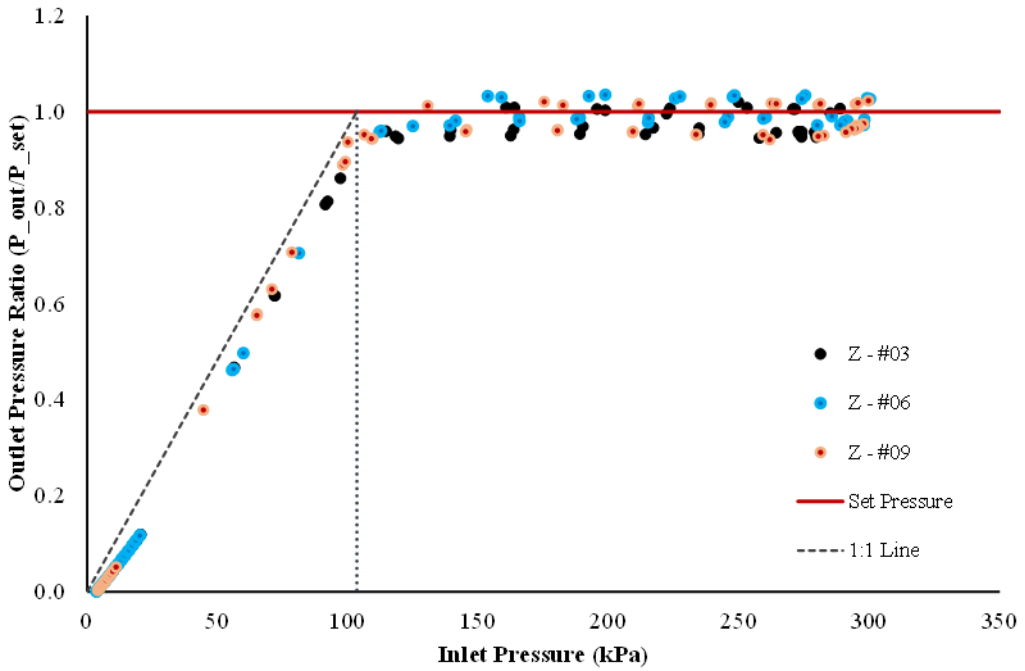

Figure 5-117: Comparison of Z high pressure regulator hysteresis envelopes tested from three different units at 0.3 L/s

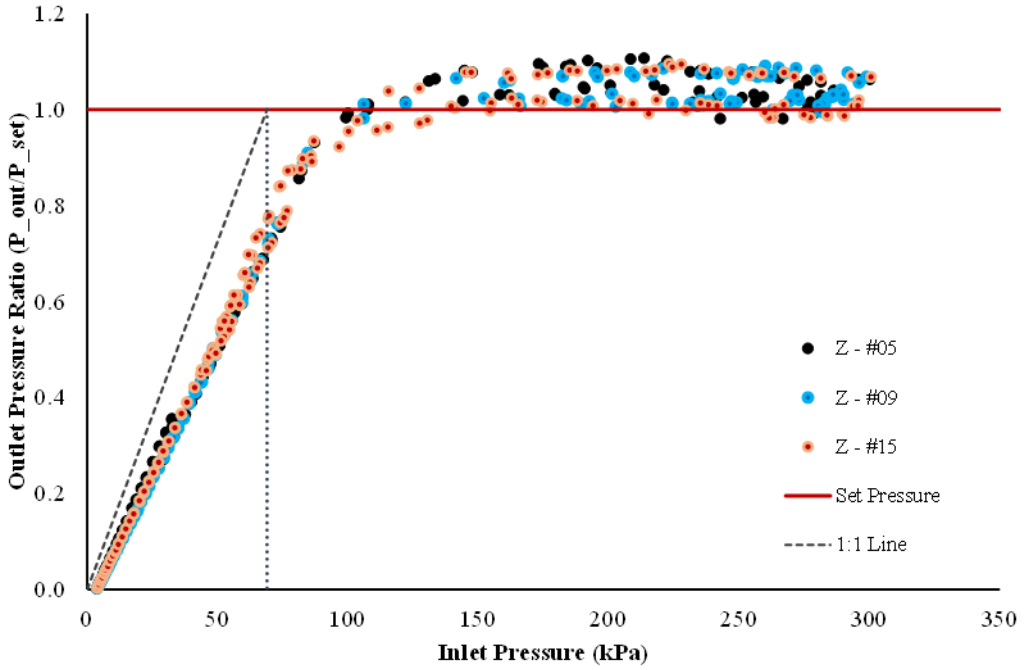

Figure 5-118: Comparison of Z low pressure regulator hysteresis envelopes tested from three different units at 0.6 L/s

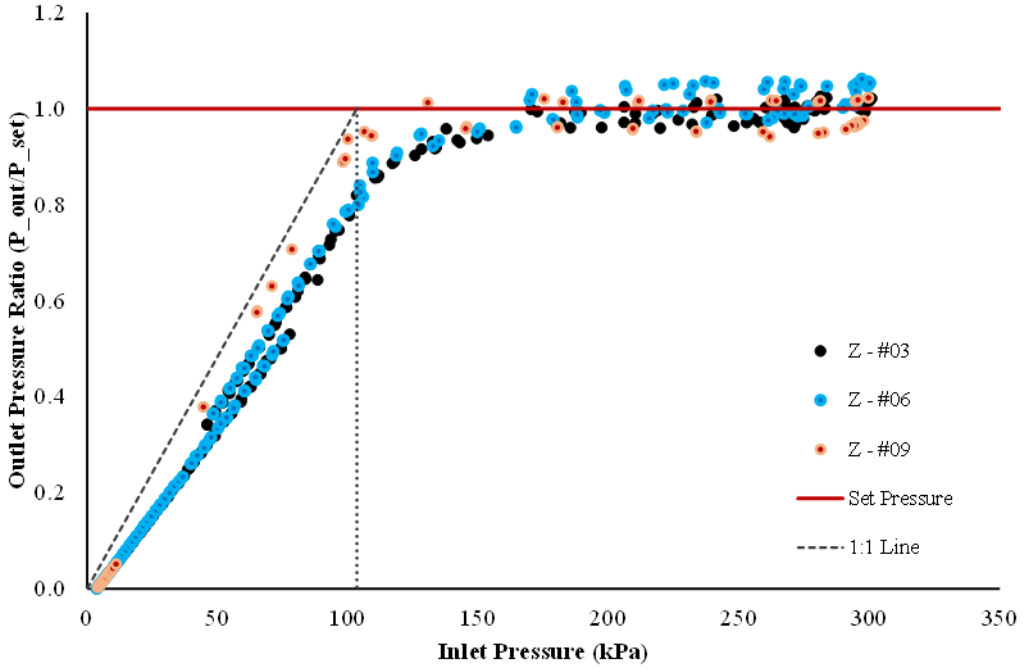

Figure 5-119: Comparison of Z high pressure regulator hysteresis envelopes tested from three different units at 0.6 L/s

5.6.6 *Continuing Hysteresis*

A different approach to the conventional hysteresis characterisation criteria was employed to simulate the nature and characteristic behaviour of the hysteresis curve that could result from normal irrigation practices when CP&LMs encounter at least one or all of the causes of unsteady conditions. In these situations, the inlet pressure will be hunting between the rising and falling limbs such that the outlet pressure impact will be responding to these pressure fluctuations. The idea was to develop a full comprehension of hysteresis to enable accurate modelling of this important complex process. The simulation of inlet pressure fluctuation was achieved using the automatic electronic DAQ system by inserting different maximum test pressures for a single flow rate (0.3 L/s) with an average velocity of 1 m/s. This type of exploratory testing was conducting using only one pressure regulator, the low pressure model X regulator brand.

Figure 5-120 shows the simulated hysteresis envelopes along an increasing inlet pressure regime. The maximum test pressure in this single experiment was increased to a maximum 400 kPa rather than the 300 kPa used in previous tests. Is it evident that the shape of the edge of the curve when it changes from a positive direction to start falling to track the lower limb is relatively similar. The only difference is on the slope change with inlet pressure threshold, where steeper slopes are visible on the lower inlet pressures up to ~250 kPa. The slope becomes close to flat when inlet pressure is greatest (between 300 kPa and 400 kPa). This hysteresis slope is referenced from the 1:1 line in a 2-D space of inlet and outlet pressure because the discharge is constant. The average slopes of the regulation and hysteresis curves are calculated using constant C for pressure regulator mathematical model development, as explained in Section 7.2.2.

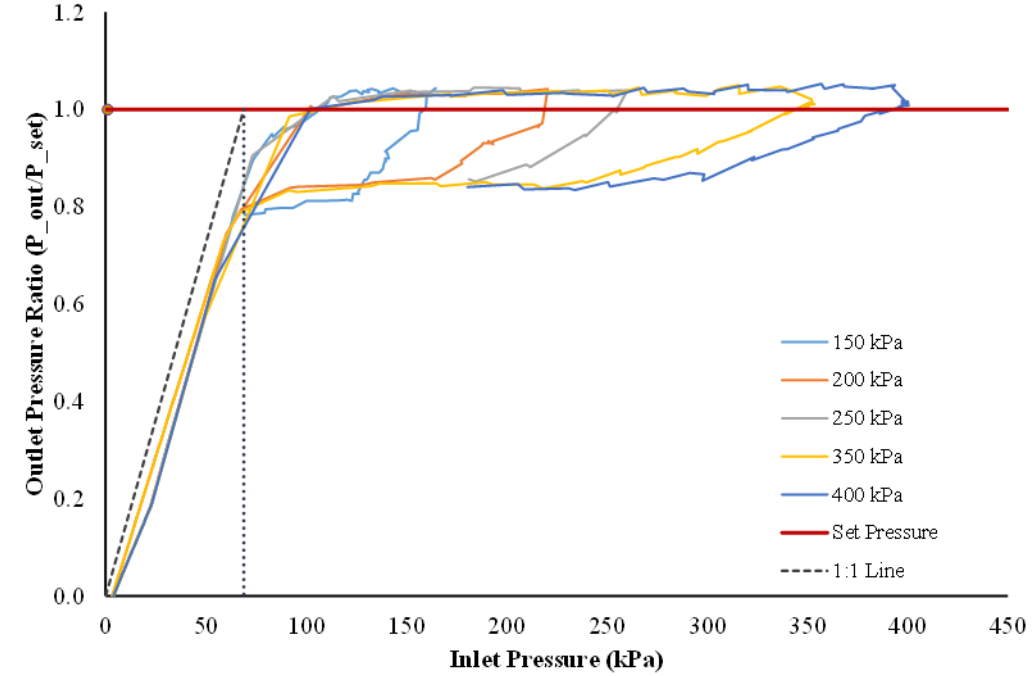

Figure 5-120: Continuing hysteresis envelopes for a low pressure X regulator model measured at 0.3 L/s

5.7 Hydraulic Response of Pressure Regulators to VRI Transients

The original concept for an experimental investigation of the response of pressure regulators to fast VRI pressure transients induced by the on-and-off pulsing of solenoid valves was explored to a very little extent. This was caused by the need for the extensive work around pressure regulator performance characterisation which required a lot of time and care to complete, as demonstrated by the amount of testing and analysis conducted in this component of the research. As such, 36 tests were conducted and a large dataset was measured at 10 kHz. This data was collected from a randomly selected small sample of previously tested pressure regulators to determine if there was any potential change in the final regulated outlet pressure when a transient is created upstream of the pressure regulator. The methodology for implementing this experiment is described in Section 4.4.4 in Chapter 4. In each of the 20 second tests, the total data points captured by each pressure transducer was equal to 200,000.

Section 5.5 of the results of hydraulic transient testing has already established that the pressure waves and hydraulic heads generated from VRI pulsing will generally increase with flow rate as a result of fluid momentum, amongst other factors. Therefore, the flow rates selected for these experiments only measured flow rates between 0.3 and 0.63 L/s. The measurements were conducted for only one or two pulses of the VRI valve, while measuring the outlet pressure response from the pressure regulator. The Y regulator brand was selected for these experiments because of the stability and consistency of the regulator performance results presented in the previous sections.

Figure 5-121 shows the results of the initial output from a 15 psi pressure regulator when there was no VRI valve pulsing influence in the test apparatus. An identical result was obtained for the 10 psi model when the inlet pressure was kept constant between the two tests, except that the outlet pressure was lower.

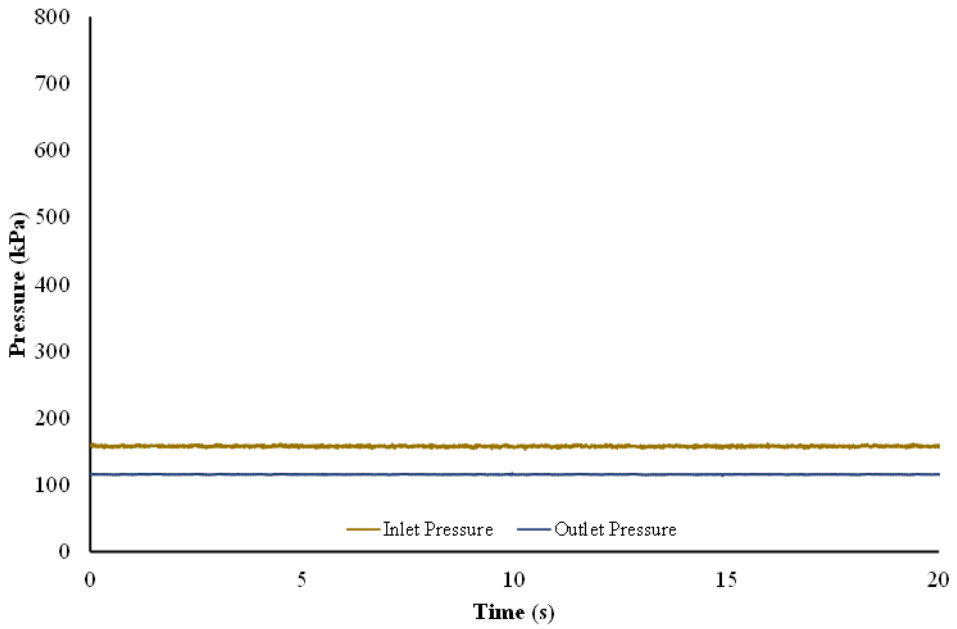

Figure 5-121: Generic pressures measured from the upstream and downstream pressure transducers in the VRI valve-pressure regulator (Y – #01 15 psi) configuration in the test-apparatus without any pulsing at 0.4 L/s

Figure 5-122 and Figure 5-123 illustrate the response of pressure regulator outlet pressures from a single pulse of a VRI solenoid valve and the subsequent pressure wave transient created to impact the inlet side of the Y regulator brand. The response pattern of the regulator outlet pressure is identical to the pressure response on the

upstream side of the regulator as a result of the VRI valve closure or opening but at a lower pressure magnitude. Figure 5-123 is the amplified form of the regulated pressure response. Small transients are also observed in the outlet pressures and this can result in momentary increase or decrease in the regulated pressure to about 17 % or (+/-12 kPa) of the nominal set pressure, and about 16 % of the actual regulated pressure for the device.

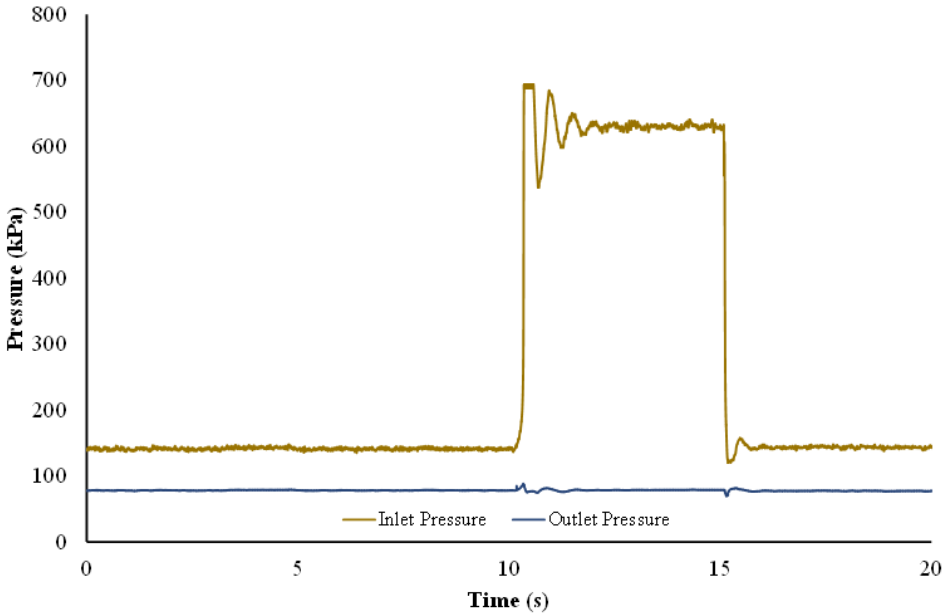

Figure 5-122: Pressure regulator outlet pressure measured with a single VRI valve transient for the low pressure model of the Y regulator brand at 0.4 L/s

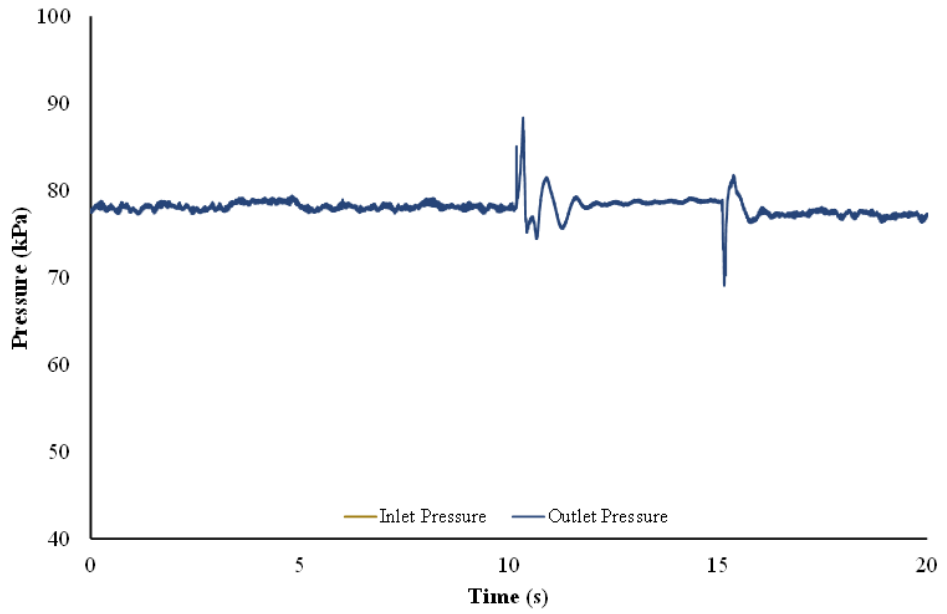

Figure 5-123: Exploded outlet pressure produced from a single VRI transient on a low pressure model of the Y regulator brand at 0.4 L/s

The transient impacted regulator outlet pressures for the high pressure model Y regulator brand are illustrated in Figure 5-124 through to Figure 5-127. The temporary increase or decrease in the regulated pressures is about 11.6 % (-/+ 12 kPa) of the nominal pressure rating of the regulator, and about 10 % of the actual regulated pressure of the regulator unit. The final regulator outlet pressure after the transients is about 2 kPa on average above or below the regulator outlet pressure before pulsing.

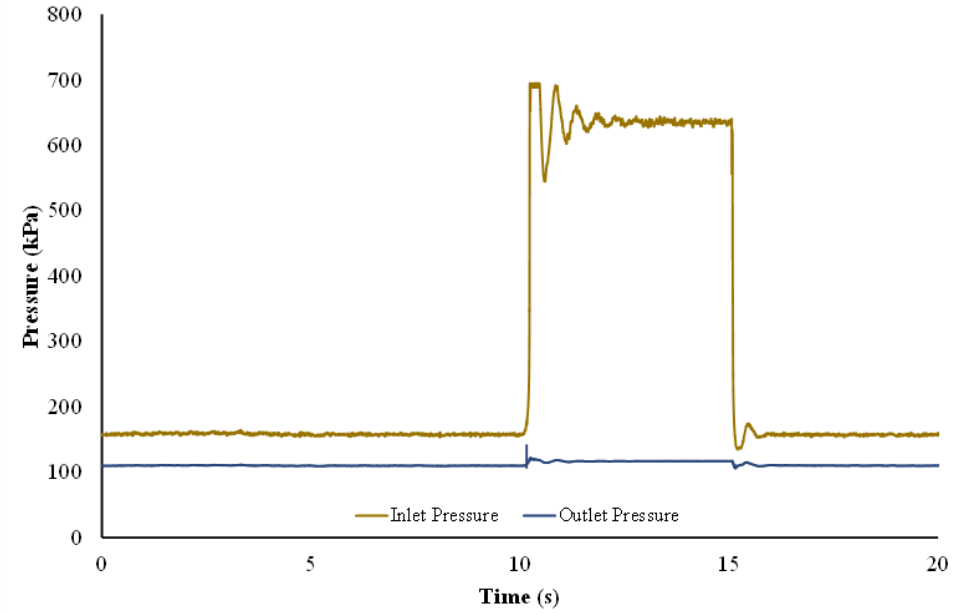

Figure 5-124: Pressure regulator outlet pressure measured with a single VRI valve transient for the high pressure model of the Y regulator brand at 0.4 L/s

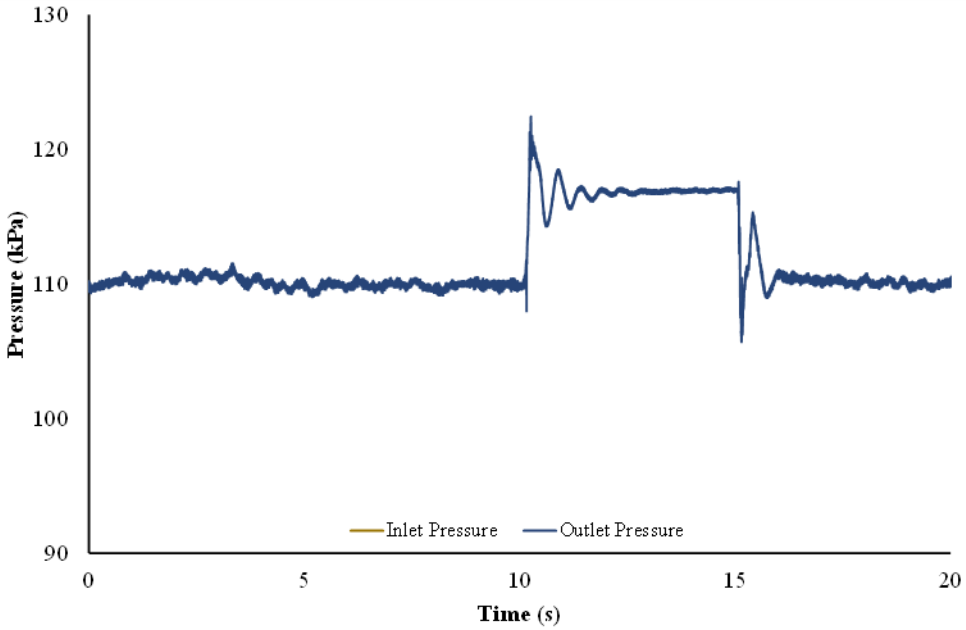

Figure 5-125: Exploded outlet pressure produced from a single VRI transient on the high pressure model of the Y regulator brand at 0.4 L/s

Figure 5-126 and Figure 5-127 represent the results of two pulses from the VRI valve and the corresponding outlet pressure from the Y pressure regulating device. The response of the pressure regulator is almost identical to the results of the single pulse. However, it was observed that a time lapse has to be allowed generally between a minimum of 5 seconds to generate a good transient from the test-apparatus.

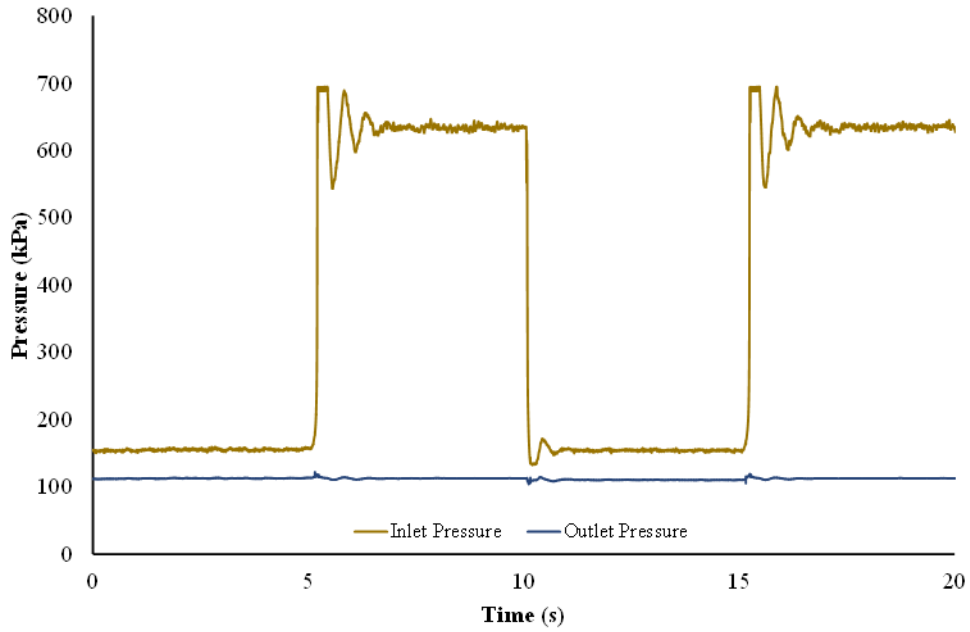

Figure 5-126: Pressure regulator outlet pressure measured with two VRI valve transients for the high pressure model of the Y regulator brand at 0.4 L/s

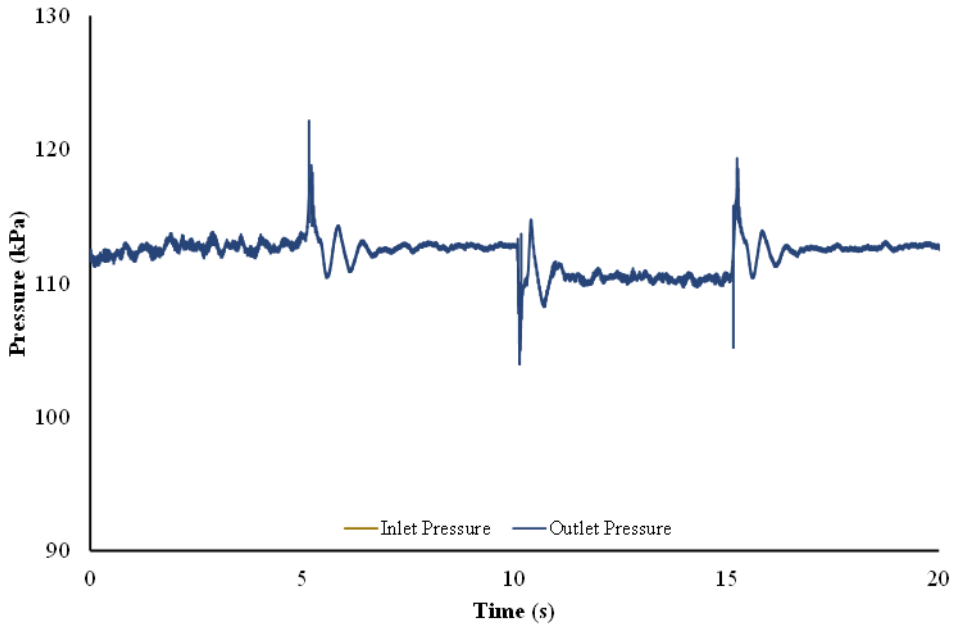

Figure 5-127: Exploded outlet pressure produced from two VRI transients on the high pressure model of the Y regulator brand at 0.4 L/s.

5.8 Summary

This section of the research completed a very detailed extensive investigation and testing of the hydraulic performance of VRI components, solenoid VRI valves and CP&LM pressure regulators. The detailed analyses and results of the different experimental tests conducted have been presented. It has been established that the minor head losses created through VRI valves are very significant and to some extent, may not qualify to be treated as minor losses, especially for one of the three commonly used VRI valve manufacturers examined. This outcome necessitated the review and modification of the universal pressure loss equation that is used for the design of CP&LMs, to be able to be used in the design of VRI machines. Regression analysis was also performed to develop minor loss coefficients for the different VRI valve brands used in VRI systems. The rationale for these minor loss coefficients is to aid VRI system design and management as there is no technical available information regarding the hydraulic performance of the VRI valves that can be used to simplify the design process.

Hydraulic transients were also investigated from the on-and-off pulsing mechanisms of VRI valves using two different built configurations (Configuration A and B) to determine the relative magnitudes of hydraulic head generated with VRI systems. The results show that the pressure head increase is significant when the inlet pressure head supply is great, and will only be reduced when the supply pressure is not sufficient. The increase in transients have also been found to be directly proportional to the flow rate, where high pressure waves and hydraulic head are associated with higher discharges. Empirical coefficients have also been developed to predict the potential maximum hydraulic head across the different nozzle size configurations used in CP&LMs retrofitted with VRI. The transients have also been found to influence pressure regulator performance.

A series of pressure regulator performance characterisation tests were conducted to determine the hydraulic performance of these regulating devices and their significance in CP&LM irrigation. The experiments were conducted on a selection of commonly used pressure regulator brands in the world. The results established a number of

hydraulic parameters which helps to understand pressure regulation performance more explicitly. The major parameters investigated include pressure regulation accuracy, pressure regulation curves, outlet pressure hysteresis, minor head losses, minor loss coefficients, and the impact of VRI transients in final regulator outlet pressure. The results show that the performance characteristics of pressure regulators are largely dependent on the regulator manufacturers for the specific hydraulic parameters tested. The regulators do to perform at the nominal pressure ratings usually nominated by the manufacturers. There is also an impact of hysteresis in the regulator outlet pressures which is caused by variations inlet pressure head. The impacts of unsteady inlet pressure head caused by fast VRI pressure transients have also been investigated.

From the outcomes of the extensive and complex pressure regulator performance test results, and the subsequent analysis completed in this research of the inherently complex nature of modern CP&LM hydraulic systems, there is a need to conduct further investigative research into the manner in which pressure regulators are modelled. The advantage that this research brings to this topic is the comprehensive regulator performance results obtained from the experiments conducted using the novel automatic multi-function test-apparatus developed. This will augment the current limited comprehension of the hydraulic performance of pressure regulators, and permit appropriate design and application of these important devices in CP&LMs. Any improved model will enable the more accurate prediction of VRI impacts on the regulator outlet pressures and sprinkler nozzle performance, to allow hydraulic designers to mitigate against the negative effects of this phenomena during the design process. Initially, there is a need to develop an understanding of the current limitations of existing pressure regulator mathematical models in predicting regulator outlet pressures. The confirmed unsteady conditions introduced by VRI require a special focus for regulation modelling as it is in line with common hydraulic conditions experienced by CP&LMs in the field. A review of the current mathematical modelling of pressure regulators is the focus of the next chapter of this thesis.

6. HYDRAULIC MODELLING OF PRESSURE REGULATION IN CP&LM IRRIGATION

6.1 Introduction

The functionality of pressure regulators is important to ensure proper uniformity and efficiency of water application for CP&LM irrigation machines. The background material on how these pressure regulating devices are implemented with CP&LMs has been covered in Chapter 1 and Chapter 2 of this thesis. This chapter explores the hydraulic modelling of the pressure regulation process. It discusses the common pressure regulator mathematical models that have been developed including an analysis of the mathematical concepts used, and an evaluation of their performance in predicting regulator outlet pressure. The discussion will highlight some of the limitations which make these models unsuitable for accurate modelling of pressure regulator performance. The results of this analysis will serve as a basis for the work presented in Chapter 7.

Before proceeding with the review and analysis of the pressure regulator mathematical models, it is imperative to first develop a precise and clear understanding of the hydraulic principles for the pressure regulation mechanisms occurring inside pressure regulators when pressurised water enters from the inlet end, through to the outlet.

6.2 Theory of Pressure Regulation

Pressure regulators, or pressure regulating valves (PRV) are a special type of spring-loaded inline valve used to limit sprinkler nozzle pressure so as to ensure optimum performance. These valves are not identical to ordinary irrigation valves that rely on continuous adjustment of discharge to cause a specific reduction in head, but they have a unique automatic operating mechanism that produces a somewhat constant outlet pressure for the sprinkler nozzle, regardless of variations in inlet pressure and

discharge. Figure 6-1 below shows a cut-away section of a PRV with all the internal components that make up the device.

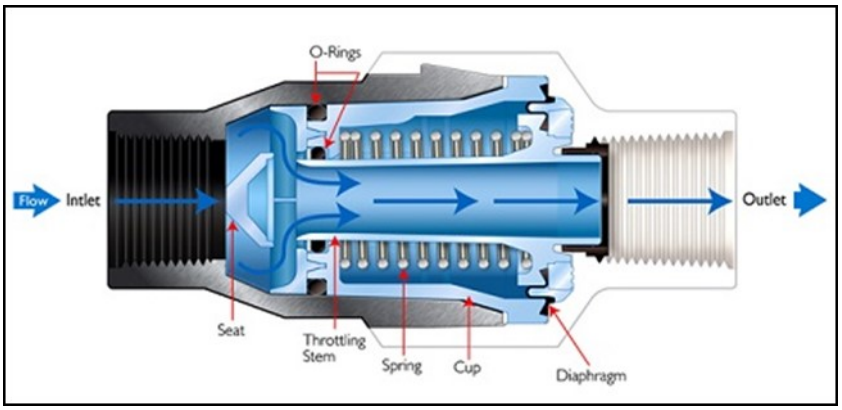

Figure 6-1: Cut-away section of a pressure regulator unit showing the internal components (Senninger Irrigation, 2018)

Water flow enters via the inlet end around a centrally located "seat" or "entry diffuser" positioned in an expanded flow cross-section to redistribute the stream of water flow into the body of the device. The entry diffuser is supported by struts which break-up and redirect the flow, providing a head loss and a flow damping mechanism in the process. The downstream side of this entry diffuser has an extended skirt, while the outer valve body has an abrupt contraction in flow diameter, which interact to aggressively re-direct water into a moveable hollow cylinder called a throttling stem or flow tube. This tube has an entry way which is bevelled, and it is this area between the entry diffuser's skirt and the tube entry that is the most critical flow area of the entire regulating device. The position of this tube inlet in relation to the downstream skirt of the entry diffuser forms the basis for the variable head loss generated by the pressure regulator valve.

Once in the tube, flow passes down its length until it is discharged into the flow outlet fitting at the downstream end of the external casing of the pressure regulator. The outer side of the bottom end of the flow tube has indentations which allows outlet water pressure to fill the void between it and the external casing. These indentations permit water entry and transmit pressure into this lower outlet void, and onto the diaphragm connected to the bottom end of the flow tube. The conical form of the flow tube also provides an annular area on which the outlet pressure acts in the upstream direction.

These pressures act on these surfaces to generate a force to move the flow tube upstream against a spring holding the tube toward the downstream end. This mechanical spring, is located in a dry chamber within the external casing, and it encircles the flow tube. The upstream end of the spring rests against the casing structure, while the downstream end of the spring is seated on the diaphragm support on the flow tube, so that the compression of the spring resists any tube movement upstream that is generated by the outlet water pressure acting on the diaphragm. It is the balance of this spring compression force and the outlet water pressure force from the diaphragm that generates the flow tube movement to regulate the outlet pressure.

To avoid filling the void between the flow tube and the external casing, the water flow path through the regulator is sealed with a rubber diaphragm at the downstream end, and with two rubber O-rings seated in the upstream of the internal regulator structure. The smaller O-ring is the most important one and seals on the outside of the flow tube, preventing water from flowing outside of the flow tube at the upstream end, and filling the void between the flow tube and the external casing. Another large O-ring also fits into another moulded seat on the upstream end of the internal regulator structure to maintain the overall upstream seal. The small O-ring acting on the outside of the flow tube generates a friction force when the flow tube displaces within the pressure regulator, which produces a hysteresis in the outlet pressure with changing inlet pressures. Hysteresis in outlet pressure is caused this an undesired friction force resisting the required free movement of the flow tube within the regulator, over that of the spring or outlet water pressure acting on the total effective diaphragm area. This friction force at the O-ring or flow tube seal, may also be supplemented by the rolling resistance of the diaphragm. Low hysteresis in outlet pressure with varying inlet pressure is important for accurate regulation. To overcome some of this hysteresis effect, manufacturers apply a lubricant around the external surface of the flow tube to reduce friction with the small O-ring. Therefore, it is expected that the hysteresis head loss will increase over time as PRVs remain exposed to heat from high temperatures, which will cause a loss of lubricant.

Although fluid head loss is generally undesirable in pumped hydraulic systems, it is what makes these pressure regulating valves work. A nominal additional head of 34.5 to 49.3 kPa (3.5 to 5 m head) is required upstream of the regulator to overcome normal fluid friction and minor head losses, and ensure that the desired outlet pressure is achieved. For instance, if 100 kPa is supplied into a regulator with a nominal set pressure of 70 kPa, the 30 kPa difference is the fluid head loss caused by the flow tube closure against the redistribution plug seat, plus the fluid friction and minor head losses through the fully-open regulator for that flow.

When all components of a pressure regulating valve have been assembled together, vents are used to prevent the valve from becoming pressurised. Venting of the spring chamber is achieved through a small cut-away section within the external casing. The bottom section of the regulator is vented into the downstream pressurised region through indentations located at the bottom of the flow tube. When a pressure regulator is in a fully open position, air is still able to flow in and out of the spring chamber at the upstream end of the regulator. Both of these incorporated designs allows the pressure regulator to function at atmospheric pressure conditions, and at no stage is the outer casing able to build up pressure which would affect the internal workings and functionality of the pressure regulator.

6.3 Identification of PRV Mathematical Models

Only four mathematical models are identified in the literature to predict the hydraulic performance of pressure regulators despite the extensive utilisation of the devices in nearly all CP&LMs around the world. These PRV mathematical models are explained in detail in the following sections.

6.3.1 *Keller and Bliesner model*

The first PRV mathematical model was proposed by Keller and Bliesner (1990) to help improve the design of CP&LMs equipped with these pressure regulating devices. This model is a mathematical description of PRV performance that was developed using

regulator performance data reported from Kincaid et al. (1987) (Figure 6-2 and Figure 6-3). It is expressed mathematically as shown in Equation 6.1.

$$P_j = P_{pr} - \left(P_{cv}\right)_j = P_{pr} - K_{KB}\left(\frac{q_j}{cv}\right)^2 \qquad 6.1$$

where P_j is the available regulator outlet pressure (kPa or psi) at radius r_j, P_{pr} is a constant value for the manufacturer's regulator type and is the average outlet pressure (kPa or psi) of that regulator type at very low discharges, $(P_{cv})_j$ is the minimum pressure loss across the regulator (kPa or psi) that varies with desired outlet discharge q_j (L/s or USgpm) at radius r_j, cv is the constant discharge for each manufacturer's regulator type (L/s or USgpm) when pressure loss across the regulator model equals one (in corresponding units), and K_{KB} is a pressure loss of unity with units corresponding (kPa or psi) to that being used.

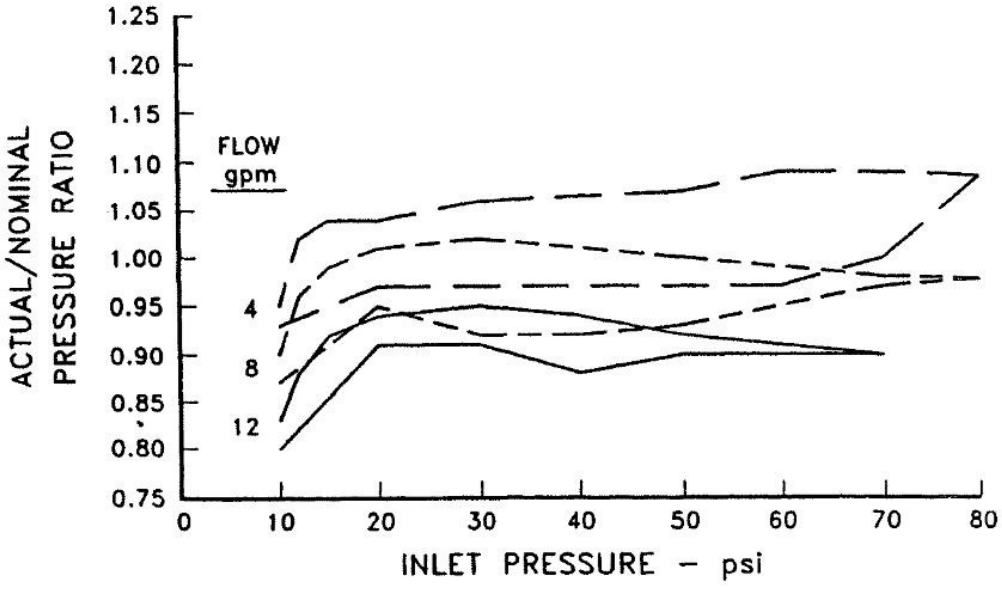

Figure 6-2: Regulation curves for a 69 kPa (10 psi) pressure regulator from Kincaid et al. (1987) as reported by Keller and Bliesner (1990)

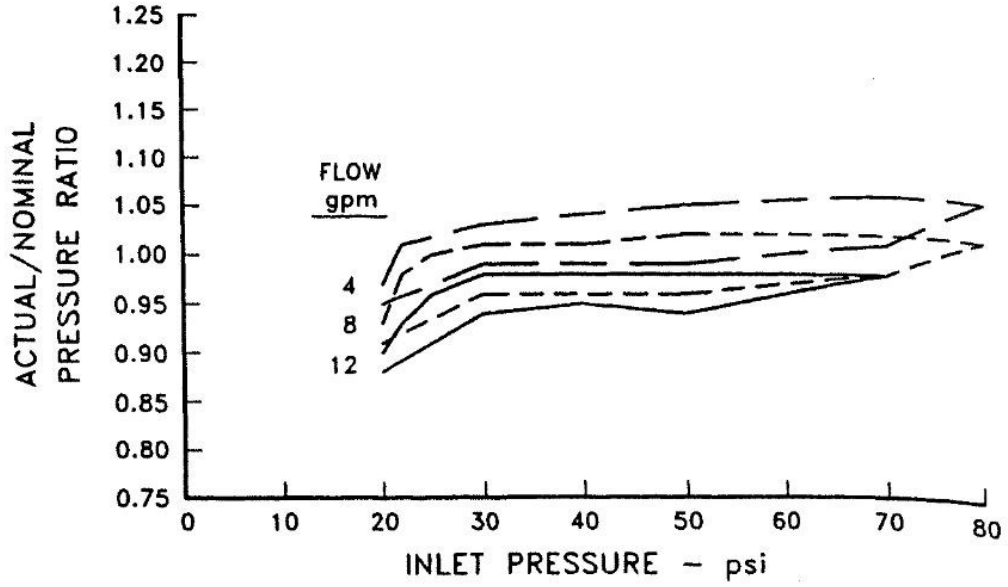

Figure 6-3: Regulation curves for a 138 kPa (20 psi) pressure regulator from Kincaid et al. (1987) as reported by Keller and Bliesner (1990)

This PRV model is derived on the basis of the functional characteristics of PRVs which work to hold the downstream pressure constant. However, this downstream pressure is dependent on the discharge through the regulators. Keller and Bliesner (1990) proposed that this discharge dependency is predictable and therefore could be easily incorporated into the design of sprinkler nozzle and/or regulator packages. In this way, the sprinkler package nozzle sizes selected to operate at different radii, were adjusted for any expected additional pressure loss due to flow rates through the regulator body. For one manufacturer's pressure regulator type a *cv* equal to 0.24 L/s (10 USgpm), was proposed regardless of the pressure setting. This means that the constant pressure for the manufacturer's regulator type is further reduced by the product of a constant, $K_{KB}/(cv^2)$, with units of pressure/discharge squared for each manufacturer's regulator type, and the nozzle discharge q_j at each radius r_j.

6.3.2 *Foley model*

The second PRV mathematical model was proposed by Foley (2010). This model consists of two equations (Equation 6.2 and 6.3) that both account for the inlet pressure head, H_{pi}, discharge, Q_o, and set pressure, *nReg*, to generate outlet pressure head. It works by using the first equation, Equation 6.2, to predict the average outlet pressure

head from the origin or zero point up to about the set pressure or turning point of the combined PRV characteristics. The second equation, Equation 6.3, predicts outlet pressure head from around the turning point or set pressure of the regulator to the maximum.

$$H_{po} = H_{pi} e^{0.039+0.0035 n\mathrm{Re}g-342Q_o} \quad 6.2$$

$$H_{po} = (nReg - 0.91) + \frac{0.047(H_{pi}+21)}{e^{1650Q_o}} \quad 6.3$$

The Foley (2010) model is a semi-empirical model that was developed based on the data from von Bernuth and Baird (1990). The model predicts pressure regulator performance for nozzle flow rates between 0.126 L/s and 1.01 L/s. It accommodates changes in outlet pressures due to changes in discharge, and does not account for hysteresis in outlet pressures other than the prediction of the average outlet pressure. This model was developed to simulate regulator performance for the nominal pressure settings of 100 kPa and 140 kPa of CP&LM pressure regulators.

6.3.3 *Junior model*

The third PRV mathematical model has been developed recently by Junior et al. (2018) and is represented by Equation 6.4. The rationale for the development of this PRV mathematical model was due to the lack of appropriate models for use to accurately predict outlet pressure from pressure regulators. It is:

$$P = a + bQ + \frac{c}{1+e^{\left[(d-(P_{in}/98.066))/f\right]}} \quad 6.4$$

where: P = regulator outlet pressure (kPa), P_{in} = inlet pressure (kPa), and Q = flow rate through the pressure regulator (m^3/h). Empirical coefficients used are a, b, c, d, and f, while 98.066 is a conversion constant for metric units from kgf/cm^2 to kPa.

This PRV model is a semi-empirical model that follows a logarithmic function with a sigmoid curve and uses a set of fitted statistical coefficients to predict the regulated PRV outlet pressure. The coefficients and boundary conditions for each pressure

setting for this particular manufacturer's regulator, are summarised in Table 6-1. The authors stated that this PRV mathematical model uses inlet pressure, discharge, and hysteresis to predict outlet pressure. They further proposed that when the inlet pressure increases infinitely beyond the upper boundary limit, the regulator outlet pressure becomes constant and follows Equation 6.5.

$$P = a + bQ + \text{constant} \tag{6.5}$$

Table 6-1: Statistical coefficients and boundary limits for using Junior et al. (2018) model to estimate pressure regulator outlet pressure

PRV Model	*a*	*b*	*c*	*d*	*f*	*Q* (L/s)	P_{in} (m head)
10 psi	-5.0871	-0.0292	5.7730	-0.9202	0.4357	0.15-1.0	5.0-80.0
15 psi	-3.5686	0.0483	4.6925	-0.2054	0.3775	0.15-1.1	5.0-80.0
20 psi	0.2162	-0.0361	1.2187	0.8951	0.2819	0.15-1.1	5.0-80.0

However, in practical conditions, the mechanical spring has certain limits of load and can therefore respond up to a certain inlet pressure thresholds. Zhang and Li (2017) emphasised the importance of the manufacturer pre-set pressure and the initial regulation pressure. Additionally, the spring is reported to vibrate heavily at certain flow rates depending on the pressure rating of the device, which is this case is determined by the spring properties. Lima et al. (2003) reported vibration of a 20 psi regulator model when inlet pressure exceeded 588.40 kPa at flow rates higher than 0.95 L/s.

6.3.4 *Zhang and Li model*

The fourth mathematical model for predicting pressure regulator performance evident in the literature was proposed by Zhang and Li (2017). This model was developed using statistical techniques with mechanical and geometric parameters of PRVs, and employed computational fluid dynamics (CFD) approaches to establish the performance indices, pre-set pressure, P_{set}, and the slope of the regulation performance line on the unregulated segment, η. The model that predicts the regulator outlet

pressures and the regulation curve are represented by two very large quadratic polynomial equations that are reported in the work completed by the authors. The PRV parameters that describe the model include, the diameter of plunger (flow tube) upstream face, d_1, height of flow orifice to seat, h, diameter of plunger downstream face, d_2, spring stiffness, K_s, and pre-stressed spring length, L_0. The analysis of the structure of model is covered in Section 6.4.4.

6.4 Review of the PRV Mathematical Models

The complex nature of the pressure regulation process requires comprehensive and appropriate modelling approaches that encompass robust and accurate mathematical expressions that can fully describe the pressure regulation mechanisms. To develop a full comprehension of the Keller and Bliesner (1990) and Junior et al. (2018) models, it is necessary to separate the individual hydraulic concepts and the mathematics involved in building these hydraulic models. The analysis will establish an understanding of the conceptualisation process of the models, and the connotations and purposes of the parameters and/or expressions involved. This analysis is based on the fundamental principles of pure hydraulics and fluid mechanics to establish any potential limitations in the development of these PRV mathematical models.

6.4.1 Review of Keller and Bliesner (1990) model

For the purposes of this analysis, the original model (Equation 6.1) is simplified and written as the following equation.

$$P_j = P_{pr} - K_{KB}\frac{q_j}{cv^2}^2 \qquad 6.6$$

The term on the left hand side of the equation, P_j, is defined in the original model as the sprinkler operating pressure at a radius r_j in the lateral of a CP&LM machine. This outlet pressure available to the sprinkler head is a result of the numerical difference between the incoming pressure head through the PRV and all of the head losses occurring inside the regulator. The discharge pressure head from the PRV is designed

to ensure that the sprinkler nozzle package operates at its optimum design pressure to ensure good water application uniformity and droplet size distribution. The general relationship between this pressure head and the discharge through the sprinkler is expressed using Equation 2.19, which can be simplified to Equation 2.20. Any increase or decrease in the sprinkler nozzle pressure will influence the discharge because any change in head is directly proportional to the square of the discharge (Equation 6.7). In the PRV mathematical model, this pressure head is determined by reducing the PRV discharge pressure, $P_{pr,}$ with an adjustment factor as shown in Equation 6.6.

$$\Delta H \alpha Q^2 \qquad 6.7$$

The first term on the right hand side of Equation 6.6, P_{pr}, is defined as the average outlet pressure at low flow rates which is usually the nominal pressure rating of PRVs. From this model description, it is clear that this outlet pressure is not the true set pressure for the device but some offset which is specific to the manufacturer. The model suggests that this outlet pressure is occurring at low flow rates. To develop a clear interpretation of the description of lowest flow rates, this implies that there is actually no head loss taking place at this particular flow rates because it is obtainable when no regulation is taking place inside the PRV device. As such, this model only predicts regulator outlet pressure by reducing the inlet pressure head with an adjustment factor which is the manufacturer offset to the nominal pressure setting of the PRV.

According to Foley (2010), and as well as on the basis of the significant PRV test results in Chapter 5 (Section 5.6), this outlet pressure is not equal to the nominal set pressure prescribed by the manufacturer, and is also different for the different PRV brands tested. Therefore, this pressure can be summarised into three components; (1) the nominal pressure setting prescribed by the manufacturer, (2) an outlet pressure offset for the manufacturer, and (3) the static minor head loss, which is a very minor head loss that can only be such at the very low flow rates at which P_{pr} has been determined. The sum of these components is mathematically illustrated in Equation 6.8.

$$P_{pr} = P_{set} + \Delta P_{offset} + h_{m-static} \quad 6.8$$

where: P_{set} is the nominal pressure setting or pressure rating of the PRV, ΔP_{offset} is the manufacturer offset to the nominal set pressure, and h_{m_static} is the static minor head loss when no regulation is taking place.

Nonetheless, although this PRV model can account for P_{pr}, once regulation commences, it does not factor any element of inlet pressure that will trigger the regulation mechanisms inside the PRV to alter P_{pr}. As a result, the inlet pressure influence on P_{pr} at a specific constant nozzle discharge is unable to be predicted. This information and its incorporation in any mathematical model is critical, to ensure that the final outlet pressure is accurate. The minimum inlet pressure threshold required above the nominal pressure rating of a PRV to induce pressure regulation is approximately 1.5 times the nominal set pressure (Mohr, 2011). Therefore, the Keller and Bliesner (1990) model is not comprehensive enough and does not have capability to model pressure regulation correctly if the principal aspect (inlet pressure) that drives all PRV operating mechanisms to produce regulation is not mathematically expressed in the model.

The PRV test results from this research have shown that there is a slight increase in the regulated outlet pressure as inlet pressure continues to rise, and the outlet pressure regulation curve will rise slightly with increases in inlet pressure, i.e. it is not a straight line. Therefore, any influence of continuous steady and sometimes unsteady increase in inlet pressure needs to be clearly defined and mathematically incorporated into any PRV model. This aspect of pressure regulation process will be discussed in detail in Chapter 7 in the development of the new PRV mathematical model.

The second expression in the Keller and Bliesner (1990) model $K_{KB}(q_j^2/cv^2)$, comprises a set of three different parameters that are integrated mathematically to establish an adjustment factor. This is a minor head loss that reduces the manufacturer specific regulator outlet pressure, P_{pr}. This expression is a product of a constant $K_{KB}/(cv^2)$, with units of pressure/discharge squared, and a nozzle discharge q_j, squared, at each radius

r_j. According to Keller and Bliesner (1990), this head loss K_{KB} is equal to 1 with units of pressure (psi or kPa), and a *cv* which is equal to flow rate through the pressure regulator that gives 1 pressure loss unit (1 psi or 1 kPa). Then the minor head loss $P_{(cv)j}$ is a variable value with q_j^2 and will not equal a constant value of 1. As such, it can be expressed using Equation 6.9.

$$P_{(cv)j} = K_{KB}\left(\frac{q_j^2}{cv^2}\right) \tag{6.9}$$

The flow coefficient *cv* is a relative measure of the flow capacity of the PRV. It is defined as the flow through a valve creating a unit pressure loss equal to 1 psi. The authors use a standard values equal to 0.24 L/s (10 USgpm) for the *cv* based on an assumption that this value is constant for PRVs of the same body configuration regardless of pressure rating. Rearranging Equation 6.9 results in the following equation which represent the minor head loss coefficient assumed by Keller and Bliesner (1990) model.

$$K_{KB} = \frac{P_{(cv)j}}{\left(\frac{q_j^2}{cv^2}\right)} \tag{6.10}$$

In fundamental hydraulics, this static minor loss is calculated using the universal minor pressure loss equation (Equation 2.16), with the minor loss coefficient *K* derived using Equation 2.17. The velocity head is calculated from water velocities occurring inside the PRVs as determined by the individual discharge rates, by first rearranging the continuity equation (Equation 2.6) to the following equations (Equations 6.12 and 6.13). Therefore, this means that the K_{KB} described by Keller and Bliesner (1990) model is not a true minor loss coefficient and can therefore not be used to accurately describe the average outlet pressure from the PRV called P_{pr}. In practice, this means that $P_{(cv)j}$ is equal to the standard minor loss equation as shown below.

$$P_{(cv)j} = h_m \tag{6.11}$$

To derive the equivalent expressions for the valve flow coefficient and flow rates producing $P_{(cv)j}$, let us first rearrange the continuity equation.

$$V = Q / A \tag{6.12}$$

and further to;

$$V = \frac{4Q}{\pi D^2} \tag{6.13}$$

Squaring the velocity from Equation 6.13 result in;

$$V^2 = \frac{16Q^2}{\pi^2 D^4} \tag{6.14}$$

The diameter D used in this calculation is the nominal dimeter of the PRVs which is different from the diameter of the flow tube, and is equal to 19.05 mm. Substituting the square of the velocities (Equation 6.14) in the minor head loss equation (Equation 2.16) result in the following equation.

$$h_m = K \frac{8Q^2}{g\pi^2 D^4} \tag{6.15}$$

Therefore, h_m, can be rearranged into Equation 6.16.

$$h_m = \frac{8K}{g\pi^2 D^4} \mathrm{x} Q^2 \tag{6.16}$$

Since we have already established that $P_{(cv)j}$ is equal to h_m, this means that Equation 6.9 will rearrange to the following equation.

$$P_{(cv)j} = \frac{8K}{g\pi^2 D^4} \mathrm{x} Q^2 \tag{6.17}$$

However, since the minor head losses inside pressure regulators can be divided into various components, including the static minor head loss and variable regulation minor head loss, this means that the K_{KB} is only a crude minor loss coefficient representing all these types of losses at a specific nozzle discharge.

Lastly but most importantly, the one important component of the regulating process inside PRVs can be termed *hysteresis*, due to the hysteresis in outlet pressure with changing inlet pressure, and it is not accounted for in this model. This component is explained in detail in Section 2.4.5.3 of Chapter 2 and Section 6.2 of this chapter. Keller and Bliesner (1990) overlooked this important process which brings about the regulating characteristics of PRVs to produce a specific outlet pressure P_j. The inability of this model to account for hysteresis suggest that it is deficient in modelling pressure regulation correctly. A detailed analysis and mathematical description of the hysteresis process will be covered in Chapter 7 in the development of a new PRV mathematical model.

The PRV model evaluation Section 6.5.1 of this chapter will also address some additional concerns that are identified in the application of this model to predict regulator outlet pressure.

6.4.2 *Review of Foley (2010) model*

The relationship between inlet pressure head and discharge to produce a final outlet pressure from a regulating device is expressed by the combined implementation of Equation 6.2 and 6.3, as explained previously in Section 6.3.2. This model is an improvement to the original model proposed by Keller and Bliesner (1990). It produces regulator outlet pressures between the two sides of the regulation curve, with a clearly defined turning point. The relationship between inlet pressure and outlet pressures for a specific discharge has a linear relationship rising from the origin, with decreasing slope for increasing discharges. The model predicts average regulator outlet pressures with an increase in inlet pressure head. This means that it takes into account of any changes in inlet pressure by producing the average outlet pressure, which in some ways, may be considered as an average of the hysteresis in outlet pressure.

The variables used in the model are the inlet pressure head H_{pi}, which in this case is set between zero and 35 m head. This inlet pressure head rises up to a maximum value that corresponds to an outlet pressure head equal to the set pressure of the regulator, at

a specific discharge, for Equation 6.2. A further increase in this inlet head will extend the outlet pressure line following the same slope. Therefore, at this point where the inlet pressure corresponds to an outlet pressure head value equal or near the regulator set pressure, Equation 6.3 is applied to simulate the further outlet pressures resulting from the further increase in inlet pressure head. The discharge range used is 0.126 L/s to 1.01 L/s. Although the nominal set pressure *nReg* used in the model is for a specific set pressure, the semi-empirical nature of the model allows for any regulator outlet pressures to be predicted by adjusting the variables to fit to experimental data using the coefficients. However, the model does not account for the differences in the regulating characteristics between common major regulator manufacturers used in most CP&LMs around the world.

6.4.3 *Review of Junior (2018) model*

Equation 6.4 represents the PRV mathematical model developed by Junior et al. (2018). This model is an improvement to the original model proposed by Keller and Bliesner (1990). It was developed empirically, and according to the authors it predicts PRV outlet pressure as a function of inlet pressure and discharge while considering hysteresis. The model achieves this by integrating these parameters with set of statistical coefficients that were developed to simplify the PRV model calculations. The PRV model was developed using data measured from a local Brazilian PRV brand, which is not popular amongst CP&LMs irrigation globally. The nominal pressure ratings were 68.95 or 70 kPa (10 PSI), 103.42 or 100 kPa (15 PSI), and 138 or 140 kPa (20 PSI). On the contrary, the PRV testing conducted in this PhD research, concentrated on brands that are used in at least 95 % of all CP&LM irrigation machines in the world. The results from these experiments showed that they perform differently, and therefore any model should be able to account for these differences in manufacturer performance, especially when considering the mathematical modelling of the performance of the devices for design improvements and operational management.

The boundary conditions and limitations of use for Junior et al. (2018) PRV mathematical model include a discharge range between 0.15 L/s and 1.0 L/s for the

low pressure (10 psi) PRV models, and between 0.15 L/s and 1.1 L/s for the intermediate pressure (15 psi) and higher pressure (20 psi) PRV models. The inlet pressure range is set between 5.0 and 80 m head or ~50 kPa and ~800 kPa as illustrated in Table 6-1. In practice, low pressure CP&LMs are operated with pressure heads from as low as 15 m (150 kPa) to 20 or 25 m (200 or 250 kPa) to ensure their lateral line pressure is sufficient for pressure regulation. In countries like Australia where energy prices are high, there seldom exists CP&LM machines regulated at 140 kPa with pressure regulators. Most machines are regulated by 70 kPa pressure regulators and to some extent 100 kPa regulators, and use sprinkler packages with nozzles that have a discharge range between 0.067 L/s to 0.63 L/s, with this higher discharge commonly found on very long machines with very large system capacities.

The model parameters are, P_{in} which is the inlet pressure to the PRV device in kPa, and Q is the discharge through the PRV as controlled by the sprinkler nozzle and is measured in m^3/h. These two key parameters are important in the mathematical relationships developed to predict the outlet pressure because they influence the coefficients used in the model. It also clear in the mathematical solution that the model is developed using pressure units of kgf/cm^2, which are not commonly used in the standard metric system. These pressure units are then converted to kPa using a conversion constant equal to 98.066 when the whole numerical computation is completed. This is likely to introduce elements of complexity and model limitations to use.

The next critical components in the model are the statistical coefficients used to solve the PRV mathematical equation to produce accurate PRV outlet pressure. The first coefficient *a*, which has a negative scale for the 70 and 100 kPa PRV models and a positive scale for the 140 kPa PRV models, is used as an adjustment factor to the PRV outlet pressure which has a dependency on the discharge by a factor *b* in the model. The adjusting factor is large for the low pressure PRV models and reduces slightly for the 100 kPa until it assumes a positive value for the highest pressure models. The relationship between the discharge and *b* is negative and is very small in terms of magnitude. The other coefficients *c*, *d*, and *f* relates to the minor head losses that occur inside the PRV and include a loss due to friction, the variable head loss due to

regulation, and energy loss due to the spring resistance to compression. The other parameter which is a constant is the natural logarithmic base e=2.718281828.

Although Junior et al. (2018) cited that this model accounts for hysteresis, they did not state how this is undertaken and it is also not clear from the interpretation of the different individual mathematical components making up the model on how the hysteresis is predicted or factored into the complete model to predict PRV outlet pressure. Instead, the coefficients described above are used to define boundary limits and adjustment factors which are not linked to hysteresis, and this creates complexity in the comprehensive and prudent utilisation of the model.

6.4.4 *Review of Zhang and Li (2017) model*

The Zhang and Li (2017) model is a statistical model that uses a series of geometric and mechanical parameters of an unnamed or unknown PRV manufacturer, to perform numerical simulations using CFD to predict regulator outlet pressures. The principal focus of this study was to determine optimal PRV parameters which satisfy the target P_{set} while maintaining a maximum η. The physical geometric parameters of the unknown PRV used in the model development include, the diameter of plunger upstream face, d_1, height of flow orifice to seat, h, and the diameter of the plunger downstream face, d_2. The mechanical properties include, spring stiffness, K_s, and pre-stressed spring length, L_0. The quadratic polynomial regression equations were fitted using a statistical software package encompassing the five highest ranking variables, as shown in Figure 6-4.

However, this approach used in the PRV model development does not conform to the approach used by other researchers, where the independent hydraulic variables of discharge, inlet pressure head, and outlet pressure turning points, are used. As a result of this approach, the model does not account for hysteresis in the regulator outlet pressures. It was also developed over a small range of discharges, between 0.1 and 0.42 L/s which is only about 67 % of the nominal nozzle discharges common for modern low pressure CP&LMs. The utilisation of the geometric parameters to model

pressure regulator performance is somewhat awkward, because it is not always possible to disassemble regulator units to obtain these dimensions. Therefore, apart from the numerous statistical coefficients used to fit the model parameters, the applicability of this model is limited in industry.

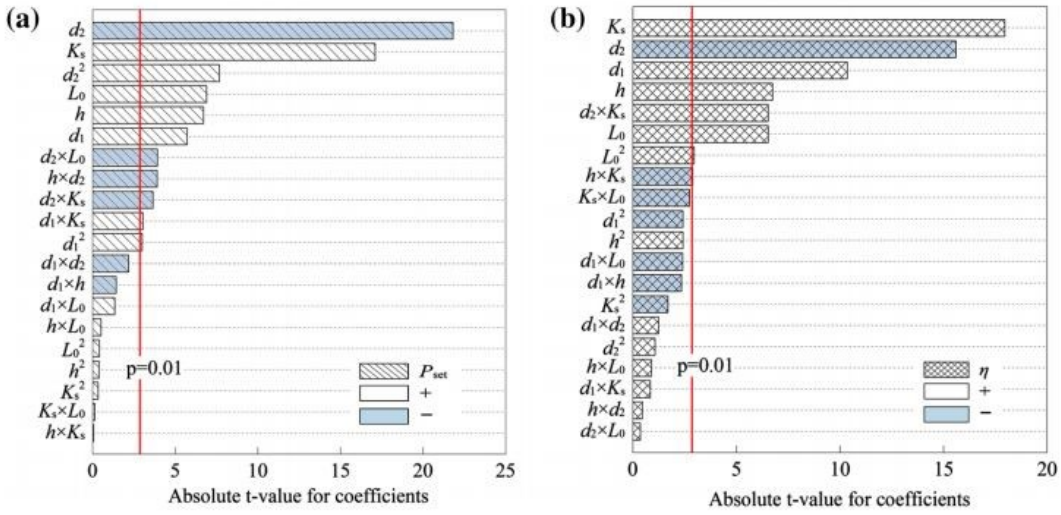

Figure 6-4: The statistical coefficients used to fit the model parameters (a) P_{set} and (b) η indices that predict the regulator outlet pressure

6.5 Evaluation of the PRV Mathematical Models

To clearly demonstrate the potential and downside of the three PRV mathematical models, it is necessary to evaluate their performance in predicting the regulator outlet pressure. The procedures that were adopted to complete the models' performance evaluation are discussed in Section 6.5.1 below. The evaluation of Foley (2010) and Zhang and Li (2017) models however, only utilised the results produced from the original performance evaluation completed by the respective authors.

6.5.1 *Evaluation Methodology*

The development and calibration processes of the novel multi-function test-apparatus (Chapter 3 and Chapter 4) detailed the boundary conditions for experimental testing of pressure regulators and explained the rationale for selecting these pressure and discharge limits. This is important because the data from these measurements is used to develop hydraulic modelling techniques that will be applied in the design and

management of VRI and pressure regulated CP&LM systems. Therefore, to simplify the performance evaluation of the existing PRV mathematical models identified, the same criteria used to develop the test boundary limits and intervals for the pressure and discharge will be used in the evaluation of these models. The objective is to provide opportunities for model performance comparisons with measured data.

The specific range of input parameters used in this model evaluation are those used to generate pressure regulation and hysteresis curves. They include an inlet pressure range between 0 and 300 kPa (0 to 30 m head), and flow rates between 0.1 and 0.63 L/s. The intervals between pressure values (2.5 kPa) are selected to produce a series of closely spaced pressure data points that are more identical to the data measured and developed in this research. However, this is not to suggest that these PRV models were originally developed in such a similar approach. The interval used for the discharge in the evaluation of the models is synonymous to that used in the experiments (0.1 L/s).

A numerical scheme was developed in MS Excel to perform analysis and 2-dimensional graphical outputs of the model performance. The results obtained from the processes followed for each PRV model, are discussed in the following sections.

6.5.1.1 Performance of Keller and Bliesner (1990) model

Figure 6-5 and Figure 6-6 below present the results of the numerical analysis and modelling of pressure regulator outlet pressure at different flow rates when using the Keller and Bliesner (1990) model. The modelled outlet pressures show that the PRV model is only capable of producing these pressures in a straight line segment parallel to the set pressure. This outcome is contrary to the author's perception that the outlet pressure increases slightly with an increase in inlet pressure after the first 35 kPa above the nominal outlet pressure setting. The model produces reduced outlet pressures with increase in discharge, although with a much wider spread across the modelled flow rates than those results from Chapter 5.

However, the overall results show that this model does not have the capability to produce initial outlet pressures below the non-regulating part of the regulation curves, and hence it is not able to characterise the onset of regulation. The initial regulation process is usually achieved at a characteristic "knee" that forms between the non-regulating and regulating legs of the pressure regulation curve. An attempt to produce this outcome from the model proved not to be possible as the outlet pressure below the inlet pressure threshold at onset of regulation only produced and maintained a parallel result of outlet pressures. The model also produces the same regulator outlet pressures from an increasing inlet pressure. It is deficient in producing lower outlet pressures when the inlet pressure is reducing, and so correctly account for the variations in the pressure received by the nozzle when a CP&LM is operating in the field. This process is what is called hysteresis in pressure regulation mechanisms.

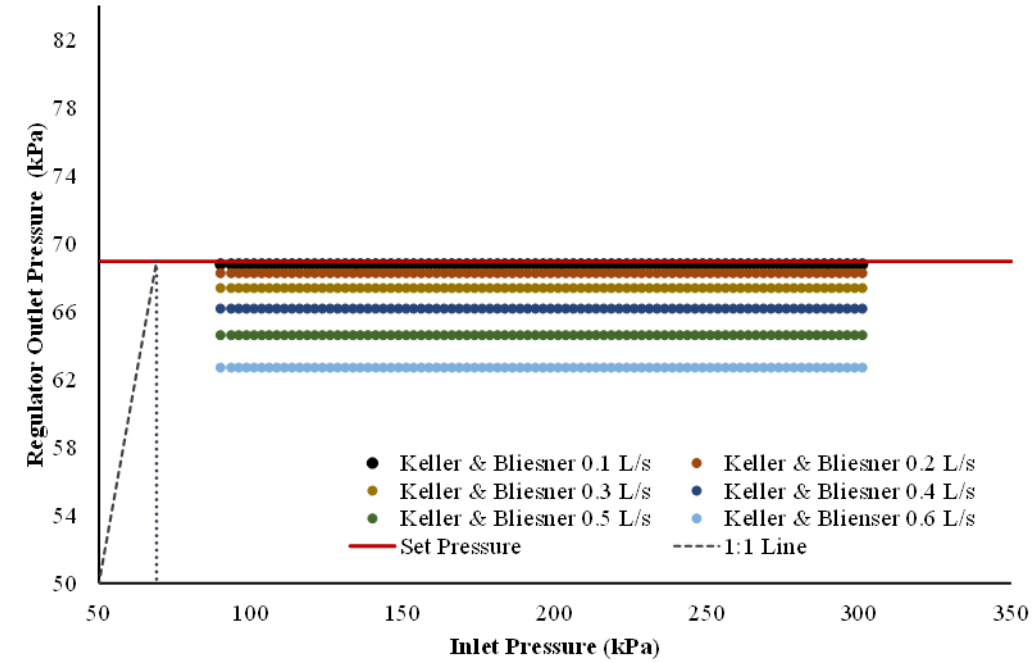

Figure 6-5: Pressure regulation curves for different flow rates modelled using Keller and Bliesner (1990) model

Figure 6-5 also shows that the model assumes a very significant head loss through the devices with increase in discharge. In practical hydraulics, the increased flow is expected to induce a drag force that will push the flow tube towards the downstream to maintain a larger opening of the area between the strut seat and the upstream inlet end of the tube. This process will reduce the head loss through the pressure regulator and therefore will result in slightly higher outlet pressure. The interactions between

the regulating mechanisms to produce this result as flow rate increases is not accounted for in the model. Nonetheless, it must be that the magnitude of this drag force is negligible, to not cause this outcome in practice. In other words, the minor head loss is much larger than any flow induced opening of the cylindrical opening of the regulating orifice.

The Keller and Bliesner (1990) model results were also plotted against measured data from the experiments described in Chapter 4 and Chapter 5 of this thesis as shown in Figure 6-6. The measured outlet pressures at the different flow rates for one of the pressure regulator brands (Z Brand 70 kPa model) prove to be different from the model results. The reduction in the regulated pressure caused by increased flow rate is different between measured and model results. The model regulated pressures are below the same pressures from the measured results. The experimental results also show that there is a slight slope along the regulation curve as inlet pressure rises, but this is not depicted in the straight curves with zero slope from the model. This shows that the model cannot predict pressure regulator outlet pressures correctly, and is therefore limited. The Keller and Bliesner (1990) therefore, cannot be used accurately for the design of pressure regulated CP&LM irrigation machines.

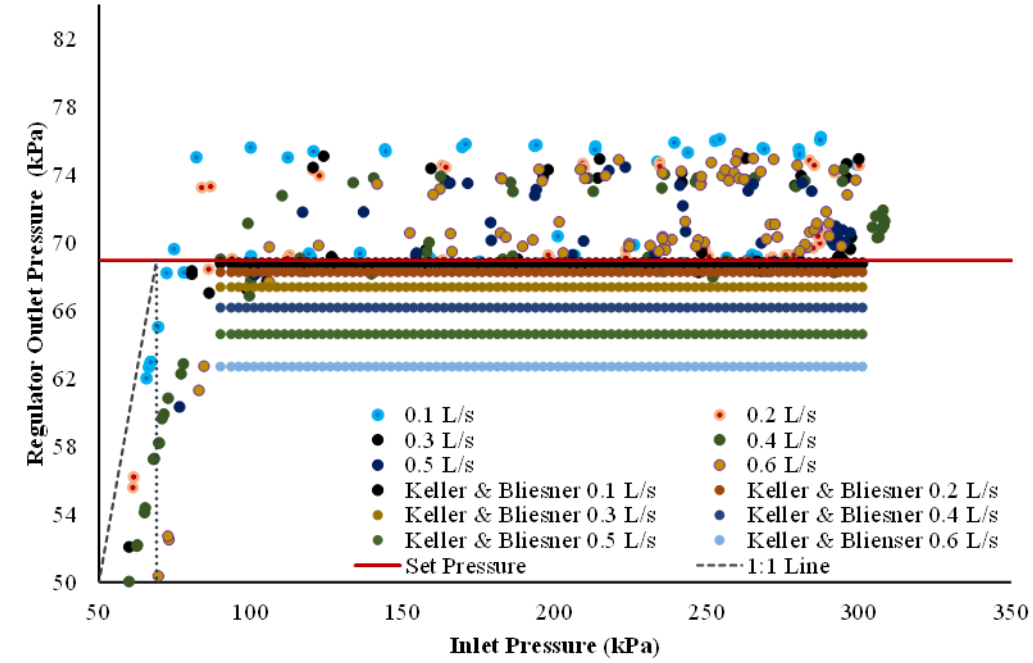

Figure 6-6: Pressure regulation curves from Keller and Bliesner (1990) model plotted against measured data for a 70 kPa Z type of regulator brand.

6.5.1.2 Summary

This performance evaluation has established that the Keller and Bliesner (1990) PRV model was originally developed for design purposes which make use of, and rely on over-simplifications of certain conditions and parameters. In this case, a model may not be representative of real world conditions as it takes into account of certain assumptions. The Keller and Bliesner (1990) model assumes that pressure regulators are ideal and will always be at pressure at any point. Therefore, it disregards any pressure changes and the performance below the regulating segment of the devices. Hence this model:

1. is a theoretical model that uses a coefficient term K_{KB}, similar to a minor head loss coefficient, which is not the true minor loss K coefficient, to adjust for the minor head loss inside the pressure regulators,

2. is not capable of producing pressure regulator outlet pressures that follow the normal pressure regulation curve. Instead, the model output is a straight line with zero slope regardless of the magnitude of inlet pressure head, which is a result of the over-simplification of the model parameters to suit design purposes,

3. is not capable of predicting regulator outlet pressures lower than the nominal set pressure of the devices,

4. produces more head loss with increases in flow rate than the results obtained from the laboratory experiments conducted in this research,

5. it assumes that the CP&LM lateral line pressure remains stable throughout the irrigation event and therefore the regulators will always be at pressure. Hence it is unable to account for hysteresis in the regulator outlet pressure. It is limited to model regulator outlet pressures assuming that the inlet pressure always track on the rising pressure limb.

6. cannot characterise the difference in outlet pressures between the non-regulating and regulating segments of the regulation curve, and the resulting turning point which is produced as a result of this important boundary between the two segments, and,

7. does not account for the differences in regulator performance amongst the different manufacturer brands.

6.5.1.3 Performance of Foley (2010) model

Figure 6-7 below represents the performance of the PRV mathematical model proposed by Foley (2010). It is evident that this model is capable of predicting regulator outlet pressures up to near the nominal set pressure for each discharge, and continues to rise with a slightly positive slope from the nominal set pressure line. Foley (2010) proposed that this positive slope on the regulated outlet pressure is necessary for the stability of the algorithms that calculate the pump operating point in an entire irrigation system. It ensures that the system resistance curve only contains one head for each discharge. Nevertheless, the model does not represent the true effects of changes in system pressure head, causing hysteresis in the regulator outlet pressure.

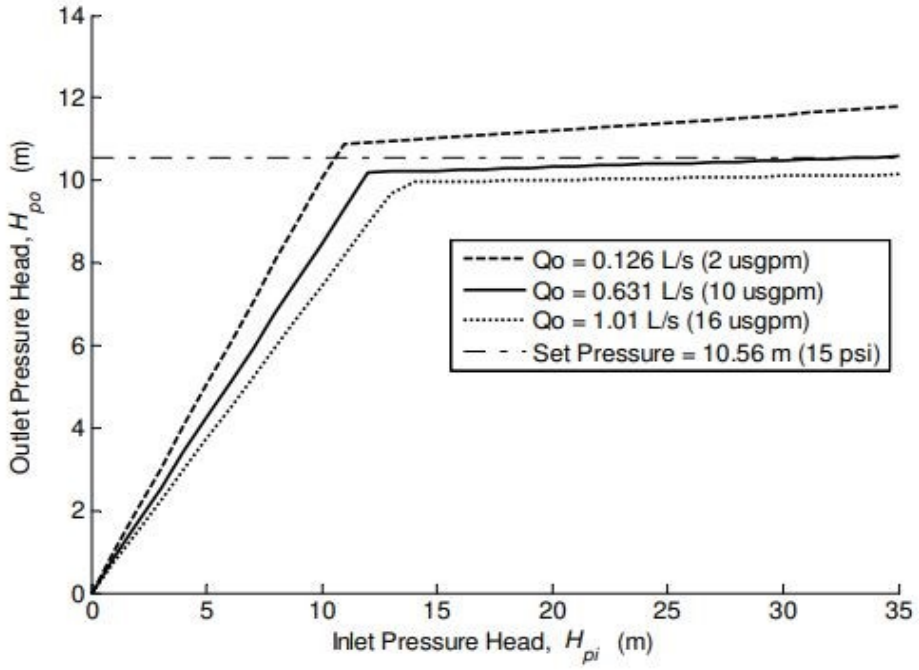

Figure 6-7: Regulator outlet pressure regulation curves for three discharges for a set pressure of 10.56 m produced from Foley (2010) model

6.5.1.4 Summary

The Foley (2010) model is a semi-empirical model that predicts regulator outlet pressure more accurately than the theoretical model of Keller and Bliesner (1990). However, it is deficient in the following:

1. predicts the effects of changes in inlet pressure head and regulator outlet pressure hysteresis as an average of the regulator outlet pressure,

2. The example given was developed for regulator nominal pressure settings higher than those used in the majority of CP&LMs, especially in Australia and other regions where low pressure models are used to minimise system energy costs,

3. while it was developed from empirical hydraulic parameters, pressure head and discharge, it does not fully explore the components of pressure regulation mechanisms, to enable the full interpretation of these regulation minor head losses, especially hysteresis, and

4. it cannot be applied to simulate regulator outlet pressures of all the common the common regulator manufacturers used in the majority of CP&LMs in the world.

6.5.1.5 Performance of Junior (2018) model

The simulation results of the PRV model proposed by Junior et al. (2018) are illustrated in Figure 6-8, Figure 6-9, and Figure 6-10 for the low pressure (10 psi) model. It is evident that this model is a slight improvement to the original model of Keller and Bliesner (1990) because it is able to produce pressure regulator outlet pressures in the low pressure non-regulating segment of the regulation curve, and during the regulation process with a clearly defined turning point between these two segments. However, the sharpness of the turning point from this model is not as pronounced as that measured with the pressure regulators in the laboratory (Figure 6-9 and Figure 6-10). The simulated results from this model are further below the 1:1

equilibrium line which shows that the modelled outlet pressures are lower than measured pressures from similar pressure regulating device.

The regulated pressure curves from each of the modelled flow rates have a steep slope from initial regulation and then attain a reasonably stable and flat slope as the inlet pressure continues to rise above the regulation threshold. This model is only capable of producing outlet pressures based on a rising limb. The authors did not state the nature of the inlet pressure change in the model, or whether they took an average of the outlet pressures from their experimental results; only this model accounts for hysteresis. As such, it is deficient in producing outlet pressures for anticipated real changes of inlet pressures on CP&LM operated on normal irrigated fields.

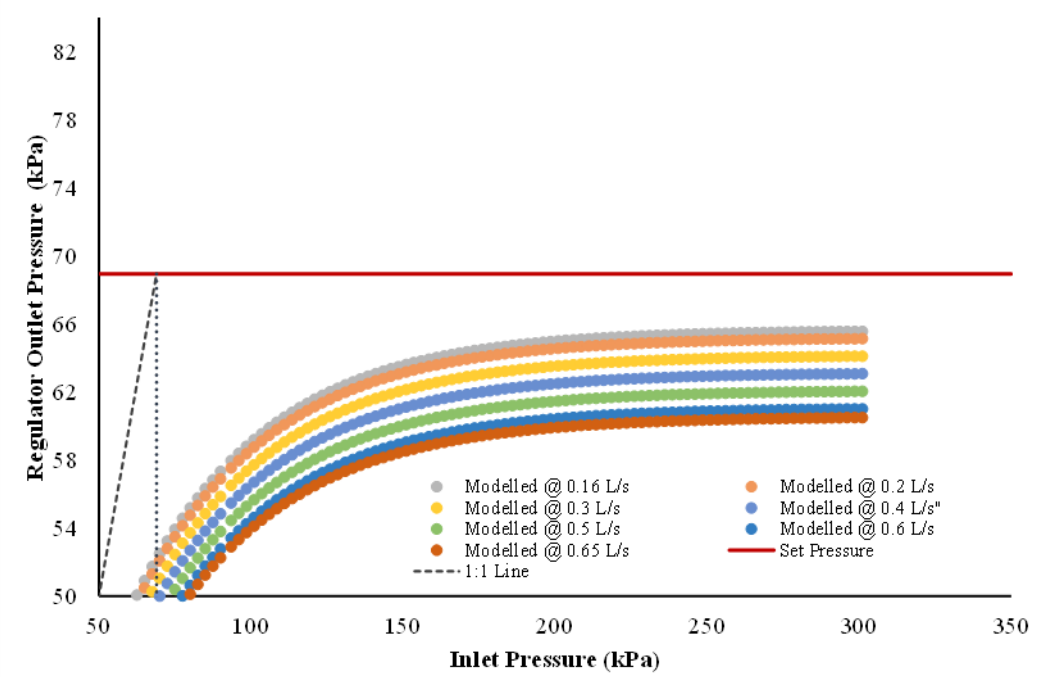

Figure 6-8: Pressure regulation curves from different flow rates modelled using Junior et al. (2018) model

The limitations of using a single, uncommon brand of pressure regulators to develop this PRV model are illustrated in both Figure 6-9 and Figure 6-10. The model underestimates the regulator outlet pressure when compared to the brands tested in this research (tested brands are used in the majority CP&LMs in the world). This outcome also emphasizes the need for a manufacturer specific adjustment factor in any new

PRV model to be able to account for these differences, so as to accurately design for these important pressure regulating devices in CP&LM irrigation.

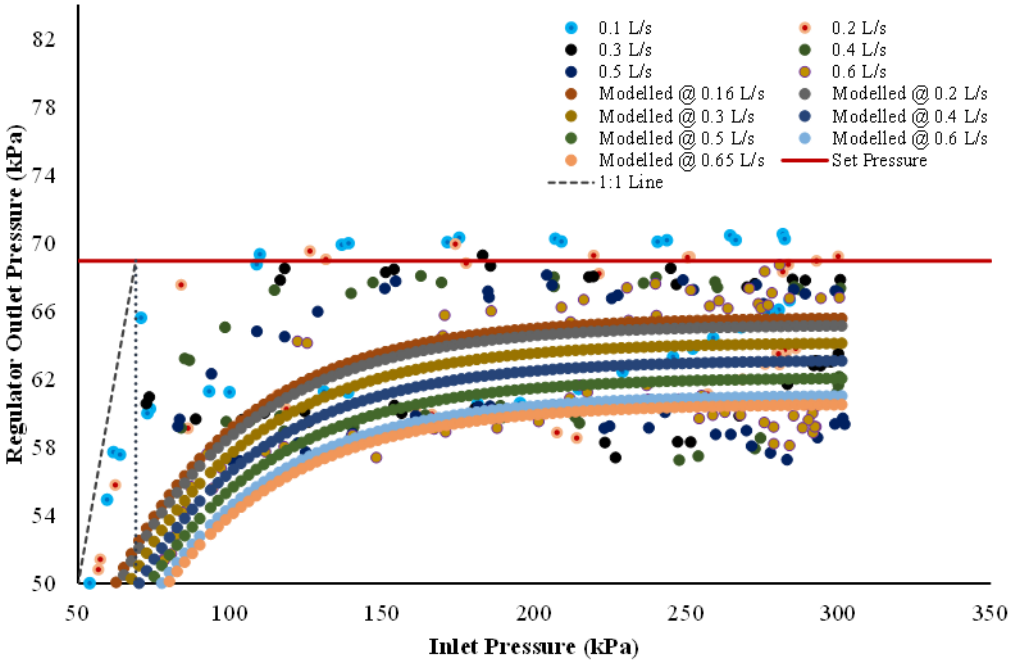

Figure 6-9: Pressure regulation curves from Junior et al. (2018) model plotted against measured data for a 70 kPa X type of regulator brand.

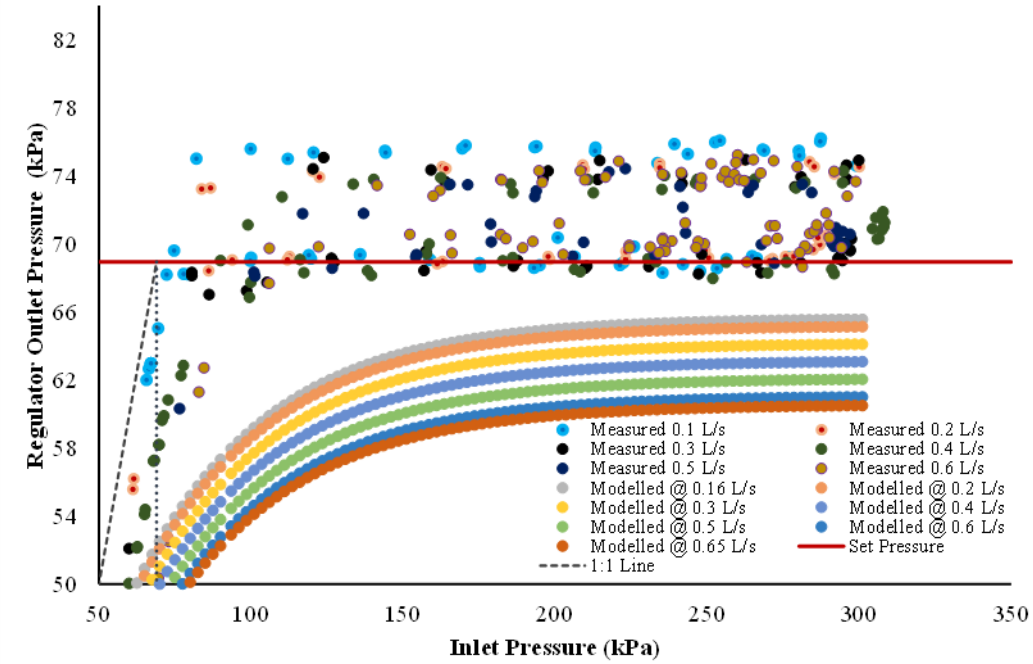

Figure 6-10: Pressure regulation curves from Junior et al. (2018) model plotted against measured data for a 70 kPa Z type of regulator brand.

6.5.1.6 Summary

The performance evaluation has established that the Junior et al. (2018) model:

1. is a semi-empirical model that incorporates a range of statistical coefficients to produce the final regulator outlet pressure, which makes the model difficult to use,

2. has a wide range of boundary operating conditions which may impact the model performance on modern CP&LMs (input pressure ranges between ~50 kPa to 800 kPa against a maximum 250 or 300 kPa for modern low pressure CP&LMs. Nozzle discharge between for the PRV model is ~0.16 L/s to 1.2 L/s whereas typical nozzle flow rates for CP&LM are between 0.067 l/s and 0.63 L/s. Lower boundary limit for nozzle discharge is higher than CP&LM nozzles in the field,

3. was developed using one particular Brazilian pressure regulator brand which is not common amongst the vast majority of CP&LMs in the world. As such, it is not representative and therefore cannot be used for the design of pressure regulated machines as proven by the laboratory results of the most common pressure regulator brands in industry,

4. underestimates the turning point and onset of hysteresis. This is complicated by the application of statistical coefficients to adjust the outlet pressure from this region of the pressure regulation curve, and

5. produces regulator outlet pressures that increase steadily with a positive slope along the regulation curve which is not consistent with the results in Chapter 5.

6.5.1.7 Performance of Zhang and Li (2017) model

The performance of the Zhang and Li (2017) model is illustrated in Figure 6-11 using an evaluation completed by the authors with test results from laboratory experiments.

The difference between measured (symbols) and simulated (lines) regulator outlet pressures is significant at the selected discharge rates. It is evident that the model underestimates the regulator outlet pressures in parts of the range of the regulation curves, and is not able to predict outlet pressure hysteresis in the regulation curves.

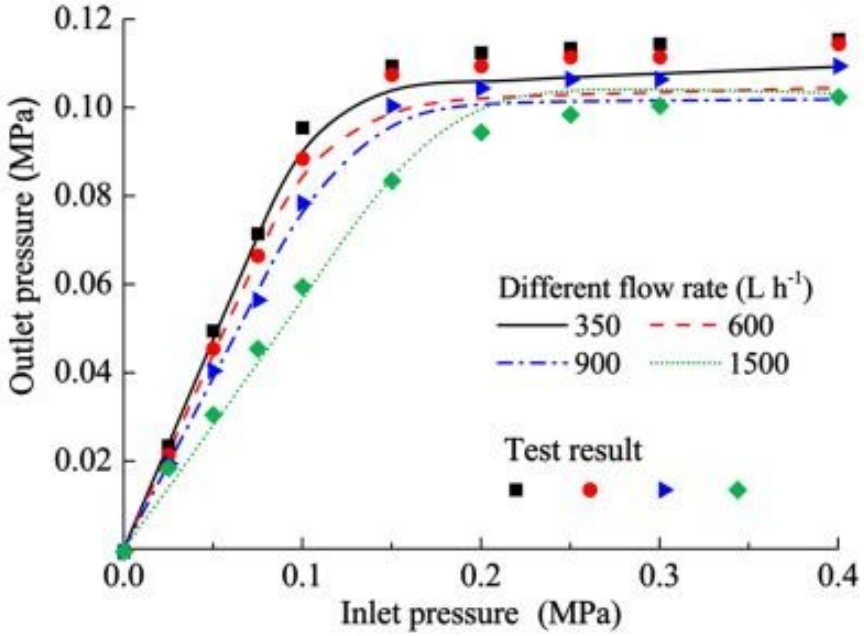

Figure 6-11: Results of the comparison between numerical CFD simulated and measured pressure regulator performance curves (Zhang and Li, 2017)

6.5.1.8 Summary

The statistical model of Zhang and Li (2017) which is developed on the basis the mechanical and structural properties of an unstated PRV manufacturer, is a complex model for use in industry, and has several limitations:

1. it simulates regulator outlet pressures using a great number of statistically derived coefficients, from geometric properties that cannot be easily determined for PRVs.

2. it does not account for hysteresis in the regulator outlet pressures, which was highlighted as an important requirement from the PRV test analysis conducted in research.

3. the model was developed using geometric parameters of an unknown PRV manufacturer. Therefore is difficult to apply this model on the major PRV manufacturers used with CP&LMs in industry.

4. it was also developed using a fraction of the nozzle discharges common under modern low pressure CP&LMs.

6.6 Conclusion

The current existing PRV mathematical models that are used to predict pressure regulator performance in CP&LM irrigation machines have been identified in this chapter. To clearly identify the capabilities and any potential deficiencies of these models, a preliminary review of the theory of pressure regulation mechanisms was conducted. Accordingly, a comprehensive analysis of the mathematical concepts involved in the development of these models was completed to develop a full understanding of their significance and relevance to the hydraulics of CP&LM irrigation machines. Two of the PRV mathematical models were also evaluated using a set of predefined parameters in conjunction with the pressure regulator performance results obtained in Chapter 5, to determine their suitability and accuracy in pressure regulation modelling. The other models were evaluated by interpreting the results of the model performance completed by the authors. The results show that these models are not suitable for modelling pressure regulation under the existing hydraulic and operational conditions for modern CP&LMs. The downside and limitations associated with each of the PRV models have been identified and summarised accordingly. The conclusions drawn from this evaluation is that, none of these mathematical models is capable of fully representing the true regulation for PRVs, especially with hysteresis. Consequently, there is a need for the development of a new and improved version of PRV mathematical model for use in the design of CP&LMs.

7. DEVELOPMENT OF A MATHEMATICAL MODEL FOR PRESSURE REGULATION OF CP&LMS

7.1 Introduction

Although pressure regulation is considered to be an important component in the hydraulic performance of CP&LMs, previous studies (as cited in Chapter 2) have shown that a full comprehension of pressure regulation during unsteady flow has eluded the irrigation engineering community. The conclusions from Chapter 6 also demonstrated that the existing PRV mathematical models are limited in accurately modelling pressure regulation. This has been due to a lack of comprehensive understanding of the intricate interconnected hydraulic processes that occur inside regulators in interaction with the CP&LM hydraulic system. Unsteady conditions in these machines occur as a result of changes in field elevation as they traverse irrigated fields, fluctuations in groundwater supply levels, and in more recent times due to the on-and-off pulsing of solenoid actuated VRI sprinkler control valves.

The conclusions drawn from Chapter 6 detail that the Keller and Bliesner (1990) model is limited in predicting regulator outlet pressure because it does not contain an explicit minor head loss and it does not account for hysteresis. Instead something similar to a minor loss coefficient was used, but it is not a true standard minor loss coefficient used in the standard minor loss hydraulic equation. Foley (2010) does not account for hysteresis other than the prediction of average regulator outlet pressures. In addition to not expressing hysteresis, the Junior et al. (2018) model uses a range of statistically fitted coefficients and operates over a wide range of hydraulic conditions that are not typical for modern low pressure CP&LMs. Finally, the Zhang and Li (2017) model uses a set of complex geometric and mechanical properties that cannot be easily established, and like the other models, it does not account for hysteresis. According to Foley (2010), and on the basis of the extensive PRV experimental results discussed in Section 5.6.5, the PRV outlet pressure is dependent on supply pressure and discharge

thresholds, static and variable minor head losses through the devices, hysteresis in the regulator outlet pressure caused by mechanical resistances associated with the flow tube movement, and is specific for each PRV manufacturer brand. This dependency shows that these devices perform very differently under a range of conditions. As a result, numerous considerations and data exploration must be completed to derive this new model.

The purpose of this chapter is to describe the development of a new PRV mathematical model that accurately describes the performance of pressure regulators within the hydraulic and operational conditions of modern low pressure CP&LMs. The aim of this development is to implement a set of mathematical equations or sub-models that together predict regulator outlet pressure. The objective of this model development is to permit accurate representation and implementation of PRVs in modern CP&LM irrigation. The first section of this chapter introduces the general nature and structure of the proposed PRV model, highlighting how it was discovered from the results of the extensive hydraulic experiments of pressure regulator performance reported in Chapter 5. Discussion of the different individual minor head losses that occur during regulation, including the development of the respective mathematical equations and sub-models that describe this process, are included. This chapter also contains a methodology for determining the values of coefficients used to implement the model accurately while also demonstrating its performance. A validation process is presented to compare the full PRV model performance against measured regulator performance results, and includes conclusions drawn from the development of this new PRV mathematical model.

7.2 Proposed General Nature of the PRV Model

The new PRV model being proposed is a hydraulic model that is developed on the basis of the empirical pressure regulator measurements obtained in Chapter 5 of this thesis. To enable the development of this mathematical model, two very important steps need to be completed. The first step is the identification and analysis of the main components of the minor head losses that occur inside pressure regulators to produce

the final regulator outlet pressure. This process is to enable the precise utilisation of the experimental data to help derive some of the complex minor losses that could not be measured by experimental means. The second step is to use fundamental hydraulic principles to develop mathematical equations that represent these minor losses, and implement them as sub-models to derive the full hydraulic pressure regulator mathematical model. The full comprehension and interpretation of these minor losses is integral in the development of this preferred hydraulic model to better describe pressure regulation. The proposed hydraulic model includes the following considerations:

- boundary conditions applicable to modern low pressure CP&LM irrigation machines,
- simulate the majority of different pressure regular brands used with CP&LMs in the global irrigation industry,
- to account for hysteresis correctly, and
- to be simple.

The pressure regulation minor head losses include, a static minor head loss, a variable regulation minor head loss, and a hysteresis minor head loss. These three minor head losses are responsible for the outlet pressure prediction model of PRVs because they function collectively to reduce inlet pressure head to produce the final regulator outlet pressure. As such, it is important to recognize that the mathematical expressions representing these minor loss are influenced by, or are at least dependent on pressure head and discharge. Therefore, to simplify the PRV model parameters to conform to a pure hydraulic model and enable a direct algebraic calculation of these expressions to produce outlet pressure, the units of measurement for the different hydraulic and experimental data from Chapter 5 were converted to metres head of water. The flow rates measured were converted to units of cubic metres per second.

The boundary operating conditions for the proposed PRV mathematical model are:

- inlet pressure head that is between zero and not exceeding a maximum of ~30 m head,

- discharge range that is between 0.1 L/s and 0.6 L/s.

The boundary conditions for operating the proposed PRV model are important for better results, because CP&LMs are now supplied to operate at relatively low pressures generally between 20 and 30 m head. They also tend to be designed with sprinkler packages with a nominal nozzle discharge range from 0.067 L/s for the 2.78 mm # (14/128 of an inch) which is the smallest for CPs, to the high extreme of 0.63 L/s for the 10.32 mm # (52/128 of an inch) in 3TN and 3NV nozzle ranges (Nelson, 2020) when regulated by 68.95 kPa (7.0 m head) and 103.42 kPa (10.56 m head) pressure regulators. However, depending on the size, most machines operate sprinklers up to 7.94 mm # (40/128 of an inch) that can generate maximum discharges of about 0.55 L/s at 7.0 m head or about 0.63 L/s at 10.56 m head.

7.3 Proposed Static Minor Head Loss sub-model

The static minor head loss that occurs through pressure regulators is a form of head loss that is identical in nature to any standard hydraulic minor loss. It has a dependency on the discharge through the regulator which is usually controlled by the nozzle orifice in CP&LM systems. In fundamental hydraulics, this static minor head loss is approximately proportional to the velocity of the fluid passing through the device, multiplied by the minor loss coefficient of that particular device (Equation 2.16). In the discussion here of this new PRV model development, the static minor head loss will be denoted as h_{m_ST}. Under ideal flow conditions, and when the pressure regulator is not regulating, there would be no head loss and the inlet pressure head would equals the outlet pressure ($P_{\_in} = P_{\_out}$) with the slope between these two pressures represented by a 1:1 line (Figure 7-1). In real flow when the static minor head loss actually exists, a new outlet pressure line with a slope that is different to the 1:1 equilibrium line would represent this minor head loss below the 1:1 line. The difference between the equilibrium line and any position along the regulated pressure line represents the static minor loss. Figure 7-1 shows a *green* line, which is an idealised static minor head loss at a lower discharge, and a *black* line which represents the minor loss for a higher discharge, superimposed over the regulation curve to represent how the minor loss

occurs during regulation below the turning point. The vertical difference between these lines and the 1:1 line represents the static minor loss difference at the two discharges.

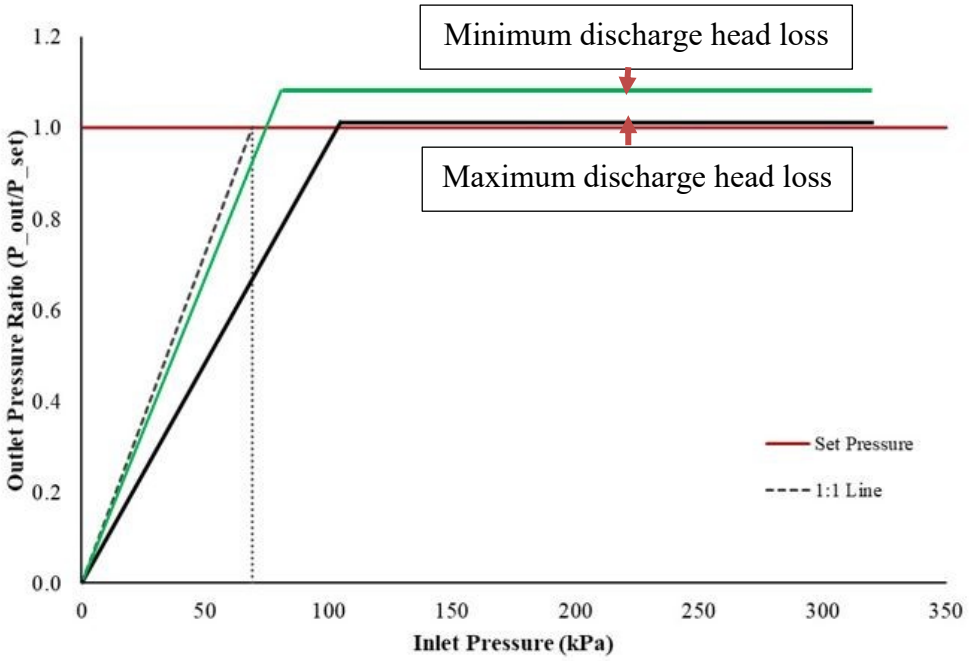

Figure 7-1: Idealised static minor head losses for low and high discharge rates through pressure regulator. The losses are not to scale but are represented in their original form of occurrence during regulation

Due to the operational nature of pressure regulators and the formation of the static minor head loss component during regulation, it is not possible to rely only on simple hydraulic minor loss calculations to derive and clearly represent this minor head loss. Therefore, to develop a full understanding of the static minor loss, as well as the development of an appropriate static minor head loss sub-model for addition in the complete PRV mathematical model, an understanding of the following critical aspects has to be made.

(i) The maximum static minor head loss created at nominal discharges for specific nozzle sizes must be determined.

(ii) The two forms of the static minor head loss; a variable form at rising nozzle discharge, and a static form which is the maximum static head loss at nominal nozzle discharge, and

(iii) The maximum turning point (TP) of the static minor head loss in the regulation process.

The maximum static minor head loss can be mathematically expressed using a similar equation to the generic standard minor head loss hydraulic equation (Equation 2.16), with a special minor loss coefficient K_prv derived from the hydraulic experiments of pressure regulator performance characterisation. To derive the maximum static minor head loss during pressure regulation, the experiments completed in Chapter 4 were conducted with the flow tube held fully open in a stationary or "frozen" position, for all the three PRV manufacturers investigated. The results of the static minor head loss, along with the corresponding minor loss coefficients K_prv, for the X, Y, and Z pressure regulator manufacturers were obtained by linear regression analysis as shown in Figure 5-78, Figure 5-79, and Figure 5-80 in Section 5.6.5. The special minor loss coefficients K_prv for the regulators are summarised in Table 7-1. The maximum static minor loss for a specific nozzle discharge in the model is calculated by multiplying each coefficient of PRV by the velocity head, as shown in Equation 7.1.

$$h_{m\_ST} = K_{\_prv} \frac{8Q^2}{g\pi^2 D^4} \qquad 7.1$$

where: Q is the discharge through pressure regulator in m^3/s, g is the gravitational acceleration constant in m/s^2, and D is the nominal diameter of the inlet and outlet of the pressure regulator in metres (m).

Table 7-1: Minor loss coefficients K_prv for the low and high pressure X, Y, and Z pressure regulator manufacturers obtained by linear regression analysis

PRV Brand	X	Y	Z
K_prv	12.768	8.447	30.683

It has already been pointed out that at regulator outlet pressures below the turning point, the discharge is variable and it rises to the nominal discharge of the sprinkler nozzle usually at the turning point. As a result, the static minor head loss will also be variable below this turning point as it has a dependency on the discharge. Therefore, there is a need to understand this component of minor head loss when the discharge is below the nominal discharge to express it mathematically in order to build an appropriate sub-model for the static minor head loss for incorporation in the final

pressure regulator model. To interpret this, it is important to understand that the generic static minor head loss is only achieved when the outlet pressure corresponds to an inlet pressure that creates a turning point to the regulation curve. At this turning point, it is where the full nozzle discharge is reached. The different sections or components of the static minor head loss above and below the turning point of the regulator at low and high discharges are represented in Figure 7-1.

Figure 7-2 through Figure 7-7 shows magnitudes of the discharge based variation in the static minor head loss for the X, Y, and Z PRV manufacturers. The graphs show the static minor head loss predictions overlain on individual measured pressure regulator performance data, as reported previously in Chapter 5. It is evident that the minor loss is a function of discharge. It is lower and close to the 1:1 line for the small nozzle discharge, and is larger and further away to the right of the 1:1 line for the largest nozzle discharge. The differences in static minor head loss between nominal nozzle discharges at maximum static minor head loss is represented by the gap between the green and black straight lines next to the 1:1 line, where the green line represents the slope of the static minor loss at the lowest discharge of 0.1 L/s, while the black line represents the slope of the static minor loss at 0.6 L/s. The static minor head loss at this non-regulating segment is larger for the low pressure models when compared to the minor loss in the high pressure models for the same discharge across all three manufacturers. It is also apparent that the variable static minor loss component below the turning point is larger for the X regulator brand, followed by the Z brand, and is smallest for regulator Y brand.

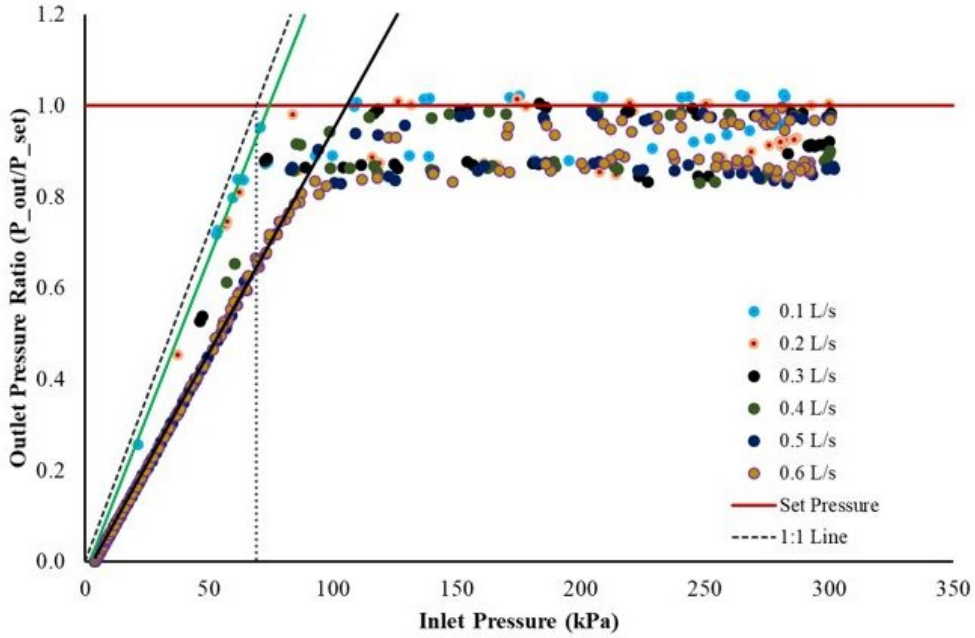

Figure 7-2: Comparison of static minor head loss at 0.1 L/s and 0.6 L/s to the 1:1 line for the X low pressure regulator model

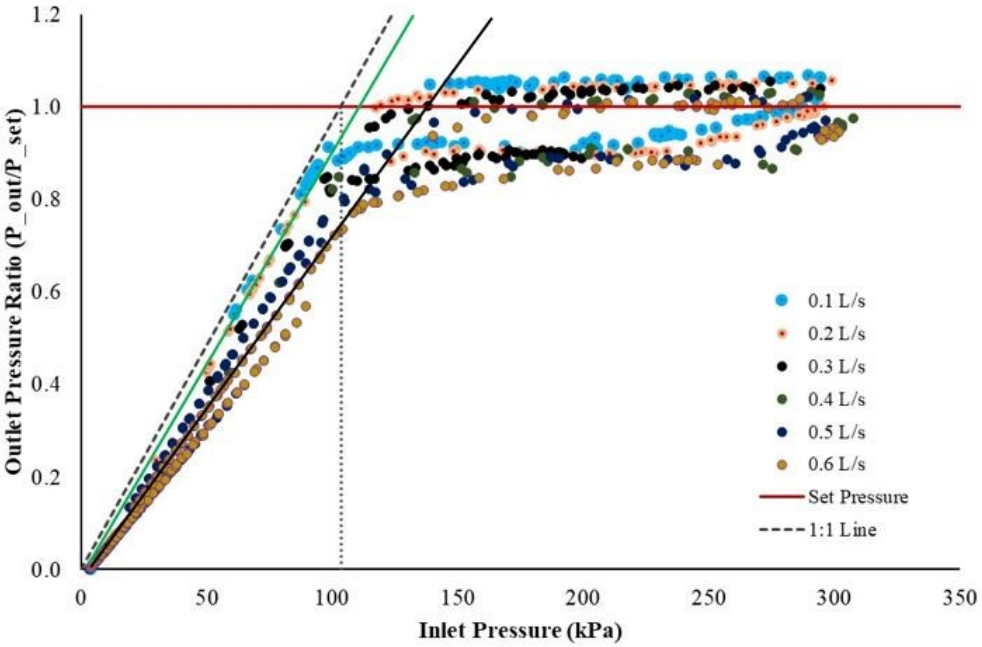

Figure 7-3: Comparison of static minor head loss at 0.1 L/s and 0.6 L/s to the 1:1 line for the X high pressure regulator model

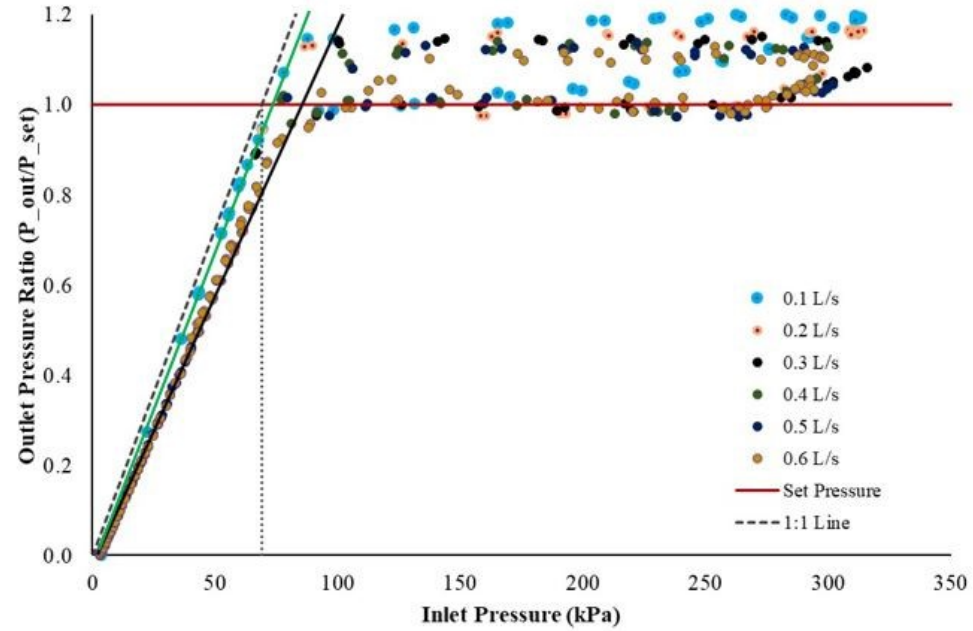

Figure 7-4: Comparison of static minor head loss at 0.1 L/s and 0.6 L/s to the 1:1 line for the Y low pressure regulator model

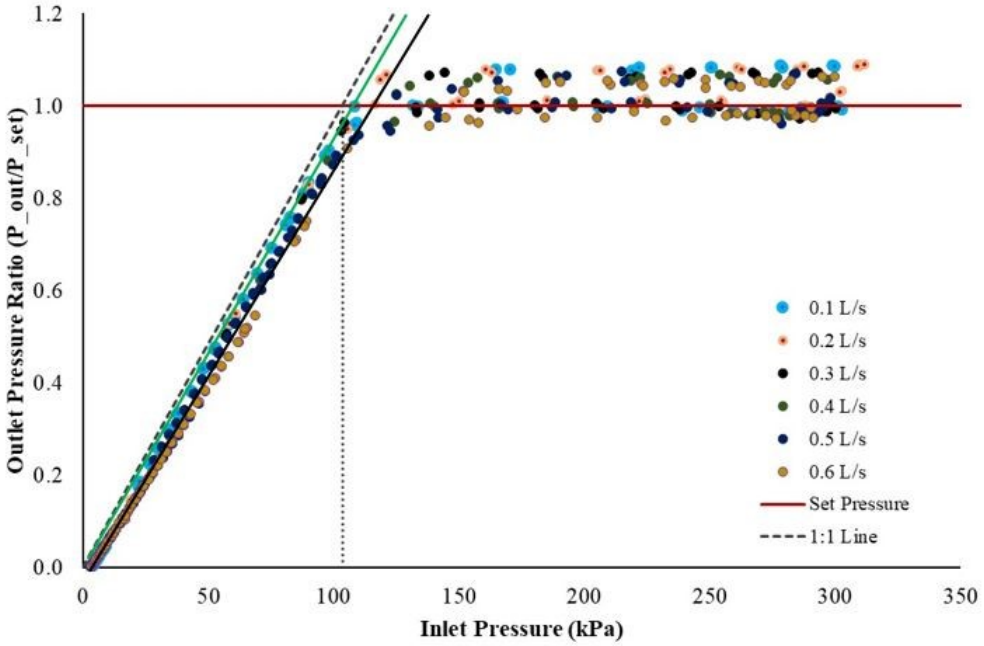

Figure 7-5: : Comparison of static minor head loss at 0.1 L/s and 0.6 L/s to the 1:1 line for the Y high pressure regulator model

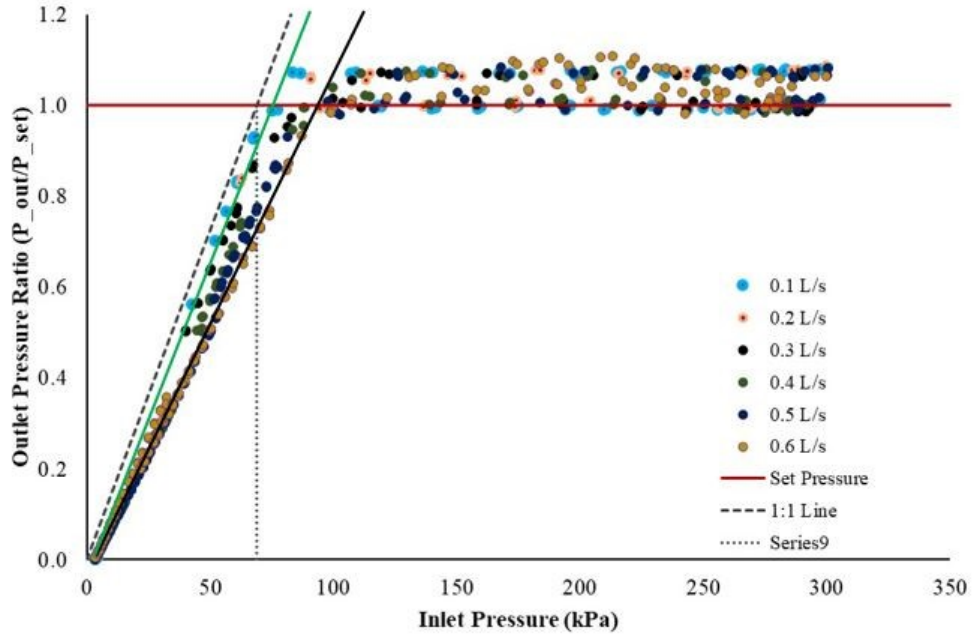

Figure 7-6: Comparison of static minor head loss at 0.1 L/s and 0.6 L/s to the 1:1 line for the Z low pressure regulator model

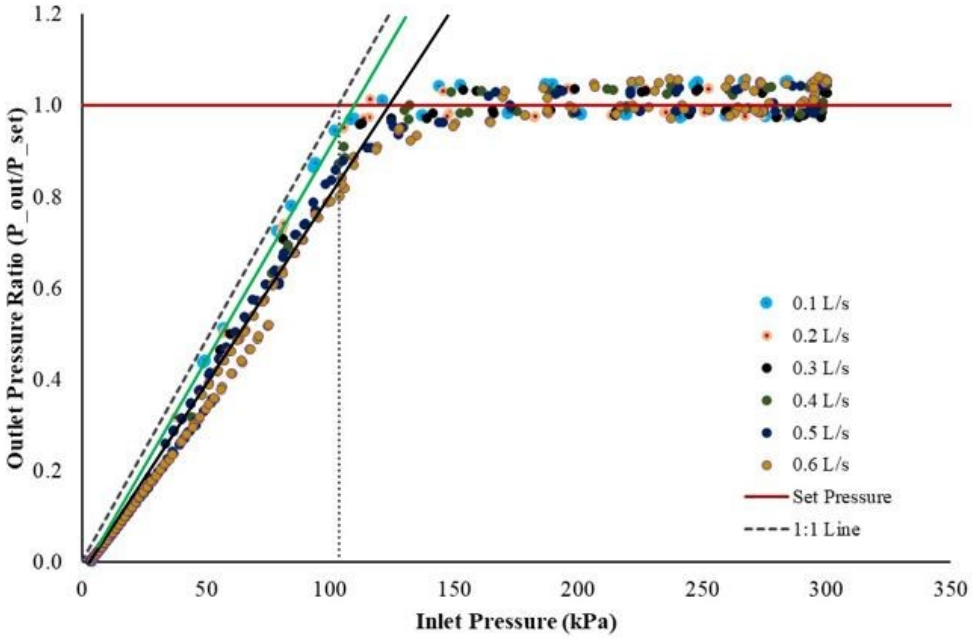

Figure 7-7: : Comparison of static minor head loss at 0.1 L/s and 0.6 L/s to the 1:1 line for the Z high pressure regulator model

To calculate the variable component of the static minor head loss which is denoted h_{m_Sv} below the turning point for a specific discharge, Equation 7.1 is multiplied by a factor which is developed as the ratio of inlet pressure head to the maximum constant

static minor head loss at the turning point, adjusted by a manufacturer offset to the nominal set pressure by using a coefficient D'. The methodology of deriving and implementing the coefficient D' is explained in detail in Section 7.6.

$$h_{m\_Sv} = K_{\_prv} \frac{8Q^2}{g\pi^2 D^4} \frac{P_{\_in}}{P_{\_set} + D' h_{m\_ST}} \qquad 7.2$$

where: h_{m_Sv} is the variable static minor loss below the turning point, $P_{\_set}$ is the nominal set pressure rating of pressure regulator, and D' is a constant for adjusting $P_{\_set}$ by a specific offset of the pressure regulator.

This equation (Equation 7.2) will be integrated into a larger mathematical expression to predict the static minor head loss above and below the inlet pressure where regulation initiates, at the discharge selected. In this form, it represents the complete hydraulic sub-model for the static minor head loss component in the PRV model. The graphical form of the static minor head above and below the turning point in the regulation curve is shown in Figure 7-8. This static minor loss curve is also obtainable from the direct subtraction of the variable regulation minor head loss in Section 7.4 when it is known, from the inlet pressure head supplied to the regulator.

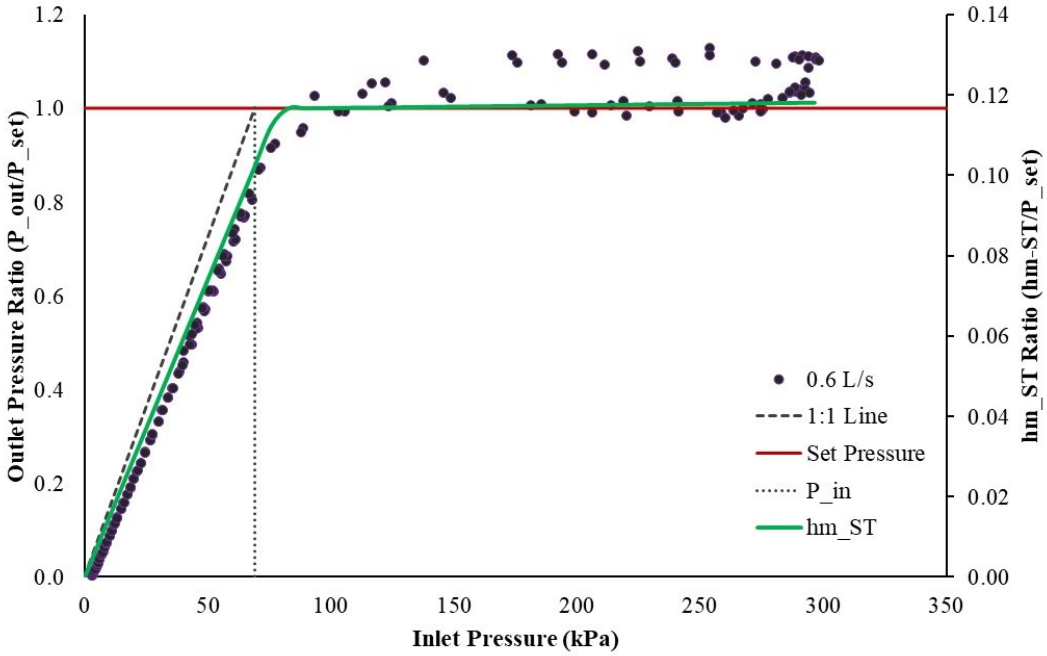

Figure 7-8: Predicted static minor head loss (h_{m_ST}) during regulation calculated and plotted against the measured outlet pressures for a manufacturer Y low pressure regulator model at 0.6 L/s

The third component which helps in the delineation of the two sides of the static minor head loss is the maximum turning points for the regulator outlet pressures at corresponding inlet pressures for the selected discharges. These maximum turning points are obtained from the regulation curves measured in the hydraulic experiments, and are used to in determination of the model coefficients described in Section 7.6.

7.4 Proposed Variable Regulation Minor Head Loss sub-model

The variable regulation minor head loss component, denoted h_{m_V}, is a head loss solely associated with the regulating actions of the PRV. It comes into effect with rising inlet pressure when it has reached the turning point on the $P_{\_out}$ versus $P_{\_in}$ plot where the regulation process initiates. It is one of the most complex regulation minor losses and is difficult to characterise by experimental means, because is it occurs when the regulation mechanisms are in full action. The variable regulation head loss occurs as a result of changes in the length of the cylindrical opening between the downstream side of the skirt of the diffuser and the upstream edge of the flow tube. This minor head loss is typically the largest component of the pressure regulator head loss during normal operation. It is called a "variable regulation head loss" because its magnitude changes primarily as a result of the displacement of the flow tube inside the regulator and can vary independently of the discharge. This is induced by the imbalance of forces between the spring compression force and the water pressure force acting on the diaphragm to move the flow tube. It increases when the area of opening is small with the flow tube positioned very close to the skirt, and reduces as the tube moves downstream away from the skirt at lower inlet pressures. Figure 7-9 shows the theoretical form of the variable regulation minor head loss sub-model during regulation. The variable regulation head loss increases with increasing inlet pressure and its magnitude will depend on the maximum inlet pressure head threshold as the regulator outlet pressure will be almost constant at a specific discharge. This variable regulation head loss is caused by the interactions between the rising inlet pressure head and the static minor head loss. Figure 7-10 shows a graphical representation of the variable regulation minor head loss during pressure regulation when plotted against

measured data. From this figure (Figure 7-10), it is apparent that it maintains a near constant zero value until the turning point for a regulator outlet pressure, where it suddenly increases and rises to its maximum, depending on inlet pressure head and discharge.

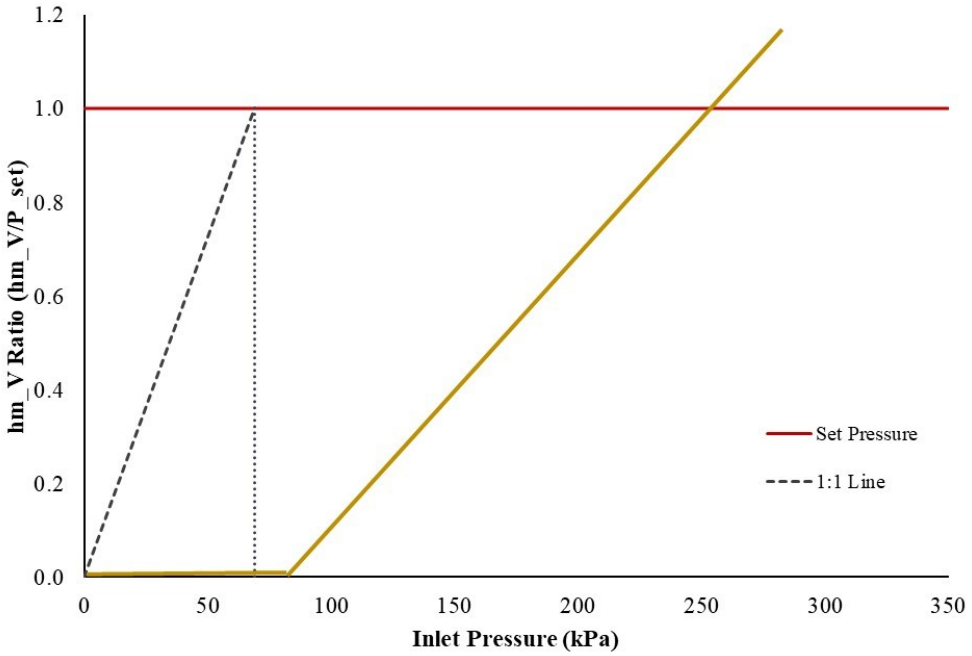

Figure 7-9: Idealised variable regulation minor head loss h_{m_V} during regulation of a PRV device at a particular discharge

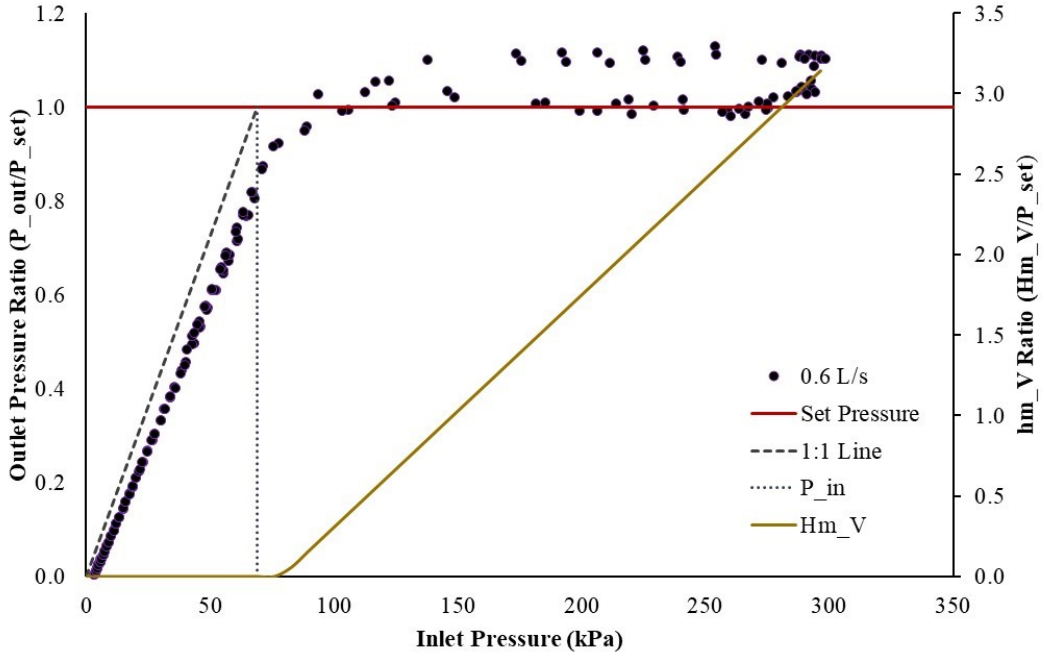

Figure 7-10: Predicted variable regulation minor head loss h_{m_V} calculated and plotted against measured outlet pressures for a manufacturer Y low pressure regulator model at 0.6 L/s

If the regulation minor losses were identical to simple hydraulic systems, the variable regulation minor head loss sub-model h_{m_V} could be established from the algebraic difference between inlet pressure head and the static minor head loss for a particular nozzle discharge, as shown in the equation below.

$$h_{m\_V} = P_{\_in} - h_{m\_ST} + P_{\_set} \tag{7.3}$$

However, this mathematical approach is not very precise because it produces variable regulation head losses greater than zero below the turning point, implying the existence of the variable regulation minor head loss below the turning point. Using Equation 7.3 would also be mathematically incorrect because the regulator outlet pressure has a special reference to the nominal set pressure for each model of regulator and an offset for each manufacturer. Therefore, to enable the variable regulation minor head loss to increase suddenly at the turning point of the regulator outlet pressure, a hyperbolic mathematical function (Equation 7.4) is used, so that the variable regulation minor head loss is determined correctly for all $P_{\_in}$ using Equation 7.5. This sub-model for the variable regulation minor head loss is the second sub-model developed for the entire PRV model.

$$\gamma = (0.5(\tanh(P_{\_in}(P_{\_set} + D' h_{m\_ST}))) + 1)) \tag{7.4}$$

$$h_{m\_V} = \gamma C' (P_{\_in} - (P_{\_set} + D' h_{m\_ST}))(C' \text{x} 1.00E-08 + Q^2) \tag{7.5}$$

where: γ is the hyperbolic mathematical function that suddenly rises at the turning point of the regulation curve, and C' is a constant for adjusting the slope of the regulation curve after the turning point. The process of determining this constant is covered in Section 7.5.

From the results of the hydraulic experiments in Chapter 5, it was established that at a continuous rising inlet pressure head during regulation, the minor losses that impact the inlet pressure head are the static and variable regulation minor head losses. As

such, the two sub-models developed in Sections 7.3 and 7.4 can now be integrated, at this stage of the PRV model development, to produce a regulator outlet pressure line that results from an increasing inlet pressure limb. The process of combining and applying these sub-models is discussed in Section 7.6 and the results from the sub-model calculations are presented. However, to complete this process, there is a need to fit coefficients to the sub-models to help adjust the model parameters in order to produce accurate regulator outlet pressures for each nozzle discharge selected, and for the three pressure regulator manufacturers, at the nominal pressure settings.

7.5 Methodology for Determining Values of C' and D' Coefficients

The static and variable regulation minor head loss sub-models require certain adjustments to produce ideal regulator outlet pressures that are representative of pressure regulator performance in the real world. Two coefficients were fitted to the data to adjust (a) the vertical position of the regulation curve along the y-axis, and (b) slope of the regulation curve along the x-axis. These coefficients are denoted C' and D' respectively. The methodology for fitting the C' and D' coefficients employed error minimisation and integration using a set of maximum outlet pressure turning points ($P_{\_in}$ and $P_{\_out}$) for the two general pressure setting models for X, Y, and Z regulator manufacturers at the nozzle discharge rates between 0.1 and 0.6 L/s. These target outlet pressure turning points for the regulators were obtained from the pressure regulator performance results reported in Chapter 5. They were used to tune the regulation curves for each nozzle discharge by selecting a suitable C' constant, and then continuously adjusting D' until the regulation curve with adequate slope passes through the outlet pressure turning point. To be more precise, error minimisation for measured and predicted outlet pressure using alternate values for D' was completed to achieve more realistic graphical representation of $P_{\_out}$ curves using this model component. The error minimising technique is used mainly in the model comparison with measured data in Section 7.8.3 to produce more accurate results.

The results of the graphical output comparisons from fitting the coefficients *C′* and *D′* are presented in Table 7-2 for the low pressure models (10 psi), and in Table 7-3 for the high pressure models (15 psi), using same discharges from the experimental procedures in the laboratory for the X, Y, and Z pressure regulator manufacturers.

Table 7-2: The *C′*, and *D′* parameters obtained from graphical integration with $K_{\_prv}$ and measured outlet pressure turning points for the low pressure regulator models

Q (L/s)	X			Y			Z		
	$K_{\_prv}$	*C′*	*D′*	$K_{\_prv}$	*C′*	*D′*	$K_{\_prv}$	*C′*	*D′*
0.1	12.768	315	0.40	8.447	315	19.0	30.683	315	4.80
0.2		313	0.40		313	4.50		313	1.55
0.3		312	0.80		312	2.80		312	1.35
0.4		308	0.80		308	1.80		308	1.12
0.5		304	0.85		304	1.48		304	1.07
0.6		298	0.80		298	1.35		298	1.08

* *C′* values are in the order of: 1 x 10^3

Table 7-3: The *C′*, and *D′* parameters obtained from graphical integration with $K_{\_prv}$ and measured outlet pressure turning points for the high pressure regulator models

Q (L/s)	X			Y			Z		
	$K_{\_prv}$	*C′*	*D′*	$K_{\_prv}$	*C′*	*D′*	$K_{\_prv}$	*C′*	*D′*
0.1	12.768	315	6.00	8.447	315	27.0	30.683	315	2.80
0.2		313	2.70		313	6.00		313	1.08
0.3		312	1.20		312	3.10		312	1.05
0.4		308	1.20		308	2.10		308	0.96
0.5		304	1.15		304	1.50		304	0.97
0.6		298	0.95		298	1.30		298	0.99

* *C′* values are in the order of: 1 x 10^3

It is apparent from Table 7-2 and Table 7-3 that the coefficient C' is constant for each nominal discharge across the three pressure regulator manufacturers, and for nominal pressure settings. It is large for the lowest discharge and it reduces slightly with increases up to the maximum discharge. The factor C' impacts the slope of the predicted regulator outlet pressure line produced for increasing inlet pressures. D' is a coefficient that varies with nominal pressure settings across the three pressure regulator manufacturers, and with variation in discharge. This coefficient is responsible for the exact positioning of the outlet pressures with respect to the nominal set pressure. These coefficients are built from basic hydraulic pressure regulator performance parameters, as the overall objective of this model development is to deliver a full hydraulic based PRV mathematical model.

It should be noted that both coefficients C' and D' are independent of each other at any particular outlet pressure for the X, Y, and Z regulators. However, they need to be altered together to predict accurate outlet pressures when compared to the measured regulation curve. Thus, any change to one parameter will result in a different outlet pressure and both parameters should be re-checked when using this model.

7.6 The combined Static and Variable Regulation Minor Head Loss sub-models

The interactions between inlet pressure head, and the static and variable regulation minor head losses produce a final regulator outlet pressure received by the sprinkler nozzle when inlet pressure head is continuously rising. The fundamental hydraulic relationship between the interaction of inlet pressure head and the static and variable regulation minor head losses can be mathematically expressed using Equation 7.6. Therefore, combining the static and variable regulation minor loss sub-models developed in Section 7.3 and 7.4 produces a minor loss adjustment factor that can be used to create an outlet pressure regulation curve with a rising inlet pressure limb. This average regulator outlet pressure line can be adjusted using the coefficients C' and D' developed in Section 7.5 to produce an appropriate and representative regulation curve.

$$P_{\_out} = P_{\_in} - h_{m\_ST} - h_{m\_V} \quad 7.6$$

where: $P_{\_out}$ is the regulator outlet pressure head which is received by the sprinkler nozzle, $P_{\_in}$ is the inlet pressure head to the PRV which is an independent variable, h_{m_ST} is the static minor head loss, and h_{m_V} is the variable regulation minor head loss.

The procedure developed to implement the combinations of static and variable regulation minor head loss sub-models to offset a rising inlet pressure head follows these seven steps.

1. Firstly, identify the PRV manufacturer and pressure model to be modelled.
2. Select the appropriate regulator minor loss coefficient $K_{\_prv}$.
3. Select, and input the discharge to be modelled.
4. Select C' to be equal to the appropriate constant used for the discharge modelled.
5. Select the outlet pressure turning point (TP) for the discharge selected.
6. Input coefficient D' for the specific PRV manufacturer and pressure model for the same discharge modelled.
7. Read off the pressure regulation curve from the graphical output, or simply use the model equation to calculate the $P_{\_out}$.

7.7 Performance of Static and Variable Regulation Minor Head Loss sub-models

To demonstrate the combined performance of the static and variable regulation minor head loss sub-models, three nozzle discharges for the pressure regular manufacturers X, Y, and Z were selected. They were the lowest at 0.1 L/s, median discharge at 0.3 L/s, and the highest discharge at 0.6 L/s. Input pressures in the combined sub-model calculation were selected from 0 to approximately 30 m head, at 0.7 m head (1 psi) increments. The calculations produced a total of 44 pressure head and discharge data points which were used in the model to produce regulation curves. The maximum

turning points (*TPs*) $P_{\_in}$ and $P_{\_out}$ were used for each of the discharges selected for the low and high models across the three manufacturers. These *TPs* were obtained from the experimental results, to ensure that the model utilises the hydraulic parameters measured from the regulators. The approach taken here aims to make the model more robust and precise in its performance, than the models discussed in Chapter 6. The C' and D' coefficients in Table 7-2 and Table 7-3 were used to complete the model calculations.

7.7.1 *Calculation of PRV Outlet Pressures for Manufacture X*

Demonstration of the PRV model performance on the low and high pressure regulator models for manufacturer X are presented here. The turning points for the discharge rates selected on both low and high pressure models of the regulator manufacturer X are presented in Table 7-4. C' and D' parameters are summarised in Table 7-2 and Table 7-3, and the calculation is completed using the procedure described in 7.6 above.

Table 7-4: Maximum Pressure TPs for example calculations of the PRV model pressure regulator X models

Q (L/s)	Maximum Pressure Turning Points (*TPs*)			
	7.0 (m head)		10.6 (m head)	
	$P_{\_in}$	$P_{\_out}$	$P_{\_in}$	$P_{\_out}$
0.1	7.85	6.93	12.13	11.00
0.3	9.01	6.88	13.25	10.70
0.6	10.60	6.42	14.48	10.40

The results of the PRV model calculations and graphical outputs for Manufacturer X pressure regulators at 0.1 L/s, 0.3 L/s, and 0.6 L/s are illustrated in Figure 7-11 for the low pressure model and Figure 7-12 for the high pressure model.

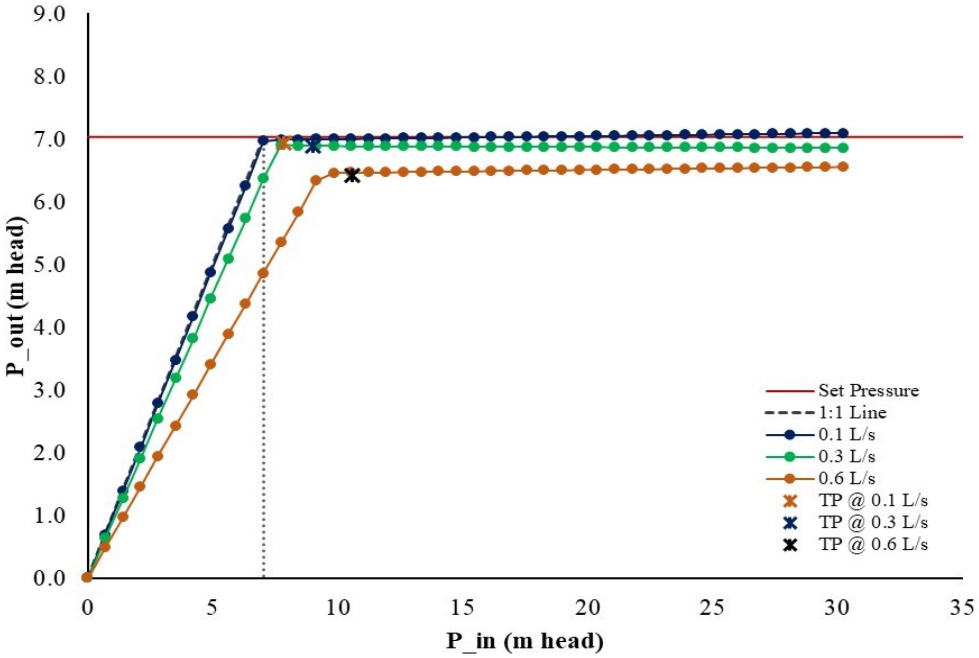

Figure 7-11: Modelled regulation curves for manufacturer X low pressure regulator model at 0.1 L/s, 0.3 L/s, and 0.6 L/s

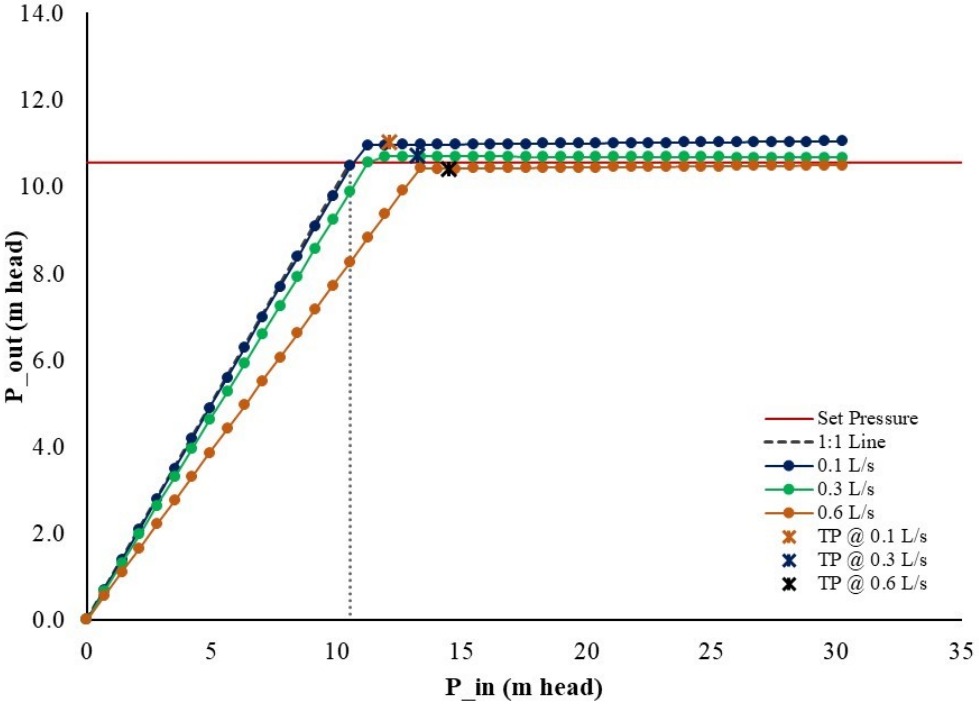

Figure 7-12: Modelled regulation curves for manufacturer X high pressure regulator model at 0.1 L/s, 0.3 L/s, and 0.6 L/s

7.7.2 Calculation of PRV Outlet Pressures for Manufacturer Y

The parameters for implementing the model calculations for the manufacturer Y pressure regulators are summarised in Table 7-5. The same tables of coefficients implemented in Section 7.8.1 are used to complete the model calculations. The results are shown in Figure 7-13 and Figure 7-14 for the low and high pressure regulator models, respectively.

Table 7-5: Maximum Pressure TPs for example calculations of the PRV model pressure regulator Y models

Q (L/s)	Maximum Pressure Turning Points (*TPs*)			
	7.0 (m head)		10.6 (m head)	
	P_in	P_out	P_in	P_out
0.1	9.60	8.01	12.90	11.97
0.3	9.99	7.88	13.15	11.52
0.6	12.03	7.71	14.28	11.18

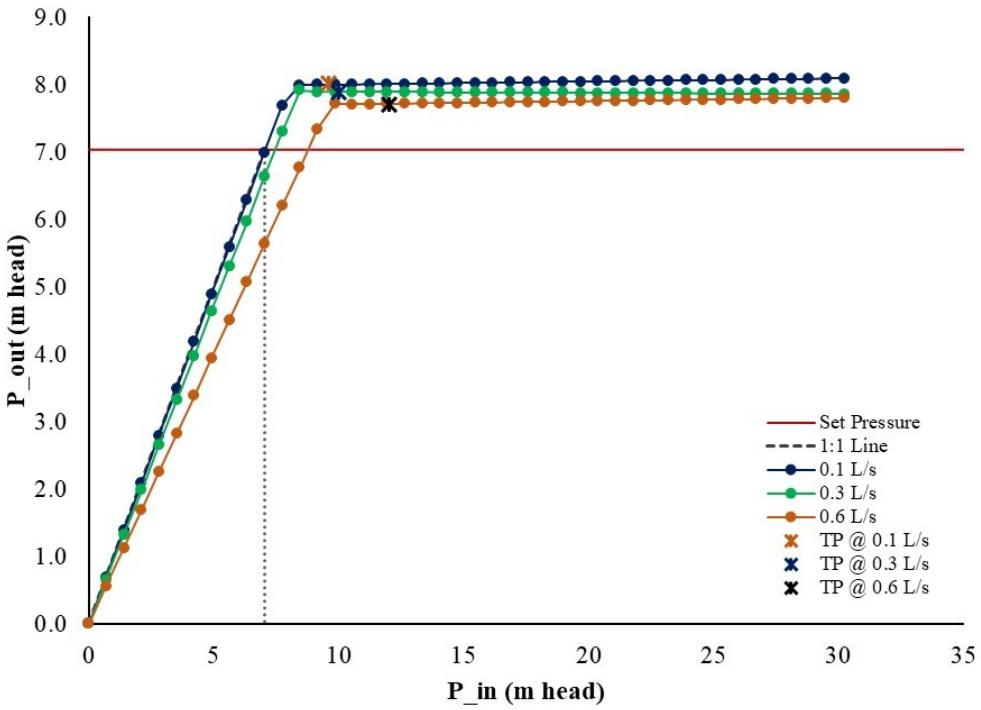

Figure 7-13: Modelled regulation curves for manufacturer Y low pressure regulator model at 0.1 L/s, 0.3 L/s, and 0.6 L/s

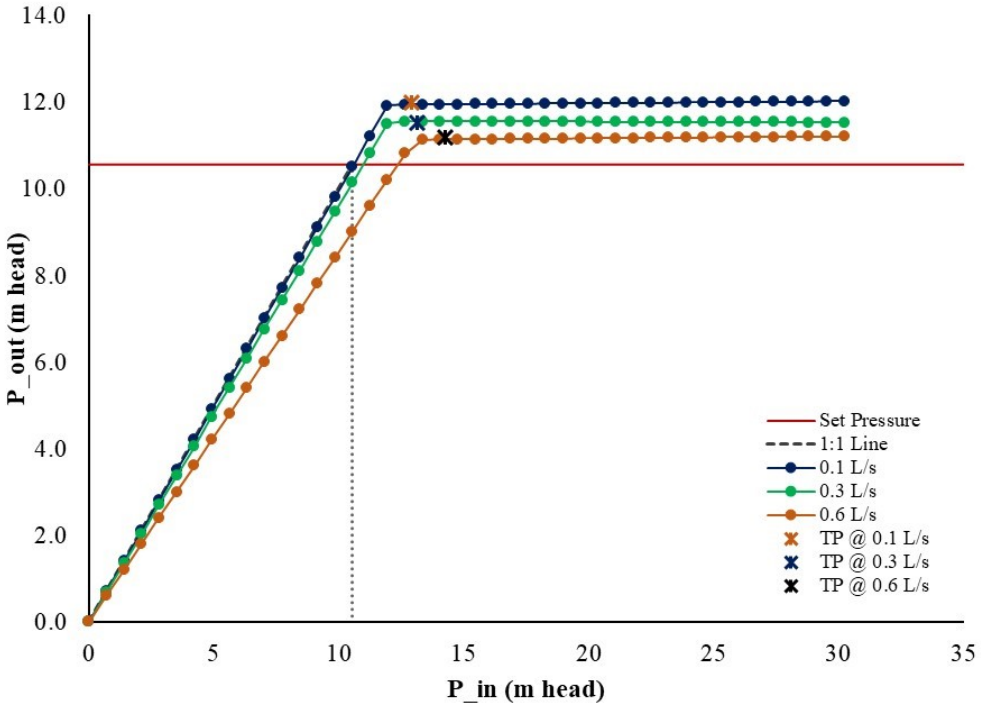

Figure 7-14: Modelled regulation curves for manufacturer Y high pressure regulator model at 0.1 L/s, 0.3 L/s, and 0.6 L/s

7.7.3 *Calculation of PRV Outlet Pressures for Manufacturer Z*

The model calculation parameters for the manufacturer Z pressure regulators are presented in Table 7-6. The results of the calculations are presented in Figure 7-15 and Figure 7-16 for both the low and high pressure regulator models.

Table 7-6: Maximum Pressure TPs for example calculations of the PRV model pressure regulator Z models

Q (L/s)	Maximum Pressure Turning Points (*TPs*)			
	7.0 (m head)		10.6 (m head)	
	$P_{\_in}$	$P_{\_out}$	$P_{\_in}$	$P_{\_out}$
0.1	8.36	7.75	12.33	10.90
0.3	8.87	7.59	13.25	10.63
0.6	11.21	7.49	15.90	10.48

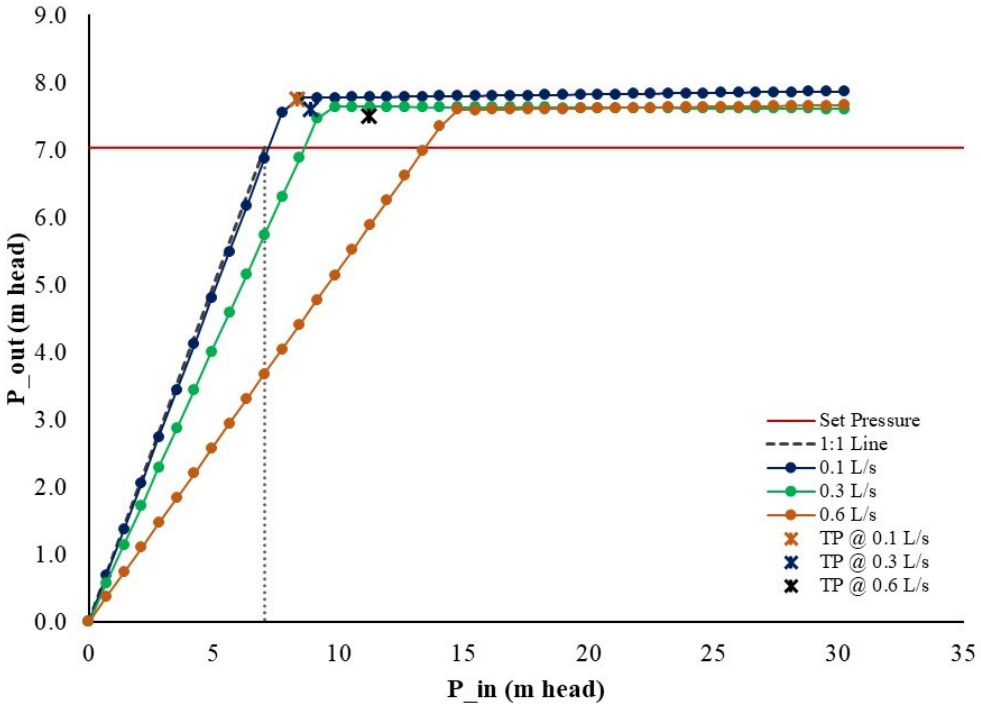

Figure 7-15: Modelled regulation curves for manufacturer Z low pressure regulator model at 0.1 L/s, 0.3 L/s, and 0.6 L/s

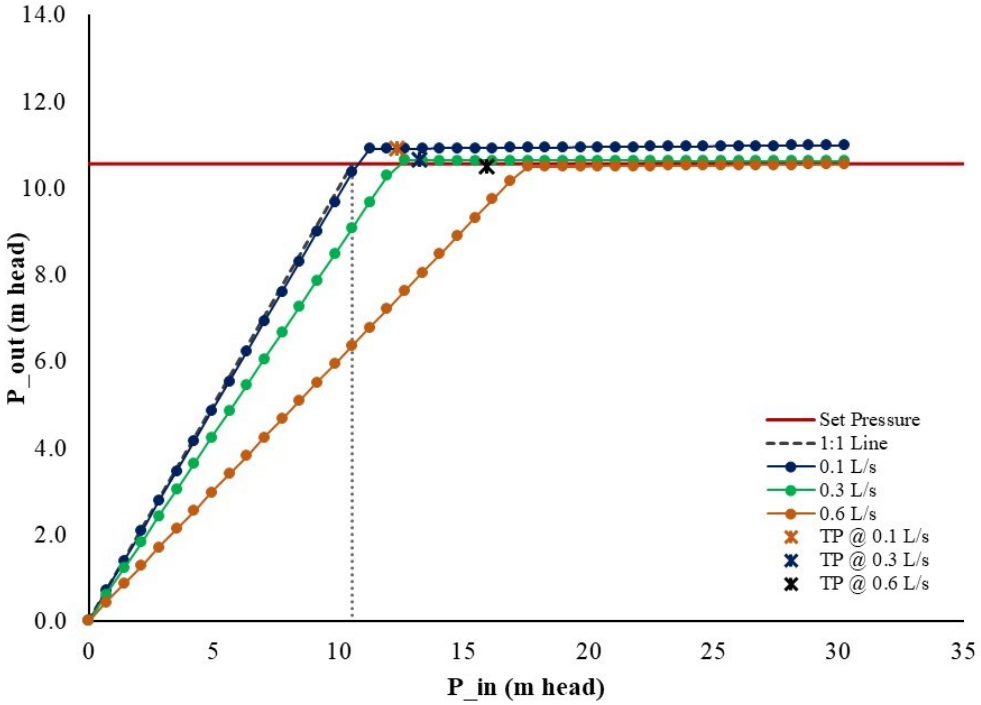

Figure 7-16: Modelled regulation curves for manufacturer Z high pressure regulator model at 0.1 L/s, 0.3 L/s, and 0.6 L/s

7.8 Proposed Hysteresis Minor Head Loss sub-model

The third important and most complex minor head loss in pressure regulation is termed the *hysteresis* minor head loss. This process is not accounted for in the Keller and Bliesner (1990) model, and is also not accounted for by the Junior et al. (2018) model. The failure to account for hysteresis in the hydraulic modelling of pressure regulation results in a significant underestimation and imprecise description of the entire pressure regulation process, especially in unsteady conditions usually experienced by modern low pressure CP&LMs. By definition, hysteresis is the phenomenon in which the value of a physical property lags behind changes in the effect causing it, or the dependency of the state of a system on its history. In pressure regulators, the lag in outlet pressure change is caused by mechanical friction between the rubber O-ring and the flow tube, as the tube entry moves in relation to the downstream side of the diffuser skirt. This movement hysteresis results in a different outlet pressure than that created solely by the variable regulation head loss inside the regulator. In most CP&LM situations, this often results from changes in inlet pressure caused by machine elevation changes, fluctuations in groundwater supply levels, and the on-and-off pulsing of VRI sprinkler control valves. From the results of the experiments, it is clear that this additional minor head loss component due to hysteresis can cause serious reductions in the regulator outlet pressure, resulting in further reductions in the operating duty point for CP&LMs.

The combination of the static and variable regulation minor head loss sub-models in Sections 7.6 and 7.7 to produce an average outlet pressure regulation curve has been previously explained. This average regulator outlet pressure curve, or regulation line, is taken to be as a result of increasing inlet pressures during regulation. It sets the maximum upper boundary of the outlet pressure under any regulation process, and will therefore be used as a reference point for the effect of the hysteresis minor head losses on the regulator outlet pressure curve. This upper boundary of regulation provides an opportunity to simplify the process of factoring the hysteresis minor head loss. This phenomena represents the flow tube passing through the inner surface of the O-ring remaining closer to the diffuser skirt with falling inlet pressures, creating this additional hysteresis minor head loss in the regulator.

To derive the hysteresis minor head loss sub-model which for the purposes of this PRV model development is denoted h_{m_H}, the measured differences between the outlet pressure regulation curves produced by an increasing and decreasing inlet pressures were used. Figure 7-17 below shows the theoretical representation of the h_{m_H} sub-model inside a pressure regulator when inlet pressure is rising or falling. The graph shows that the minor head loss, h_{m_H}, is very small or closer to zero when inlet pressure is rising, and it will increase to a maximum value when the inlet pressure is falling back to zero. The results from the experiments in Chapter 5 shows that the hysteresis minor head loss is dependent on the discharge. It is larger with a small discharge, and vice versa. This is caused by the compression of the spring by the diaphragm force acting on it, causing the entry of the flow tube to move very close to the downstream side of the diffuser skirt. When the regulator discharge is large, the inlet pressure plus any flow induced drag force will move the flow tube to toward the downstream, creating a somewhat smaller head loss in the regulator due to the larger flow area between the upstream entry of the flow tube and the downstream of the diffuser skirt.

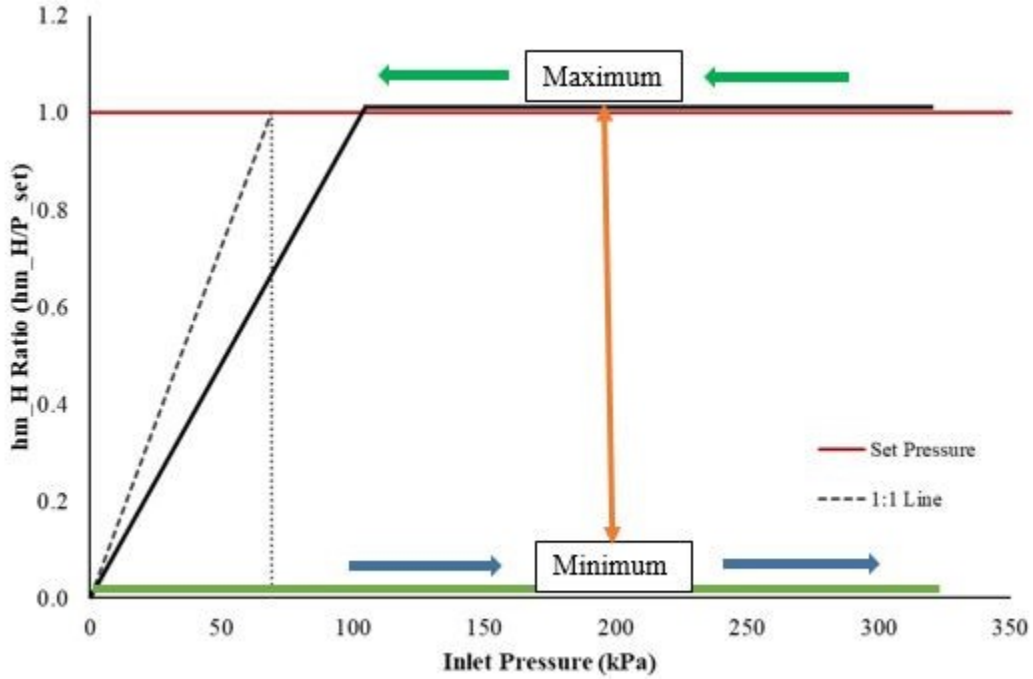

Figure 7-17: Idealised hysteresis minor head loss h_{m_H} during regulation of a PRV device at a particular discharge

Figure 7-18 to Figure 7-20 shows the magnitude of hysteresis minor head losses for pressure regulator manufacturers X, Y, and Z, across the nozzle discharges

investigated in the laboratory experiments. These graphs from the different regulator manufacturer results are in agreement with the idealised sub-model in Figure 7-17, where h_{m_H} starts from anywhere around zero and rises to the maximum head loss. These hysteresis minor head losses were derived from the hysteresis results presented in Section 5.6.5 in Chapter 5 of this thesis. It is also clear that the hysteresis minor head loss is lower for the low pressure regulator models and is higher for the high pressure models. Pressure regulators from manufacturer X have a higher hysteresis head loss when compared to the loss for the Y and Z manufacturers. Regulator manufacturer Z has the least hysteresis head loss, followed by manufacturer Y. It should be noted that the head loss may be a function of the type of lubrication used between the flow tube and the O-ring inside the pressure regulators.

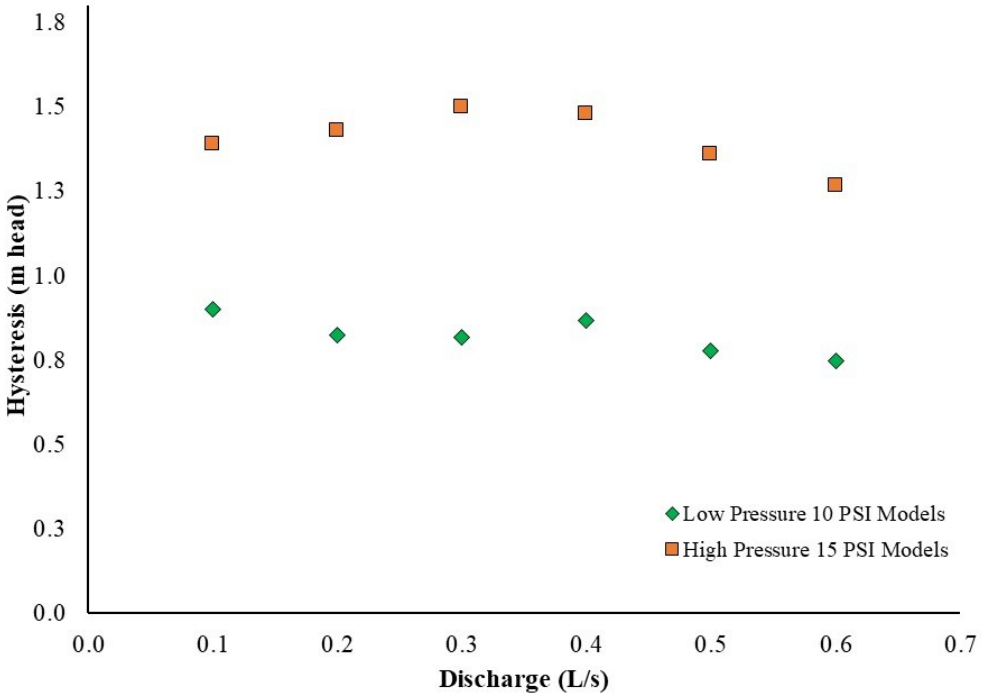

Figure 7-18: Average hysteresis minor head losses for manufacturer X low and high pressure regulator models across the nozzle discharge range investigated

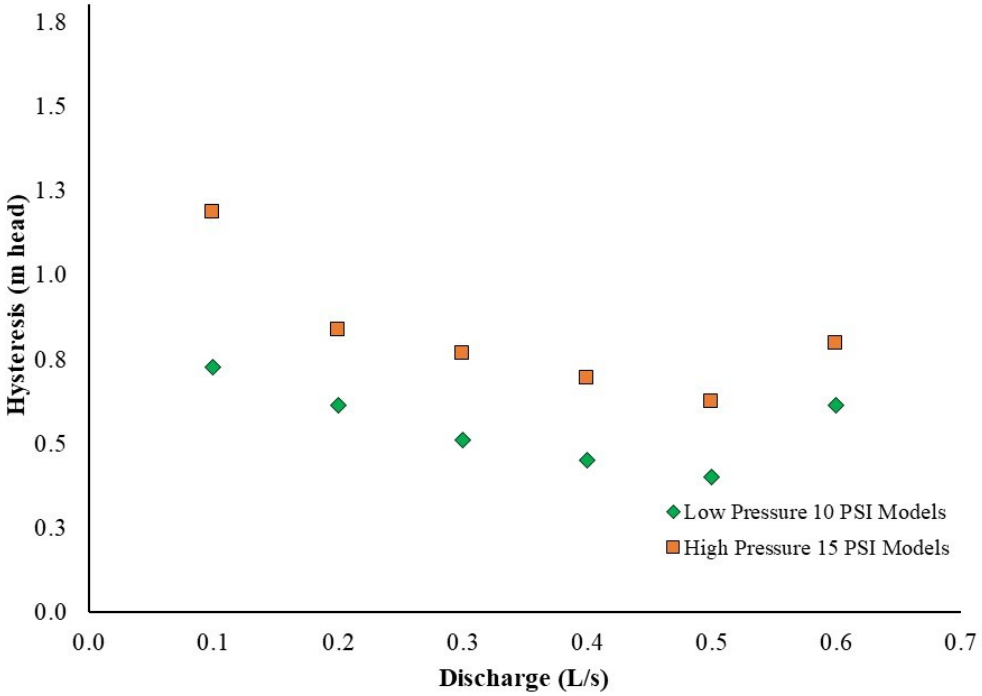

Figure 7-19: Average hysteresis minor head losses for manufacturer Y low and high pressure regulator models across the nozzle discharge range investigated

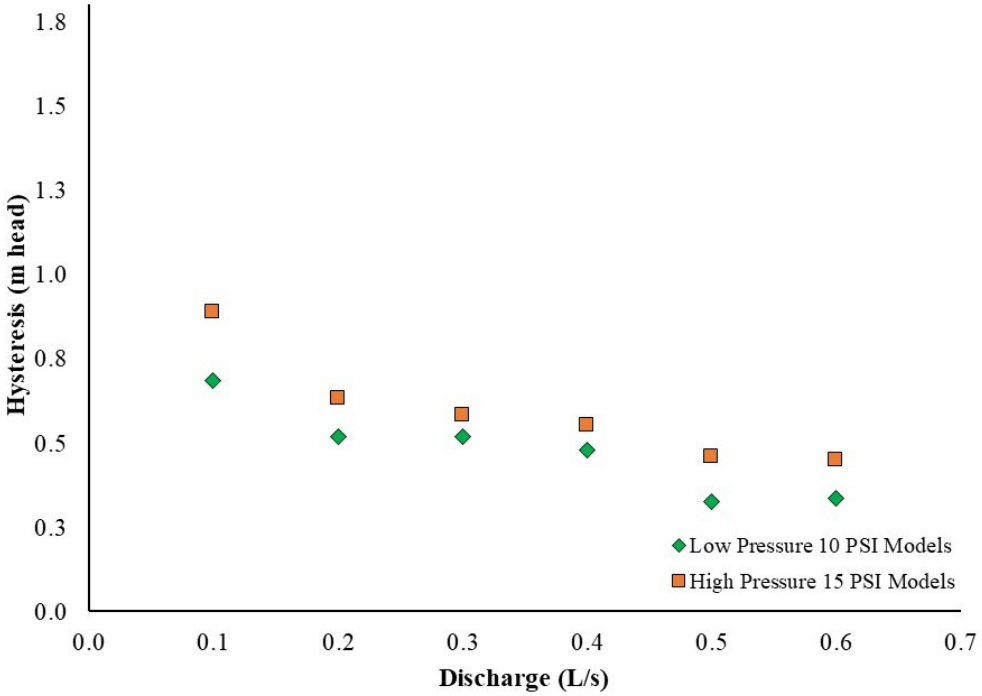

Figure 7-20: Average hysteresis minor head losses for manufacturer Z low and high pressure regulator models across the nozzle discharge range investigated

In continuing the incremental development of this novel PRV prediction model for $P_{\_out}$, the h_{m_H} produced from the hysteresis minor head loss sub-model is added to Equation 7.6 to give Equation 7.7.

$$P_{\_out} = P_{\_in} - h_{m\_ST} - h_{m\_V} - h_{m\_H} \qquad 7.7$$

When using the existing upper boundary of the outlet pressure regulation curve as a reference, a special mathematical equation is developed to predict the lower regulation curve which is caused by hysteresis. This equation factors the measured hysteresis minor head loss data from the laboratory experiments with the D' coefficient for the different pressure regulator manufacturers to enable slope adjustment of the regulation curves due to hysteresis, in addition to the maximum outlet pressure data from the upper boundary of the regulation lines produced from rising inlet pressure limbs. The utilisation of the upper regulation curve and application of an offset for the hysteresis head loss simplifies the mathematical process because the static and variable regulation loss sub-models and the C' and D' coefficient are already accounted for. The only critical parameters in this prediction model then become the hysteresis head loss and D' for outlet pressure adjustment.

Since the results of the laboratory experiments demonstrated that the lower limb of regulation resulting from hysteresis does not come into contact with the rising outlet pressure limb, it was concluded that there is a very small hysteresis head loss that takes place below the turning point before the head loss reaches a near zero value at very low inlet pressures. This small hysteresis minor head loss resulting from the tube's movement is an addition to the static minor head loss created by the discharge which offsets the regulation curve for the selected discharge away from the 1:1 line. Therefore, to clearly describe the hysteresis minor loss sub-model, two equations (Equations 7.7 and 7.8) are integrated into one large equation to enable the prediction of the outlet pressures above the set nominal outlet press, and below this set outlet pressure when inlet pressure is falling. This latter section of the regulation curve generated by hysteresis below the nominal set outlet pressure is calculated using Equation 7.8, while Equation 7.7 predicts the outlet pressures and the regulation curve

above the set outlet pressure during full regulation when hysteresis minor head loss comes into effect.

$$P_{\_out} = (P_{\_in} - h_{m\_ST} - h_{m\_V} - h_{m\_H})(\frac{P_{\_in}}{P_{\_set} + D' h_{m\_ST}}) \quad 7.8$$

This sub-model of $P_{\_out}$ due to hysteresis, when combined with the static and variable regulation minor head loss sub-models, allows for the prediction of regulator outlet pressures during the unsteady flow conditions experienced by pressure regulators in CP&LMs. The outcome is two outlet pressure regulation curves for the same discharge, one for the rising inlet pressure limb obtained from the combined static and variable regulation sub-models only (Equation 7.6), and the second representing the regulation curves resulting from falling inlet pressures as impacted by hysteresis (Equation 7.7 and 7.8). Both regulation curves have a common origin of zero, rising very close to each other until they eventually depart at or near the turning point. Beyond this region, the regulation curves run parallel to each other by a magnitude which is equal to the hysteresis head loss, h_{m_H}. Therefore, it can be concluded that these series of mathematical equations provide the upper and lower limits in which the regulator outlet pressures actually exist, with every single increase and decrease in inlet pressure head. Between these upper and lower boundaries of the regulation curves, there is a series of multiple regulator outlet pressure curves that result from numerous different hysteresis minor losses. The calculations and graphical examples of these sub-model predicted regulation curves to represent the full PRV model performance are presented in Section 7.9.

Although this full PRV outlet pressure prediction model currently does not mathematically represent the shape of the regulation curve with a unit change in inlet pressure, the slopes of the regulation curves have been determined experimentally using different inlet pressure heads as reported in Section 5.6.6. Figure 5-120 shows that the slopes of the outlet pressure regulation curve due to hysteresis are steeper for low inlet pressures, and are flatter for high inlet pressures. The idealised representation of this phenomenon when super-imposed in the theoretical scheme of the proposed $h_{m\text{-}H}$ sub-model is illustrated in Figure 7-21.

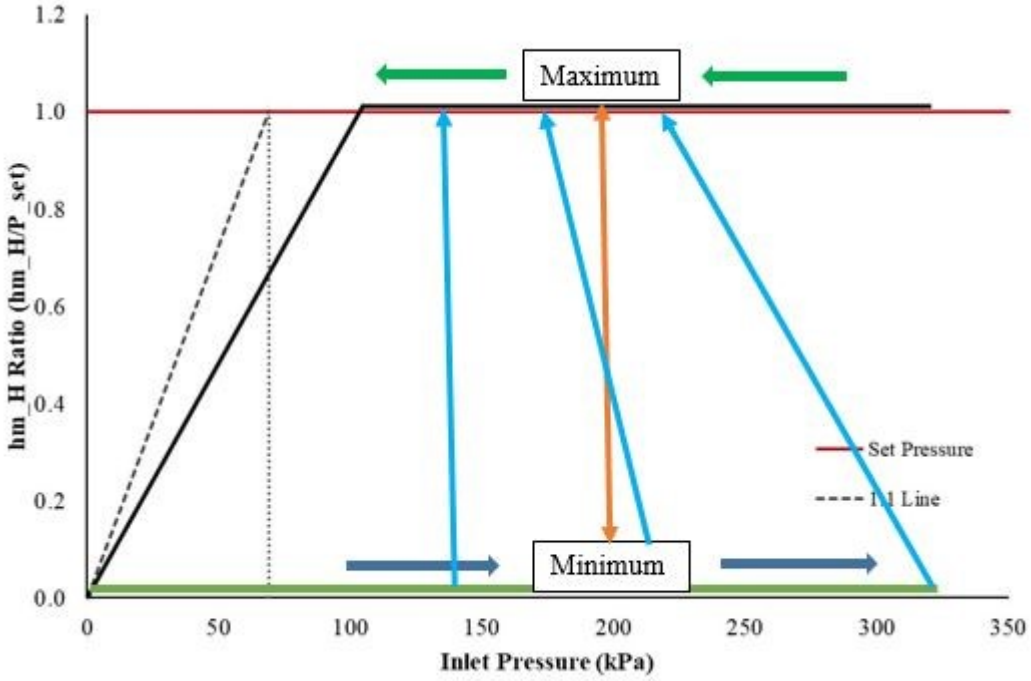

Figure 7-21: Idealised h_{m_H} sub-model showing slope variation with increase in inlet pressure head

7.9 Performance of Full PRV Model

The performance of the static and variable regulation sub-models which forms part of the full PRV model have been presented in Section 7.7. In this approach, the performance was described through calculated example results and graphical outputs of the combined static and variable regulation minor head loss sub-models to produce average outlet pressure regulation curves over increasing inlet pressure limbs. The full PRV model performance evaluation involves the integration of the hysteresis sub-model to produce calculated examples and graphical outputs for the lower limb of outlet pressure regulation curves when inlet pressure head is falling. The segregation of the model performance results is because the performance is different for the combined static and variable regulation minor loss sub-models, and the addition of the hysteresis loss sub-model also produces different results.

The performance results of the complete PRV model (Equation 7.7 and 7.8) when the hysteresis minor head loss sub-model is added to the static and variable regulation minor head loss sub-models are presented here. Only the low and highest discharges

of 0.1 L/s and 0.6 L/s were modelled to predict regulator outlet pressures using the full PRV mathematical model. The hysteresis minor head loss is used in this type of calculation process to produce the lower leg of the regulation curve using the criteria described in Section 7.8.

7.9.1 *Graphs of PRV Outlet Pressures for Manufacturer X*

Figure 7-22 and Figure 7-23 show the predicted regulation curves for the low and high pressure regulator models from manufacturer X using the newly developed PRV model. The regulation curves for the rising and falling inlet pressures are indicated by H_{p_R} and H_{p_F}, respectively. It is apparent that the hysteresis minor head loss is large at low discharges and decreases with increasing discharge for all pressure regulators. The larger regulator outlet pressures at the falling pressure limb for the 0.1 L/s data is due to low static minor head loss at this discharge. Otherwise the hysteresis head loss component at this low discharge is large for the X pressure regulators.

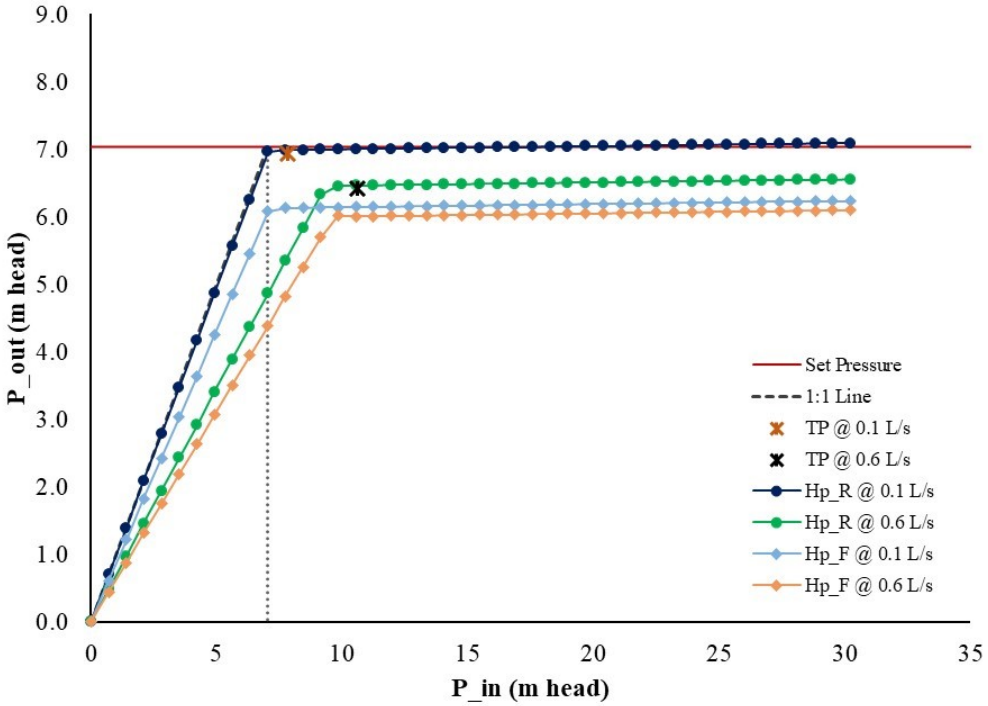

Figure 7-22: Predicted outlet pressure regulation curves for the low pressure regulator model from manufacturer X for both rising and falling inlet pressure head at 0.1 L/s and 0.6 L/s respectively

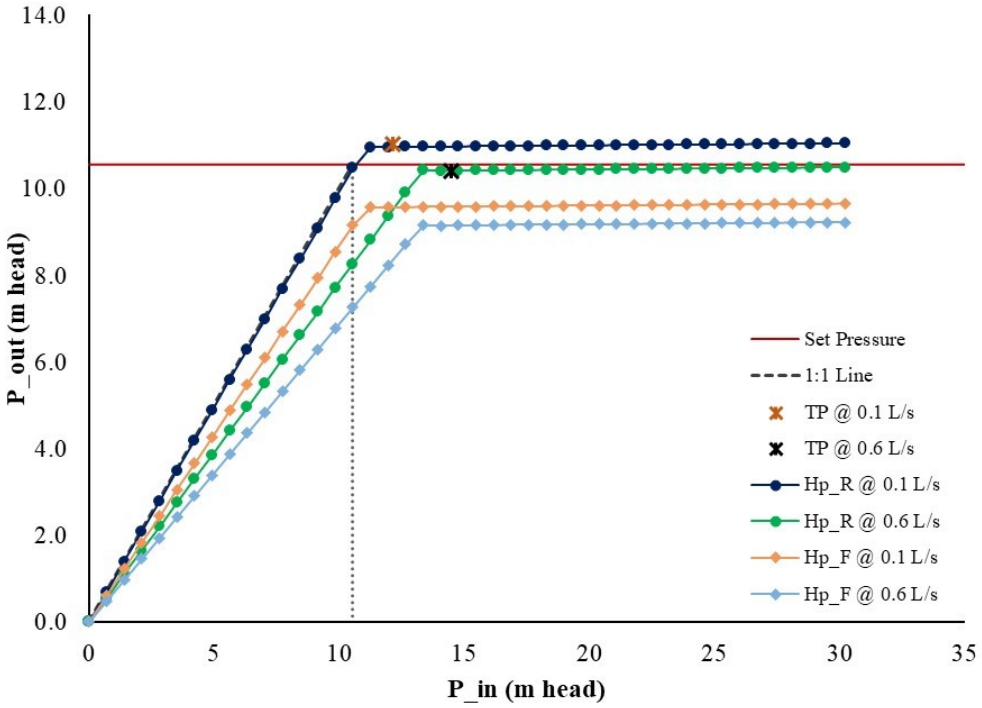

Figure 7-23: Predicted outlet pressure regulation curves for the high pressure regulator model from manufacturer X for both rising and falling inlet pressure head at 0.1 L/s and 0.6 L/s respectively

7.9.2 *Graphs of PRV Outlet Pressures for Manufacturer Y*

The regulation curves of rising inlet pressures and falling inlet pressures for the low and high pressure regulator models from manufacturer Y are shown in Figure 7-24 and Figure 7-25. It is evident that the predicted regulator outlet pressure curves are only influenced by discharge and the amount of hysteresis head loss. The outlet pressure decreases with discharge, but it is not impacted in the same way by the hysteresis. The hysteresis head loss is larger at low discharges in a similar way as observed for manufacturer X.

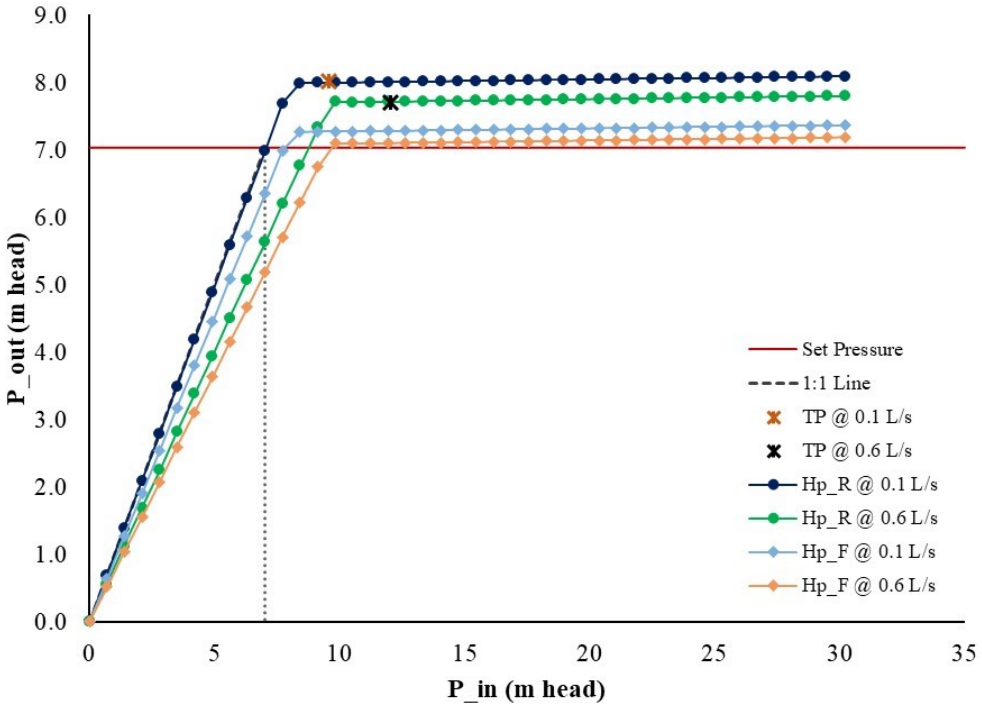

Figure 7-24: Predicted outlet pressure regulation curves for the low pressure regulator model from manufacturer Y for both rising and falling inlet pressure head at 0.1 L/s and 0.6 L/s respectively

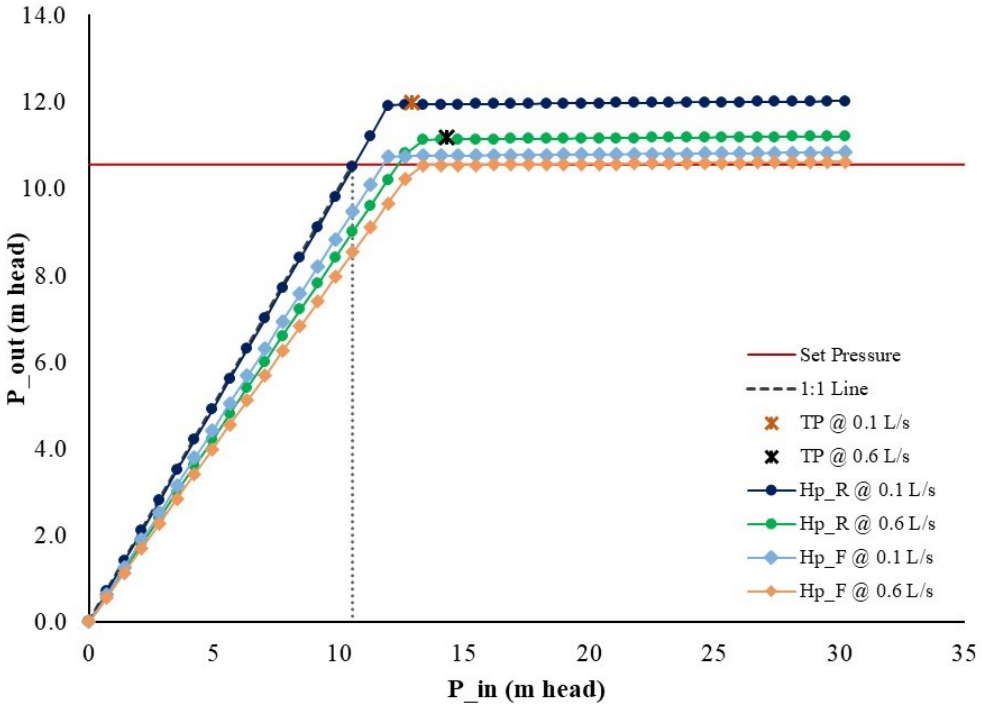

Figure 7-25: Predicted outlet pressure regulation curves for the high pressure regulator model from manufacturer Y for both rising and falling inlet pressure head at 0.1 L/s and 0.6 L/s respectively

7.9.3 *Graphs of PRV Outlet Pressures for Manufacturer Z*

The regulated outlet pressure curves of rising and falling inlet pressures for the low and high pressure regulator models from manufacturer Z are shown in the graphs below. It is clear that the predicted regulator outlet pressure curves are only influenced by discharge and the amount of hysteresis head loss. The outlet pressure decreases with increasing discharge, but it is not impacted in the same way by the hysteresis head loss as observed for other manufacturers. The hysteresis head loss is larger at low discharges and reduces with increases in discharge. For this regulator manufacturer, the regulator outlet pressures during hysteresis are at least equal at the two extreme nozzle discharges for the high pressure models. The outlet pressure increases with increasing in discharge for the low pressure model due to very low hysteresis.

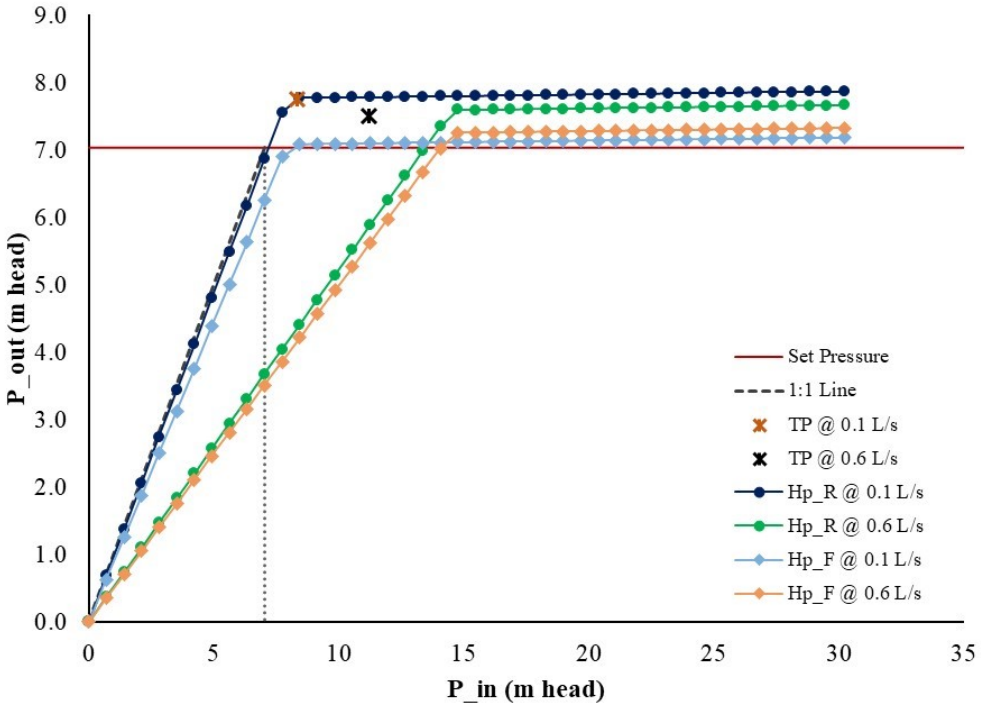

Figure 7-26: Predicted outlet pressure regulation curves for the low pressure regulator model from manufacturer Z for both rising and falling inlet pressure head at 0.1 L/s and 0.6 L/s respectively

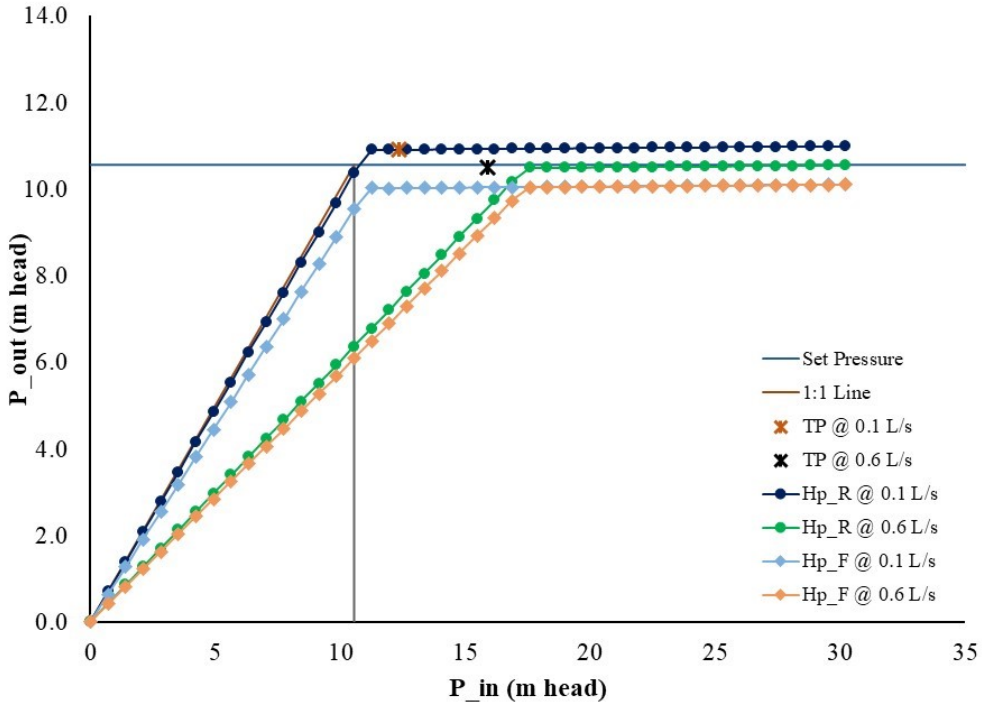

Figure 7-27: Predicted outlet pressure regulation curves for the high pressure regulator model from manufacturer Z for both rising and falling inlet pressure head at 0.1 L/s and 0.6 L/s respectively

7.10 Validation of the new PRV Model

Since the parameters used to develop the PRV model were established from experimental data, a very simple non-statistical comparison was performed between model predicted regulator outlet pressures and the actual measured results of regulator outlet pressures reported in Chapter 5. This demonstrates the accuracy of the new model's prediction of regulated outlet pressures, and how they compare with measured data. The comparison was completed for the low pressure nominal setting for all three pressure regulator manufactures. The comparison results are presented in Figure 7-28, Figure 7-29, and Figure 7-30, where the measured data was plotted against model predicted regulator outlet pressures for the two extreme nozzle discharges at 0.1 L/s and 0.6 L/s, respectively. The measured data was taken from the pressure regulator performance results presented in Section 5.6.5 in Chapter 5, Figure 5-85, Figure 5-87, and Figure 5-92.

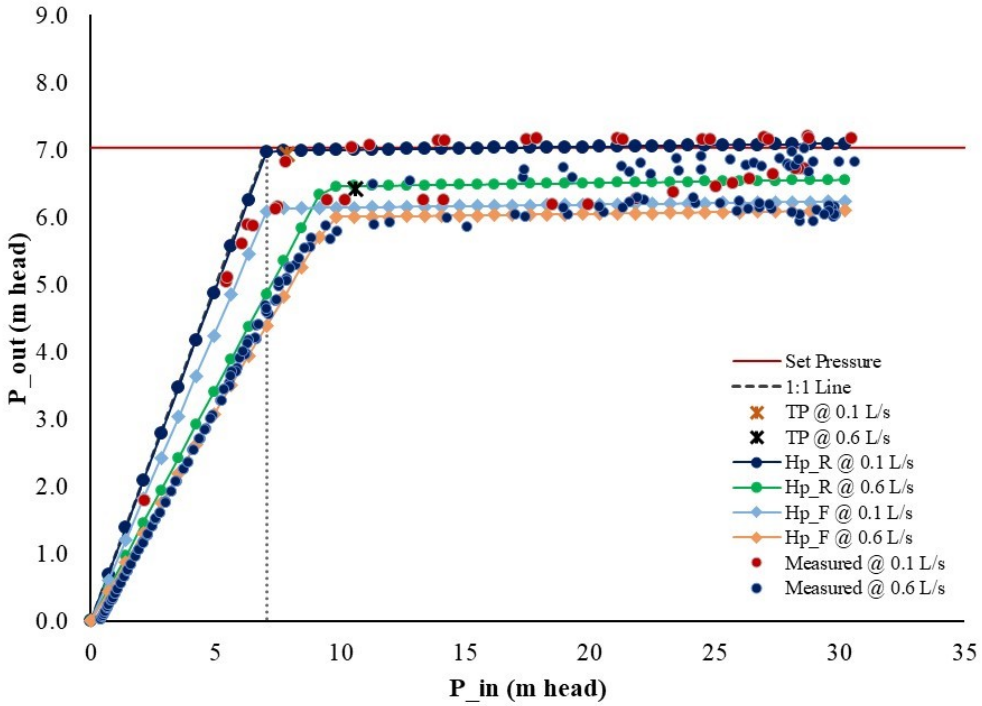

Figure 7-28: Comparison of model predicted versus measured regulator outlet pressures for the low pressure regulator model from manufacturer X at 0.1 L/s and 0.6 L/s

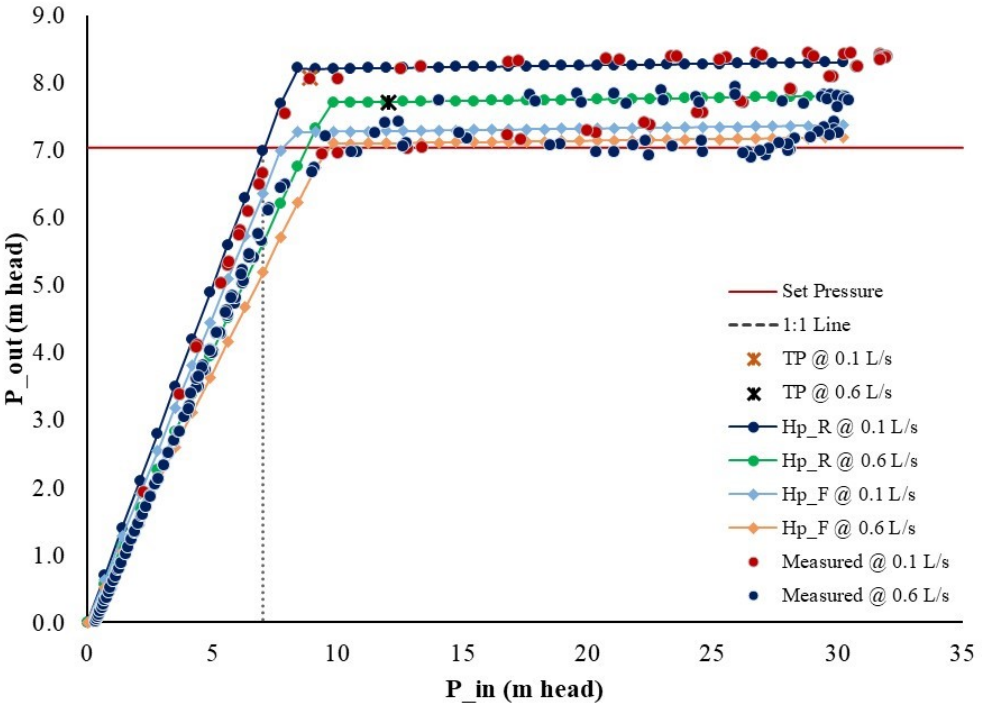

Figure 7-29: Comparison of model predicted versus measured regulator outlet pressures for the low pressure regulator model from manufacturer Y at 0.1 L/s and 0.6 L/s

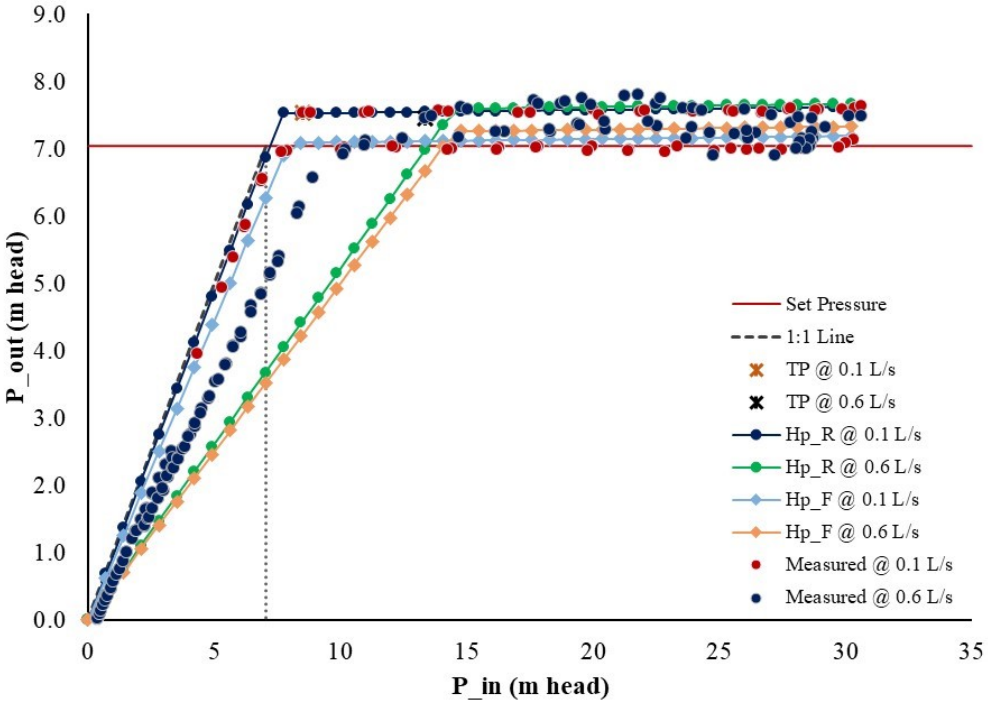

Figure 7-30: Comparison of model predicted versus measured regulator outlet pressures for the low pressure regulator model from manufacturer Z at 0.1 L/s and 0.6 L/s

From these figures, it is apparent that the hydraulic model is capable of accurately predicting regulator performance for each of the three manufacturers at the different selected discharges. There is a negligible difference between predicted and measured regulator outlet pressures, which was achieved by using the error minimisation technique by adjusting for the outlet pressure and slopes of the regulation curves at each discharge modelled, as explained in Section 7.5. In cases where the model could not predict the regulator outlet pressures with high accuracy, it is likely that the spring vibration was too high, caused by a combination of high inlet pressure head and discharge. This is noticeable at 0.6 L/s of the regulator manufacturer X where the outlet pressure data points were scattered around the average regulation line when the inlet pressure head was close to the maximum (Figure 7-28).

Nonetheless, like any model, the new PRV outlet pressure prediction model has limitations. It is currently not capable of predicting the shape or slope of the decline in outlet pressure when it has reached a maximum head, before fully attaining the lower boundary when inlet pressure head is falling and hysteresis is at a maximum. The

mathematical description and incorporation of this capability is required in any further development of the h_{m_H} sub-model, so as to also permit the prediction of this response by regulators. It has been experimentally determined as shown in Figure 5-120 in Section 5.6.6. This was however, not explored in this model development due to time constraints. The PRV model also predicted turning points at slightly higher inlet pressures than the actual measured turning points at the highest discharge for the manufacturer Z pressure regulator.

Overall, based on the PRV model calculated graphical results presented above, it can be concluded that this mathematical model, which is a semi-empirical hydraulic model developed for predicting the hydraulic performance of pressure regulators used with CP&LMs:

- Simulates regulator outlet pressures from the origin rising up to the turning point, which is close to the nominal set pressure rating of the regulator, for each discharge selected.
- Produces clearly defined regulator outlet pressure turning points that are close to the turning points of the 1:1 line.
- Accounts for the reduction in regulator outlet pressures with increases in discharge.
- Accounts for hysteresis in the regulator outlet pressure by simulating the average upper and lower boundaries of regulation curves in which any outlet pressure points resulting from changes inlet pressure head are contained.
- Predicts the reduction in hysteresis minor head losses with increases in discharge.
- Simulates regulator outlet pressures from three common manufacturers used with CP&LMs in industry.

While it is clear that this model can accurately predict the regulator outlet pressures to produce average regulation curves during hysteresis, there are further improvements that can still be made in the hysteresis sub-model so that the full PRV prediction model is able to simulate a single outlet pressure that can be located anywhere between the upper and lower limits of the regulation curves. However, this process of further

development could not be completed within the scope and timelines of this thesis. The preliminary hypothesis of the hysteresis sub-model further development is that the model should be able to incorporate, knowledge of the previous position of inlet pressure head, $P_{\_in}$, and knowledge of the previous hysteresis minor head loss, h_{m_H}, using a time step, t. This process can be described using the following conceptual model.

$$h_{m\_H(t)} = h_{m\_H(t-1)} + fn(P_{\_in(t)}, P_{\_in(t-1)}) \qquad 7.9$$

7.11 Summary

This chapter describes the development of a new PRV mathematical model to predict pressure regulator outlet pressure in modern low pressure CP&LMs. This hydraulic model was developed using the empirical results of the hydraulic experiments of pressure regulator performance characterisation that were conducted in the USQ Hydraulics Laboratory. This new mathematical model encompasses three sub-models that represent each of the minor head loss components occurring inside pressure regulators. Pressure regulator performance has not been accurately described previously in this level of detail. The sub-models were developed using a set of mathematical equations that are based on fundamental hydraulic principles, and are combined to complete a large mathematical equation to predict the regulator outlet pressures for the upper and lower limits of outlet pressure regulation curves accounting for the hysteresis of the rising and falling inlet pressures. Model coefficients were fitted using error minimisation techniques, and permit accurate prediction of regulator outlet pressure. The performance and validation of the new PRV model provided good agreement between measured and predicted regulator outlet pressure. The ideal operating conditions and limitations of use for PRV model have also been outlined. A conceptual model for the required further improvements of the hysteresis sub-model is proposed, to enable the prediction of any single actual regulator outlet pressure during regulation.

8. DISCUSSION

8.1 Introduction

The development of CP&LMs has been continual with a large number of modifications completed since their introduction in the 1950s. They were converted from high pressure impact sprinklers to low energy precision application (LEPA) systems which are now implemented with pressure regulators, amongst other improvements. The most recent innovation involves retrofitting these machines with VRI technology to modify their water application patterns and achieve variable-rate or site-specific irrigation. This focus of the discussion in this chapter is the application of VRI on CP&LMs, and the hydraulic implications of retrofitting this technology on these machines, inferred from results of the extensive hydraulic experiments conducted in this research. The more comprehensive understanding of pressure regulation and the resulting new mathematical model developed for the purpose of numerically describing their performance are discussed, along with associated limitations. This chapter will reflect on the objectives and main aim of this thesis, and how these have been achieved.

8.2 Implications of Retrofitting VRI on CP&LMs

VRI systems have been developed for use with CP&LMs to tailor water applications within specific irrigation management zones. The objective is to generate water and energy savings while also realising improvements in crop yields. However, the literature review established that the return on investment (ROI) for VRI is very low due to high investment costs and the lack of tangible benefits from using the technology. Consequently, growers have consistently been losing interest in purchasing VRI equipment, with utilisation declining from those growers who had already invested in the technology. Recent studies (Hedley et al., 2011, O'Shaughnessy et al., 2019) show that savings greater than 15 % in energy, 27 % in water, and 10 % increase in crop yield, are required to justify investment. However, in

countries like Australia and New Zealand, VRI is reportedly used to reduce water logging on CP&LMs wheel tracks and machine downtime due to bogging (Krishna, 2016).

The literature review also concluded that the design of VRI on CP&LMs is commonly completed without any attempts to account for the minor head loss characteristics of the solenoid valves used. The hydraulic characteristics of VRI valves are more often ignored due to difficulties in establishing the important technical information about their performance. Therefore, the VRI hydraulic experiments completed in this research to determine, the minor head losses for solenoid VRI valves, the occurrence of hydraulic transients or water hammer and its magnitude during pulsing, and the impacts of pulsing on pressure regulator performance, were all novel. They were needed to address the VRI problems in industry because there has been no single attempt previously undertaken to investigate the hydraulic performance of VRI systems. Nearly all VRI research has so far been focusing on improving the generation of irrigation prescriptions using advanced scheduling techniques such as real-time moisture sensing technologies. Previous work has also focussed on validating and demonstrating the proposed benefits, but ignores potential changes to the hydraulic behaviour of the machine. The motivation for conducting this hydraulic research was instigated by the manner in which VRI alters the normal discharge of sprinkler heads. It achieves this by cycling the opening and closing of solenoid valves in a non-sequential approach along CP&LM spans, to tailor irrigation depths to the specific requirements of discrete soil management units in irrigated fields. This mode of operation triggered questions around the integrity of CP&LM hydraulic systems when introduced to these type of fast unsteady conditions. The special research interest was justified by the fact that the VRI hydraulic characteristics are not accounted for in the designs of machines retrofitted with this technology. As a result, an extensive exploratory experimentation program was commissioned to solicit data on each of these hydraulic phenomena, to help improve the design of these irrigation machines.

8.2.1 *Additional VRI valve Minor Head Loss*

A good understanding of the magnitude of minor head losses in irrigation components is integral to successful design process, which ensures that the design operating head is adequate to meet system head requirements. A total of 144 experimental tests were completed to determine the minor head losses across three common VRI valve manufacturers. Eighteen (18) of these tests were completed for each VRI valve unit at the selected nozzle discharges, and were replicated three times, as presented in Chapter 4 and Chapter 5. While the results proved to be conclusive, it would have been more appropriate to test the number of samples statistically calculated for associated accessories in Table 4-2 of Chapter 4. However, due to budget constraints and time limitations, purposive sampling was used to determine a reasonable number of test units for VRI valves, and results were found to be acceptable. This statistical technique is also reported to have worked flawlessly for Fraisse (1994).

The minor head losses resulting from addition of VRI hardware were found to be as high as 4 m for one manufacturer, while the other two manufacturers had up to 1.2 m head loss at the tested nozzle discharges. Minor losses are proportional to the velocity head. These losses are usually estimated to be equal to 10 % of total system head loss in other pressurised pipelines (Kincaid and Heermann, 1970). However, the additional head loss introduced by VRI valves into some CP&LM designs are very impactful on the final design operating head and discharge. The magnitude of the minor head loss at 4 m head is approximately 25 % of the total head for a majority of modern low pressure CP&LMs operating at 16.5 m head, as demonstrated in Section 5.4.2 in Chapter 5. The head loss can be approximately 14 % of the total system head loss for machines with a design operating head of 30 m, which is equal to the maximum test pressure used in the hydraulic experiments. The minor head loss of 1.2 m for the two manufacturers is about 7.5 % of total head for machines operating at 16.5 m head and about 4 % for machines operating at 30 m head. The much larger head loss through the one manufacturer is believed to be a result of the diaphragm sealing mechanism, as it exhibited an abrupt rise of approximately 2 m head loss immediately after, and very close to zero velocity head. Therefore, the conclusions drawn from the literature that VRI equipment is expensive in terms of capital cost and provides few benefits, are

further confirmed with the results and findings from the VRI component testing in this research. The results have implications in the manner in which VRI CP&LMs are designed because the additional VRI valve head loss will result in steeper system resistance curves, which impact on system pumping heads and capital cost, and the ongoing operating costs. It can be concluded from the results that the minor head losses from VRI valves are significant, and are not always within the 10 % threshold for hydraulic minor losses which is used as a rule of thumb in the design guidelines. Higher capital costs are therefore inevitably absorbed due to the need to review and upgrade pumping systems that meet higher system head requirements, especially on existing machines that are retrofitted with VRI. This can be in excess of the initial capital cost of the VRI equipment itself.

In new VRI CP&LMs installations, the additional operating head of the machines due to VRI valves may be wasted energy especially for machines irrigating single non-cash crops on generally flat terrain. A design solution (Equation 5.4) was proposed in Chapter 5, where the original standard total pressure head loss equation for designing ordinary conventional CP&LMs was modified by incorporating a new term, h_{m_vri}, to account for the additional minor head loss from VRI valves. The solution was developed together with empirical coefficients that can help design engineers to simulate the hydraulic characteristics of each of the specific solenoid VRI valves used in the design of the VRI machines. If the hydraulic designer is unable to incorporate the necessary upgrades in existing pumping supply systems for conventional machines, the additional VRI energy losses will impact the system head and will cause hydraulic situations where pressure regulators would be unable to regulate properly, thereby resulting in poor water application uniformity and reduced crop yields. In countries like USA where it is common practice to use very high pressure models of regulators (20 psi or more), the impact of uncorrected machine hydraulics will have a serious impact on regulation. Depending on the magnitude of any additional head loss, the hydraulic designer only has the option of reducing the sprinkler package total discharge whilst trying to maintain suitable water requirements for the crop and soil.

On-going additional operating costs throughout the season, caused by the additional energy losses created by VRI valves, reduces their likely benefit. These higher energy

costs would generally mask the benefits accrued from reductions in water usage with improved scheduling and irrigation, especially in farming enterprises where the water cost is not significant. As such, VRI will continue to remain unprofitable until the hydraulic head losses are well integrated into CP&LM design processes. To be cost effective, economic assessments are required during the design stage to determine the feasibility of VRI for different crops and soils. In addition, the findings where one manufacturer has a very unique and large valve head loss that does not conform to the normal minor head loss characteristics stipulated in the standard hydraulic design guidelines, VRI users would need to be advised of the specific range of head losses between manufacturers to help them make informed investment decisions that offers great benefit. While it will be more beneficial to influence the whole industry through VRI valve manufacturers, by reviewing their valve designs and optimising them to those that minimise head loss, it is unlikely that this can be achieved unless they can realise an economic benefit from it, or until they are ultimately exposed. An improvement in VRI equipment manufacturing will help reduce the amount of head loss, and subsequently reduce the total system design heads for VRI CP&LMs, thus increasing the profitability of the technology. Consequently, the results from this research will help to advise designers and irrigators to make good choices when selecting between VRI valves and purchasing them, especially when they have a choice for retrofitting.

8.2.2 *VRI Pulsing and Propagation of Hydraulic Transients*

The principal idea that motivated the undertaking of this research was the on-and-off pulsing and cycling mode of VRI operation, as mentioned previously in Section 8.2 of this chapter. Based on this phenomenon, a hypothesis was formed that VRI pulsing was expected to cause pressure transients commonly known as water hammer that will impact on the hydraulic performance of CP&LMs. The results of VRI valve testing completed in this research confirmed this hypothesis and postulations. A total of 84 experiments were completed with two VRI valve configurations, using one type of solenoid VRI valve to determine the occurrence of water hammer or pressure transients during pulsing. The VRI valves selected for testing this phenomena was from the manufacturer with the highest amount of minor head loss. The reason for selecting this

one particular brand was the magnitude of the minor head loss, and the time constraints for building multiple solenoid control algorithms, as explained in Chapter 4. The results highlighted that pulsing does indeed create water hammer in VRI machines. The transients generated during on-and-off pulsing of VRI valves are significant, and they were found to be between three and four times the typical system operating head. Investigations of the water hammer effects were measured on pressure regulator performance. The hydraulic response of regulator outlet pressure to fast pressure wave transients was conducted using a total of 36 experiments configured with a VRI valve and a pressure regulator, as described previously in Chapter 4. The results confirmed the hypothesis from this research that VRI pulsing impacts pressure regulator performance. It was discovered that the transients cause an average variation that is equal to about 0.2 m head in the final regulator outlet pressure. The temporary variation in regulator outlet pressure was significant at a maximum of 17 % of the nominal set pressure, and 16 % of the actual regulated pressure, for the highest nozzle discharge on the regulator manufacturer tested.

These transients will impact the longevity of CP&LM machine components since their maximum design operating heads and allowable design stresses can be compromised by prolonged repetition of pressure spikes from VRI pulsing. Therefore, when designing VRI machines, there is a need to understand component lifespan with the maximum number of cycles or pulses before they fail, or before significant changes in their performance characteristics occur. While these transients were investigated on a small pipe rig, and shown to be significant, it is worth examining these on larger pipe diameters representative of CP&LM spans to check for any potential hydraulic dampening. This hydraulic investigation is important to understand the true magnitude of the hydraulic heads created, so as to correctly select machine components during design. In machines equipped with flexible sprinkler drop hoses, the hydraulic dampening may be caused by a slight expansion of the droppers in response to any temporary increase in system head, and this may reduce the severity of the transients on machine integrity. Therefore, there is a likely benefit from testing and validating these experiments using techniques such as large diameter pipe rigs, multiple VRI valve combinations and pulsing cycles, to examine the impact on performance especially the simultaneous opening and closing of the solenoid valves.

Overall, the results of the novel experiments conducted on solenoid VRI valves testing in this research will assist hydraulic designers of VRI CP&LMs and irrigators to select VRI equipment more appropriately, and use the hydraulic equations developed, to ensure that these machines are economical in design, safe to operate, and cost-effective to run. It is my belief that the small performance differences observed within each group of VRI valve test units, are a result of manufacturing differences. Henceforth, this emphasizes the need for larger samples to fully understand the performance differences within each sample and, account for the extent of manufacturing variation.

8.3 Development of a Novel Automatic Test Apparatus

While measurement and testing of irrigation accessories such as irrigation valves and pressure regulators can be guided by special procedures provided by the International Standards Organisation (ISO), these guidelines were found to be limited and somewhat outdated for modern irrigation equipment such as pulsing solenoid valves. In addition, these are not very detailed for the characterisation of pressure regulator performance. Therefore, this limitation was overcome by developing a novel automatic test-apparatus and associated test methodology for data collection, as provided in Chapter 3 and Chapter 4.

The novel special characteristics of this test-apparatus included an ability to integrate advanced high precision water measuring equipment, water pressure and temperature sensing equipment into a LabVIEW data acquisition software that automatically controlled the hydraulic experiments using control signals generated by sensors in the experimental rig. The automatic control was achieved through a set of electronically-actuated control valves that received signals from the automatic data acquisition software. This configuration provided enough capability to simulate the on-and-off pulsing of VRI valves, and the simulation of the complex operation of CP&LM pressure regulators, while providing advanced automatic data collection. This capability provided very critical and useful information on the hydraulic performance characteristics of VRI valves and pressure regulators. The most critical features were the abilities, to control the operation of all experimental parameters via the desktop

graphical-user interface provided by LabVIEW, which included test discharge, pulsing frequencies for solenoids, and the desired positions of the test-rig control valves. The new apparatus had a smart and unique method for automatically characterising pressure regulator hysteresis, as described in Chapter 4. The outcomes from the analysis of this technical information is highly valuable in the correct hydraulic design and operation of VRI equipped CP&LMs, as well as machines equipped with pressure regulators. As well, the successful development and application of this novel test-rig offers an opportunity for design engineers and researchers to further utilise these techniques to develop valuable information for other irrigation accessories. This research also provides an opportunity to amend the ISO Standards 9644:2008 and 10522:1993 with modern state-of-the-art procedures that are commensurate with modern irrigation technological advancements. This latter conclusion is consistent with the recommendations of Junior et al. (2018).

8.4 PRV Performance Characterisation and Modelling

An accurate understanding of the true nature of the hydraulic performance of pressure regulators is very limited within industry, and there is a substantial difference of opinion amongst researchers regarding the actual performance of these important regulating devices. The literature identifies the lack of suitable testing procedures for characterising the complex nature of pressure regulator performance, as responsible for these limitations. In addition, the mathematical models used to predict pressure regulator performance were found to be unsuitable. The limitations of these models are those relating to the models either being too theoretical or statistical, or not accounting for the true complete elements of pressure regulation mechanisms, such as hysteresis in outlet pressure. The limitations have been summarised in Chapter 6 of this thesis.

A total of 618 extensive and time-consuming hydraulic tests were completed for the five different groups of experiments designed for the operational characterisation of pressure regulator performance, taking advantage of the test capabilities of the novel test-apparatus described in Section 8.3 of this chapter. The novel test protocol

developed, provided a range of diverse datasets that enabled a full understanding of pressure regulator performance for three major manufacturers in the irrigation industry to be captured. This automatic testing also allowed for the full characterisation of the hysteresis of outlet pressure during operation, which previous researchers had failed to adequately comprehend due to the limitations of manually controlled experiments. The limitations of these previous manual approaches had been inevitable to human error at predetermined point measurements. This was often not representative for pressure regulators as they function based on the movement of a flow tube against a compression spring to provide a particular outlet pressure. The novel approach employed in this research allowed the test-rig to automatically alter inlet pressures while maintaining a constant regulator discharge and continuously measuring a large number of data points across the full range of inlet pressures applied.

From these results, it was established that pressure regulators do not limit pressure to the nominal pressure ratings prescribed by manufacturers. The actual outlet pressure is different for each manufacturer, and depending on the manufacturer, was either above or below the nominal setting. Therefore, these results will help designers to select appropriate regulator models and adjust corresponding nozzle sprinkler discharge totals when designing pressure regulated CP&LMs, to ensure the water requirements of irrigated crops are satisfied. The results also indicated that the regulator outlet pressure is impacted by hysteresis in outlet pressure, which is caused by variations in inlet pressure head. Similarly, the variations experienced in groundwater supply levels caused by fluctuations in water table drawdown, will impact the regulator performance in a similar manner, resulting in poor water application uniformity. This is largely expected on LMs where the decline in system head will reduce pressure regulator outlet pressure below the minimum required operating pressure head for the sprinkler nozzle package across the entire length of the machine. While a significant number (total of 80 units) of pressure regulator units were tested within the available time and resources, they were less than the number determined by the statistical means reported in Table 4-2 of Chapter 4.

The great quantity of data developed from these hydraulic experiments allowed for the development of a better understanding of the different individual pressure regulation mechanisms inside CP&LM regulators. This improved understanding of regulation from this good test data, also helped to provide a clear perspective on the true nature of pressure regulator performance, and will be invaluable in resolving the conflicted opinion amongst researchers on how these devices perform. It was evident that the average regulator outlet pressure is about 93 % of the nominal set pressure for the manufacturer X regulators, 107 % times the nominal set pressure for manufacturer Y, and is 101 % times the nominal set pressure for manufacturer Z regulators, in steady conditions. Therefore, the common mistake that hydraulic design engineers and other many industry practitioners make when dealing with pressure regulated CP&LMs causes significant variations in the operating point of these machines because they assume that regulators operate at their nominal set pressures. For instance, if an un-uniformed CP&LM designer selects low pressure models of the manufacturer X regulators, the pump discharge will be lower than the actual duty point required to efficiently operate these machines. The system operating point will be different if regulators for this machine are replaced with other manufacturers' regulators. The expected magnitudes of the discharge change for a particular change in head are explained in Chapter 2 of this thesis. If a correctly designed LM with a total of 500 of the #42 nozzles (8.33 mm diameter and nominal flow rate = 0.62 L/s) is to be regulated by 68.95 kPa of manufacturer X regulators, the total system discharge will be less than the expected 310 L/s. The same LM machine will be over-designed when each of the manufacturers Y and Z are selected to regulate sprinkler heads. The outcomes of poor regulator performance understanding, are that the supposedly well designed machines operate inefficiently and cause poor water application uniformities and subsequent reductions in crop yields, in addition to the increases in capital and operating costs of these irrigation machines. The implications are exacerbated in CP&LMs supplied from groundwater sources. Under these conditions, the fluctuations in water table further creates hysteresis in regulator outlet pressures of the already poorly matched system duty points, resulting in further declines in irrigation and pumping efficiencies. The gross misinterpretation of actual regulator performance is also demonstrated by Zerihun et al. (2019), where the nominal set pressure was used to simulate the hydraulic performance of a LM machine equipped with pressure regulators.

The novel aspect of this quantity of hydraulic data of pressure regulator performance, is that it enabled the development of a new mathematical model for industry to use, and to overcome the challenges of imprecise modelling of pressure regulation. Without this new model, elements of the good hydraulic test data could not be explored any further to improve pressure regulation understanding, or be beneficial to industry to help improve the design of CP&LMs that are equipped with the devices. Hence, the development of the PRV model was novel. Unlike previous PRV models, this new hydraulic model is built from three sub-models derived directly from the minor head losses that reduce inlet pressure head to produce outlet pressure. The advantage of this model is that it is built on the basis of pure hydraulic fundamentals, and accounts for hysteresis in outlet pressure. It produces the upper and lower boundaries of the outlet pressure regulation curves, in which the actual individual outlet pressures exist for an increasing and decreasing inlet pressures. Currently, there has been no simulation model that could accurately predict regulator outlet pressure hysteresis. Therefore, the new PRV model would help designers to accurately assess their selection of low and high pressure models from different manufacturers, and combine these with appropriately sized nozzle packages functioning at the correct operating heads to ensure accurate amounts of irrigation water are applied to crops with pressure regulated CP&LMs. The regulator nominal set pressures used in the design can now be verified by using this model to ensure that the most precise actual regulator outlet pressures and total discharges are achieved. This will ensure that the design operating point of the machines are that required to irrigate very efficiently. The correct application of this new PRV model should alert the LM designer to adjust the nozzle package to an appropriate size that delivers the total discharge at the right pressure for the selected regulator manufacturer. In the event that the model predicts a lower outlet pressure than the nominal pressure rating of the manufacturer at the nozzle discharge, the designer has the option of selecting the next better regulator manufacturer by using the model to perform multiple simulations. This would help maintain the stability of the algorithms used to calculate the operating points of CP&LMs, as well as the correct selection amongst the different types of available sprinkler packages for CP&LMs.

As expected of any model, the new PRV model developed has limitations. It is not capable of predicting the shape of the decline in outlet pressure at maximum test

pressure, during the transition between the upper and lower boundaries of the regulated outlet pressure, caused by hysteresis. However, this shape has been experimentally determined as shown in the outlet pressure hysteresis results reported in Section 5.6.6 of Chapter 5. Further improvements of the $h_{m\text{-}H}$ sub-model are proposed and will address this short coming. The model also predicted the outlet pressure turning points at higher pressures than the measured turning points at the highest nozzle discharge for one manufacturer. Therefore, further development is still required to fully represent the true nature of the characteristic shape of the hysteresis envelopes in the model, and the actual position of a single outlet pressure when a change is effected on the inlet pressure head.

8.5 Achievement of Research Objectives

The aim of this research was to develop and implement an advanced automatic measurement system in the hydraulic characterisation of pulsing solenoid VRI valves and CP&LM pressure regulators. The ultimate goal was to develop hydraulic modelling strategies that can be employed to improve the hydraulic design of VRI CP&LMs. Current designs are completed without considering the hydraulic impacts introduced by the additional accessories and their unique pulsing mode of operation in the irrigation machines.

Objective 1: A novel automatic measurement system was developed for performing series of simulated hydraulic experiments for solenoid VRI valves and CP&LM pressure regulators in the USQ Engineering Hydraulics Laboratory. This included control algorithms and pulsing frequencies for solenoid valves that were incorporated in the LabVIEW software and data acquisition system.

Objective 2: Appropriate test procedures for the groups of novel experiments conducted in this research were developed through incremental testing and modifications of the test-apparatus, until accurate, repeatable, and reliable results were obtained.

Objective 3: Characterisation of the minor head losses on common solenoid VRI valves manufacturers were completed. Empirical coefficients and mathematical equations for simulating the hydraulic performance of VRI valves were developed. These equations led to the modification of the standard total pressure head loss equation for the hydraulic design of VRI CP&LMs.

Objective 4: The propagation of hydraulic transients and the occurrence of water hammer during VRI pulsing was investigated, including the characterisation of the relative magnitude of hydraulic heads created.

Objective 5: Extensive characterisation of the complex hydraulic performance characteristics of CP&LM pressure regulators was achieved using the advanced capabilities of the novel automatic test-rig developed.

Objective 6: The testing of the hydraulic response of pressure regulators from impacts of fast pressure transients created during VRI pulsing was completed, with the results showing that the transients can affect regulator performance.

Objective 7: From the great quantity of pressure regulator performance data created, a pressure regulator mathematical model was developed to help engineers, designers, researchers, and growers to address the design problems for VRI retrofits on pressure regulated CP&LMs.

Therefore, this research successfully achieved the aim of using advanced experimental measurement techniques to model the hydraulic impacts of retrofitting VRI technology on CP&LMs operating with pressure regulators.

8.6 Research Contribution to Theory and Practice

This research was conducted to develop an understanding of the hydraulic performance of CP&LM irrigation machines retrofitted with VRI technology. It is the first work to be completed in the hydraulics space because nearly all VRI research and development has so far been focussed on building prototype systems that can help demonstrate the proposed benefits, with the ultimate aim of promoting the adoption of the VRI technology. In doing so, this novel work covered a wide range of topic areas from developing a suitable test method that can be employed to simulate and measure the hydraulic performance characteristics of VRI equipment and pressure regulators. The overall goal was to enable the proposition of hydraulic design improvements for VRI equipped CP&LMs. A summary of the major contributions to theory and practice arising from this research is as follows.

- A proof of concept that electronic measurement and testing systems are technically feasible for conducting complex experiments where very large datasets are sought. This has been demonstrated and achieved by integrating instrumentation and electronics equipment with visual software programming, sensing equipment, and hydraulics equipment, to build an advanced automatic test-apparatus for simulating and characterising the hydraulic performance of VRI valves and CP&LM pressure regulators.

- Novel procedures and test protocols for investigating hydraulic transients during VRI pulsing, and the advanced pressure regulator characterisation of outlet hysteresis.

- Novel procedures and test protocols for characterising the hydraulic response of pressure regulators to pressure transients introduced by VRI.

- Development of a large quantity of data for the hydraulic performance characteristics of common VRI valves and major pressure regulator manufacturers used in the irrigation industry. This critical information helps to build a very comprehensive and robust theory about the hydraulics of these important CP&LM irrigation components.

- A hydraulic model for pressure regulators to be used in industry to complete accurate and seamless hydraulic designs of self-propelled CP&LM irrigation machines.

The research has led to the development of a novel automatic multi-function hydraulic measurement apparatus that can be employed to complete testing of identical experiments. The advanced test method will serve as a good basis for improving ISO Standards 9644:2008 and 10522:1993 in line with modern irrigation technological advancements. The research has also enabled the development of mathematical equations and empirical coefficients that can be used to simulate VRI and pressure regulator performance, while also permitting improvements in the hydraulic design of VRI machines. Finally, a new pressure regulator mathematical model has been developed for the precise and accurate prediction of pressure regulator performance within the hydraulic and operational conditions of modern low pressure CP&LMs. This model will improve the hydraulic design of CP&LMs and optimise their performance in the field, while reducing the capital and operational costs of these machines. Further improvements of the PRV model will enable engineers, designers, and researchers, to be able to simulate and understand the actual regulator outlet pressures in hydraulic situations of CP&LMs. It will also help manufacturers to review the mechanical and geometrical properties of pressure regulators to improve their levels of accuracy and precise performance.

9. CONCLUSIONS AND FUTURE RESEARCH

9.1 Conclusions

This research investigated the hydraulics phenomena of VRI technology when implemented with pressure regulated CP&LM irrigation machines. Although the basic concepts of VRI were defined in the early 1990s, with VRI development and commercialisation beginning around 2010, there has been no attempt to investigate the hydraulic impacts of retrofitting this technology on these irrigation machines. It has also been established that the hydraulic performance of CP&LM pressure regulators is not adequately understood in industry. The main aim of this study was to determine the effects of retrofitting pulsing solenoid valves on the hydraulic performance of pressure regulated CP&LMs, in order to develop mathematical equations and hydraulic modelling techniques that can be used to improve the hydraulic design of VRI CP&LM irrigation machines.

Extensive simulated laboratory experiments were completed in the Engineering Hydraulics Laboratory (Z113) at USQ, Toowoomba Australia. Firstly, a novel automatic multi-function testing apparatus was developed to perform and control these experiments, and so to measure the hydraulic performance data resulting from the experiments. The novel automatic measuring apparatus incorporated a LabVIEW DAQ system, and a set of high precision sensors, electromagnetic flow meter, and electronic control valves. A series of tests were performed on the VRI valves and pressure regulators by automatically operating and controlling the experiments using the LabVIEW software. Four groups of experiments were conducted, including (i) VRI valve minor pressure head losses and (ii) hydraulic transients from VRI valves pulsing (iii) pressure regulator performance tests, and (iv) the hydraulic response of pressure regulators to VRI transients. The datasets were used to establish the hydraulic performance characteristics of VRI valves and pressure regulators, including mathematical equations and empirical coefficients that enables modelling of the hydraulic performance of these irrigation components. The novel hydraulic characteristics of VRI valves enabled the modification of the total pressure head loss

equation for the design of VRI machines. Accordingly, the comprehensiveness of the large datasets for the complex pressure regulator performance characteristics established in this research, enabled the development of a hydraulic model for use to overcome the limitations of imprecise modelling of pressure regulation during the design of CP&LMs. The novel experimental test-rig and methodologies developed in this study would allow anyone interested to characterise the hydraulic performance of any new VRI CP&LM components from manufacturers or products that are introduced to the industry. These special testing methods will also inform the ISO standards for testing irrigation components to be in line with new technologies that are developed. The results obtained from this study will provide important information to hydraulic engineers and designers, VRI equipment manufacturers, researchers, and the users of this technology, to better manage its implementation and reception. It will also inform the current on-going research aimed at demonstrating the benefits of VRI. Consequently, based on this extensive research work, the study concludes that:

1. Advanced automatic measurement and testing systems are technically feasible, and are a smarter way of executing complex experiments and recording of very large datasets.

2. Solenoid VRI valves create a significant amount of head loss, and this is impactful in some CP&LM designs. The head loss for one manufacturer, was found to be approximately 25 % of head at the centre of low pressure CP&LMs.

3. The on-and-off pulsing of solenoid VRI valves introduces water hammer and pressure wave transients in CP&LMs retrofitted with VRI. The on-and-off pulsing creates unsteady conditions that impact the regulator outlet pressure in CP&LMs equipped with pressure regulators. The transients create a temporary rise in regulator outlet pressure that is very significant when compared to the nominal pressure setting of CP&LM pressure regulators.

4. The regulated outlet pressures received by sprinkler heads in CP&LMs is not equal to the nominal pressure rating usually specified by the manufacturers. This depends on the regulator design characteristics as determined by the respective manufacturers.

5. A new PRV model has been developed to help improve the design and implementation of pressure regulators in industry. This model is an improvement to the existing PRV models, because it is a full hydraulic model and is capable of predicting pressure regulator performance more accurately. Its greatest advantage is the ability to account for hysteresis in regulator outlet pressures, for the major regulator manufactures and nominal pressure settings used on CP&LMs.

9.2 Recommended Future Research

This study is a first step towards the development of a hydraulic understanding of VRI technology, and is also contributing to a limited research around pressure regulation. The study has been successful in developing the hydraulic performance characteristics of VRI valves and pressure regulators, including the building of mathematical approaches for modelling the performance of these important devices. However, this work has been completed using a limited set of test equipment due to resource and time constraints. In addition, these experiments were completed under simulated laboratory conditions. Consequently, there are several areas of research that still need to be addressed in future studies, including:

1. The need to test and characterise a larger sample of the different individual VRI valves and pressure regulators used with CP&LMs in industry in order to understand the magnitude of the variation due to manufacturing.

2. Employing computer simulation and modelling techniques such as CFD to optimise the internal design geometry of the one particular solenoid VRI valve with the highest minor head loss, to recommend some design improvements. A similar approach to that of Zhang and Li (2017) can be employed with a desired pre-set minor head loss for a selected number of discharges, to improve the mechanical design of the valves.

3. Measurements and validation of the results of water hammer and pressure transients from VRI pulsing using a large diameter pipe rig representative to

CP&LM spans, with multiple numbers of solenoids combinations and pulsing frequencies, to determine any potential for hydraulic dampening.

4. Further investigation and development of in-depth understanding of the impact of fast pressure wave transients on pressure regulator performance, to interpret the potential displacement of the flow tube induced by transients which is responsible for the differences in final regulated outlet pressures.

5. Further improvements of the hysteresis sub-model in the full PRV outlet pressure prediction model are required to permit accurate prediction of any regulator outlet pressures within the upper and lower limits of the regulation curves currently predicted by this PRV model developed. The conceptual ideas of the necessary improvements in the sub-model have been outlined in this research.

6. Refining the precision of the automatic test-apparatus to reduce noise in measurements to produce very smooth curves of data, especially with hysteresis characterisation.

7. Finally, when the hydraulics of VRI equipment are well integrated in the designs of CP&LMs, the other important aspects of VRI performance that are currently being investigated with little success can be improved by developing suitable algorithms. This include amongst others, the challenges associated with infield evaluations of water application uniformity for VRI machines, as discussed in Section 1.3.5.

REFERENCES

ABS 2019. Water use on Australian farms.

Adamkowski, A. & Lewandowski, M. 2012. Investigation of hydraulic transients in a pipeline with column separation. *Journal of Hydraulic Engineering,* 138**,** 935-944.

Al-Kufaishi, S., Blackmore, B. & Sourell, H. 2006. The feasibility of using variable rate water application under a central pivot irrigation system. *Irrigation and Drainage Systems,* 20**,** 317-327.

Allen, R. G., Keller, J. & Martin, D. 2000. *Center pivot system design*, Irrigation Association Falls Church, VA.

Anwar, A. A. 2000. Correction factors for center pivots with end guns. *Journal of Irrigation and Drainage Engineering,* 126**,** 113-118.

Araujo, A., Colombo, A., Barbosa, B. D. A., Almeida, I., Buono da Silva Baptista, V. & Diotto, A. 2017. Effects of wear of pressure regulating valves from a centre pivot irrigation in its uniformity of water application and optimum depth of bean irrigation. *IV Inovagri International Meeting.*

Armindo, R. A. & Botrel, T. A. 2012. Performance and radial distribution profiles of a variable flow rate sprinkler developed for precision irrigation. *Scientia Agricola,* 69**,** 160-167.

Armindo, R. A., Botrel, T. A. & Garzella, T. C. 2011. Flow rate sprinkler development for site-specific irrigation. *Irrigation Science,* 29**,** 233-240.

Barker, J. B., Bhatti, S., Heeren, D. M., Neale, C. M. & Rudnick, D. R. 2019. Variable Rate Irrigation of Maize and Soybean in West-Central Nebraska Under Full and Deficit Irrigation. *Frontiers in Big Data,* 2**,** 34.

Beccard, R. & Heermann, D. 1981. Performance of pumping plant-center pivot sprinkler irrigation systems [Irrigation]. *Paper-American Society of Agricultural Engineers (USA). Microfiche collection. no. fiche 81-2548.*

Boulos, P. F., Karney, B. W., Wood, D. J. & Lingireddy, S. 2005. Hydraulic transient guidelines for protecting water distribution systems. *Journal (American Water Works Association),* 97**,** 111-124.

Bradbury, S. F. & Ricketts, M. G. 2014. Irrigation systems and methods. Google Patents.

Bralts, V. F., Wu, I.-P. & Gitlin, H. M. 1981. Manufacturing variation and drip irrigation uniformity. *Transactions of the ASAE,* 24**,** 113-0119.

Burt, C. M. 2013. Pressure Regulating Valve Characteristics. *Irrigation Association.*

Camp, C. & Sadler, E. 1994. Center pivot irrigation system for site-specific water and nutrient management. *Paper*.

Camp, C., Sadler, E., Evans, D., Usrey, L. & Omary, M. 1998. Modified center pivot system for precision management of water and nutrients. *Applied Engineering in Agriculture,* 14**,** 23-31.

Casanova, J. J., O'Shaughnessy, S. A., Evett, S. R. & Rush, C. M. 2014. Development of a wireless computer vision instrument to detect biotic stress in wheat. *Sensors (Basel),* 14**,** 17753-69.

Chadwick, A. & Morfett, J. 2002. *Hydraulics in civil and environmental engineering*, Crc Press.

Chaudhry, M. H. 1979. Applied hydraulic transients. Springer.

Chavez, J., Pierce, F. & Evans, R. 2010. Compensating inherent linear move water application errors using a variable rate irrigation system. *Irrigation science,* 28**,** 203-210.

Christiansen, J. 1942. Hydraulics of sprinkling systems for irrigation. *Trans. Amer. Soc. Civ. Eng,* 107**,** 221-239.

Chu, S. T. & Moe, D. L. 1972. Hydraulics of a center pivot system. *Transactions of the ASAE,* 15**,** 894-0896.

Covas, D. I., Libraga, J., Ribeiro, R., Carriço, N., Ramos, H. M. & de Almeida, A. B. Measurement of hydraulic transients in a metal pipe rig: effects of free-air, cavitation and pipe axial-deformation. Proceedings to the 11th International Conference on Pressure Surges, 2012. 679-689.

Darko, R. O., Shouqi, Y., Junping, L., Haofang, Y. & Xingye, Z. 2017. Overview of advances in improving uniformity and water use efficiency of sprinkler irrigation. *International Journal of Agricultural and Biological Engineering,* 10**,** 1-15.

De Fraiture, C., Molden, D. & Wichelns, D. 2010. Investing in water for food, ecosystems, and livelihoods: An overview of the comprehensive assessment of water management in agriculture. *Agricultural Water Management,* 97**,** 495-501.

Doerge, T. 1999. Defining management zones for precision farming. *Crop Insights,* 8**,** 1-5.

Duke, H., Buchleiter, G., Heermann, D. & Chapman, J. Site specific management of water and chemicals using self-propelled sprinkler irrigation systems. Precision agriculture'97: papers presented at the first European Conference on Precision Agriculture, Warwick University Conference Centre, UK, 7-10 September 1997, 1997. Oxford; Herndon, VA: BIOS Scientific Pub., c1997.

Eberhard, J., McHugh, A., Scobie, M., Schmidt, E., McCarthy, A., Uddin, M. J., McKeering, L. & Poulter, R. 2013. Improving irrigation efficiency through precision irrigation in South East Queensland.

Evans, R. G., LaRue, J., Stone, K. C. & King, B. A. 2013. Adoption of site-specific variable rate sprinkler irrigation systems. *Irrigation Science,* 31**,** 871-887.

Foley, J., Greve, A., Huth, N. & Silburn, D. Comparison of soil conductivity measured by ERT and EM38 geophysical methods along irrigated paddock transects on

Black Vertosol soils. Proceedings of 16th Agronomy Conference, 2012. 14-18.

Foley, J. & Raine, S. 2001. Centre pivot and lateral move machines in the Australian cotton industry. *University of Southern Queensland: Toowoomba, Qld*.

Foley, J. & Smith, R. Performance evaluation of commercial CP and LM machines. 2011 Society for Engineering in Agriculture Conference: Diverse Challenges, Innovative Solutions, 2011. Engineers Australia, 169.

Foley, J. P. 2008. Centre pivot and lateral move machines. *WATERpak.*

Foley, J. P. 2010. *Performance Improvement of Centre Pivots & Lateral Moves.* PhD, University of Southern Queensland.

Foley, J. P. 2019. *RE: Centre Pivots and Lateral Moves.*

Fraisse, C. 1994. *Variable water application with moving irrigation systems.* PhD, Colorado State University.

Fraisse, C., Heermann, D. & Duke, H. Modified linear move system for experimental water application. Advances in planning, design and management of irrigation systems as related to sustainable land use, Leuven (Belgium), 14-17 Sep 1992, 1993.

Fraisse, C., Heermann, D. & Duke, H. 1995. Simulation of variable water application with linear-move irrigation systems. *Transactions of the ASAE,* 38**,** 1371-1376.

Fraisse, C., Sudduth, K. & Kitchen, N. 2001. Delineation of site-specific management zones by unsupervised classification of topographic attributes and soil electrical conductivity. *Transactions of the ASAE,* 44**,** 155.

Grisso, R., Alley, M., Holshouser, D. & Thomason, W. 2009. Precision farming tools. *Soil electrical conductivity*.

Grisso, R. D., Alley, M. M., Thomason, W. E., Holshouser, D. L. & Roberson, G. T. 2011. Precision farming tools: variable-rate application.

Hamill, L. 2011. *Understanding hydraulics*, Macmillan International Higher Education.

Han, Y. J., Khalilian, A., Owino, T. O., Farahani, H. J. & Moore, S. 2009. Development of Clemson variable-rate lateral irrigation system. *Computers and Electronics in Agriculture,* 68**,** 108-113.

Hedley, C., Bradbury, S., Watson, E., Dalrymple, H. & Wright, J. 2011. Farm scale trials of variable rate irrigation to assess the benefits of modifying existing sprinkler systems for precision applicationr. *International Journal of Agricultural Management,* 1**,** 51-55.

Hezarjaribi, A. & SourellL, H. 2008. Variable Water Application Depths from a Centre Pivot Irrigation Control System. *Tarım Makinaları Bilimi Dergisi,* 4.

James, L. G. 1982. Modeling the Performance of Center Pivot Irrigation Systems Operating on Variable Topography. 25.

Jensen, M. & Fratini, A. 1957. Adjusted" F" factors for sprinkler lateral design. *Agri. Eng.,* 38**,** 247.

Junior, T., de Araujo, A., de Camargo, A., Saretta, E. & Frizzone, J. 2018. Operational characterization of pressure regulating valves. *The Scientific World Journal,* 2018.

Keller, J. & Bliesner, R. D. 1990. Sprinkle and trickle irrigation.

Kincaid, D. & Heermann, D. 1970. Pressure distribution on a center-pivot sprinkler irrigation system. *Transactions of the ASAE,* 13**,** 556-0558.

Kincaid, D. C., Busch, R. J., McCann, I. R. & Nabil, M. 1987. Evaluation of Very Low Pressure Sprinkler Irrigation and Reservoir Tillage for Efficient Use of Water and Energy: Final Report. Agricultural Research Service, Kimberly, ID (USA); Idaho Univ., Moscow (USA). Dept. of Agricultural Engineering; Idaho Univ., Aberdeen (USA). Dept. of Agricultural Engineering.

King, B. & Kincaid, D. 1996. Variable flow sprinkler for site-specific water and nutrient management. *ASAE Paper*.

King, B. & Kincaid, D. 2004. A variable flow rate sprinkler for site-specific irrigation management. *Applied engineering in agriculture,* 20**,** 765.

King, B. & Wall, R. 1998. SUPERVISORY CONTROL AND DATAACQUISITION SYSTEM FOR SITE-SPECIFIC CENTER PIVOT IRRIGATION. *Applied Engineering in Agriculture,* 14**,** 135-144.

King, B., Wall, R., Kincaid, D. & Westermann, D. 1997. Field scale performance of a variable rate sprinkler for variable water and nutrient application.

King, B., Wall, R., Kincaid, D. & Westermann, D. 2005. Field testing of a variable rate sprinkler and control system for site-specific water and nutrient application. *Applied engineering in agriculture,* 21**,** 847-853.

King, B. A., Foster, G. L., Kincaid, D. C. & Wood, R. B. 1998. Variable flow sprinkler head. Google Patents.

King, B. A., Stark, J. & Wall, R. W. 2006. Comparison of site-specific and conventional uniform irrigation management for potatoes. *Applied Engineering in Agriculture,* 22**,** 677-688.

Kisekka, I., Oker, T., Nguyen, G., Aguilar, J. & Rogers, D. 2017. Revisiting precision mobile drip irrigation under limited water. *Irrigation Science,* 35**,** 483-500.

Koech, R. 2012. *Automated real time optimisation for control of furrow irrigation.* University of Southern Queensland.

Kranz, W. L., Irmak, S., Martin, D. L. & Yonts, C. D. 1997. *Flow Control Devices for Center Pivot Irrigation Systems*, Cooperative Extension, Institute of Agriculture and Natural Resources, University of Nebraska--Lincoln.

Krishna, K. R. 2016. *Push Button Agriculture Robotics, Drones, Satellite-Guided Soil and Crop Management*.

Lambert, S., Hay, F., Norton, T., Cotching, B. & Terhorst, A. 2013. Design and demonstration of precision agriculture irrigation applied to different vegetable crops. *Armidale NSW Australia 10-11th September 2009***,** 93.

Larock, B. E., Jeppson, R. W. & Watters, G. Z. 1999. *Hydraulics of pipeline systems*, CRC press.

LaRue, J. L. Variable Rate Irrigation 2010 Field Results. 2011 Louisville, Kentucky, August 7-10, 2011, 2011. American Society of Agricultural and Biological Engineers, 1.

Li, Y., Shi, Z., Wu, C.-f., Li, H.-y. & Li, F. 2008. Determination of potential management zones from soil electrical conductivity, yield and crop data. *Journal of Zhejiang University Science B,* 9**,** 68-76.

Lima, S. C., Frizzone, J. A., Costa, R. N., Souza, F. d., Pereira, A. S., Machado, C. C. & Valnir Júnior, M. 2003. Performance curves of new and used pressure regulating valves. *Revista Brasileira de Engenharia Agrícola e Ambiental,* 7**,** 201-209.

Lo, T. H. 2015. *Quantification of variable rate irrigation benefits and spatial variability in root zone water holding capacity.* MS thesis, Lincoln, Neb.: University of Nebrakska-Lincoln, Department of Biological Systems Engineering.

Lo, T. H., Heeren, D. M., Martin, D. L., Mateos, L., Luck, J. D. & Eisenhauer, D. E. 2016. Pumpage reduction by using variable-rate irrigation to mine undepleted soil water. *Transactions of the ASABE,* 59**,** 1285-1298.

Lo, T. H., Heeren, D. M., Mateos, L., Luck, J. D., Martin, D. L. & Eisenhauer, D. E. Potential irrigation reductions from increasing precipitation utilization with variable rate irrigation. 2015 ASABE/IA Irrigation Symposium: Emerging Technologies for Sustainable Irrigation-A Tribute to the Career of Terry Howell, Sr. Conference Proceedings, 2015. American Society of Agricultural and Biological Engineers, 1-11.

Lowenberg-DeBoer, J. 2018. The Variable Rate Irrigation Management Challenge. *The Oxford Handbook of Food, Water and Society.*

Luedtke, B. 2013. Drilling Down, Pumping Up: A History of Center-Pivot Irrigation and Hydraulic Fracturing in Kansas.

Magazine, A. S. 1976. Centre pivot irrigation. *Scientific American.*

McCann, I., King, B. & Stark, J. 1997. Variable rate water and chemical application for continuous-move sprinkler irrigation systems. *Applied Engineering in Agriculture,* 13**,** 609-615.

McCann, I. R. & Stark, J. C. 1993. Method and apparatus for variable application of irrigation water and chemicals. Google Patents.

McCarthy, A. 2010. *Improved irrigation of cotton via real-time, adaptive control of large mobile irrigation machines.* University of Southern Queensland.

McCarthy, A. & Foley, J. 2017. Technology: Rural: Smarter irrigation using variable-rate centre pivots. *Irrigation Australia: The Official Journal of Irrigation Australia,* 33**,** 6.

McCarthy, A., Hancock, N. & Raine, S. 2015. Holistic control system design for large mobile irrigation machines. *Machine Vision and Mechatronics in Practice.* Springer.

McCarthy, A. C., Hancock, N. H. & Raine, S. R. 2011. Advanced process control of irrigation: the current state and an analysis to aid future development. *Irrigation Science,* 31**,** 183-192.

McCarthy, A. C., Hancock, N. H. & Raine, S. R. 2014. Simulation of irrigation control strategies for cotton using Model Predictive Control within the VARIwise simulation framework. *Computers and Electronics in Agriculture,* 101**,** 135-147.

Mkhwanazi, M. 2014. *Developing a modified SEBAL algorithm that is responsive to advection by using limited weather data.* Colorado State University. Libraries.

Mohr, D. 2011. *Performance characterisation of pressure regulation devices used in broad-acre irrigation.* BEng Honours, University of Southern Queensland.

O'Shaughnessy, S. A., Evett, S. R., Colaizzi, P. D. & Howell, T. A. 2011. Using radiation thermography and thermometry to evaluate crop water stress in soybean and cotton. *Agricultural Water Management,* 98**,** 1523-1535.

O'Shaughnessy, S. A. & Colaizzi, P. D. 2017. Performance of precision mobile drip irrigation in the Texas High Plains region. *Agronomy,* 7**,** 68.

O'Shaughnessy, S. A. & Evett, S. R. Zone edge effects with variable rate irrigation. Proceedings of the Central Plains Irrigation Conference, 2015.

O'Shaughnessy, S. A., Evett, S. R. & Colaizzi, P. D. 2015. Dynamic prescription maps for site-specific variable rate irrigation of cotton. *Agricultural Water Management,* 159**,** 123-138.

O'Shaughnessy, S. A., Evett, S. R., Colaizzi, P. D., Andrade, M. A., Marek, T. H., Heeren, D. M., Lamm, F. R. & LaRue, J. L. 2019. Identifying advantages and disadvantages of variable rate irrigation: An updated review. *Applied Engineering in Agriculture,* 35**,** 837-852.

O'Shaughnessy, S. A., Urrego, Y. F., Evett, S. R., Colaizzi, P. D. & Howell, T. A. 2013. Assessing application uniformity of a variable rate irrigation system in a windy location. *Applied Engineering in Agriculture,* 29**,** 497-510.

Olson, B. L. PMDI Field Test Results from Sheridan County. Proceedings for 2006 Central Plains Irrigation Conference, Colby, Kansas, Feb 21-22, 2006. 44.

Omary, M., Camp, C. & Sadler, E. 1997. Center pivot irrigation system modification to provide variable water application depths. *Applied Engineering in Agriculture,* 13**,** 235-239.

Perry, C. & Pocknee, S. Precision pivot irrigation controls to optimize water application. Understanding & addressing conservation and recycled water irrigation, the Proceedings of the 2003 irrigation association meeting. San Diego, CA, 2003. 86-92.

Perry, C., Pocknee, S., Hansen, O., Kvien, C., Vellidis, G. & Hart, E. Development and testing of a variable-rate pivot irrigation control system. ASAE Meeting Presentation, Chicago, Illinois, USA, Paper, 2002.

Phocaides, A. 2007. *Handbook on pressurized irrigation techniques*, Food & Agriculture Org.

Pieterse, L. 2014. *Variable Rate Irrigation* [Online]. Available: https://spudsmart.com/tuber-talk-spud-smart-fall-2014/ [Accessed].

Rackers, A. D. 2011. *Development and application of variable rate irrigation techniques on non-uniform soils using center-pivot irrigation systems.* 1517412 M.S., University of Missouri - Columbia.

Raine, S. & Foley, J. 2002. Comparing Application Systems for Cotton Irrigation-What are the Pros and Cons?

Ramos, H., Tamminen, S. & Covas, D. 2009. Water Supply System Performance for Different Pipe Materials Part II: Sensitivity Analysis to Pressure Variation. *Water Resources Management,* 23**,** 367-393.

Rogers, D. H. Evaluation of pressure regulators from center pivot nozzle packages. 2010 CENTRAL PLAINS IRRIGATION CONFERENCE, 2010. 58.

Ryan, T. P. 2013. *Sample Size Determination and Power*, Wiley.

Sadler, E. J., Camp, C. R., Evans, D. E. & Millen, J. 2002. Spatial variation of corn response to irrigation. *Transactions of the ASAE,* 45**,** 1869.

Sadler, J., Evans, R., Buchleiter, G. & King, B. 2000. Venturing into precision agriculture. *Irrigation journal*.

Santiesteban, T. G. 2011. Benefits of Pressure Regulation in Irrigation.

Smith, R. & Baillie, J. Defining precision irrigation: A new approach to irrigation management. Irrigation Australia 2009: Irrigation Australia Irrigation and Drainage Conference: Proceedings, 2009. Irrigation Australia Ltd., 1-6.

Smith, R. J., Raine, S. R., McCarthy, A. C. & Hancock, N. H. 2009. Managing Spatial and Temporal Variability in Irrigated Agriculture Through Adaptive Control. *Australian Journal of Multi-Disciplinary Engineering,* 7**,** 79-90.

Stone, K. C., Bauer, P. J. & Sigua, G. C. 2016. Irrigation management using an expert system, soil water potentials, and vegetative indices for spatial applications. *Transactions of the ASABE,* 59**,** 941-948.

Sui, R. & Fisher, D. K. 2015. Field test of a center pivot irrigation system. *Applied Engineering in Agriculture,* 31**,** 83-88.

Sui, R., Fisher, D. K. & Reddy, K. N. 2015. Yield response to variable rate irrigation in corn. *Journal of Agricultural Science,* 7**,** 11.

Tadić Ananić, M. & Gjetvaj, G. 2017. Water hammer in irrigation systems. *Građevinar,* 69**,** 633-638.

Tullis, J. P. 1989. *Hydraulics of pipelines: Pumps, valves, cavitation, transients*, John Wiley & Sons.

Turner, J. R. & Thayer, J. 2001. *Introduction to Analysis of Variance: Design, Analyis & Interpretation*, SAGE Publications.

USDA-NASS 2013. Farm and ranch irrigation survey. *US Department of Agriculture, National Agricultural Statistics Service*.

Valiantzas, J. D. & Dercas, N. 2005. Hydraulic analysis of multidiameter center-pivot sprinkler laterals. *Journal of irrigation and drainage engineering,* 131**,** 137-146.

von Bernuth, R. & Baird, D. 1990. Characterizing pressure regulator performance. *Transactions of the ASAE,* 33**,** 145-150.

von Bernuth, R. D. & Baird, D. R. 1987. Pressure regulator characteristics. *American Society of Agricultural Engineers (Microfiche collection)(USA)*.

Wall, R., King, B. & McCann, I. 1996. Center-pivot irrigation system control and data communications network for real-time variable water application. *Precision Agriculture*, 757-766.

Waller, P. & Yitayew, M. 2015. *Irrigation and drainage engineering*, Springer.

Wan, W. & Mao, X. 2016. Shock Wave Speed and Transient Response of PE Pipe with Steel-Mesh Reinforcement. *Shock and Vibration,* 2016, 10.

White, S. C. 2007. Partial root zone drying and deficit irrigation in cotton for use under large mobile irrigation machines. *PhD, University of Southern Queensland, Toowoomba*.

Workman, L. 2011. Water Hammer & Pressure Surges in PVC Systems. *Version 1. Expert4PVC Consulting.*

Yari, A., Madramootoo, C. A., Woods, S. A. & Adamchuk, V. I. 2017. Performance evaluation of constant versus variable rate irrigation. *Irrigation and Drainage,* 66, 501-509.

Younus, M. S. 2019. *Irrigation performance of centre pivot end-guns operating in windy conditions.* University of Southern Queensland.

Zerihun, D., Sanchez, C., Thorp, K. & Hagler, M. 2019. Hydraulics of Linear-Move Sprinkler Irrigation Systems, III: Model Evaluation. *Irrigat Drainage Sys Eng,* 8, 2.

Zhang, C. & Li, G. 2017. Optimization of a direct-acting pressure regulator for irrigation systems based on CFD simulation and response surface methodology. *Irrigation Science,* 35, 383-395.

Zhang, N., Wang, M. & Wang, N. 2002. Precision agriculture—a worldwide overview. *Computers and electronics in agriculture,* 36, 113-132.

Zhao, W., Li, J. & Li, Y. 2016. Review on variable rate irrigation with continuously moving sprinkler machines. *Transactions of the Chinese Society of Agricultural Engineering,* 32, 1-7.

Zhao, W., Li, J., Yang, R. & Li, Y. 2015. Field evaluating system performance of a variable centre pivot irrigation system. *Internnational Commision on Irrigation and Drainage*.

Appendix A: Calibration of Pressure Transducers

Measured Data and Regression Analysis for Calibrating the 400 kPa Druck PMP 4030 Pressure Sensing Transducer

The pressure readings generated using a Druck PV211 pneumatic pressure hand pump with a Druck DPI 802 display and voltage readings measured from the LabVIEW DAQ software. The calibration measurements were repeated three times at the same pressure supplied to the sensor, as denoted by the superscripts.

Table A 1: Pressure and voltage readings for performing regression analysis for the 400 kPa PT

Pressure (kPa)	Voltage (V)[1]	Voltage (V)[2]	Voltage (V)[3]
404.30	5.07	5.07	5.07
390.70	4.90	4.90	4.90
371.50	4.66	4.66	4.66
345.70	4.34	4.34	4.34
330.70	4.15	4.15	4.15
320.00	4.02	4.02	4.02
309.00	3.88	3.88	3.88
281.40	3.53	3.53	3.53
250.20	3.14	3.14	3.14
244.60	3.07	3.07	3.07
235.10	2.95	2.95	2.95
210.00	2.64	2.64	2.64
205.80	2.59	2.59	2.59
182.10	2.29	2.29	2.29
173.80	2.18	2.19	2.19
141.60	1.78	1.78	1.78
131.00	1.65	1.65	1.65
125.30	1.58	1.58	1.58
112.00	1.41	1.41	1.41
102.30	1.29	1.29	1.29
89.70	1.13	1.13	1.13
79.10	1.00	1.00	1.00
67.00	0.85	0.85	0.85
59.40	0.75	0.76	0.75
52.10	0.66	0.66	0.66
41.30	0.53	0.53	0.53
21.50	0.28	0.28	0.28
15.70	0.21	0.21	0.21
11.10	0.15	0.15	0.15
8.40	0.12	0.12	0.12
4.00	0.06	0.06	0.06
0.0	0.01	0.011	0.01

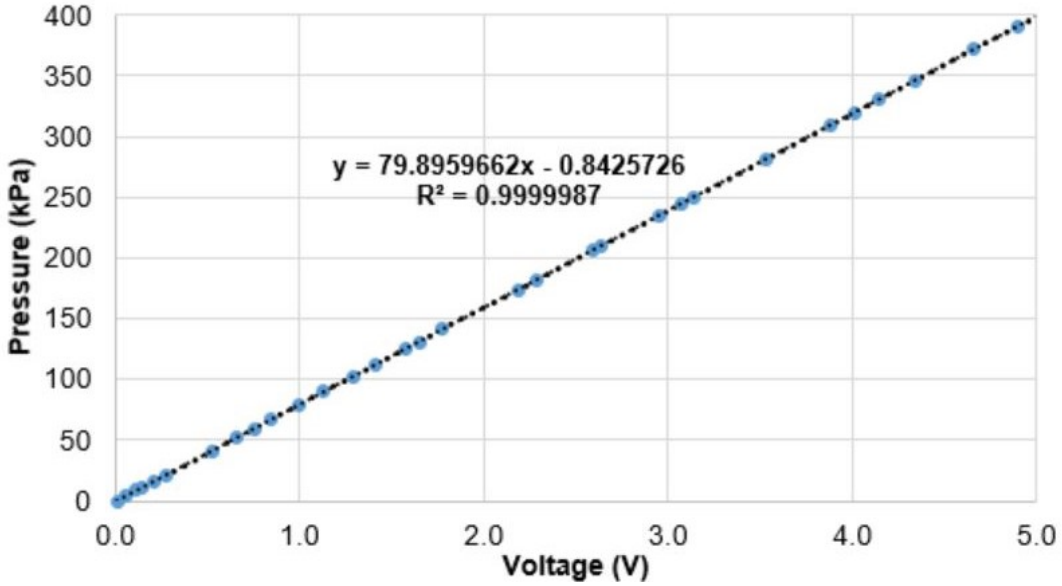

Figure A 1: Graph showing linear regression results and regression equation for the PT 400 kPa Druck pressure sensing transducer

Measured Data and Regression Analysis for Calibrating the 250 kPa Druck PMP 4030 Pressure Sensing Transducers

The pressure readings generated using a Druck PV211 pneumatic pressure hand pump with a Druck DPI 802 display and voltage readings measured from the LabVIEW DAQ software for the PT-1. The calibration measurements were repeated three times at the same pressure supplied to the sensor, as denoted by the superscripts.

Table A 2: Pressure and voltage readings for performing regression analysis for PT-1 250 kPa

Pressure (kPa)	Voltage (V)[1]	Voltage (V)[2]	Voltage (V)[3]
251.00	5.00	5.00	5.00
243.60	4.85	4.85	4.85
233.30	4.64	4.64	4.64
223.70	4.45	4.45	4.45
215.80	4.29	4.29	4.29
207.40	4.12	4.12	4.12
196.20	3.90	3.90	3.90
187.30	3.72	3.72	3.72
160.30	3.18	3.18	3.18
142.60	2.82	2.82	2.82
136.40	2.70	2.70	2.70
126.20	2.49	2.50	2.50
112.10	2.21	2.21	2.21
109.60	2.16	2.16	2.16
98.80	1.95	1.95	1.95
78.30	1.54	1.54	1.54
73.40	1.44	1.44	1.44
57.00	1.11	1.11	1.11
53.00	1.03	1.03	1.03
49.90	0.97	0.97	0.97
43.80	0.84	0.84	0.84
30.00	0.57	0.57	0.57
26.50	0.50	0.49	0.50
21.50	0.40	0.40	0.40
16.00	0.29	0.29	0.29
11.00	0.19	0.19	0.19
7.40	0.12	0.12	0.12
5.70	0.08	0.08	0.08
3.10	0.03	0.03	0.03
0.00	0.02	0.02	0.02

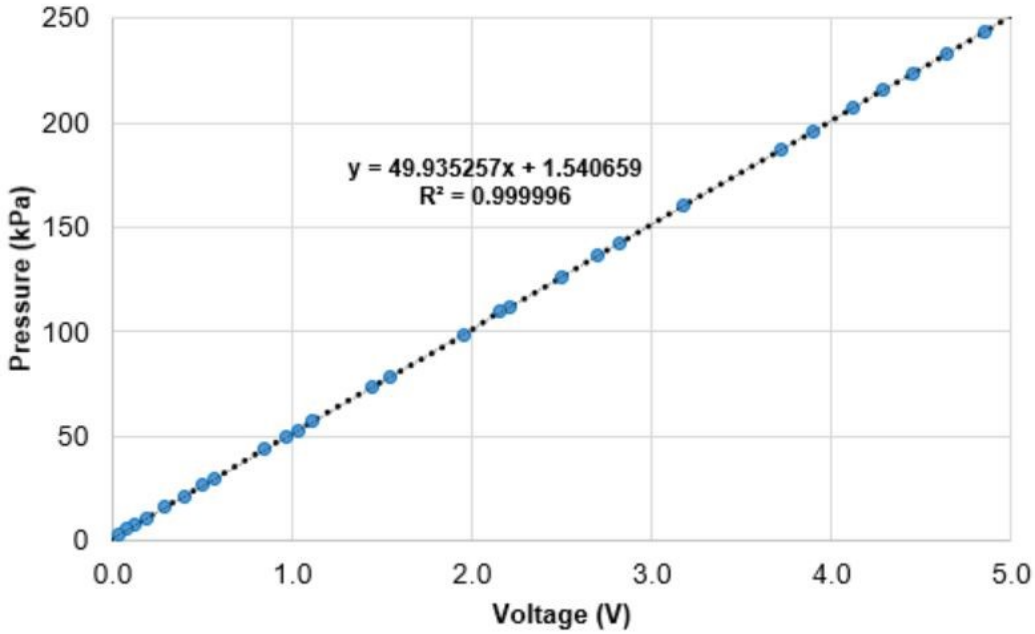

Figure A 2: Graph showing linear regression results and regression equation for the PT-1 250 kPa Druck pressure sensing transducer

Pressure readings generated using a Druck PV211 pneumatic pressure hand pump with a Druck DPI 802 display and voltage readings measured from the LabVIEW DAQ software for the PT-2. The calibration measurements were repeated three times at the same pressure supplied to the sensor, as denoted by the superscripts.

Table A 3: Pressure and voltage readings for performing regression analysis for PT-2 250 kPa

Pressure (kPa)	Voltage (V)[1]	Voltage (V)[2]
254.40	5.00	254.40
246.50	4.85	246.50
244.00	4.80	244.00
232.80	4.60	232.80
217.10	4.30	217.10
201.30	4.00	201.30
195.90	3.90	195.90
182.30	3.64	182.30
170.80	3.42	170.80
146.20	2.95	146.20
129.70	2.63	129.70
120.10	2.45	120.10
102.20	2.10	102.20
88.90	1.85	88.90
77.80	1.64	77.80
61.30	1.32	61.30
35.40	0.82	35.40
28.20	0.68	28.20
17.10	0.46	17.10
5.00	0.23	5.00
4.70	0.22	4.70
1.60	0.16	1.60
0.0	0.12	0.0

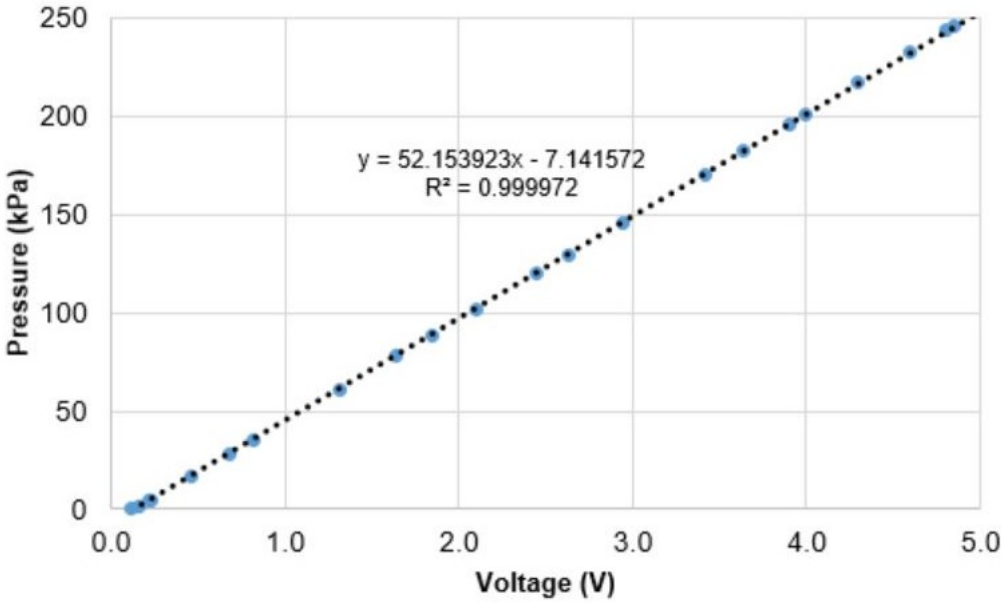

Figure A 3: Graph showing linear regression results and regression equation for the PT-2 250 kPa Druck pressure sensing transducer

Appendix B: Calibration of Electromagnetic Flowmeter

Measured Data and Regression Analysis for Calibrating LabVIEW DAQ using the ABB MagMaster Electromagnetic Flowmeter and 467.7 Ohm Resistor

Discharge readings were measured from the LCD display of the MagMaster Electromagnetic flowmeter while voltage readings were measured from the LabVIEW DAQ software, and current measured using a Fluke 115 TRUE RMS Multimeter.

Table A 4: Current, voltage, and discharge readings for performing regression analysis for calibrating the LabVIEW DAQ software

Discharge (L/s)	Voltage (V)	Current (mA)
0.00	1.86	0.00398
0.10	2.66	0.00569
0.21	3.58	0.00765
0.30	4.31	0.00922
0.39	5.10	0.01090
0.49	5.94	0.01270
0.51	6.03	0.01289
0.60	6.83	0.01460
0.70	7.68	0.01642
0.80	8.50	0.01817
0.92	9.53	0.02038

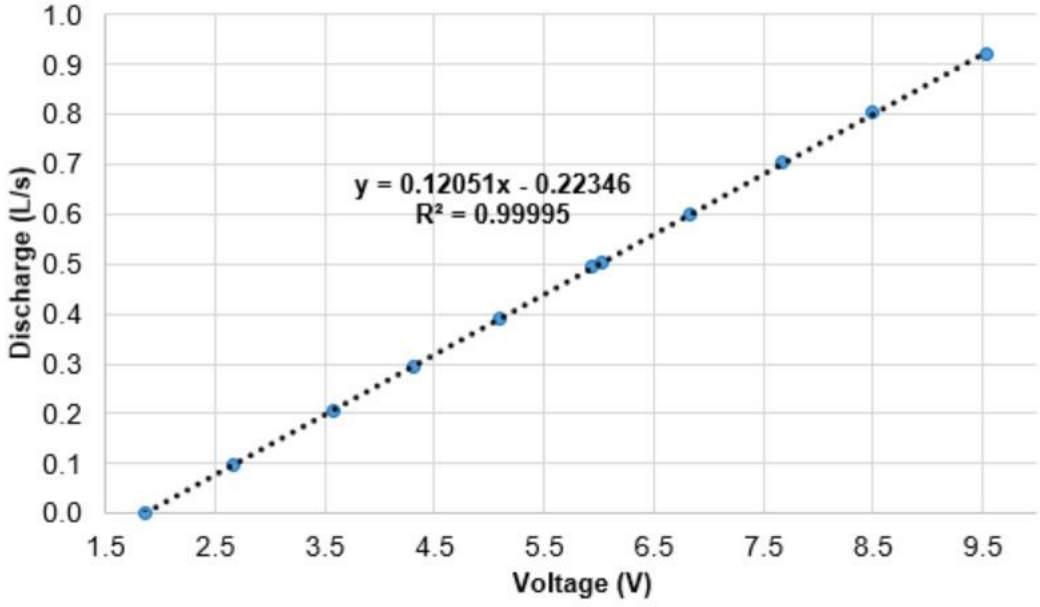

Figure A 4: Graph showing linear regression results and regression equation for the LabVIEW DAQ software

Validation of Discharge Measurements from ABB MagMaster Electromagnetic Flowmeter

Introduction

The purpose of this undertaking was to validate the discharge measurements obtained from the ABB MagMaster electromagnetic flowmeter used in the LabVIEW automatic multi-function hydraulic measurement apparatus. The idea was to ensure that accurate and precise discharge readings were measured during the experimental testing program conducted in Z113 Hydraulics Laboratory.

Procedure

The validation process employed a 15 L water drum that was first calibrated using a 1000 mL graduated plastic measuring cylinder. The measuring cylinder was filled with water to the meniscus of its maximum volume and the contents were emptied in the water drum until a known volume was reached. This volume was marked with a marker and a ruler on the side of the drum by following the meniscus of the water inside the drum. To ensure that the calibration process was quick, one side of the top section of the drum was the cut so that the height of the drum in that section was equal to the meniscus of the calibrated volume. This procedure enabled ease of filling with a garden hose that was connected at the downstream of the test-rig, such that when the known volume was reached, the water will start overflowing in the cut-away section. The time taken to fill this tank when a pre-set or known discharge was being passed through the test-rig and displayed in the flow meter digital LCD display, was measured using a timer or stopwatch. Measurements were taken five times, for two different flow rates and the results are presented in the tables below.

Table A 5: Results of discharge measurements using a 15 L drum at test-rig flow setting of 0.20 L/s

Test	Volume (L)	Time (s)	Discharge (L/s)	% variation
T_1	14	70.0	0.200	0
T_2	14	70.0	0.200	0
T_3	14	71.0	0.197	1.5
T_4	14	72.0	0.194	3.0
T_5	14	71.0	0.197	1.5
Average	**14**	**70.8**	**0.198**	**1.2**

Table A 6: Results of discharge measurements using a 15 L drum at test-rig flow setting of 0.35 L/s

Test	Volume (L)	Time (s)	Discharge (L/s)	% variation
T_1	14	40.0	0.350	0
T_2	14	41.0	0.342	2.3
T_3	14	40.0	0.350	0
T_4	14	40.0	0.350	0
T_5	14	40.0	0.350	0
Average	**14**	**40.2**	**0.348**	**0.6**

Analysis

The measurements in the tables above were analysed using the following equation.

$$Q = V/t$$

where: Q = discharge in litres per second (L/s), V = volume in litres (L), and t = time in seconds (s)

Appendix C: Schematics of the LabVIEW Program Test Methods

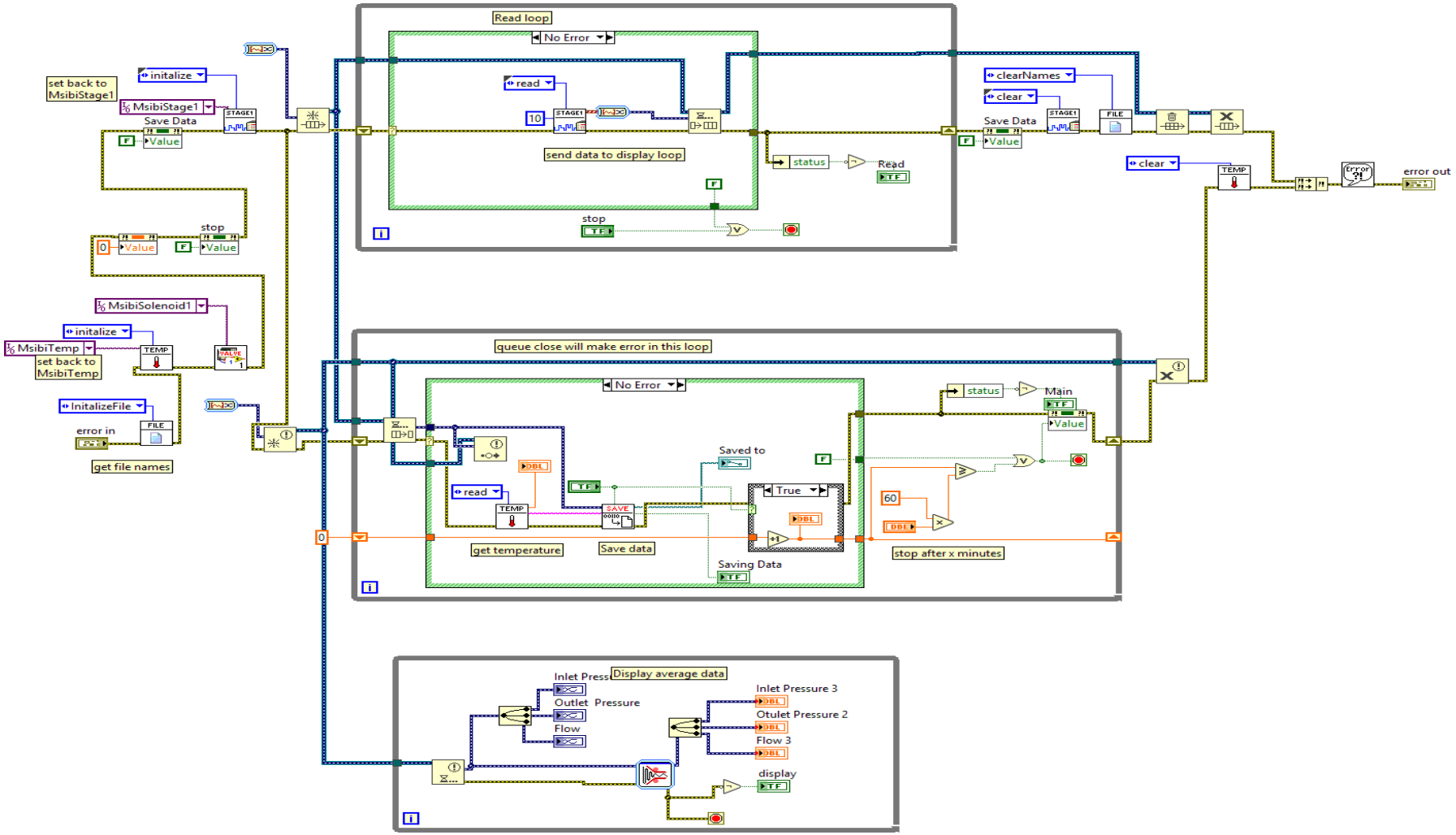

Figure C 1: Schematic of the LabVIEW code developed for Stage 1 testing

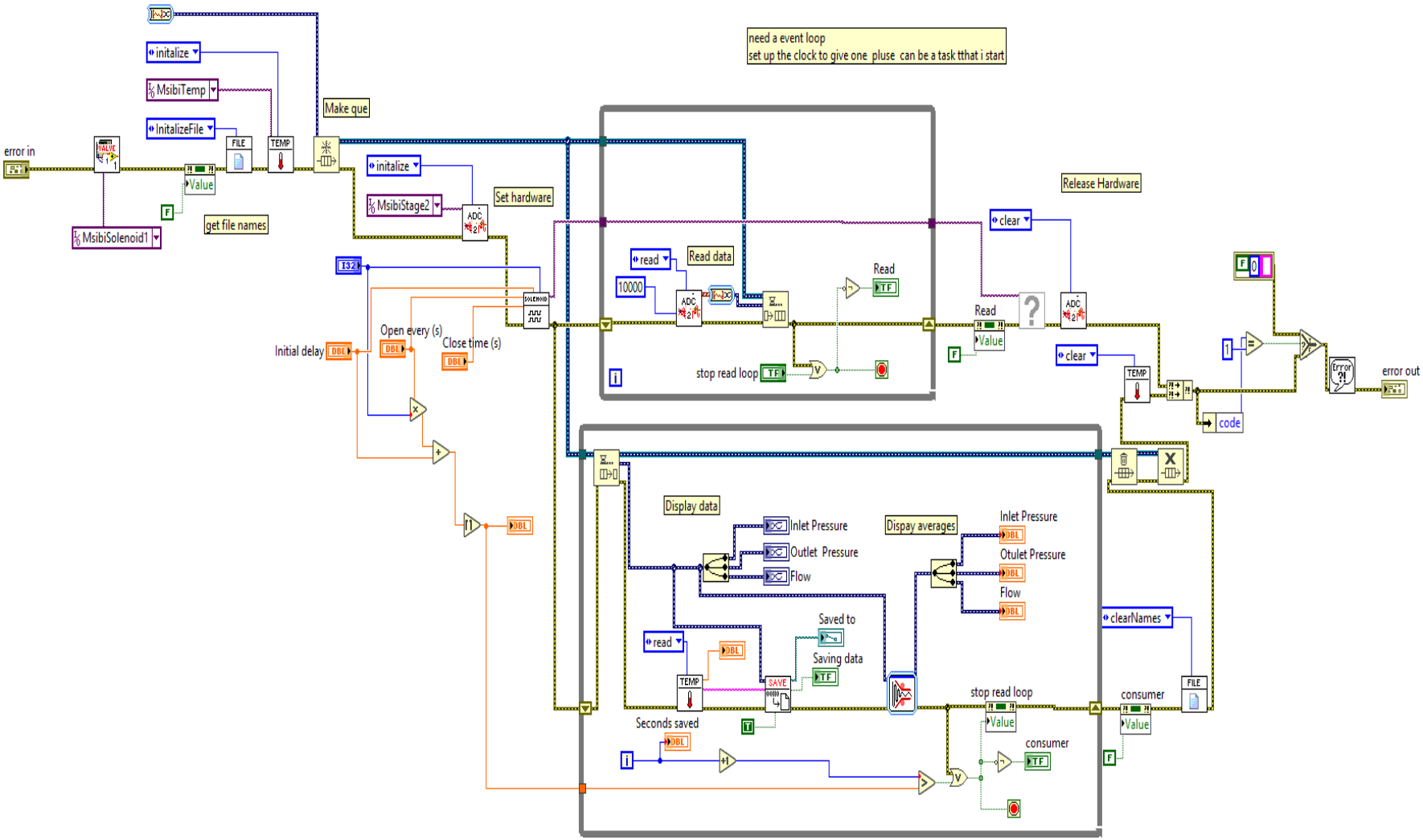

Figure C 2: Schematic of the LabVIEW code developed for Stage 2 testing

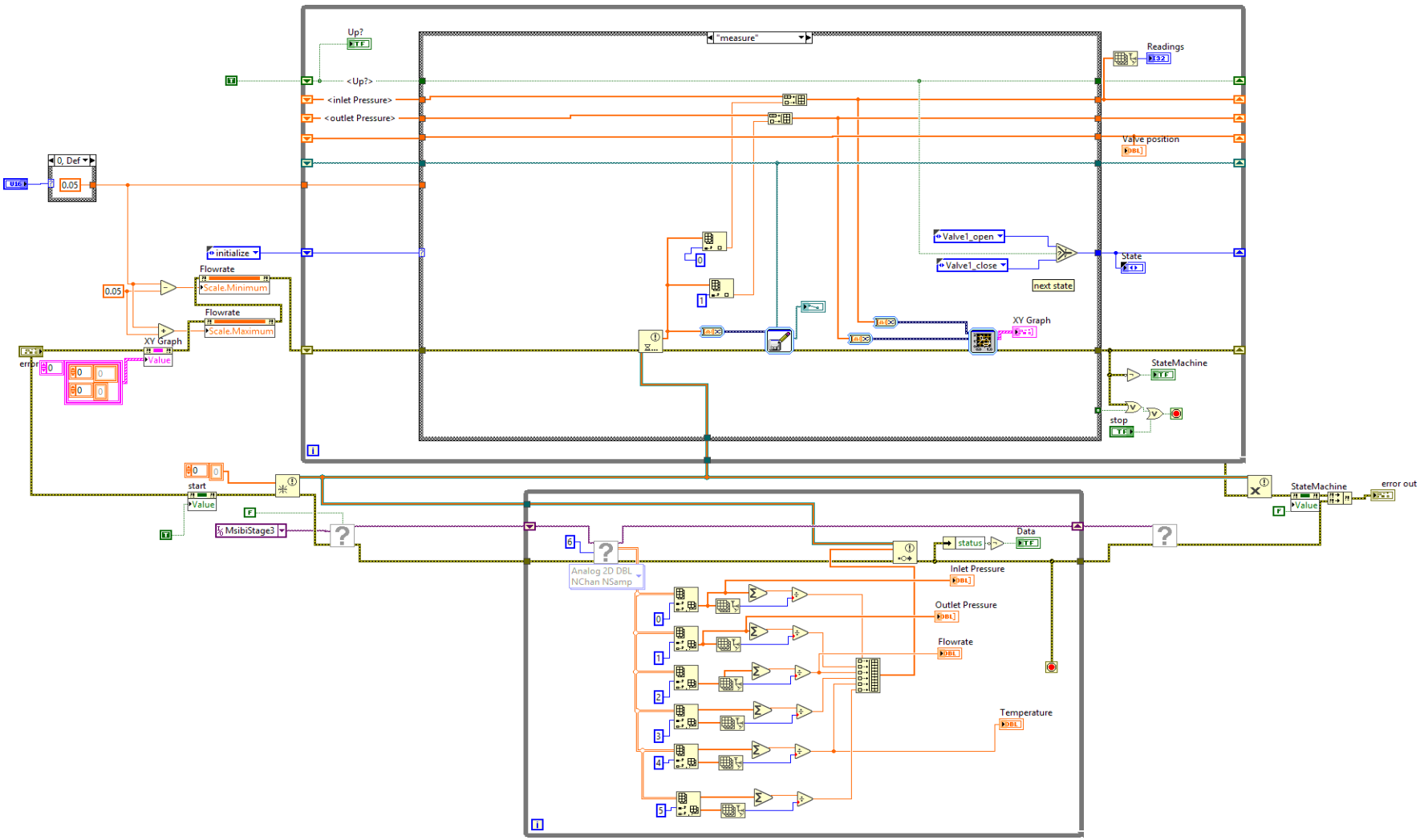

Figure C 3: Schematic of the LabVIEW code developed for Stage 3 testing

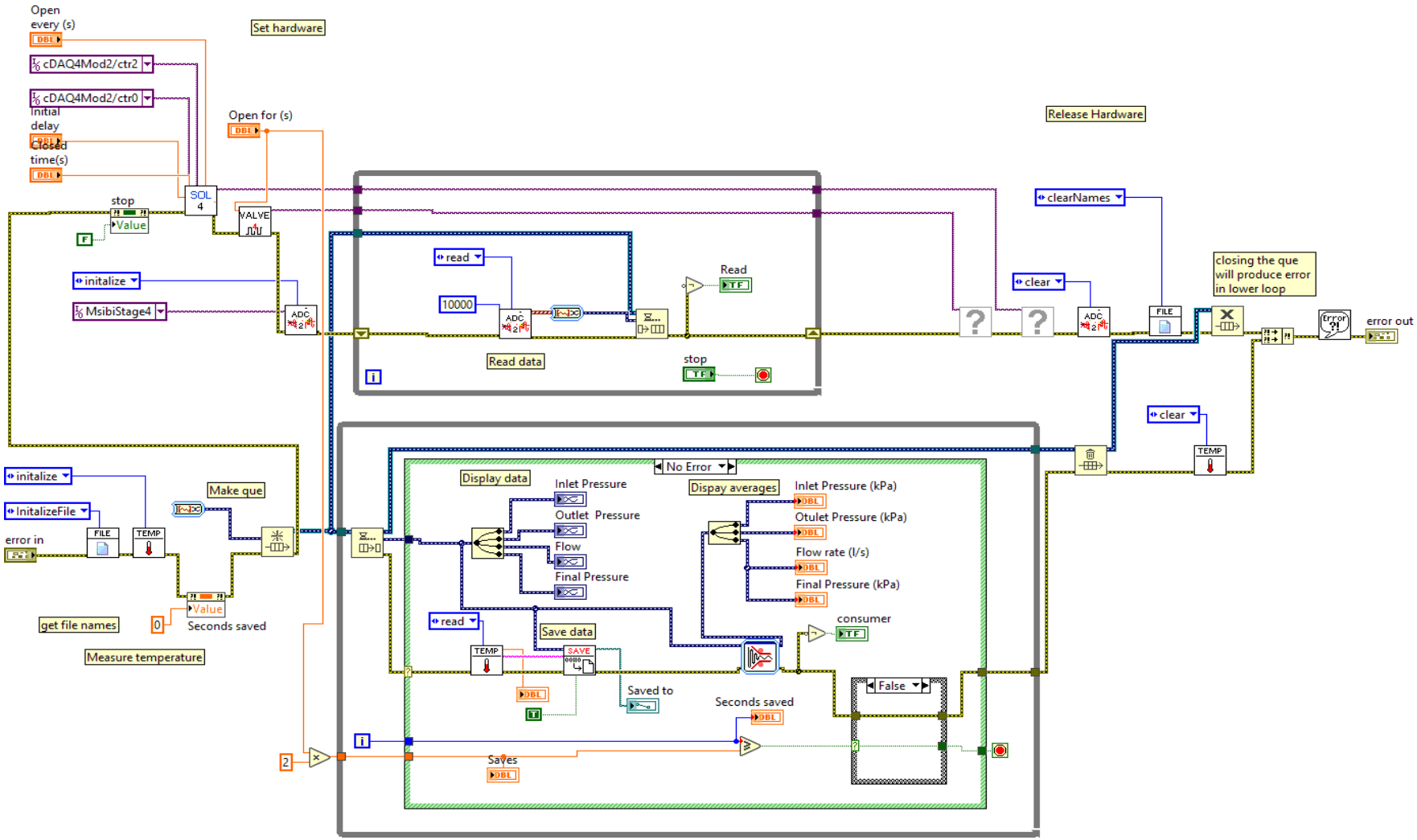

Figure C 4: Schematic of the LabVIEW code developed for Stage 4 testing